EXPERIMENTAL INVESTIGATION OF A REGENERATIVE CATALYTIC REACTOR

Submitted in fulfilment of the requirements for the degree of

Doctor of Philosophy

at

The University of Leeds

by

N. ABDULLAH, B.Sc. (Leeds)

under the direction of

P. J. HEGGS, Ph.D., C.Eng., M.I.Chem.E.

Department of Chemical Engineering,
Houldsworth School of Applied Science,
The University of Leeds,
LEEDS,
LS2 9JT

April 1983

ABSTRACT

A pilot plant is developed to investigate the Regenerative Cyclic Reactor (RCR) system. The proposed RCR system utilizes the inherent characteristics of the thermal regenerator to provide control over the temperature profiles along the reactor in order to enhance the reactant conversion. The RCR system is a transient adiabatic reactor which avoids the radial temperature gradients set up in tubular reactors. The reaction being investigated, the dehydrogenation of ethylbenzene to styrene, uses steam as a diluent. The steam is also used as the temperature regeneration medium.

The pilot plant design accommodates a steady state adiabatic reactor (SSAR) arrangement (one and two stage processes) as well as a one bed RCR system. Thus it is possible to compare the transient and steady state reactors.

With only electrical heating available, radiative electrical firebar heaters are used to generate the high system temperatures. Mathematical models are used to aid the heater design and to predict the temperatures for steady state operation. Other models are used to help in assessing the power load step up and step down rates.

The small flowrates, long pipe lengths, and the high temperature levels pose considerable problems in heat loss compensation over the system. Models are developed to assess the transfer resistances limiting the operational temperatures on ceramic bead insulated resistance wires. Heat shields utilizing these wires and a copper plate covering are successfully commissioned. Mathematical descriptions of these shields are also developed. A combination of these shields and heat tracing tapes enables reactor temperatures within the industrial operation range to be attained.

A series of transient runs of varying duration for the RCR, as well as steady state runs are carried out. Comparisons show that much higher

conversions are obtained for the RCR than the SSAR. A significant increase in conversion and the time taken to achieve steady state conversion occurs as the catalyst is regenerated by the steam. Steady state conversions for the early runs show some agreement with model predictions based on steady state kinetics. The transient runs and the later steady state runs show conversions much higher than those predicted by mathematical models.

ACKNOWLEDGEMENTS

To Dr. P. J. Heggs for his guidance and encouragement in his supervision of the research.

To the staff and faculty of the Department of Chemical Engineering for their assistance during the project, especially Mr. L. Bailey for his assistance with computational problems.

To Professor C. McGreavy for the use of the facilities in the Department of Chemical Engineering.

To the technical and workshop staff of the Houldsworth School for their patience and help during the building and the commissioning of the styrene apparatus.

To the Aga Khan Education Department, Nairobi for the research bursary award.

To the Aga Khan Aid Committee, London and the Aga Khan Jubilee Fund, Nairobi for their financial assistance.

To Miss Judith Squires who typed this thesis, for her patience and for the excellence of the end product.

To Gulnar for her inspiration, solace and persistence in not the easiest of times.

Finally, to my parents and Mr. Sadrudin S. H. Kara for whom this represents a culmination of hard work and dedication to my success.

CONTENTS

CORE CONTENTS

Page

LIST OF FIGURES

LIST OF TABLES

LIST OF PLATES

CHAPTER 1

INTRODUCTION TO THE RESEARCH

CHAPTER 1

INTRODUCTION TO THE RESEARCH

1.1 Introduction

Steady state adiabatic packed bed reactors are used in industry because of their relatively simple design and process model solutions, and the low capital costs. However, they do not provide the maximum conversion possible as compared to an isothermal reactor, especially if the reaction is highly endothermic or exothermic and equilibrium controlled.

This research aims to experimentally examine the advantages of utilizing a transient adiabatic packed bed reactor to enhance the conversions which would be obtained in a steady state adiabatic reactor (SSAR). The influence of periodic operation in fixed bed reactors has been investigated recently[1,2,3,4,5,6] in great depth. Methods employed include temperature and concentration forcing by changes in feed inlet conditions, as well as utilizing high frequency pulse methods. The transient control over process parameters results in yields and conversions unobtainable under steady state operations. This research investigates the possibilities of utilizing the thermal characteristics of a regenerator to provide more favourable temperature profiles along the reactor bed. This is the Regenerative Catalytic Reactor (RCR). Heggs[11-13], Cockcroft[10-13], Assaf[9] and Gavalas[7,8] have all examined the RCR by developing mathematical models and solutions. Assaf[9] and Cockcroft[10] showed that the RCR can achieve more favourable temperature profiles by utilizing the heat capacity of the packed bed to either provide a heat sink for exothermic reactions or a heat source for endothermic reactions. This results in significant improvements in conversion.

This work is concerned with developing a pilot plant to investigate both the RCR and the SSAR systems, thus providing means by which direct

comparisons can be made. The reaction to be investigated is the dehydrogenation of ethylbenzene to styrene. A commercial styrene system on the lines of the RCR was developed and used during the 1940's, but this was purely as a means of regenerating catalyst activity[14]. The reaction is highly endothermic and equilibrium controlled. Cockcroft[10] developed the RCR network for the styrene reaction, and his study forms the starting point for this research.

The details of the RCR system are expanded upon in Section 1.2, whilst Section 1.3 explores the advantages and disadvantages of the present industrial reactors for the dehydrogenation of ethylbenzene to styrene. Section 1.4 outlines the research programme.

1.2 The Styrene Regenerative Cyclic Reactor (RCR) System

The RCR system (Figure 1.1) uses the dehydrogenation catalyst as the heat storage medium to transfer heat from the hot phase to the cold phase. For an endothermic reaction, the reactant feed is the cold phase. The dehydrogenation of ethylbenzene utilizes steam as a feed diluent and therefore the steam is the obvious choice for the hot phase. The RCR system requires at least two beds to work simultaneously. At any time, one bed is carrying out the regeneration stroke (the heating of the catalyst by the steam), whilst the other has the reaction stroke in progress. After a short period, the flows are switched between the two beds (Period 2, Figure 1.1). The mode can be counter-current or co-current. Cockcroft[10] showed that for the styrene RCR the mode of flow makes very little difference to the conversion (less than 0.3%). After a number of cycles, the temperature profiles along the reactor length at a given time during any cycle are the same for successive cycles. Cyclic steady state is then said to have been reached.

The duration of each cycle determines the conversion obtained. The longer the duration of any cycle, the closer the approach to steady

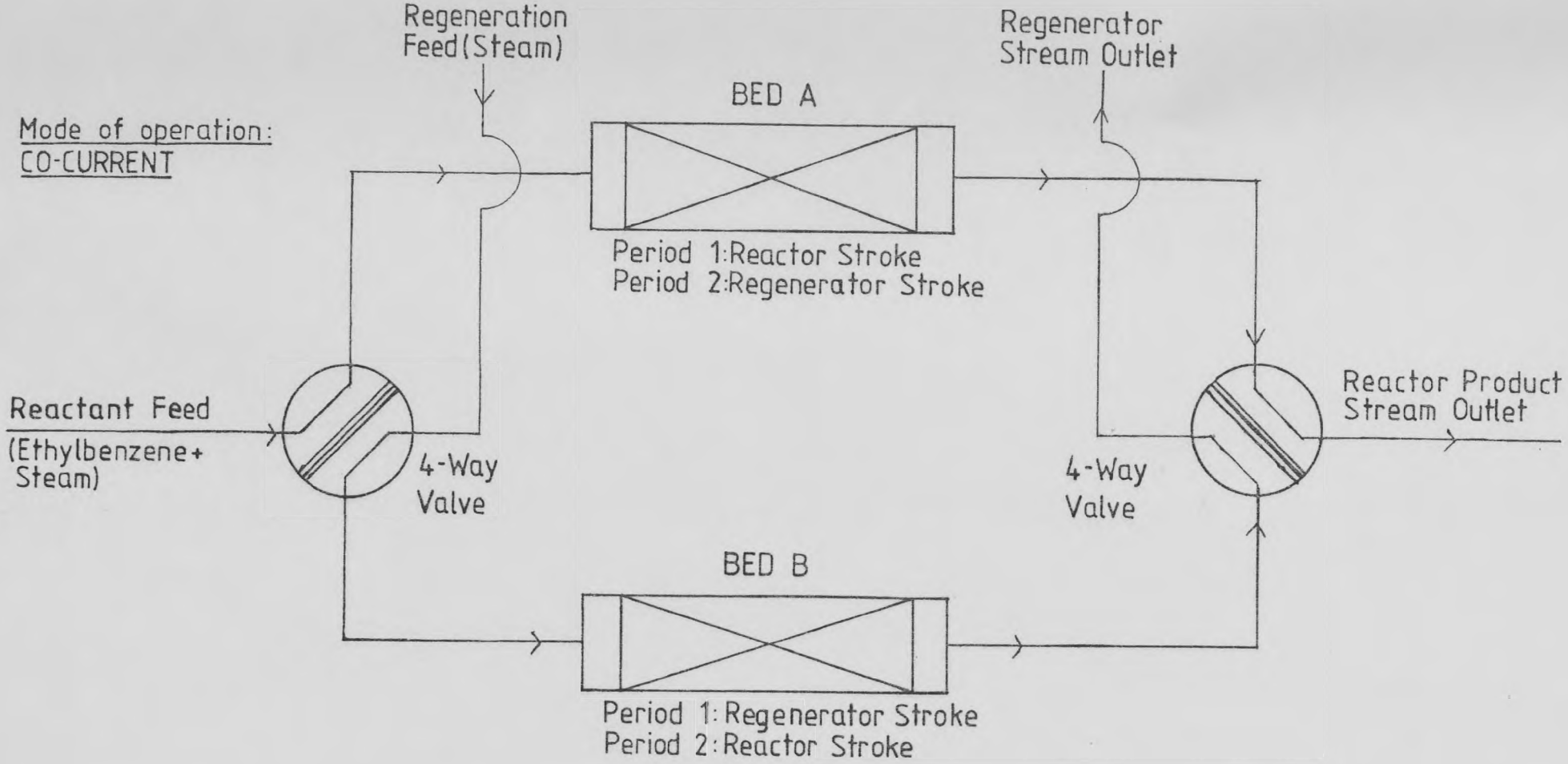

FIGURE 1.1: A Simple Regenerative Cyclic Reactor (RCR) System

state. In addition, the rate of heat transfer falls as the temperature of the catalyst and hot phase approach each other. Therefore, a short period is desirable to obtain high average conversions and high rates of heat transfer. Cockcroft[10] showed that an increase in bed heat capacity has similar effects to that of a reduction in period. Therefore, the introduction of an inert packing along the reactor length can allow the RCR system periods of operation for a fixed conversion to be varied.

The fall in overall conversion through the transient state to the eventual steady state operation is therefore the first subject to be investigated as it determines the cycle duration for the RCR.

Further details of Cockcroft's work can be found in Appendix A9, as well as References (10 - 13), whilst Schmidt and Willmott[44] present a detailed study of the properties and mechanisms of the regenerator.

1.3 The Conventional Industrial Styrene Reactors

The only major means of styrene production today is by the dehydrogenation of ethylbenzene in the presence of steam[15,16,17,20,21,22,23]. The oxidative dehydrogenation using oxygen or air is under investigation[18,19] but the rapid deactivation of the platinum catalysts makes it an uneconomical proposition at the present time. Monsanto[22] have recently developed a system operating under vacuum, but maintaining the steam/ethylbenzene adiabatic process. Literature on this is very scarce. However, the majority of the commercial systems still utilize either the SSAR (one bed or two bed) or the steady state multitubular reactors, operated at above atmospheric pressure.

1.3.1 Steady state adiabatic reactors (SSAR)

The major styrene producers, e.g. Dow[16,20], UOP[14,24], Monsanto[21] and B.P., and contractors, e.g. Badger[24], Lummus[24] etc. employ the two stage (Figure 1.2) or single stage steady state adiabatic catalyst

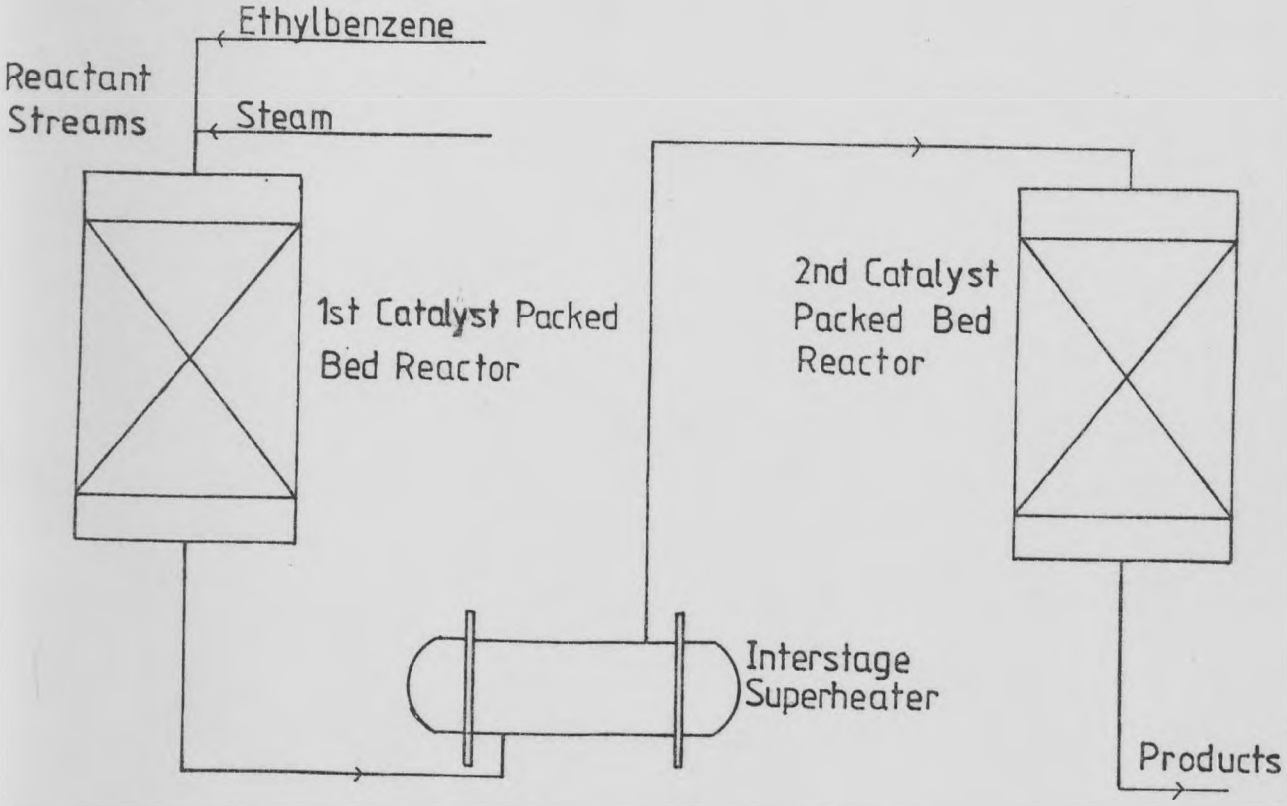

FIGURE 1.2: A Simple Two Bed Steady State Adiabatic Reactor System (SSAR)

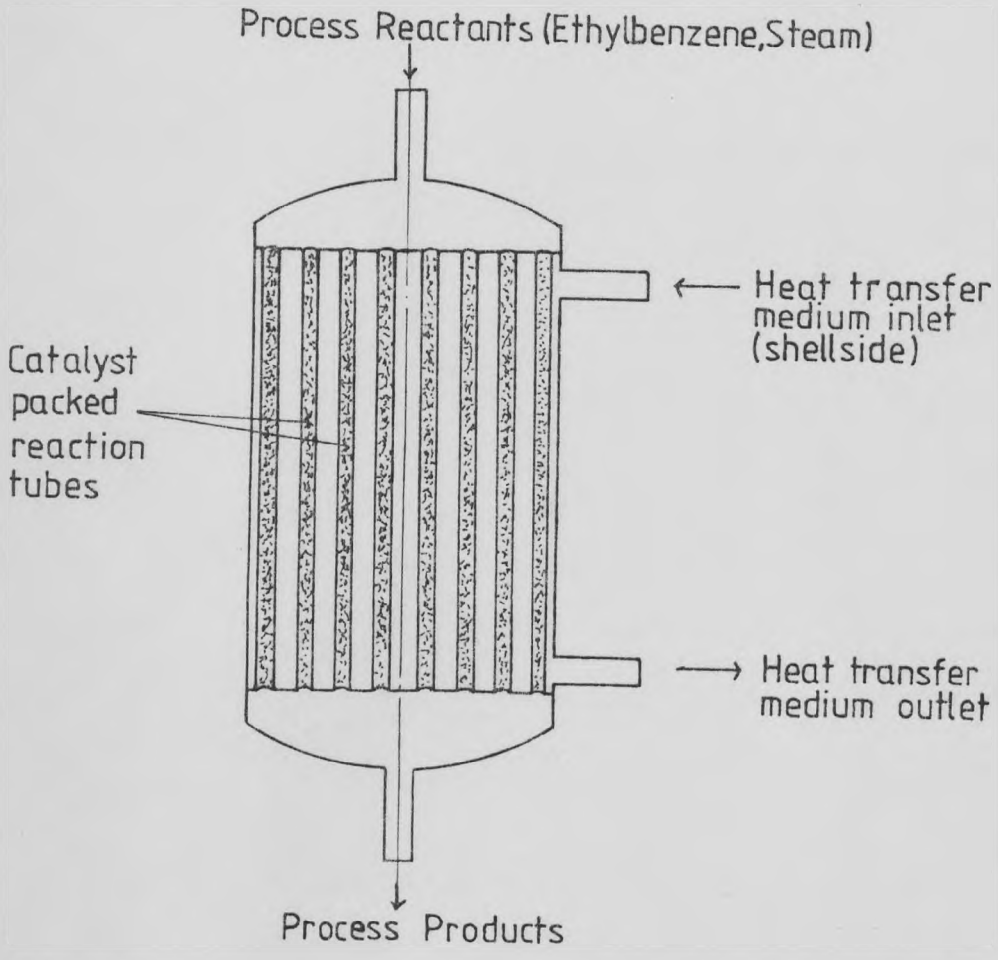

FIGURE 1.3: A Simple Multitubular Reactor

packed bed reactor system. The design of such systems is geared towards minimizing reactor size, thus simplifying design and parameter control. Hence operation has to be at the highest allowable inlet temperature to obtain the maximum possible conversion for a fixed bed size. For reversible reactions, the equilibrium conversion represents the maximum attainable level. To achieve this an infinitely long bed would be required. Thus the industrial reactors tend to be inefficient allowing room for great improvement. For both exothermic and endothermic reactions, the heat of reaction opposes the achievement of higher conversions, and the temperature profiles along the bed drive against the equilibrium situation. This results in falling equilibrium conversion along the reactor, reducing the driving force available. The two stage SSAR (Figure 1.2) uses an interstage heater to obtain more favourable reaction conditions for the endothermic styrene reaction[20,21]. As the RCR also employed two beds, the changeover to a commercial RCR does not necessitate the need for new reactors.

Cockcroft[10,11] showed through his modelling studies that a two stage SSAR operating at a bed inlet temperature of 650^{o}C would produce a conversion of 63.7% whilst a RCR system under similar operating conditions would give a conversion of 67.7%, an overall conversion improvement of 6.3%. Section 2.1.4 further examines this work. The SSAR system is the industrial reactor type that is most relevant to this study.

1.3.2 Multitubular reactors

Only BASF[23] use these for styrene manufacture. These reactors transfer heat through the reactor tubes to enable more favourable conversions to result through higher reactor temperatures along the bed (Figure 1.3). The complex construction makes such reactors costly. The complex heat transfer mechanisms make these reactors difficult to model and control. The lack of adequate temperature control also causes peaks and troughs in

the zones of the greatest reaction rate. The heat flux also sets up radial temperature gradients. This causes large variations in the rate across the tube, especially if side reactions are significant.

1.3.3 The isothermal ideal

This is difficult to obtain due to the varying temperature profiles, and the difficulty in controlling and compensating for the large and varying reaction heat flux along the bed due to the highly endothermic nature of the dehydrogenation reaction.

The RCR uses the relatively simple construction of the adiabatic reactors, and together with the bed temperature profile control provided by the regenerator cycle, it enables some approach to be made towards obtaining the maximum isothermal conversion without the difficulties in temperature control of the multitubular reactors.

1.4 The Research Programme

The aim of this study is to develop a pilot plant that would enable studies to be carried out on the RCR system as well as the SSAR system, using the styrene manufacture as the desired process reaction.

The project will include the design, safety and hazard precautions, the fabrication, construction, instrumentation and the commissioning of the pilot plant. Since only electrical heating capacity is to be used, novel radiation superheaters will be used to achieve the high temperatures. The commissioning will include the compensation for the relatively high heat losses expected, and will consider various methods of maintaining the high temperature levels of the system (up to 750^{o}C).

After successful commissioning, a series of steady state and transient runs of varying duration will be performed at various temperature levels. The steady state runs will be compared with the predictions of Cockcroft[10] using his reactor models that utilize the most reliable set

of steady state kinetics available in literature. The conversion to styrene will be the main criterion for the comparison .

The transient experiments will be directly compared with the corresponding steady state ones, as well as the model predictions of Cockcroft[10]. His transient models are based on steady state kinetics and this study should provide comment and discussion on the viability of using such kinetics to describe the transient reaction process.

The achievement of these objectives would then confirm the viability of the RCR system and make way for further and extensive research to be carried out, and various guidelines will be presented as an initial direction for such studies.

CHAPTER 2

THE DEHYDROGENATION REACTION AND THE DEVELOPMENT OF THE EXPERIMENTAL APPARATUS FLOWSHEET

CHAPTER 2

THE DEHYDROGENATION REACTION AND THE DEVELOPMENT OF THE EXPERIMENTAL APPARATUS FLOWSHEET

Introduction

A summary of the reaction conditions, kinetics and industrial performance is presented. A brief section also deals with Cockcroft's[10] simulation studies and conclusions which form the basis and starting point for this experimental study. An initial layout and working of the experimental rig is outlined. After safety considerations and modifications, a new layout is described. Various other safety measures to be taken are also mentioned.

2.1 The Dehydrogenation Reaction

The dehydrogenation reaction chosen to illustrate the proposed reactor system is the only commercial process used for the production of styrene[15-17], although the catalytic oxidation of ethylbenzene has also been proposed[18,19].

This reaction:

$$C_6H_5\ CH_2 - CH_3 \rightleftharpoons C_6H_5\ CH = CH_2 + H_2 \qquad (2.1)$$

is reversible, endothermic and accompanied by an increase in volume. Hence a high equilibrium conversion is favoured by a high reaction temperature and a low ethylbenzene partial pressure. The low partial pressure is achieved by the usage of steam, within a molar steam/ethylbenzene ratio range of 12 - 20 for an adiabatic reactor system, and 6 - 10 for an isothermal reactor system. The use of steam removes the need for expensive vacuum technology and the possibility of any formation of explosive air/organic mixtures in the event of small leaks.

A large number of side reactions have been proposed[25,26] but only five are supported by experimental work[25] and the two most important ethylbenzene consuming side reactions are those producing benzene and toluene.

$$C_6H_5C_2H_5 \longrightarrow C_6H_6 + C_2H_4 \qquad (2.2)$$

$$C_6H_5C_2H_5 + H_2 \rightarrow C_6H_5\,CH_3 + CH_4 \qquad (2.3)$$

These reactions are considered to be irreversible[27] at the normal operating conditions.

The only other side reactions that Sheel and Crowe[25] observed to any significance, in an industrial system are:

$$C_2H_4 + 2H_2O \longrightarrow 2CO + 4H_2 \qquad (2.4)$$

$$CH_4 + H_2O \longrightarrow CO + 3H_2 \qquad (2.5)$$

$$CO + H_2O \longrightarrow CO_2 + H_2 \qquad (2.6)$$

The dehydrogenation catalyst consists mainly of Fe_2O_3 with 2 - 5% chromia, and small amounts of other metallic oxides and alkali salts are bonded. These trace compounds vary between manufacturers[24]. The alkali salts promote the reaction:

$$C + 2H_2O \longrightarrow CO + 2H_2 \qquad (2.7)$$

minimising the problem of carbon deposition, and eliminating the need for catalyst regeneration.

2.1.1 System temperature limitations

(i) The catalyst tends to sinter if the bed temperatures exceed 660°C[24,36].

(ii) The pyrolysis of ethylbenzene becomes greatly significant after 540°C. Hence superheated steam is required to raise the reactant mixture to around 650°C, the highest bed entry temperature used in industrial systems. The presence of steam suppresses the pyrolysis until temperatures in excess of 650°C[28].

2.1.2 Reaction kinetics

Cockcroft[10] carried out a detailed investigation into the kinetics available in literature. Those of Sheel and Crowe[25], Davidson and Shah[26,34], Wenner and Dybdal[27], Abel et al[29], Modell[30], Eckert et al[31] and Carra and Forni[32] were examined in detail. Only the rate expression by Carra and Forni for the major styrene reaction 2.1 was found to be satisfactorily derived and predicted the expected behaviour as far as conversion, efficiency, temperature behaviour are concerned.

For the benzene and toluene producing reactions 2.2 and 2.3, Cockcroft derived rate expressions from the experimental data of Bogdanova et al[33]. With no further data available, Cockcroft had to use the rate expressions of Sheel and Crowe[25] for the gaseous reactions 2.4 - 2.6. This set forms the so called 'derived kinetics' that Cockcroft used in his modelling studies. Nevertheless, the data of Bogdanova[33] is subject to uncertainties as to the reactor inlet conditions[10]. This necessitates the need to carry out some steady state runs to examine all the kinetics published in order to obtain reliable steady state results for direct comparison with the transient results. Appendix A6 contains the 'derived kinetics' expressions of Cockcroft.

2.1.3 Industrial reactor performance

The following are the definitions of the terms used to define commercial systems:

$$\text{Conversion of Component A} = \frac{\text{moles of A produced}}{\text{moles of ethylbenzene passed}}$$

$$\text{Efficiency} = \frac{\text{moles of styrene produced}}{\text{moles of ethylbenzene consumed}}$$

If the term 'conversion' is not referred to any particular component, it will infer as conversion to styrene.

(i) Single bed adiabatic reactors (see Figure 2.1)

These operate with inlet temperatures of around 600 - 650°C and inlet pressure of 1.3 - 1.8 bar with a molar steam/ethylbenzene ratio of around 15[17,20,25]. The steam provides the heat of reaction, and the temperature falls along the bed giving an outlet temperature of 550 - 600°C. The conversion is 35 - 40% with an efficiency of 87 - 89%. The low conversion leads to a large ethylbenzene recycle, and hence recently the move towards two stage adiabatic systems.

(ii) Two stage adiabatic reactors (see Figure 2.2)

Interstage heating is used to raise the second bed inlet temperature to a maximum of 630°C. To overcome the extra pressure drop, the inlet pressure to the first reactor is generally around 3 bar, and the two stage conversion emerges around 55 - 63%[20,21,24]. The higher pressure and conversion together with the pyrolysis at the interstage heater results in lower efficiencies (84 - 86%) than that of a single bed reactor[24]. Multibed reactors of more than two

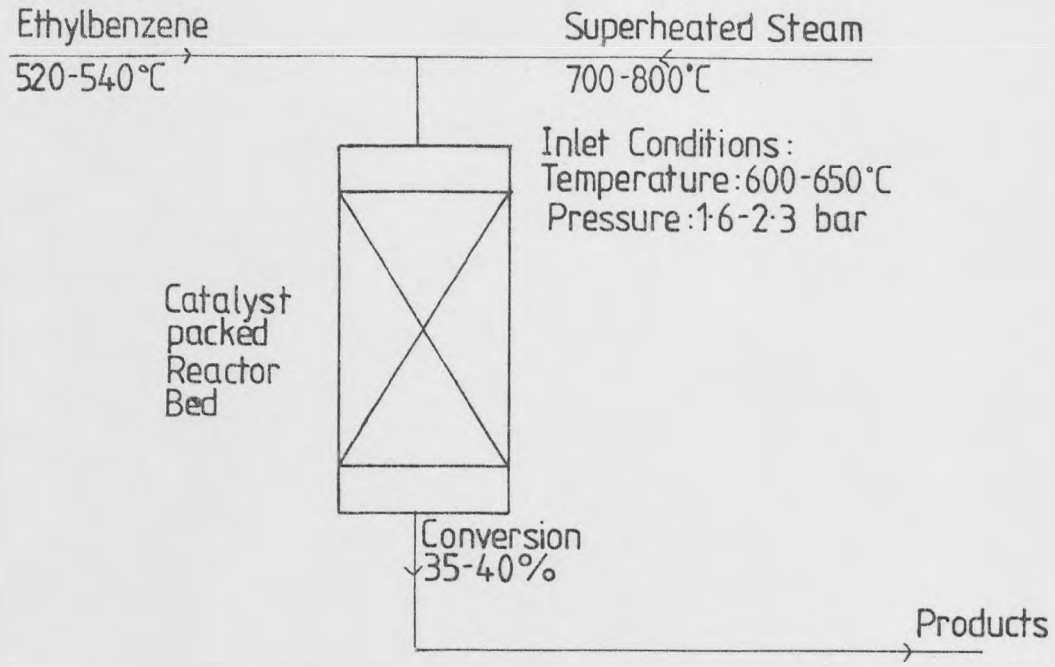

FIGURE 2.1: The Styrene Manufacture One Bed SSAR

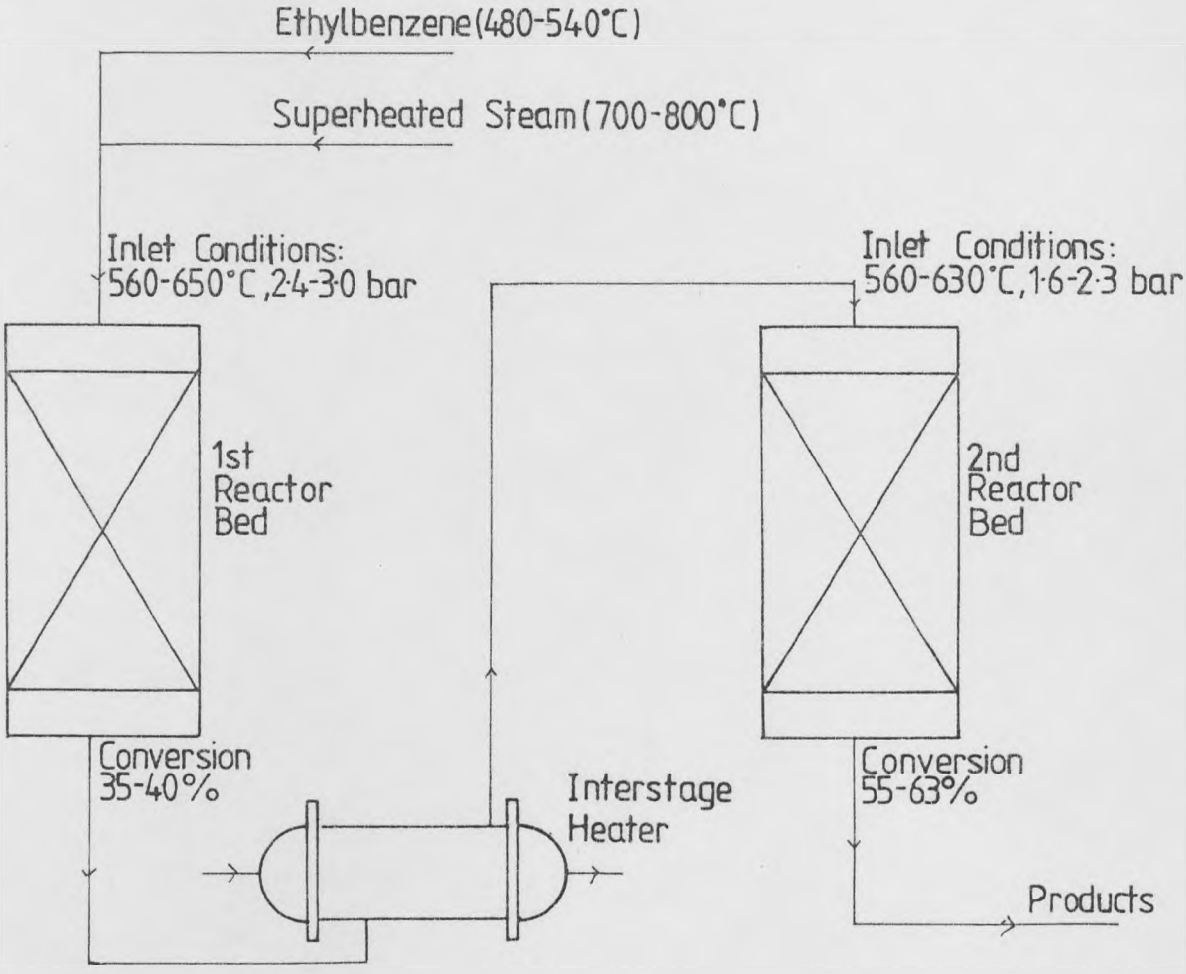

FIGURE 2.2: The Styrene Manufacture Two Bed SSAR

units are extremely rare due to the high capital costs.

(iii) Externally heated tubular reactors (see Figure 2.3)

BASF operate these with a conversion of 40% and an efficiency of around 90%[23]. Since the steam does not supply the reaction heat, so the molar steam/ethylbenzene ratio used is only around 6. The temperature rises from 580°C at the reactor inlet to 610°C at the exit[35]. The cost of the reactor and the associated heat transfer equipment is high and so the adiabatic systems are preferred. The conversions in all three reactor types are some way from those of an isothermal system, and Cockcroft's studies showed that considerable improvements are possible using the RCR and precise figures for this are in the next section.

2.1.4 Scope for improvement of the RCR on the SSAR

In literature, the maximum conversion quoted for the two stage SSAR is 63.7% with an efficiency of 85.7%. Cockcroft[10] showed that the maximum conversion of the cyclic system is the isothermal steady state value, this being 72% for this pilot plant. Thus the conversion range of the RCR is 64 - 72%. Cockcroft obtained the average conversion for the RCR as being 67.7% using the same steam/ethylbenzene ratio and catalyst volume, with the improved efficiency of 88.6%. The period time of the RCR governs the average RCR conversion and this has to be further investigated. Cockcroft also showed that the RCR can operate with lower steam/ethylbenzene ratios with only a small drop in conversion this is an added advantage since the steam cost is the crucial economic factor for this system. Precise figures are not available for this study.

Cockcroft's study is conclusive enough for an experimental study on the transient behaviour of the RCR to be carried out.

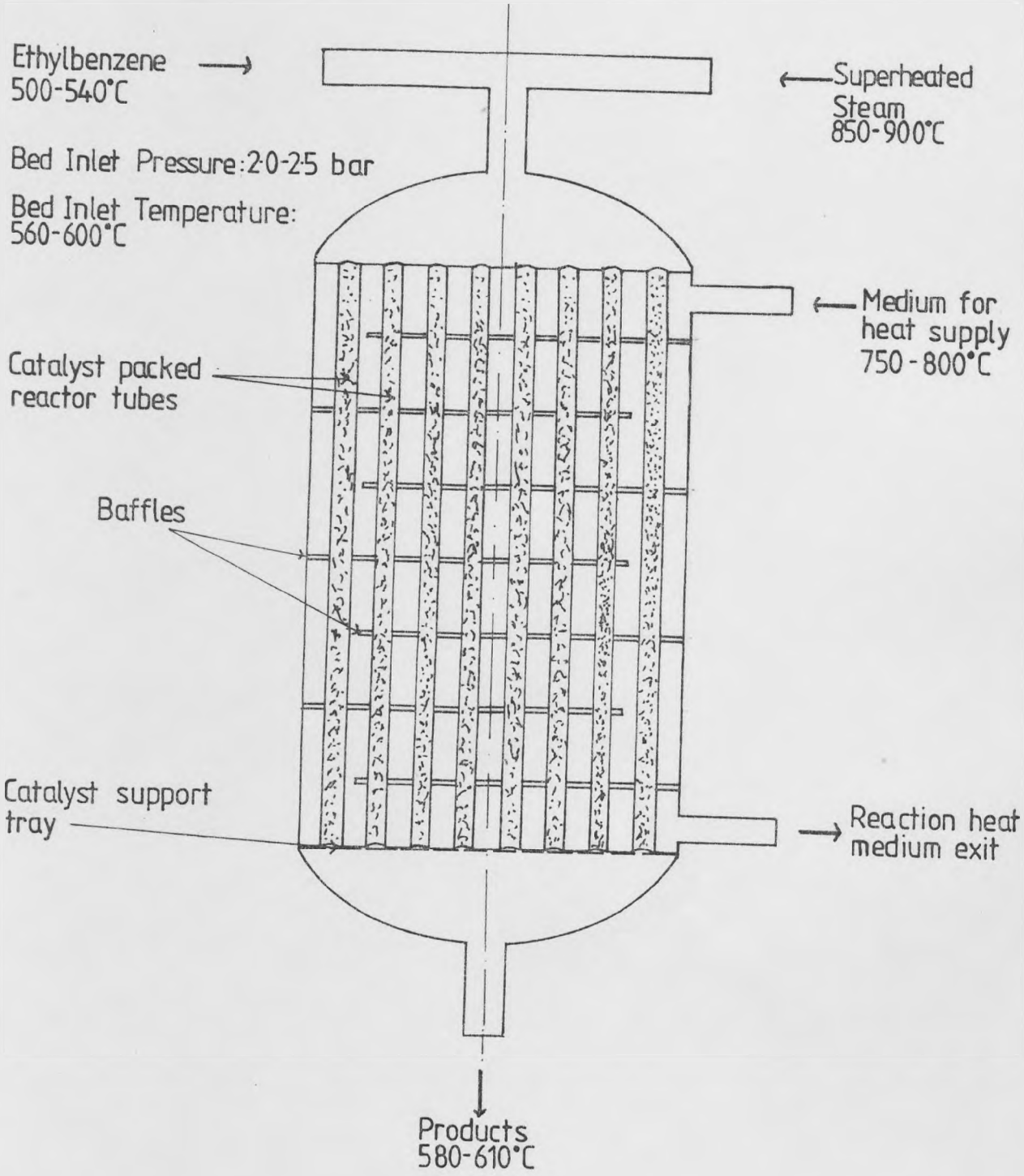

FIGURE 2.3: A Multitubular Reactor for Styrene Manufacture

2.2 Initial Flowsheet of the Experimental Apparatus

The first flowsheet of the system aims to:-

(i) accommodate the two stage SSAR with the RCR, together with the ethylbenzene feed, the steam feed, and the preheating gas lines, and

(ii) eliminate the recycle, due to the difficulty in operating steam ejectors that function well at such high temperatures, and such low loads, and also avoid the purchase of expensive, high temperature on-off ball valves.

The layout of the system is thus restricted to the co-current set-up of the RCR, with the switching of the flows carried out at relatively low temperatures by standard solenoid valves.

Figure 2.4 shows the flowsheet of the initial layout of the experimental rig. The system can investigate the one stage SSAR, the two stage SSAR and the co-current RCR, as well as the transient adiabatic reactor.

2.2.1 The description of the working of the apparatus

The reactors, the connecting pipework and all associated equipment are preheated by air, as a supply of inert gas is not available in the laboratory. The preheating is necessary to avoid any condensed steam in the system that can poison the catalyst. The manufacturers (e.g. Shell, Girdler) recommend preheating of the catalyst to 350 - 400^{o}C before switching to steam. They also advise against the use of air above 500^{o}C during heating or cooling[36]. The heating duty is carried out by the two steam superheaters (SSH1 and SSH2) on the main steam feed line, SL1, and by the ethylbenzene superheater (EBSH) on the hydrocarbon feed line, SL2.

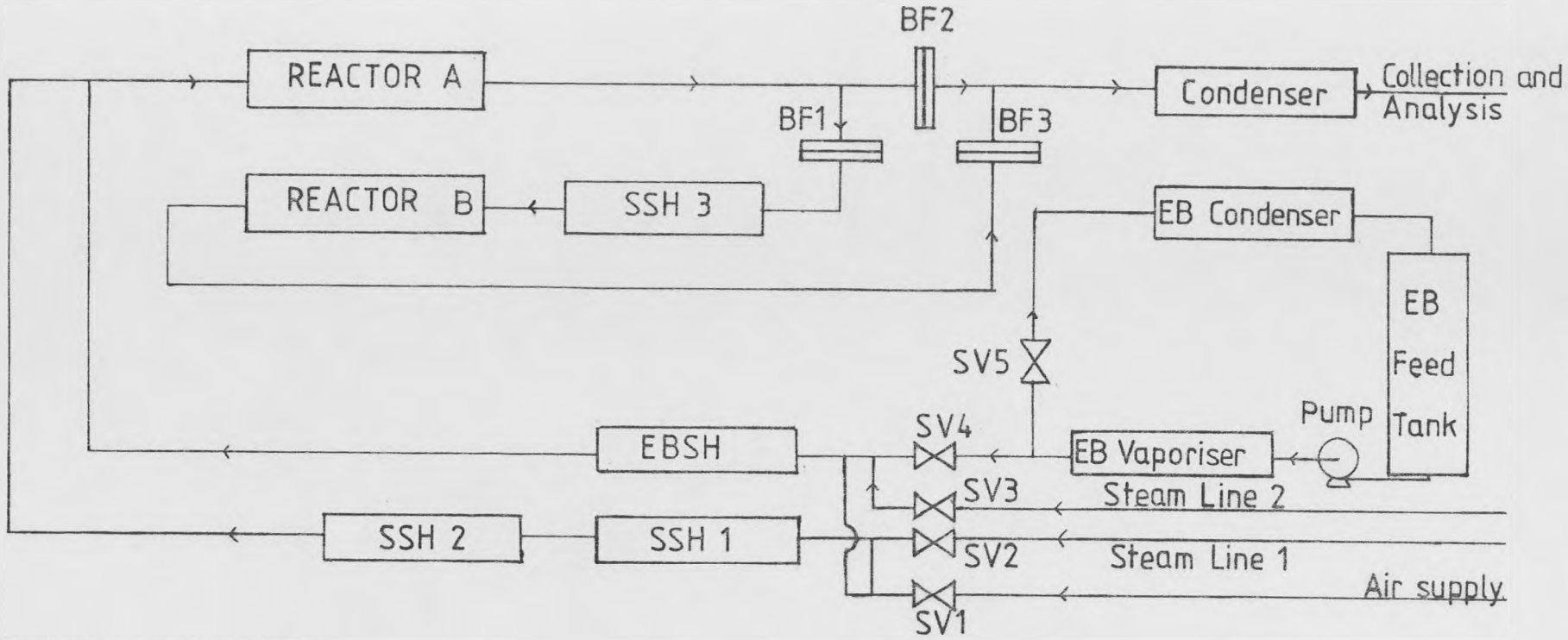

BLANK FLANGE ARRANGEMENT

Two bed SSAR system: BF1, BF3 open, BF2 closed

One bed SSAR, RCR systems: BF2 open, BF1, BF3 closed

SOLENOID VALVE SWITCHING

Air preheating: SV1 open, rest closed

Steam heating: SV2, SV3 open, rest closed

SSAR run, RCR reaction period: SV2, SV4 open, rest closed

RCR regeneration period: SV2, SV3, SV5 open, SV1, SV4 closed

BF - Blank flange
EB - Ethylbenzene
SSH - Steam superheater
EBSH - Ethylbenzene superheater
SV - Solenoid valve

FIGURE 2.4: Flowsheet of the Proposed Experimental Apparatus

The laboratory steam supply (supply pressure 90 psig, 7.12 bar) is throttled to the required pressure and heated by the superheater SSH1 and SSH2 on the main steam line (SL1) and by EBSH on the hydrocarbon line (SL2). The steam line SL2 is designed to supply the hydrocarbon line with a quantity of steam equal in heat capacity to the ethylbenzene so as to keep the EBSH at the required temperature when the reaction is not in progress. This heat capacity also enables the pipework and the reactor beds to maintain their temperature profiles.

Two reactors, A and B, are connected by an interstage superheater (SSH3) and a series of blank flanges which can be opened, thereby determining which reactor system is operating. This is described in detail later in this section.

The ethylbenzene is stored in the feedtank and is pumped by a precision metering pump, through the vaporiser, and on to EBSH and the reactors, or alternatively back to the feedtank via a condenser (EBC). The various modes of operation are described later.

The products from the reactor system are cooled and then condensed by the main system condenser (MC) and carried to the various sampling tanks and collection equipment via a gas-liquid separator. The air can be exhausted at the top of the dual coiled main condenser.

2.2.2 Description of the various reactor arrangements

The following reactor set-ups all assume that the reactor system concerned has been preheated to the desired temperatures, initially by air, and after 400°C, by steam. Solenoid valves SV1, SV2 and SV3 control the flow of air or steam to the superheater and the reactors (refer to Figure 2.4 for all arrangements).

(i) The one stage SSAR

Flanges open: BF2 Flanges closed BF1, BF3

Solenoid valves open: SV2, SV4 Solenoid valves closed: SV1, SV3 and SV5

The steam feed is superheated to around 750°C by SSH1 and SSH2, and mixes with the ethylbenzene that has been vaporised by the vaporiser EBV, and superheated by EBSH to around 540°C, and the mixture passed through Reactor A. The product steam by-passes Reactor B and SSH3 on its way to the main condenser and collection.

(ii) The one bed transient reactor

The set-up is identical to the one bed SSAR, except that the ethylbenzene is only passed for the limited period, unlike the SSAR where the hydrocarbon is passed until steady state is achieved. At the end of the transient run, solenoid valves SV4 and SV3 reverse their state to stop the run.

(iii) The two stage SSAR

Flanges open: BF1, BF3 Flanges closed: BF2

Solenoid valves open: SV2, SV4 Solenoid valves closed: SV1, SV3 and SV5

The emerging product from the first reaction is passed through the interstage superheater SSH3, and becomes the feed for Reactor B, before being directed to the main condenser and the collection equipment.

(iv) The RCR

Due to the symmetry of the RCR, only one bed need be investigated. There are two stages in the RCR:

(a) The regenerative (heating) cycle

Flanges open: BF2 Flanges closed: BF1, BF3

Solenoid valves open: SV2, SV3, SV5 Solenoid valves closed: SV1, SV4

The feed steam on SL1 is heated to 750°C and mixed with the make up steam on SL2, that is heated to 540°C. When the required temperature profile has been obtained across the bed, the reacting cycle can be carried out. Solenoid valves SV3, SV4 and SV5 are switched manually, controlling the cycle in progress.

(b) The reacting (cooling) cycle

Flanges open: BF2 Flanges closed: BF1, BF3

Solenoid valves open: SV2, SV4 Solenoid valves closed: SV1, SV3, SV5

The feed steam and the feed ethylbenzene mix and pass onto Reactor A, as per the one stage SSAR, but only for the duration of the cyclic period. At the end of the reacting cycle, the solenoid valves switch back to the regenerative cycle, and the ethylbenzene is returned to the feed tank via the condenser, EBC. The metering pump can easily adjust to the change in the delivery head, without alteration to the flowrate.

The switching of the cycles can be carried out until cyclic steady state is achieved. Composite samples can be taken by the diversion of the product stream to the sampling tanks.

Attention must now be paid to the safety and the elimination of any hazards. This inevitably will result in the changing of the initial flowsheet and layout.

2.3 Safety and Hazard Considerations

The safety measures that will be taken will try to conform to the relevant British Standards, within the financial limitations on this project

bearing in mind that some of the British Standards have been specially prepared for large commercial systems. The relevant British Standards for this project are:-

BS 4137[37] for electrical wiring and circuits

BS 229[40] for flameproof enclosures

BS 889[39] for electrical lighting and power supply

BS 1259[38] for intrinsically safe electrical apparatus.

In addition to the above, certain recommendations of Riddlestone[41] and the National Fire Protection Association[42] have also been implemented.

Adequate safety measures need to be taken against:

(i) overpressure in the steam lines;

(ii) vapour accumulation in the room, e.g. from leaks and collecting tanks;

(iii) fire and ignition catalysts around the system, e.g. electric sparks, arcs etc.;

(iv) hydrocarbon vapour or liquid contacting hot air from the preheating of the rig to provide ignition conditions.

The provision of steam pressure relief valves is vital. So is the need of high capacity fan extractors for each room. Of course, these extractors require flameproof enclosures, as would the metering pump, the 240 V switch boxes, fuse boxes and distribution boxes. The solenoid valves are operated off 24 V D.C. to provide intrinsically safe circuits[38]. The spark produced here would be incapable of triggering ignition.

Vapour accumulation can be reduced by providing adequate turbulence around the system, as well as by reducing the chance of air to hydrocarbon contact. This is aided here by the presence of the steam which would shroud the organic. The molar steam/organic ratio of 14:1 reduces the chances of the pure organic contacting sufficient oxygen to produce the right mixture for combustion.

The use of the correct seals and gaskets is vital, and so is the pressure testing to eliminate any chance of leakages. The most vulnerable lines are the pure hydrocarbon lines, and protection of this is difficult. This necessitates the provision of an enclosure for the ethylbenzene superheating, and product sampling collecting equipment, so as to protect the rest of the rig from the most vulnerable lines.

2.4 Modifications and Precautions Taken After Consideration to Safety

(i) Isolation of all pure hydrocarbon lines, and all sampling lines:

This is done by housing the full ethylbenzene vaporising and condensing cycle, as well as the main system condenser and sampling equipment in an external room, built on the roof and outside the main laboratory. The external room is equipped with air extractors and air and gas exhaust lines to the atmosphere. Figure 2.5 shows the new flowsheet and the layout of the experimental rig for both the external and control rooms.

(ii) Blanketing of hydrocarbon containers with nitrogen:

This prevents the accumulation of organic vapours in near-empty tanks. The ethylbenzene feedtank and all the sampling and collection tanks will all be blanketed with low pressure nitrogen (1.35 bar, 5 psig).

(iii) Provision of air extractors:

Both the control and the external rooms will each have a 'PMA6' air extractor, flameproofed with a clearance rate of 10.5 m^3/min, enough to clear the control room volume every three minutes.

(iv) The provision of gas-tight enclosures for all switches, switch boxes, distribution and fuse boxes certified by the Yorkshire Electricity Board, as well as ensuring flameproof standard for the metering pump, air extractor, moving coil instruments and the 'Panic Button' enclosures.

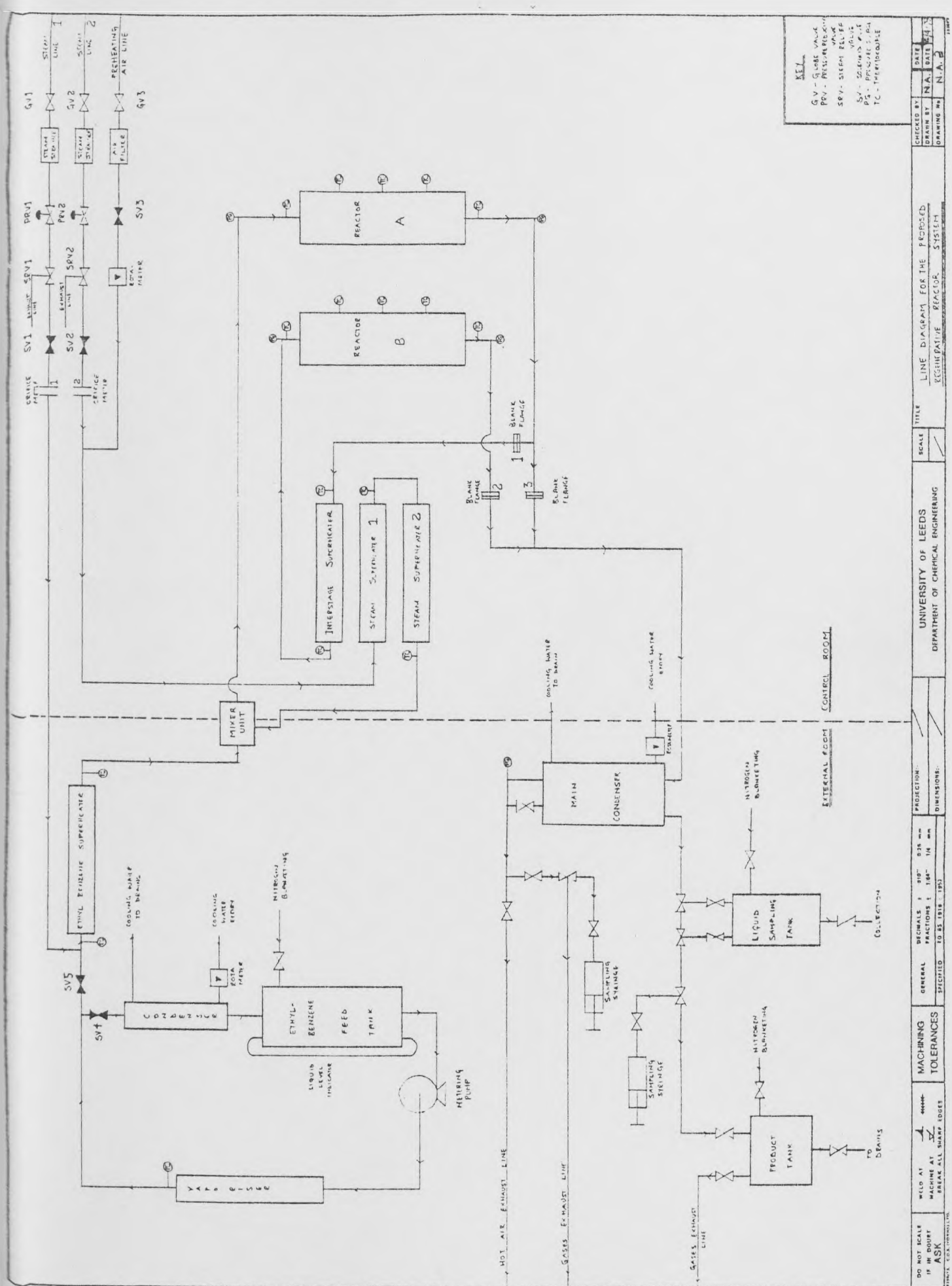

FIGURE 2.5: Apparatus Flowsheet After Modifications for Safety

(v) The solenoid valves are run off 24 V D.C., providing an intrinsically safe circuit. The steam line solenoid valves are reverse acting, i.e. open when de-energised so as to shroud the system with steam in case of power failure.

(vi) The preheating air line exhaust is isolated at the top of the main condenser, avoiding the contact of hot air with any organic vapour.

(vii) All power controllers are thyristor-fired controllers, housed in gasket sealed enclosures. The controllers are also provided with a heat sink to reduce the chances of overheating during operation.

(viii) A 'Panic Button' is provided at the entry of the control room to cut off the power to all circuits in case of an emergency.

The gas product lines are exhausted to the atmosphere since they contain very small amounts of combustible gases.

With the layout of the plant finalised, the detailed design can be carried out and the actual construction of the experimental apparatus can commence upon fabrication of the individual items.

CHAPTER 3

DESIGN, CONSTRUCTION AND INSTRUMENTATION OF THE STYRENE EXPERIMENTAL APPARATUS

CHAPTER 3

DESIGN, CONSTRUCTION AND INSTRUMENTATION OF THE STYRENE EXPERIMENTAL APPARATUS

Introduction

Full mass and heat balances are carried out for the experimental rig using the six major reactions. All the major equipment is designed, e.g. the reactors, condensers, superheaters etc. Figure 2.4 shows the major equipment that needs designing. The correct instrumentation for the flow measurements are selected for the air, steam and ethylbenzene lines. All the pipework is correctly sized with the aim of minimising the pressure drop, at the same time avoiding laminar flow in the major feed lines (Re > 6,000). The temperature measurement instrumentation is carefully checked for the range of error in the readings that would be indicated before the chosen method is implemented. The pressure and electrical instrumentation is also carefully selected with great emphasis on safety. Finally, the apparatus is constructed along the lines of the layout flowsheets produced (Appendix A1). The apparatus commissioning can then begin.

3.1 Mass and Heat Balance Modelling for the Apparatus

A typical industrial mass velocity of 16,000 kg/hr m^3 is used as an initial design basis for the pilot plant. Figure 3.1 shows the various flowrates for the major feed lines. The smallest flow that a commercial steam regulator valve can control is about 3.6 kg/hr. Therefore 4.0 kg/hr steam is the smallest flow that will be used on the pilot plant. The ethylbenzene flow on SL2 and the steam flow on SL1 are governed by this flow. The equivalent heat capacity allows 2.95 kg/hr of ethylbenzene (on SL2). Assuming a 14:1::steam:ethylbenzene molar ratio, the steam flowrate

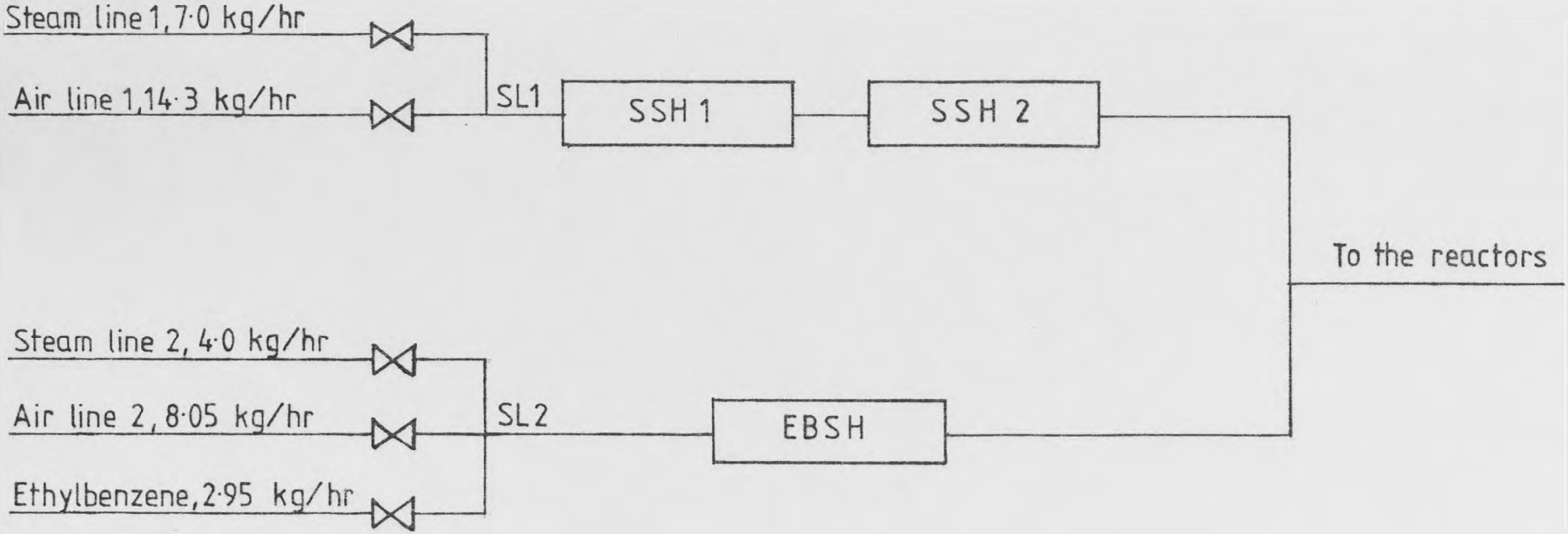

FIGURE 3.1: Design Flowrates for the Experimental Apparatus

on SL1 works out to 7.0 kg/hr. The mass and heat balances are carried out by using the I.C.I. 'Flowpack' program[43]. Cockcroft[13] details the use of this program for a similar system and so only the results are presented here. The program models the six reactions (2.1) to (2.6). Cockcroft[10,13] and Sheel and Crowe[25] reason out that the three ethylbenzene consuming reactions (2.1) - (2.3) can provide a good basis for design. Thus, the modelling can be limited to these reactions. The conversions of Sheel and Crowe[25] are used for the 'Flowpack' models. Table 3.1 shows the expected conversions for the six reactions, for the two stages of the SSAR, and the "best" possible case, i.e. the isothermal maximum. All values are based on data from Sheel and Crowe[25] and various patent claims[24]. Table 3.2 shows the flowrates that can be expected for the conversions stated in Table 3.1. Figure 3.1 shows the design flowrates for the system. The air lines carry an equivalent heat capacity to the steam feeds.

3.2 The Apparatus Piping and Reactor Sizing

The major aim here is to minimise the present losses and avoid laminar flow in the feed lines. An initial estimate of 20 metres of pipe length is made, and an allowance of 1.5 m for the two reactors. The pressure drop across the reactors must not exceed 21.5 kN/m^2 per metres (1 psi per ft), keeping to pressure entry and exit figures in the patents[20-24]. At the same time the pipe pressure drop should not exceed more than 14 kN/m^2 after the reactor section. The use of ½" BSP (1.58 cm I.D.) lines on SL1 (Re = 11657) and SL2 (Re = 6661), and 1" BSP line (2.66 cm I.D.) for the mixed stream (Re = 10879) avoids laminar flow, yet uses pipe sizes for which high temperature and pressure equipment is readily available (min. size ½" BSP, 1.58 cm I.D.). The above pipe sizing would give a maximum pressure drop of 73 kN/m^2 per 100 m of pipe, which is acceptable. The total system piping loss then will not exceed 15 kN/m^2. The reactors need to be of 10.2 cm Ø packed section to achieve a pressure drop of less than 21 kN/m^2

TABLE 3.1

'Flowpack' Conversions for the Six Major Reactions for the Three Reactor Types, all with an Inlet Temperature of 650°C

Reaction Number	ΔH (kJ kg^{-1} mol^{-1})		Fixed Conversion for Flowpack Modelling		
	527°C	627°C	1st Stage: SSAR	2nd Stage: SSAR	Isothermal Stage
2.1	124803	125261	0.4040	0.3090	0.7200
2.2	102782	101984	0.0376	0.0288	0.0671
2.3	- 63932	- 65255	0.0361	0.0276	0.0644
2.4	- 36968	- 35918	0.0046	0.0035	0.0082
2.5	223499	225516	0.0009	0.0007	0.0016
2.6	222692	232856	0.0055	0.0042	0.0098

TABLE 3.2

'Flowpack' Product Flowrate Results for the Three Reactor Types

Component	Emerging Product Flowrate (kg hr^{-1})		
	1st Stage: SSAR	2nd Stage: SSAR	Isothermal Stage
Ethylbenzene	1.53	0.97	0.44
Styrene	1.16	1.63	2.07
Benzene	0.08	0.11	0.15
Toluene	0.09	0.13	0.16
Water	6.90	6.87	6.84
Hydrogen	0.03	0.05	0.06
Ethylene	0.01	0.01	0.01
Methane	0.01	0.01	0.02
Carbon Monoxide	0.01	0.01	0.01
Carbon Dioxide	0.09	0.13	0.17

per metre of packed reactor. The modified Ergun formula by Heggs and Handley[69] is used to calculate the reactor pressure drop (Equation (3.1)):

$$\frac{\Delta P}{L} = \frac{2.63\ (1-e)\ G_M^2}{\rho e^2\ d_p} + \frac{1093\ (1-e)^2\ \mu\ G_M}{\rho e^2\ d_p^2} \qquad (3.1)$$

The catalyst particle size is 3.2 mm Ø by 6.4 mm length cylindrical size. A 10.2 cm (4" BSP) diameter reactor would reduce the channelling of the gases at the ends (d/D > 20, the general minimum figure used). The reactors require expansion and contraction cones. Charts by Simpson[45] show that a divergence angle of 20^o is required to keep a low pressure drop (< 10 kN/m^2 per cone). Figure 3.2 shows the cones and the reactors, all fabricated from Sch. 40 stainless steel 316. The reactors are lined with Kaowool paper[46] 4 mm thick, to reduce the heat transfer from the gas and catalyst to the metal wall. Cockcroft[10] showed that the use of a 2 mm lining reduces the effective heat transfer to the metal wall to a sixth of the value without the lining. The effect of this lining on the conversion is less than 0.2%[10] on the steady state and transient reactors. It does, however, slow the approach to steady state, but this is not a vital factor in this study.

3.3 Steam Line Orifice Assemblies and Heater Designs

The two steam lines have their flowrates measured by orifice meters, with the pressure drop measured by water-on-mercury manometers. Both orifice plates and their assemblies are designed from charts and methods of Spink[47], and conform to the mechanical design requirements of BS 1042[48]. Both plates are designed to give a mercury load of at least 5 cm Hg for the design flowrate, so as to get a good and accurate difference in manometer levels. The mechanical design is that for a D x D assembly[48] and the

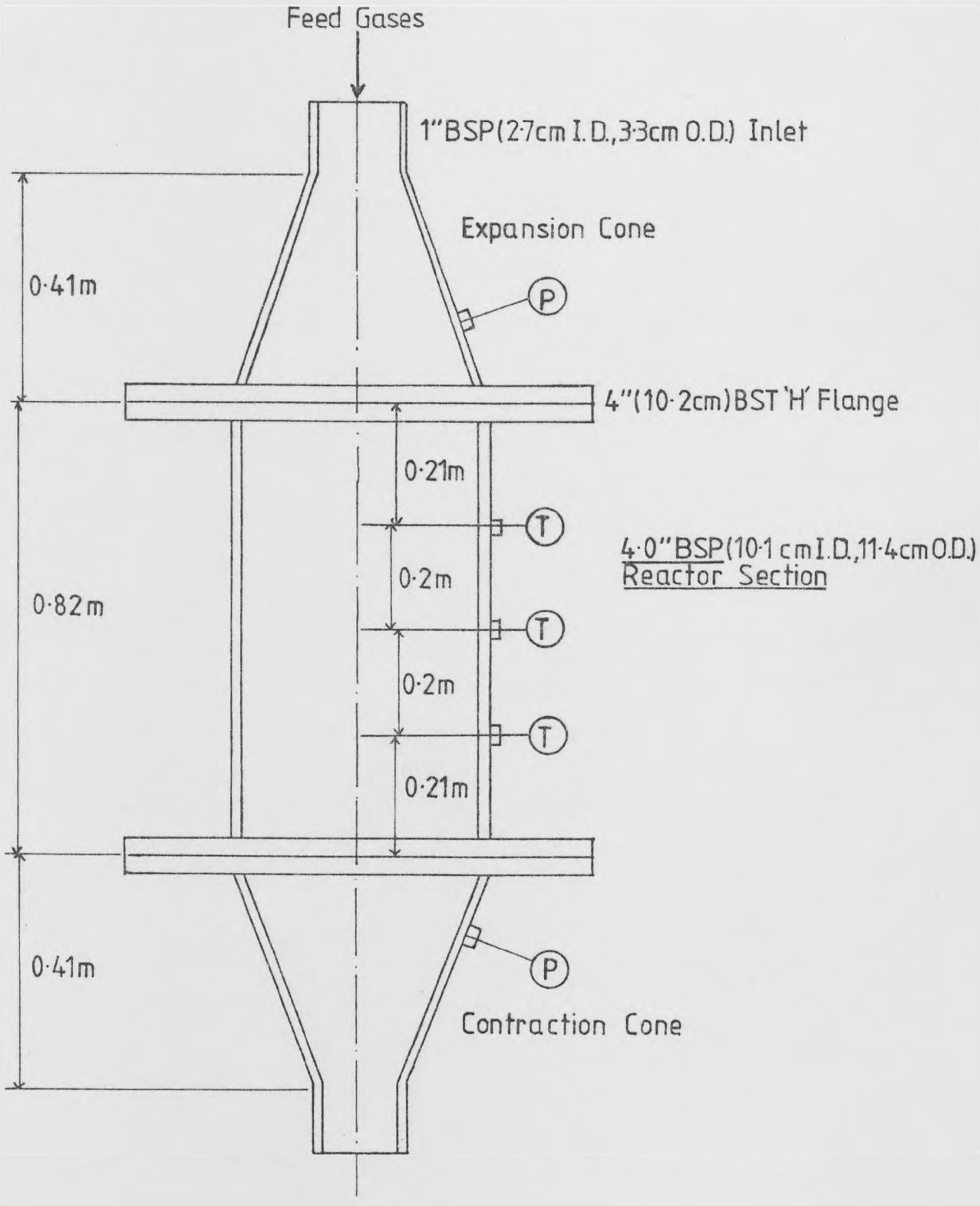

FIGURE 3.2: The Reactor and its Associated Cones

mounting is by a gasket sealed carrier ring arrangement.

Design calculations are based on Spink's[47] formula:

$$S = \frac{8.04 \times 10^{-9} W_m}{359 D^2 F_a F_m F_c Y \sqrt{\gamma_f} \sqrt{h_m}} \qquad (3.2)$$

where $F_a = 1.006$, $F_m = 0.962$ and $F_c = 1.003$ using charts for a mercury/water measuring system. A design factor of 1.15 is allowed on the steam flowrates. Table 3.3 shows the sizing of the two orifice plates. Appendix A3.1 carries a more detailed look at the design procedure, as well as a drawing of the assembly (Figure A3.1).

TABLE 3.3

Orifice Plate Sizes for the Two Steam Lines

Steam Line	Orifice Design Flowrate (kg hr^{-1})	Orifice Diameter (cm)	I.D. of Pipe (cm)
1	7.95	0.452	0.197
2	4.23	0.328	0.197

To prevent steam from condensing in the steam lines prior to entry to the superheater, and affecting the orifice meter pressure drops, both lines are provided with 'Kanthal'[49] A-1 resistance wire heaters, wound from the shut-off valve, over the pressure regulator system, the orifice assemblies, and right up to the entry to the superheaters. Ceramic 'fish' beads provide the electrical insulation of the resistance wire. The electrical design is capable of supplying the power to compensate for the latent heat of vaporisation of design steam flowrate. Table 3.4 indicates the maximum power capacity of these preheaters. Appendix A4 contains the corresponding

electrical circuit diagrams.

TABLE 3.4

Preheater Capacities for the Two Steam Lines

Steam Line	Heater	Resistance (Ω m^{-1})	Total Resistance (Ω)	Maximum Power (Watts)
SL1	SL1W	2.53	50.6	1140.0
SL2	SL2W	5.04	100.8	571.2

3.4 Ethylbenzene Storage, Pumping and Vaporisation

The feed tank can hold enough ethylbenzene for a 10 hr continuous run, i.e. 34 litres. The feedtank is blanketed with nitrogen. The pump is an 'E-2 Metripump'[50] metering pump, capable of delivery up to 104 cc/min against a maximum head of 7.8 bar. The vaporiser is a simple single tube film vaporiser as per the design method by Lord et al[51], using a nucleate boiling calculation. The heat duty required is 1000 watts, and a "Ghlom"[52] resistance wire heater is wound over the 0.5 m length of the vaporiser. The vaporiser has a maximum power capacity of 1500 W, i.e. a resistance of 37.7 Ω. The length of the wire is determined by using the recommendations by Kanthal[49] of not exceeding a surface loading of 6 W/cm^2 on the Ni/Cr alloys that are used in high temperature heaters. A condensate chamber is provided on top of the vaporiser. The vaporiser is of $\frac{3}{8}$" BSP, Sch. 40 (1.71 cm O.D., 1.25 cm I.D.), SS316 piping. The condensate chamber also has a thermocouple entry gland welded on. A full design of the vaporiser can be found in Appendix A3.2, together with a diagram (Figure A3.2).

3.5 Design of the Mixer

The mixer unit aims to achieve complete penetration of the high velocity stream, i.e. the steam from SL1, into the lower velocity stream, i.e. the ethylbenzene or steam from SL2. Figure 3.3 shows the general design aimed for. Two zones exist for which detailed design needs to be carried out:-

(i) The penetration section

The manifold allows circulation of the penetrating gas around the penetration pipe, which has a set of nozzles through which the penetration can occur. Here choked flow has to be maintained, at the same time the penetration medium should be distributed evenly around the penetration pipe. The steam should also penetrate right to the centre of this pipe. Choked flow is designed for as per Kay[53]. For 1.68 bar steam at 750°C, the diameter for choked flow is 0.21 cm. Therefore, the nozzle diameters should not exceed this diameter.

A set of nozzles, varying in diameter from 1/64" (0.04 cm) to 5/64" (0.2 cm) are drilled in rows of ten, and the spread is shown in Figure 3.4. The smaller diameter row is nearest to the penetrating gas inlet so as to provide the greatest resistance to flow, contributing to the spreading of the gas all round the manifold. The largest nozzle diameter is checked for penetration distance from charts by Patrick[54]. Some charts tabulate the distance to which 90% of the flow can penetrate, against varying pressure drives. The penetration is governed by the ratio of the two stream velocities and pressures. For this case, assuming steam against steam, the penetration distance is 3.05 cm, more than adequate for the mixing zone where the centre of the pipe is 0.635 cm from the 0.2 cm nozzles (the largest penetration

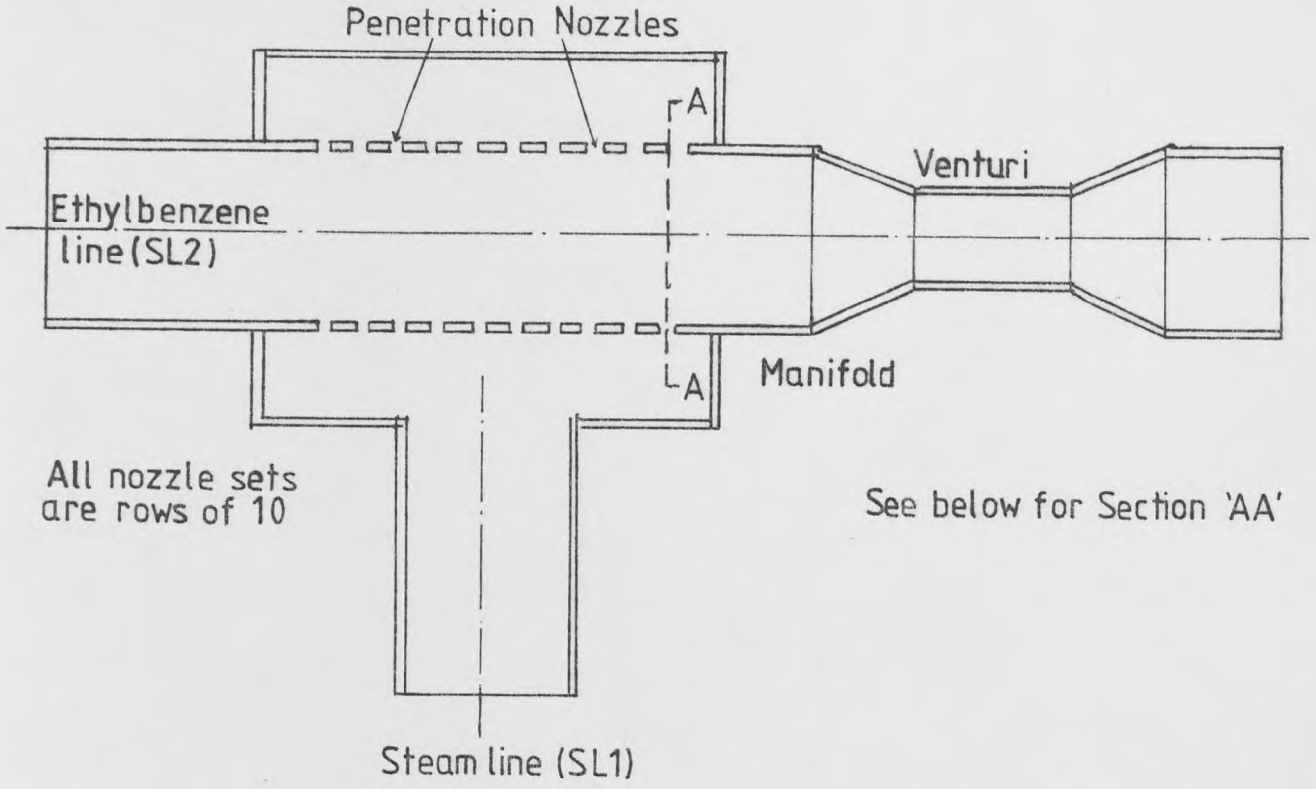

FIGURE 3.3: Basic Design of the Mixer

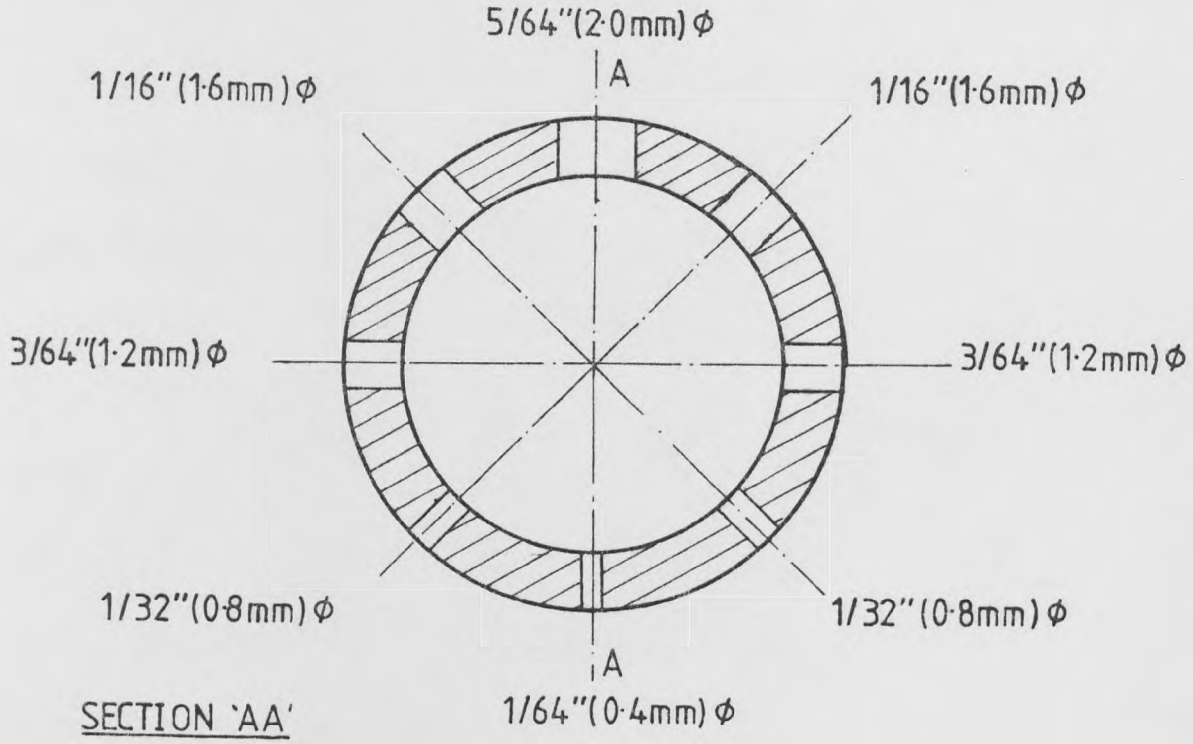

FIGURE 3.4: The Nozzle Sizing for the Penetration Zone of the Mixer

nozzle diameter). A detailed design and a drawing can be found in Appendix A3.3.

(ii) The venturi section

After the penetration section, the venturi further helps the mixing by temporarily increasing the turbulence of the mixed streams (the Reynolds number is doubled over the venturi section).

3.6 System Condenser Designs

3.6.1 Ethylbenzene condenser

This is designed to cool ethylbenzene vapour from 180°C down to ethylbenzene liquid at 20°C, and the design is broken down into three sections:

(i) the desuperheat section;

(ii) the condensation section;

(iii) the subcooling section.

The design is that of a single tube counter-current heat exchanger, with the coolant (water) allowed a rise of 5 centigrade degrees in temperature to perform the duty. A ½" BSP (1.58 cm I.D.) tube enclosed in a 2" BSP (5.25 cm I.D.) coolant shell forms the basic design. The length of the condenser is worked out for each of the three sections mentioned above. Appendix A3.4 contains a detailed design and drawing.

(i) The desuperheat section

The vapour is cooled from 180°C to saturation, at 2 bar, i.e. 164°C. Kreith[55] suggests the correlation:

$$Nu = \frac{h_{DS}\, D_H}{k} = 1.86 \left(Re \,.\, Pr \,.\, \frac{L}{D_H} \right)^{0.33} \left(\frac{\mu_b}{\mu_s} \right)^{0.14} \qquad (3.3)$$

for the evaluation of the heat transfer coefficient for laminar flow (Re = 220).

(ii) The condensation section (at 164°C)

The Colburn et al[56] and Collier[57] detail the design of this section. The simple Nusselt equation for laminar flow (Re = 29):

$$h_c \left(\frac{\mu_f^2}{k^3 \rho^2 g} \right)^{1/3} = 1.47 \left(\frac{4\Gamma}{\mu_f} \right)^{-1/3} \qquad (3.4)$$

is used to work out the heat transfer coefficient for this section.

(iii) The subcooling section

The fluid Reynolds Number (Re = 30) indicates laminar flow. The subcooling heat transfer coefficient h_{SC} is evaluated using Equation (3.3).

Equation (3.3) is also used for evaluating the heat transfer coefficient for the coolant (38.5 kg/hr water, Re = 130).

An iternative calculation is then carried out for each of the three sections to evaluate the condenser length, after evaluating the overall heat transfer coefficient. The final lengths are:

Length of desuperheat section	5.6 cm
Length of cooling section	30.5 cm
Length of subcooling section	4.6 cm

A condenser length of 0.6 m is thus more than sufficient.

3.6.2 The system's main condenser

The method of design is similar to that of the ethylbenzene condenser. However, due to the high duties, the single pass design results in the tube

length being rather long (≃ 6 m). Therefore a coiled design is pursued. Coulson and Richardson[58] indicate that as long as the coil angle does not fall below 15°, no correction factors are required to the standard design for a straight single pass tube condenser. The coil is enclosed in a drum 1.3 m high and 0.3 m diameter. Two coils are found to be necessary to maintain the coil angle of at least 15°. One coil carries out the desuperheating of the product gases from a maximum design temperature of 650°C to a condensation temperature of 115°C (the product gas is assumed to be all steam, instead of 89.5% steam the mass balances in Section 3.2 show). The second coil carries out the condensing and desuperheating duties. Figure 3.5 shows this arrangement. A full detailed design and drawing can be found in Appendix A3.4. A summary of the three sections is presented here.

(i) The desuperheating section

The Reynolds Number is 13,290, and therefore the flow is turbulent. The heat transfer coefficient, h_{DS}, is calculated from Equation (3.5):

$$\frac{h_{DS}\ D_H}{k} = 0.023\ Re^{0.8}\ .\ Pr^{0.3} \qquad (3.5)$$

The value of h_{DS} is 182.6 $W/m^2\ K$.

The length of the desuperheating section works out to be 4 metres.

(ii) The condensing section

The Reynolds number works out as 1019, indicating laminar flow. Equation (3.4) works out the heat transfer coefficient which has a value of 4952 $W/m^2\ K$.

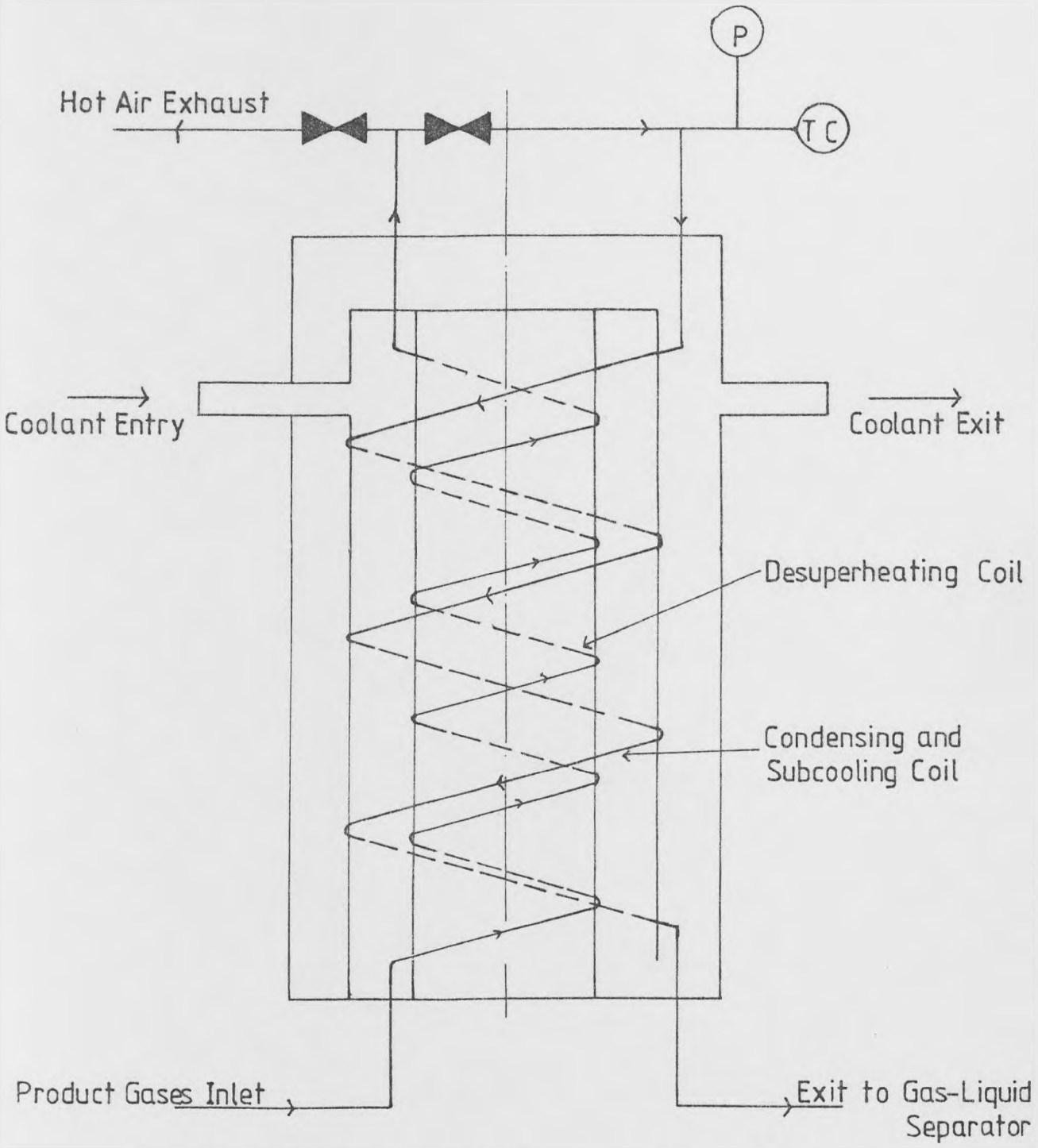

FIGURE 3.5: The Basic Design of the Main Condenser

(iii) The subcooling section

The heat transfer coefficient is evaluated from Equation (3.3) since the flow is laminar (Re = 1019). The value of h_{SC} is 6242 W/m^2 K. An iterative procedure similar to the design of the ethylbenzene condenser generates the length of the condensing and subcooling coil as 2 metres.

(iv) The coolant

The total heat duty to be removed by the water is 9101 watts. Allowing a 30 centigrade degree rise in the water temperature, the flowrate required is 250 kg/hr. The maximum tube surface temperature is 78°C. Therefore, boiling at the tube surface is not possible. The coolant Reynolds Number is 1507. The laminar flow implies the use of Equation (3.3) to evaluate the heat transfer coefficient, whose value is 1893 W/m^2 °C.

The desuperheating coil is wound around a core of 19 cm at an angle of 120°, and the condensing and subcooling coil is wound around a core of 15.2 cm at an angle of 45°.

Note on References for Physical Properties and Data Acquisition

The references used throughout this work are those of Perry[59], British Steam Specialities[60], Gallant[61], B.P. Chemicals[62], N.A.S.A.[63] and Kreith[55].

The full pipework data in Metric and BSP sizing can be found in British Steel Corporation[95] and British Steam Specialities[60] catalogues.

3.7 The Superheater Design

The superheating duties are to be performed by electrical firebar annular heat exchangers, utilising domestic ceramic firebar as the power source. Figure 3.6 shows the general design of the superheater. The firebar

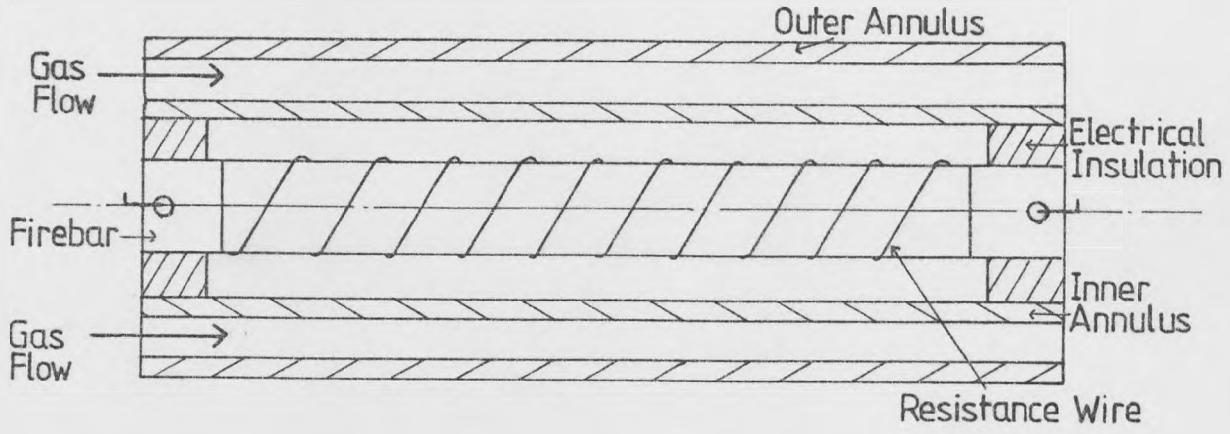

FIGURE 3.6: Simple Annulus Representation of the Radiation Superheater

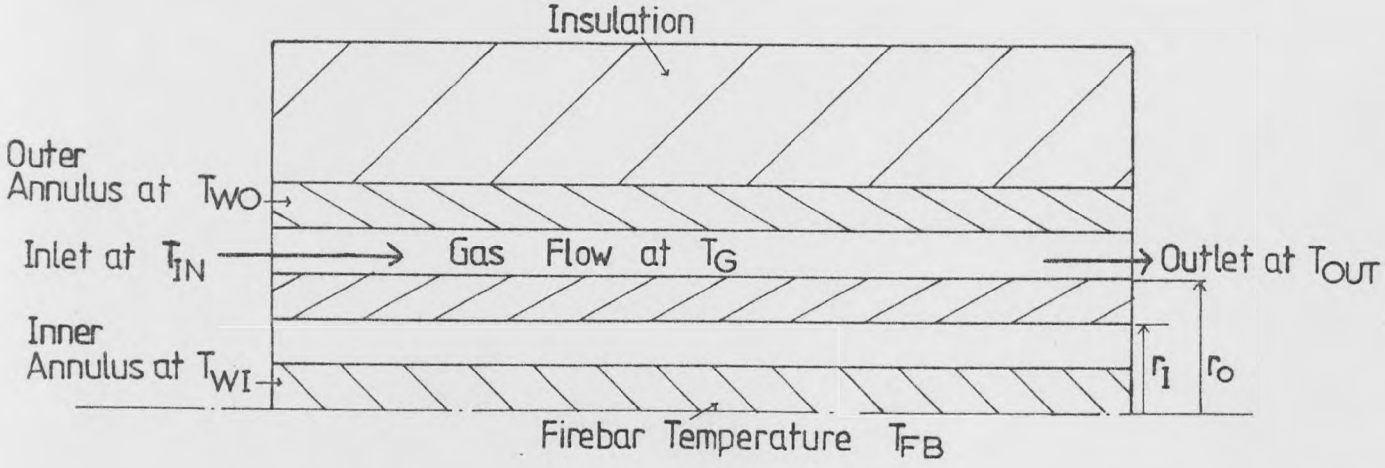

FIGURE 3.7: Model Notation for the Simple Design Method

is electrically insulated from the inner annulus of the superheater. The gas being heated is passed through the two annuli. The cylinders are of stainless steel. The compact design, and the high heat transfer coefficients and efficiencies obtainable make this type of heat exchanger particularly useful for pilot plants. The three duties that have to be carried out by the radiation superheater are:-

(i) superheating 7.0 kg/hr steam from saturation at about 2.7 bar to 750°C (to be carried out by superheater SSH1 and SSH2).

(ii) superheating 2.95 kg/hr ethylbenzene or 4.0 kg/hr steam from 140°C to 520°C (to be carried out by superheater EBSH).

(iii) the reheating of the reactor A product stream from 590°C to 650°C (to be carried out by superheater SSH3).

There are certain constraints on the design and operation of such heaters that need a more in-depth study before fabricating and commissioning of the heater can begin. The main constraints on the operation are:-

(i) the maximum power per firebar is 2 kW[64].

(ii) the maximum continuous operating temperature of the 80/20 Nickel/Chromium resistance wire firebar is 1200°C[52,64].

(iii) the ethylbenzene pyrolysis becomes significant after 540°C[28].

Therefore the heating surface temperature of the EBSH should be as low as possible, not exceeding 600°C if possible (this will be confirmed by actual runs).

A simple design method is used to check if it is possible to achieve the required duties within the above constraints. Then a more detailed, numerical method is used to investigate the various temperature regions in such a heater. Only if this design meets the above mentioned constraints will the superheater be fabricated.

3.7.1 The simple (analytical) design method

The three assumptions made are:-

(i) the wall temperatures are uniform with respect to angular and axial position.

(ii) the inner annular wall temperature is the same as the outer annular wall temperature, i.e. $T_{WI} = T_{WO} = T_W$ (see Figure 3.7).

(iii) the firebar and the inner tube can be considered to be infinitely long cylinder.

Although these assumptions do not truly represent the actual situation, they do give a good approximation of the temperatures and these values are good temperature estimates for the iterative methods of the more detailed numerical model.

Consider the arrangement in Figure 3.6. The heat load on the firebar can be calculated as:-

$$Q_{FB} = h A_s \Delta T_{ln} = \frac{h A_s (T_{GOUT} - T_{GIN})}{\ln \left(\frac{T_W - T_{GOUT}}{T_W - T_{GIN}} \right)}$$

$$\rightarrow \quad T_W = (T_{GIN} - T_{GOUT} \exp^x)/(1 - \exp^x) \qquad (3.6)$$

where $$x = h A_s (T_{GOUT} - T_{GIN})/Q_{FB} \qquad (3.7)$$

The firebar temperature can be calculated from:-

$$Q_{FB} = \mathcal{F}_{FB \rightarrow W} A_{SFB} \sigma (T_{FB}^4 - T_W^4) \quad (3.8)$$

where $\mathcal{F}_{FB \rightarrow W}$ is calculated using $\varepsilon_{FB} = 0.85$ for 'furnace splotched' 80/20 Ni/Cr resistance wire, and $\varepsilon_W = 0.95$ for furnace splotched Tropic FD or SS316, from which the annulus is fabricated. This method shows that the temperatures can meet the constraints (see Table 3.5).

TABLE 3.5

Major Superheater Temperatures Using the Simple (analytical) Design Method

Superheater	T_I °C	T_O °C	T_W °C	T_{FB} °C	Medium
SSH1	160°C	590°C	632°C	924°C	steam
SSH2	590°C	750°C	777°C	878°C	steam
SSH3	590°C	650°C	687°C	865°C	steam
EBSH	140°C	520°C	613°C	778°C	Ethylbenzene

3.7.2 The detailed (numerical analysis) design method

The assumptions made are:-

(i) the wall temperatures are uniform with angular position.

(ii) the radiation from each surface is at the average temperature along the length.

(iii) the gases are transparent. Charts from McAdams[65] for steam show that is the case ($\varepsilon < 0.01$).

(iv) small beam length.

(v) high convection coefficients.

The heat balances for the system are (see Figure 3.8 for the notation):-

(i) The gas phase: $$M_G C_{PG} \frac{d T_G}{dx} = h(x)\ 2\pi\ r_{WIO}(T_{WI}-T_G) + h(x)\ 2\pi\ r_{WOI}\ (T_{WO} - T_G) \quad (3.9)$$

(ii) The firebar: $$\frac{k_{FB}\ A_{xFB}}{(2\pi r_{FB}\ n)^2} \frac{d^2\ T_{FB}}{dx^2} + Q_T - A_{SFB}\ q_{OUT\ FB} + A_{SFB}\ q_{IN\ FB} = 0 \quad (3.10)$$

(iii) The inner annular wall:

$$k_{WI}\ A_{xWI}\ \frac{d^2\ T_{WI}}{dx^2} - h(x)\ 2\pi r_{WIO}\ (T_{WI} - T_G) - A_{SWII}\ q_{OUT\ WII} - A_{S\ WIO}\ q_{OUT\ WIO} + A_{S\ WII}\ q_{IN\ WII} + A_{SWIO}\ q_{IN\ WIO} = 0 \quad (3.11)$$

(iv) The outer annular wall:

$$k_{WO}\ A_{xWO}\ \frac{d^2\ T_{WO}}{dx^2} - h(x)\ 2\pi r_{WOI}\ (T_{WO} - T_G) - A_{SWOI}\ q_{OUT} + A_{SWOI}\ q_{IN} - U2\pi r_O\ (T_{WO} - T_A) = 0 \quad (3.12)$$

Equations (3.9) - (3.12) are a non-linear set of ordinary differential equations and are solved by numerical methods. The initial temperatures are those generated by the simple analytical design method. The non-linearity is removed by quasi-linearisation and the resulting set of equations are solved by finite differences. The equations are decoupled and solved in order. The process is repeated until convergence is obtained.

Radiation equations and view factors

In Equation (3.10), q_{OUTFB}, the radiosity, J, can be expressed as:-

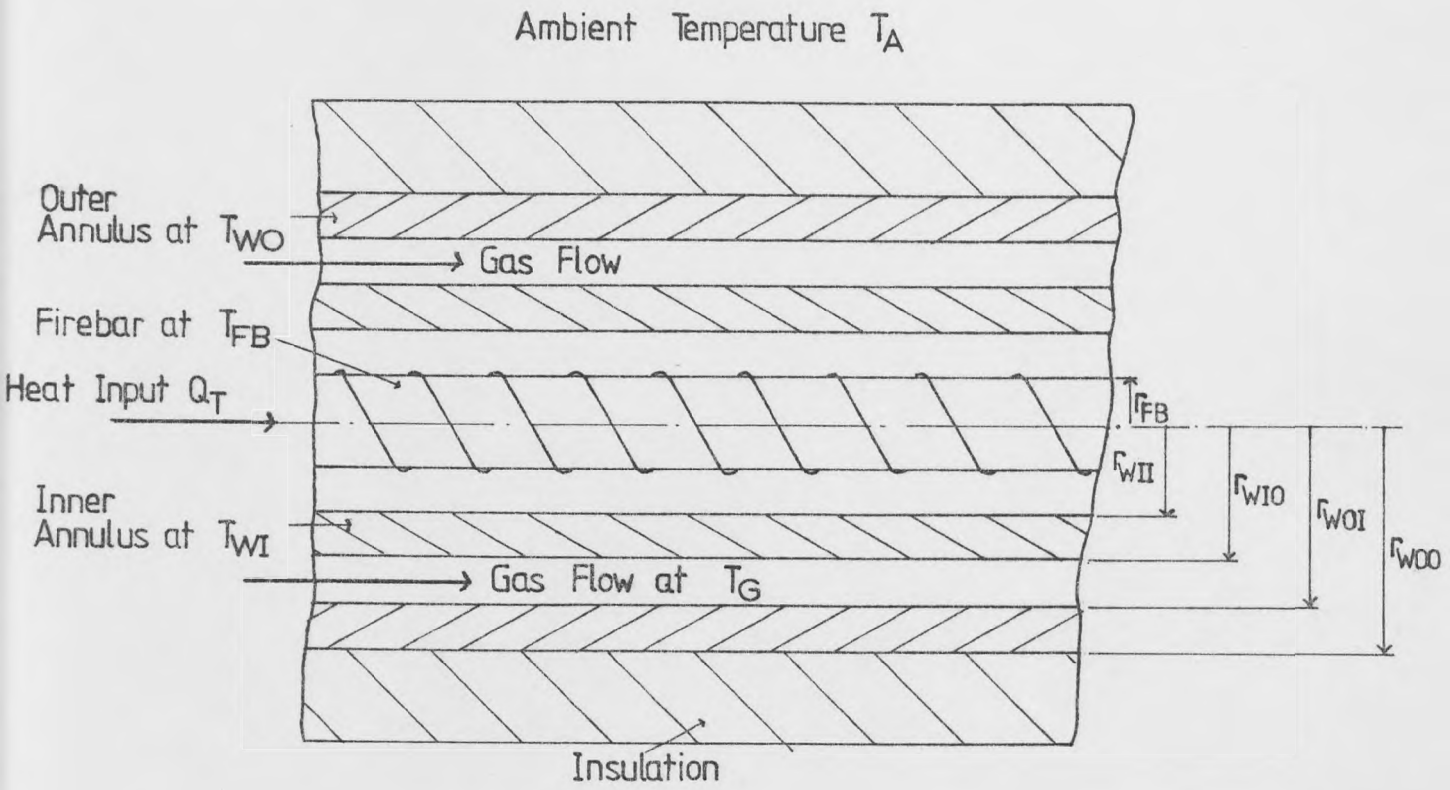

FIGURE 3.8: Model Notation for the Detailed Design Method

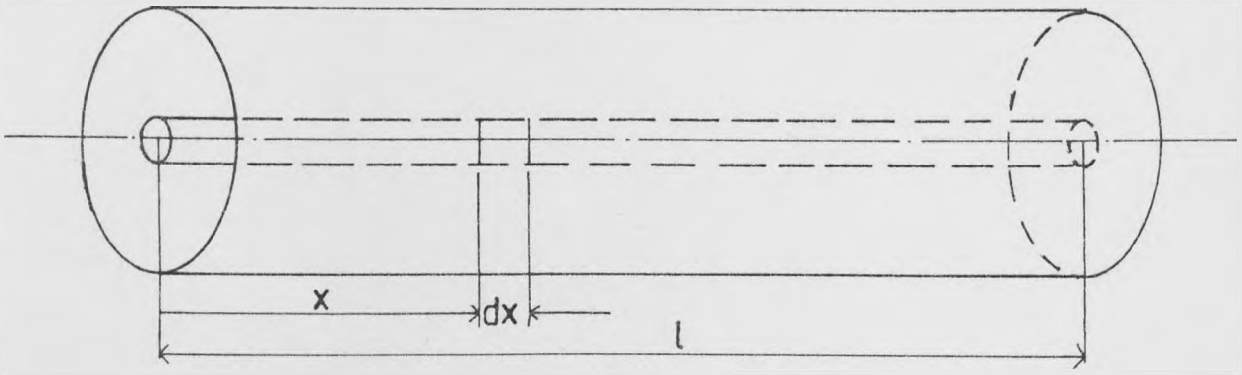

FIGURE 3.9: Radiation Shape Factor Notation for the Detailed Design Method

$$q_{OUTFB} = J = \varepsilon_{FB} \sigma T_{FB}^4 + (1 - \varepsilon_{FB}) q_{IN\ FB} \qquad (3.13)$$

and $q_{IN\ FB}$, the irradiation, G, can be expressed as:-

$$q_{IN\ FB} = G = \varepsilon_{BH}\ \sigma\ T_{WIB}^4\ E_{dx\to B}(x) + \varepsilon_{TH}\ \sigma\ T_{WIT}^4\ E_{dx\to B}(1-x) +$$

$$\varepsilon_{WI}\ \sigma\ T_{WI.AV.}^4\ L_{dx\to WI} \qquad (3.14)$$

where $E_{dx\to B}(x)$ is the view factor of the end between two concentric cylinders to an element dx on the inner cylinder, and $L_{dx\to WI}$ is the view factor of the outer surface of the two concentric cylinders to the element dx on the inner cylinder. Similar equations are obtained for $q_{OUT,WII}$, $q_{OUT,WIO}$, $q_{IN,WII}$, $q_{IN,WIO}$, $q_{OUT,WOI}$ and $q_{IN,WOI}$.

The view factors are worked out from equations by Leuenberger and Person[66] whose equations express the shape factors as ratios of the lengths and radii, and their angular properties, depending on the position of the element dx (see Figure 3.9).

Table 3.6 shows the results obtained for this detailed design. Comparison with Table 3.5 shows that the simple design method is quite accurate, a criterion on which the decision to implement the radiation superheaters can be based.

The designs show that with some inevitable practical adjustments to some temperatures (e.g. EBSH outlet temperature may need dropping by 5 or 10 degrees), the restrictions on the surface and firebar temperatures can be met, and so radiation superheaters are utilised.

Mechanical design notes

The superheaters are fabricated from Tropic FD, and utilise 'Super Twisteel' and asbestos wool seals. Flanges and flange caps ensure that the firebar element can be changed without any pipework being adjusted or

TABLE 3.6

Major Superheater Temperatures Evaluated Using the Detailed Design Method

Heater	Medium	T_{IN} °C	T_{OUT} °C	T_{FB} °C		T_{WI}		T_{WO}	
				Maximum	Average	Maximum	Average	Maximum	Average
SSH1	Air	20	420	886	884	572	547	492	410
SSH2	Air	420	680	889	886	723	709	687	661
SSH1	Steam	160	590	931	928	678	656	614	565
SSH2	Steam	590	750	884	881	791	783	767	751
EBSH	Ethylbenzene	140	520	795	793	627	600	605	595
SSH3	Steam	295	640	874	871	710	699	669	651

dismounted. Special firebar stabilizing rods and ceramic (alumina/silica) discs ensure electrical insulation and provide the means for power circuit connections. Full drawings of the superheater and the firebar supports are included in Appendix A3.6.

3.8 Materials of Construction, the Pipework and its Fittings

Due to the corrosive nature of steam, all lines and equipment in contact with steam are fabricated from Ni/Cr enforced stainless steels (SS316, SS321, or SS304).

Pipework

The pipework is all in seamless SS316 Sch. 40[95] for ⅛" (1.03 cm I.D.), ⅜" (1.25 cm I.D.), ½" (1.58 cm I.D.), 1" (2.66 cm I.D.) BSP sizes designed to withstand 850°C and 8.0 bar maximum. Full details of the accurate BSP and its metric equivalent schedule 40 sizing can be traced in BSC catalogues[95].

Fittings

All flanges are to BS10, Table H, in SS316. Ermeto olive seal fittings in SS316 are used on lines with maximum service temperatures up to 330°C, and screwed and weld fittings in SS316 used elsewhere. All screwed joints that do not need disconnection after the final alignments are welded to protect against leakages. All union threads are coated with 'BOSS' Graphite/Manganese pipe joint compound that sets at around 250°C to give a reinforced seal.

All flanges use 'Flexitallic' asbestos/stainless steel compressible ring gaskets (maximum operating temperature 800°C). Non-standard sealing surfaces use 'Super Twisteel' (maximum temperature 1000°C) or 'Klingerite 1000' (maximum temperature 550°C) non-renewable mesh gaskets.

Valves

The system solenoid valves are 'Alcon' ACP-4X valves with solenoids run off 24 V D.C., and have 'PTFE' seals.

The steam line controls valves, i.e. globe valves, relief valves, pressure regulator valves are 'Bailey' models cast off bronze, with the regulator valves having special reducer springs fitted for the small steam flow rates.

Non-return valves are installed after solenoid valves SV2, SV3 and SV5 preventing back flow in case of circuit faults or sealing problems. (see Figure 2.5 for location of the solenoid valves).

A special 'MPL' 2 bar back pressure valve is fitted to the delivery line of the metering pump.

Nitrogen blanketing and differential pressure lines

Ordinary copper ¼" (0.64 cm O.D.) pipes with brass 'ENOT' accessories are used.

Rig insulation

Two kinds of insulation are used on the rig. For temperatures up to 250^{o}C, Fibreglass based 'Super McEvoy B' insulation blanket is used. For all other high temperature insulation, 'Kaowool Bulk A' fibrewood and 'Kaowool' blanketing insulation of bulk density 96 kg/m^{3} is used. Insulation properties can be found in the Morganite Ceramic Fibres Ltd. Data Book[46].

Appendix A2 shows the layout of the control instrumentation for the air and steam supply lines.

3.9 Apparatus Instrumentation

3.9.1 Flow instrumentations

(i) Air flow measurement - A 'GEC-Elliot' metric series 18 rotameter with duralumin float weighted by a stainless steel ball is used. The calibration

is as per in the GEC-Elliot Handbook[67], with the following non-standard data for SL1 line:-

Weight of float : 9.96 g

Mean density of float: 4.64 g/cc.

(ii) Condenser coolant measurement - The main condenser coolant line uses a metric size 18X rotameter with an all stainless steel float. Calibration is as per standard charts in[67]. The ethylbenzene condenser coolant line has a pre-calibrated 0-135 litres/hr scale on the rotameter.

All flows are manually controlled using bronze globe valves.

(iii) Steam flowrate measurement - Both steam lines have orifice assemblies connected to standard water-on-mercury manometers on the control panel, with the 'Perspex' safety shields and metal collection trays.

3.9.2 Pressure instrumentation

The steam lines, air lines, nitrogen lines and the reactor entry lines have 0-30 psig (0-3.05 bar) Bourdon pressure gauges installed on them. The reactors also have the facility to measure the differential pressure across each reactor by means of a water-on-mercury manometer.

3.9.3 Electrical instrumentation

All electrical circuits are individually fused and earthed, and all voltage regulators are thyristor-based phase controllers. Good heat sinks are provided within gasket sealed containers. The current measurements are recorded by moving coil ammeters. Full wiring diagrams of all circuits can be found in Appendix A5.

3.9.4 Temperature instrumentation

It is hoped to use Ni-Cr/Ni-Al (Chromel/Alumel) 'Pyrotenax' thermo-

couples to measure the system temperatures, the emf's being balanced and recorded on a 'Kent' Series II-16 multipoint recorder. However, there are a number of errors associated with this kind of temperature measurement network, especially at high temperatures. Before implementing the network, a small study into the magnitude of these errors is carried out.

The 'Type K' Chromel/Alumel thermocouples are available in various probe diameters from 1.0 mm upwards. The thinnest have the best temperature response, but are liable to breakage. It is hoped to use the 1.0 mm diameter probes to measure the reactor temperatures, which need the fastest responding probes. All other measurements will be carried out by the more durable 3.0 mm diameter probes. The sealing of these thermocouples is by the special 'Pyrotenax' pressure entry gland fittings, sized to a ⅛" BSP (0.68 cm O.D.) thread[68].

3.9.4.1 Temperature measurement errors

There are three kinds of errors possible on the measuring network mentioned above. These are:-

(a) reading error on the multipoint recorder: this is 2 - 3 degrees Centigrade;

(b) thermocouple error due to the materials used: (i.e. accuracy limit of the 'Type K' thermocouples). This error is dependent on the bimetallic junction used, and is quoted in the 'Pyrotenax' catalogue for 'Type K' probes[68] as:

+ 0.75% of the temperatures greater than 400°C, or ± 3 Centigrade degrees for temperatures less than 400°C. The maximum this can contribute is ± 0.75% of 750°C, i.e. ± 5.5 Centigrade degrees;

(c) thermocouple error due to the heat transfer from the gas to the probe, and onto the ambient air as heat loss: the above mentioned errors are independent of gas flowrate. A study of the probe heat loss error is necessary to judge the accuracy of the probe reading indicated on the recorder. Two areas are crucial as far as the temperature indication is concerned. These are:-

(i) the measurements at the exits of SSH2, EBSH and SSH3, and

(ii) the packed catalyst bed temperature measurements on the reactors.

Error evaluation for the superheaters

Figure 3.10 shows the arrangement common to all the system superheaters. 3 mm diameter probes are used with a probe length 1.3 cm, enclosed in a ½" BSP (1.58 cm I.D.) pipe with at least 10.2 cm 'Kaowool' blanket insulation covering the pipework.

The metal wall temperature can be calculated from:-

$$T_W = T_G - \frac{UA_{SO}}{h_I A_{SI}} (T_G - T_A) \qquad (3.15)$$

The overall heat balance is:-

$$h_{GT} (T_G - T_{TC}) = \mathcal{F}_{TC \to W} \sigma (T_{TC}^4 - T_W^4) \qquad (3.16)$$

Combining Equations (3.15) and (3.16) yields Equation (3.17) from which a value of T_G can be calculated for an indicated value by the probe, T_{TC}.

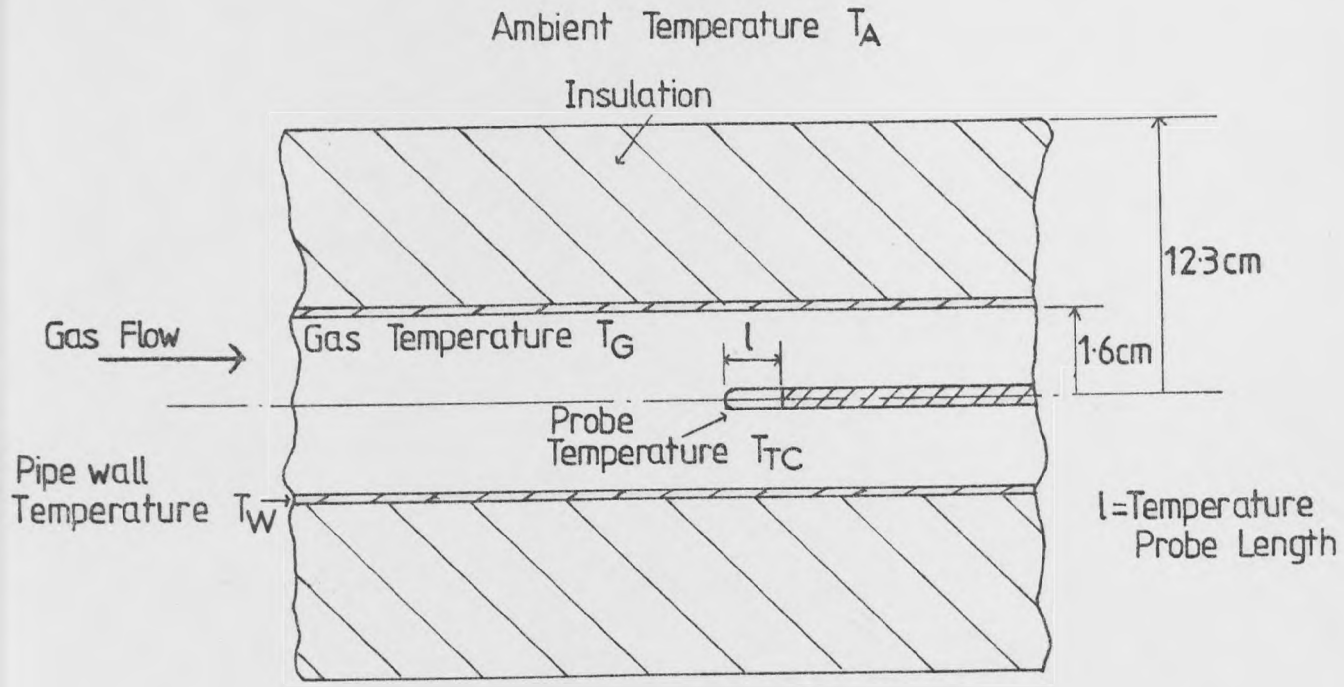

FIGURE 3.10: The Superheater Exit Temperature Sensor Set Up

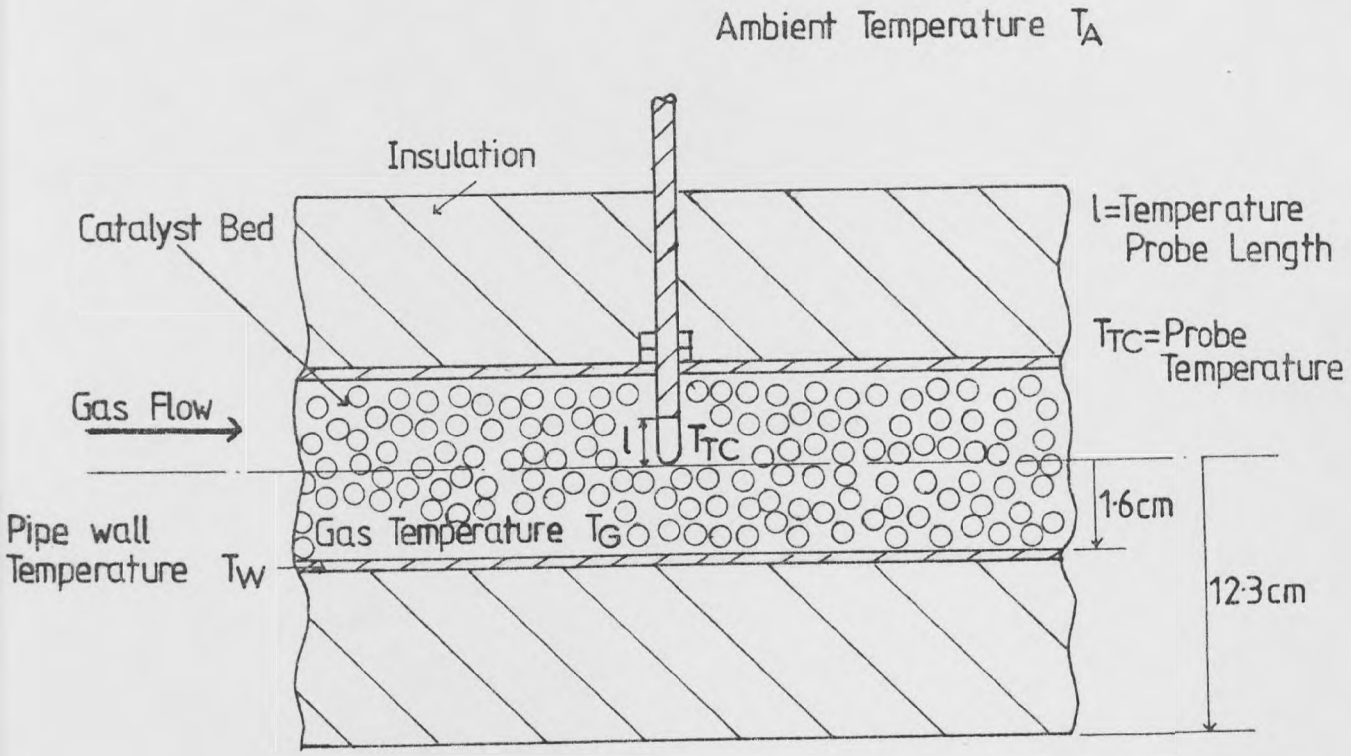

FIGURE 3.11: The Reactor Bed Temperature Sensor Arrangement

$$h_{GT}\ (T_G - T_{TC}) = \mathcal{F}_{TC \to W}\ \sigma \left[T_{TC}^4 - \left(T_G - \frac{UA_{SO}}{h_I\ A_{SI}} (T_G - T_A) \right)^4 \right] \qquad (3.17)$$

The gas heat transfer coefficient, h_I, can be calculated from standard laminar, transition and turbulent flow equations involving the Nu, Pr and Re numbers. The gas-to-probe heat transfer coefficient, h_{GT}, can be calculated from correlations in Kreith[55]. The probe can be considered either as a cylinder, or a flat plate using the lower value of h_{GT} in the error calculation. For the probe as a vertical cylinder, the correlation is:-

$$h_{GT} = 0.023\ Re^{0.8}\ Pr^{0.33}\ \frac{k}{D_H} \left(1 + \frac{6D}{L} \right) \qquad (3.18)$$

The correlation uses a hydraulic mean diameter, D_H, based Re, for the Reynolds Number.

For the probe being a flat plate, the correlation for h_{GT} is:-

$$h_{GT} = 0.664\ \frac{k}{L}\ Re_L^{0.5}\ Pr^{0.33} \qquad (3.19)$$

with Re_L as the heat Reynolds number based on the width of the plate.

T_G is calculated for each superheater, assuming that T_{TC} is the required superheater temperature, i.e. estimating the actual gas temperature for an observed temperature T_{TC}. Results are tabulated in Table 3.7.

Error evaluation for the catalyst bed probes

Figure 3.11 shows the probe location in the packed reactor. Probes of 1 mm diameter, with a sensor length of 1.3 cm are used. The gas heat transfer coefficient, h_I, is calculated from a correlation for small cylindrical packings by Heggs and Handley[69], where

TABLE 3.7

Results of the Temperature Error Calculations

Rig Section	h_I $W/m^2\,^oC$	h_{GT} $W/m^2\,^oC$	$\frac{UA}{h_I A_I}$	T_T ^oC	T_G ^oC
SSH2 Outlet	118.6	673.9	0.047	750°C	754.2°C
SSH3 Outlet	122.1	681.4	0.033	650°C	653.0°C
EBSH Outlet	57.9	486.6	0.031	540°C	542.6°C
Catalyst bed	207.3	635.4	0.014	650°C	651.7°C

$$j_h \, e = 0.26 \, Re_m^{-0.33} \qquad (3.20)$$

with Re_m being the local Reynolds number, derived in[69]. The gas-to-probe heat transfer coefficient, h_{GT} is calculated by a correlation by Whittaker in Kreith[55], where

$$h_{GT} = \frac{k}{D} \left(0.4 \, Re^{0.5} + 0.06 \, Re^{0.67} \right) Pr^{0.4} \qquad (3.21)$$

The rest of the calculations for T_G for an observed T_{TC} are identical to those for the superheaters, using Equation (3.17). The results are tabulated in Table 3.7.

Conclusions of the temperature error studies

The percentage error due to the heat loss to the ambient air is a maximum of + 0.6% whilst that due to the probe junction fabrication is $\pm$ 0.75% of the observed temperature. Hence a total error of + 1.35 to - 0.75% error can be expected due to the thermocouples. This is very small. A further $\pm$ 3 Centigrade degree error can be expected on the reading of the Kent Temperature Recorder. This all adds up to a maximum deviation of + 10.1 to - 8.6 Centigrade degrees at the maximum rig temperature of 750°C. This can be considered to be as good as a temperature sensor and indicator system can hope to achieve, whilst maintaining a fairly simple system. Hence the 'Type K' Chromel/Alumel probes can be considered satisfactory.

Appendix A5 contains the locations of the 16 point thermocouple wiring of the Kent recorder.

3.10 Notes on the Construction of the Experimental Apparatus

The layout flowsheets (Isometric projections) for both the external and control rooms are included in Appendix A1. Adequate cast iron supports are provided for all equipment and also for long lengths of pipework. Appendix A3.6 carries the details of the sampling points, the sampling and collection tanks, the lines for condensed steam drainage, and the lines for nitrogen blanketing. The correct insulation is provided for all lines. Low temperature ($< 250^{\circ}C$) lines have one layer of 1.3 cm thick fibreglass insulation, whilst all high temperature lines have two layers of 5.1 cm thick Kaowool blanket. The 'odd-shaped' equipment, e.g. the superheater, the mixer, the reactor cones etc. are enclosed in cast iron boxes that are filled with 'Kaowool Bulk A' fibrewool insulation, with at least the equivalent insulation of 2 Kaowool blanket layers. Strainers and filters are provided on the steam and air lines. Appendix A2 shows the full control and safety devices on the steam and air feed lines. Plates 1 - 5 show the major supply lines and the main system equipment, e.g. reactors, superheaters, condensers, collection tanks etc. for both the control and external rooms.

The apparatus commissioning can now begin.

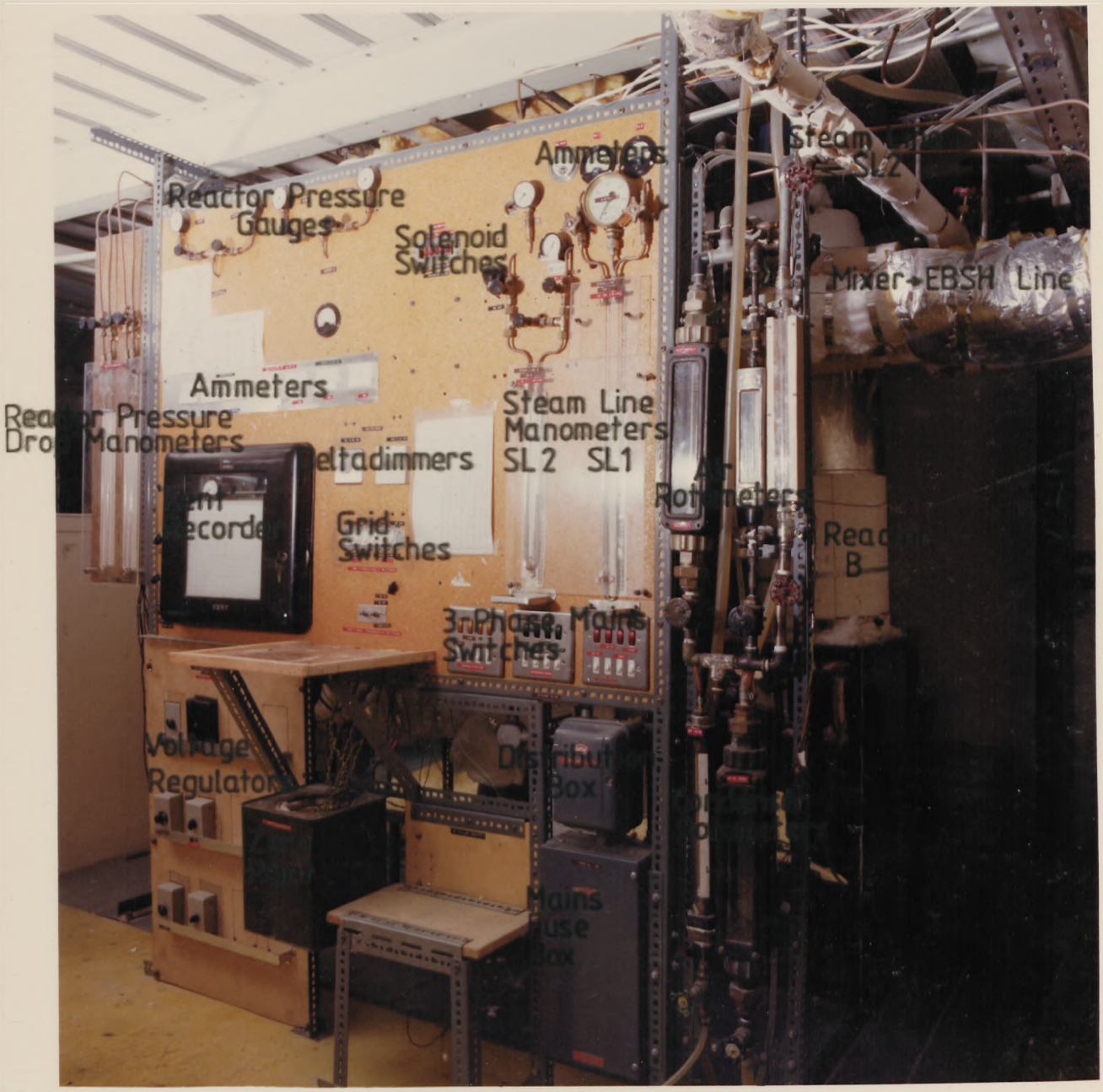

PLATE 1: The Control Panel

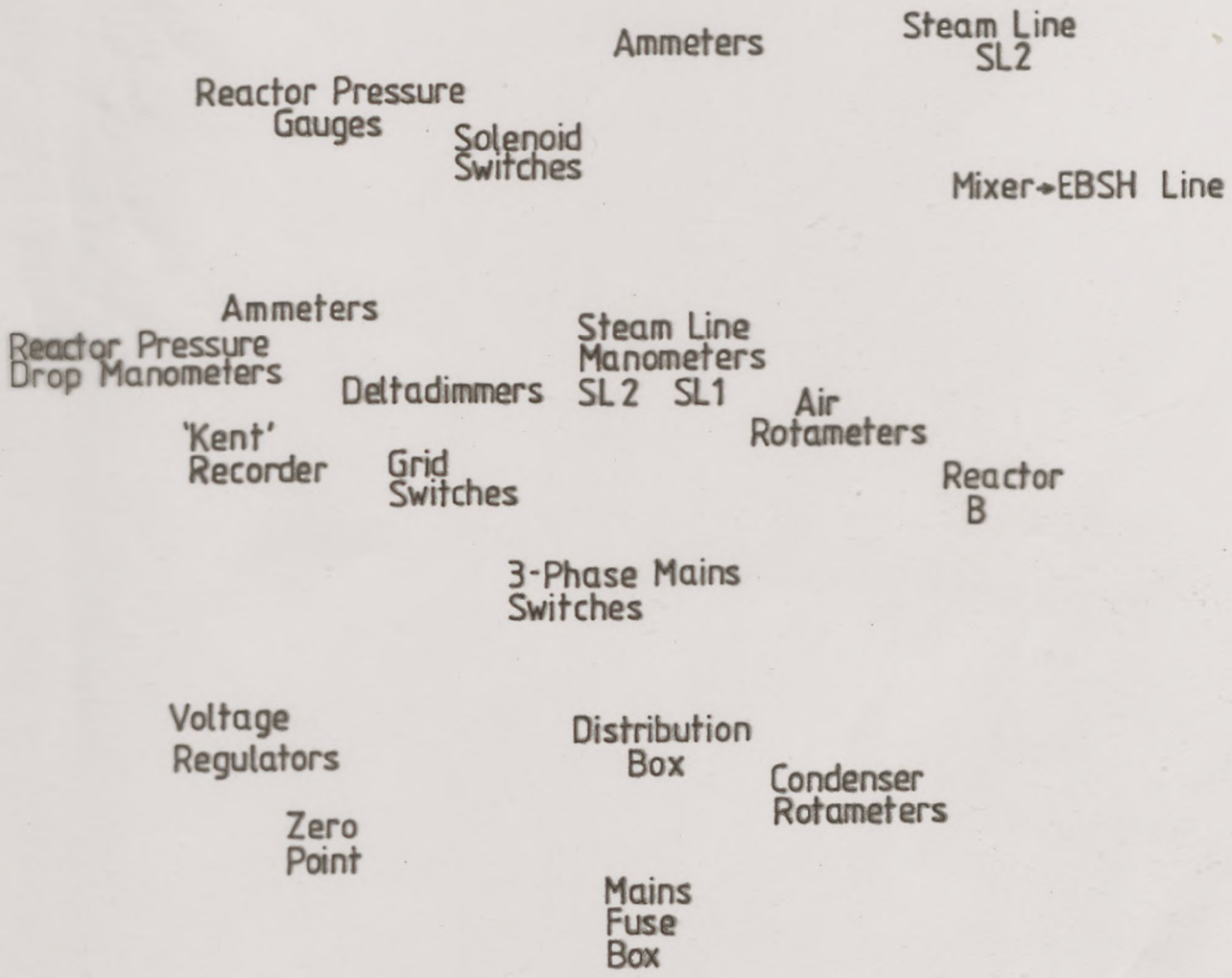

PLATE 1: The Control Panel

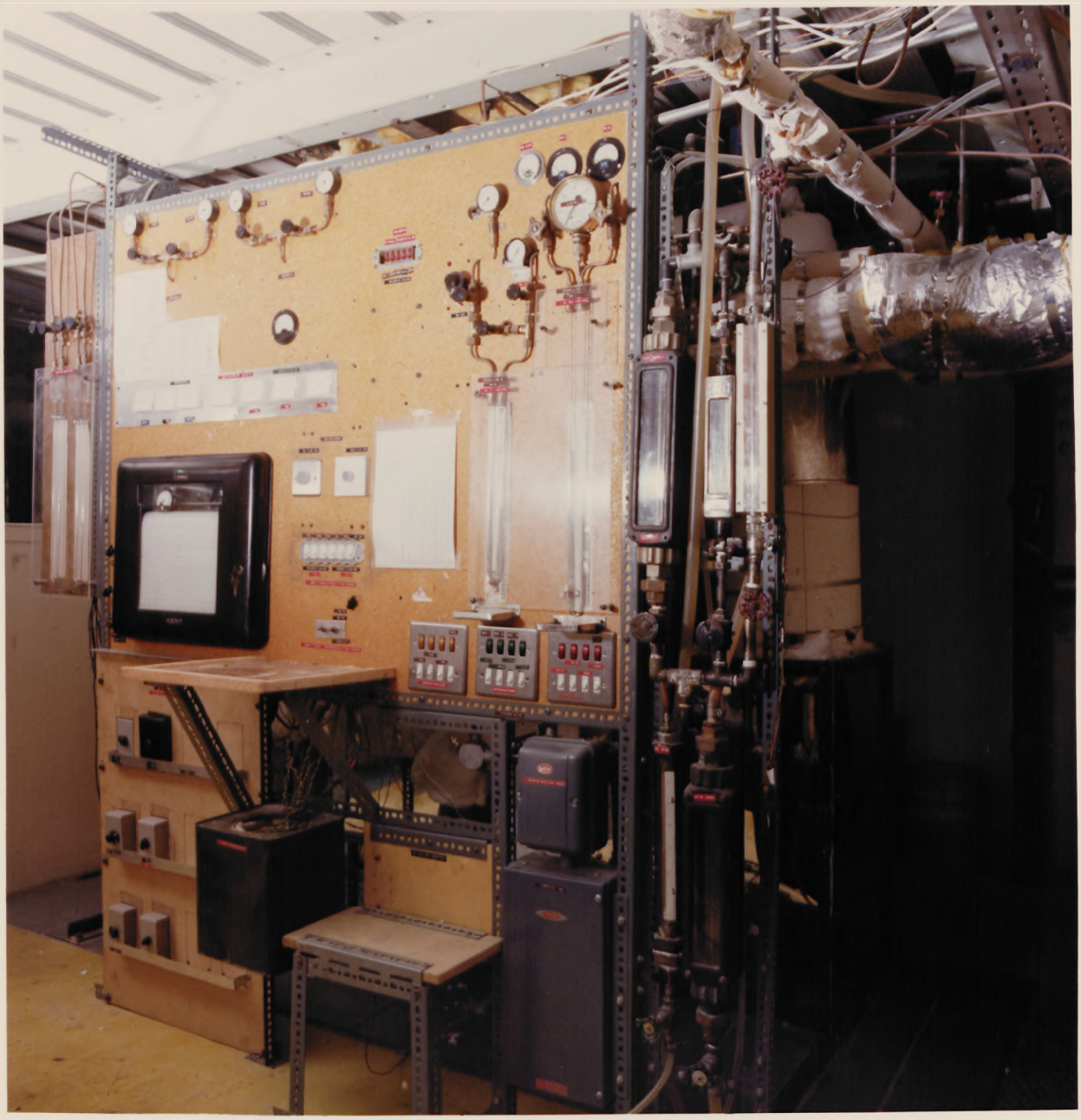

PLATE 2: Reactor A and the Superheater Box (Control Room)

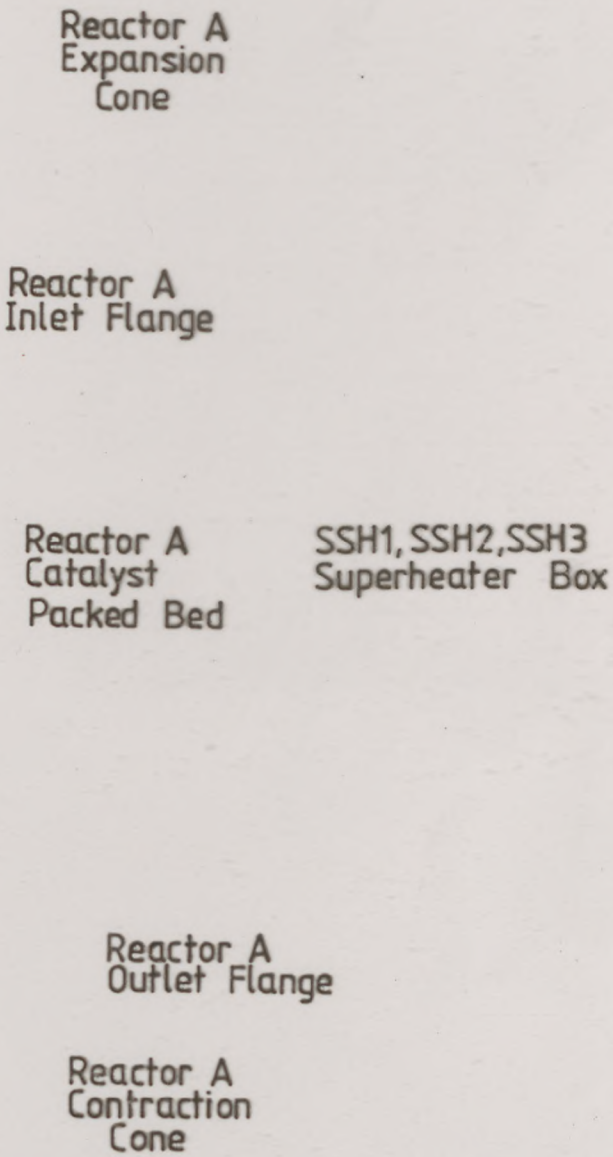

PLATE 2: Reactor A and the Superheater Box (Control Room)

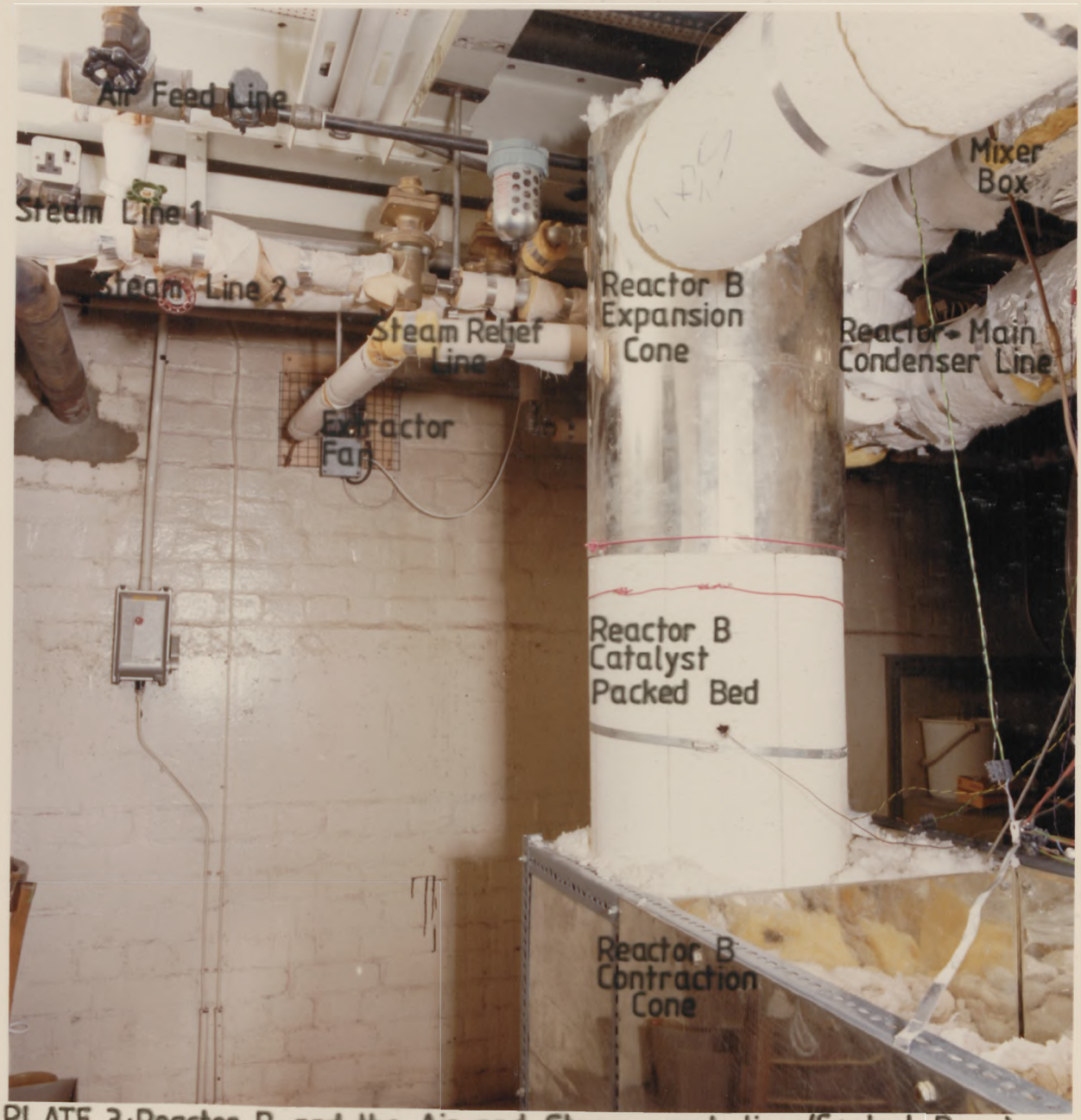

PLATE 3:Reactor B and the Air and Steam supply lines(Control Room)

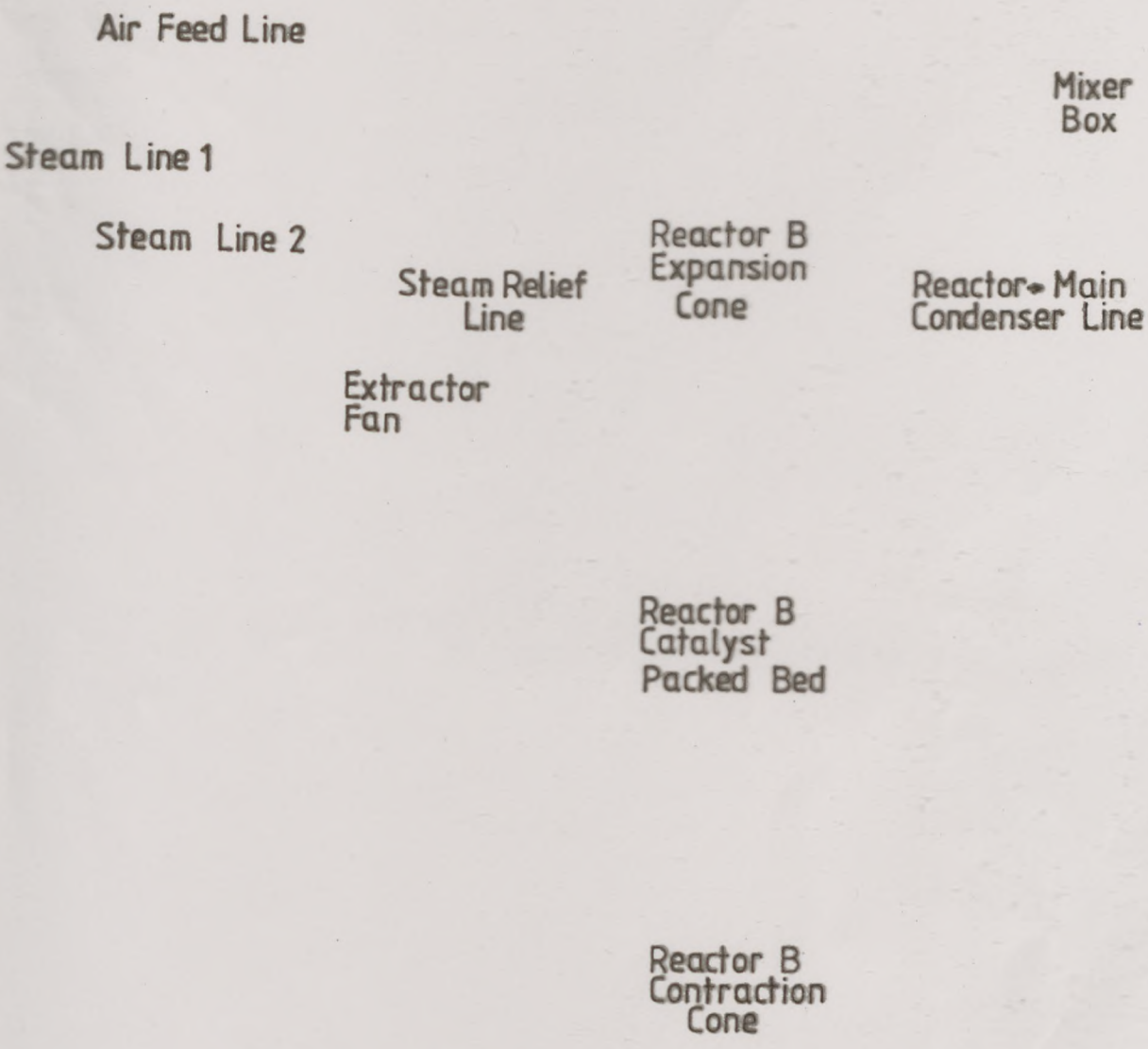

PLATE 3:Reactor B and the Air and Steam supply lines(Control Room)

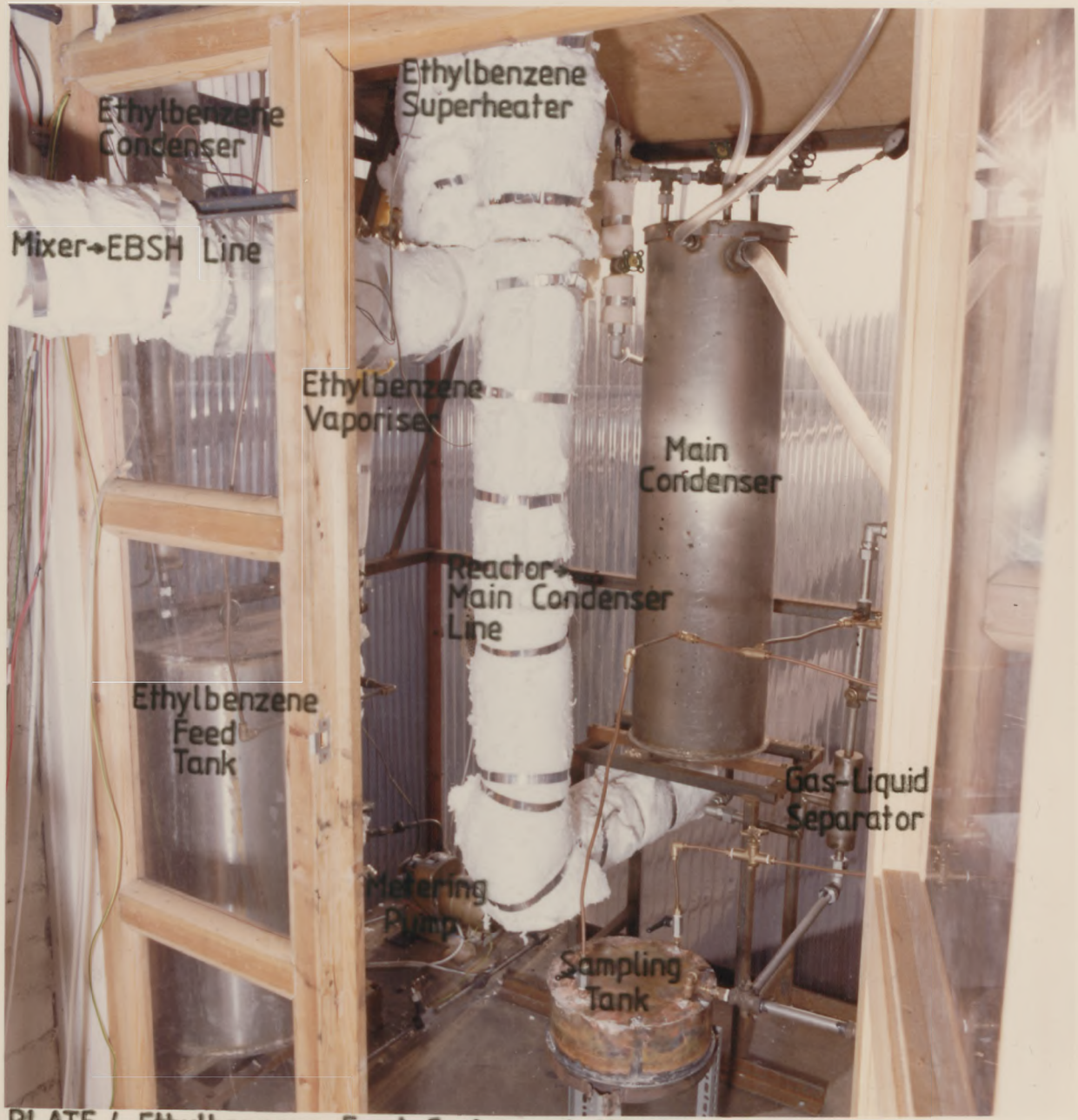

PLATE 4: Ethylbenzene Feed Cycle and the Main Condenser (External Room)

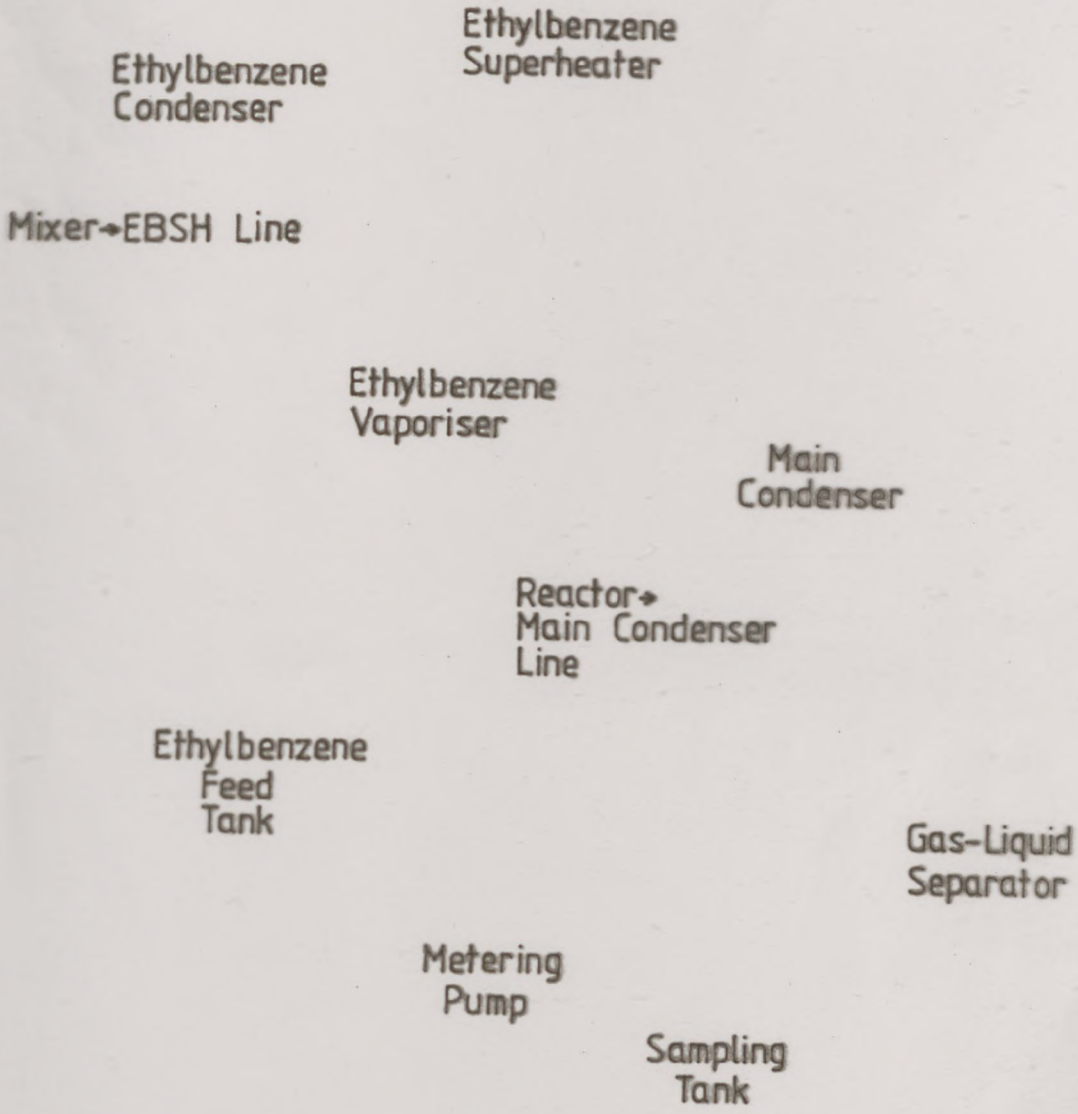

PLATE 4:Ethylbenzene Feed Cycle and the Main Condenser (External Room)

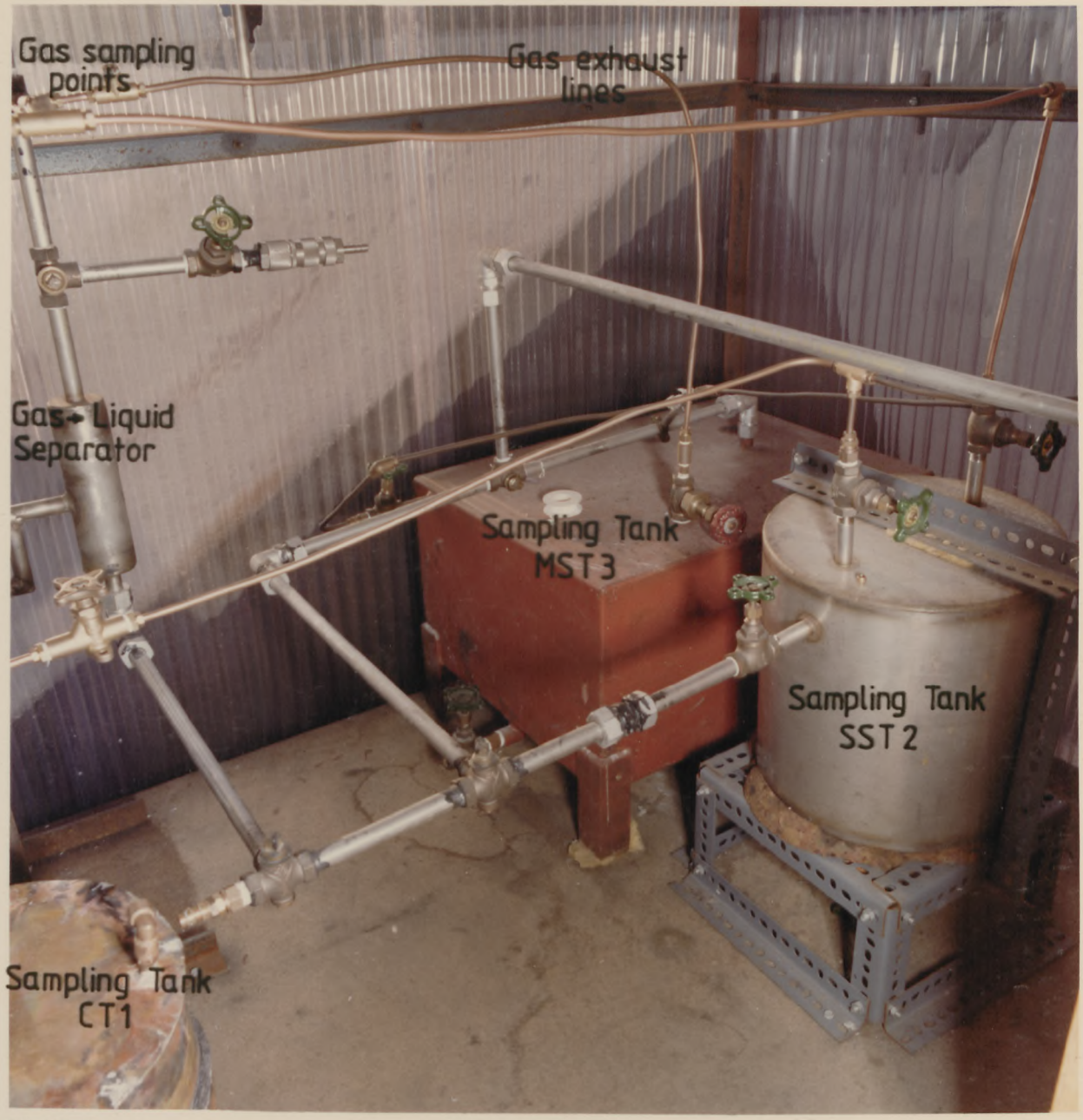

PLATE 5: Sampling and Product Collection Equipment (External Room)

Gas sampling points

Gas exhaust lines

Gas→Liquid Separator

Sampling Tank MST3

Sampling Tank SST2

Sampling Tank CT1

PLATE 5: Sampling and Product Collection Equipment (External Room)

CHAPTER 4

THE PREDICTION OF REACTOR SIZE AND THE DETERMINATION OF OPERATING CONDITIONS

CHAPTER 4

THE PREDICTION OF REACTOR SIZE AND THE DETERMINATION OF OPERATING CONDITIONS

Introduction

The volume of catalyst to be utilized is chosen such that the conversions and efficiencies fall within the range of industrial practice. The duration of the transient runs are selected so as to provide adequate product samples for analysis, and also giving noticeable changes in temperature and conversion.

The surfaces of the superheater must be aged to provide the high emissivities desired. The rates of the heating up and the cooling down for these superheaters are determined. The pressure levels throughout the system are estimated so that the operating range of the pressure regulator and relief valves can be set. Finally, the heat losses from the system are evaluated theoretically and practically, and means of compensating for these losses are suggested.

4.1 The Determination of the Reactor Bed Catalyst Volume, and the Duration of the Transient Runs

Cockcroft[10,11] developed computer programs for the SSAR and the transient reactors. Appendix A9 contains a publication which summarises the model development, and presents some results. His models use a film resistance solution, i.e. one which assumes that the intraparticle diffusion can be neglected, but includes the effect of the interphase transfer. The model equations for the heat and mass transfer are solved numerically using central difference approximations. These programs form the core on which the studies in this section are based. They have been checked for the reproducibility of Cockcroft's results before being modified for this

work. Appendix A6 contains the reactor and catalyst data, as well as the reaction kinetics used.

4.1.1 Determination of the catalyst volume, and SSAR predictions

The aim here is to utilize a catalyst volume which gives the conversion and efficiency of the styrene producing reaction within the ranges claimed by various commercial processes[24]. A two stage SSAR, utilizing interstage heating is modelled. The inlet temperature to the 1st bed is 923 K and that to the second bed is 903 K. These are the maximum temperatures for industrial SSAR systems[24]. Varying bed lengths from 0.2 m to 0.6 m are modelled. The maximum possible conversion at a particular temperature, pressure and steam ratio is the equilibrium conversion, x_e, and is represented by Equation (4.1). The equilibrium constant K_p expression is that of Wenner and Dybdal[27]:-

$$x_e = \frac{- SR + \sqrt{SR^2 + 4\ (1 + P/K_p)\ (1 + SR)}}{2\ (1 + P/K_p)} \qquad (4.1)$$

where $K_p = \exp\ (16.12 - 15350/T)$

Figure 4.1 shows the effect of pressure and temperature on the equilibrium conversion, for a steam/ethylbenzene ratio of 14:1, which is used in this experimental study. It is clear from Figure 4.1 that pressure has a considerable effect on equilibrium conversion which falls off rapidly with increase in pressure. Thus, the system pressure needs to be kept at a minimum. The inlet pressures quoted in industrial patents are in the ranges 2.4 - 3.0 bar for the first reactor and 1.6 - 2.3 bar for the second reactor. Section 4.3 reveals that the minimum reaction inlet pressures for the apparatus are significantly lower than industrial values. Therefore, the inlet pressures used for the modelling studies are those values that arise from the minimal pressure drop for the apparatus.

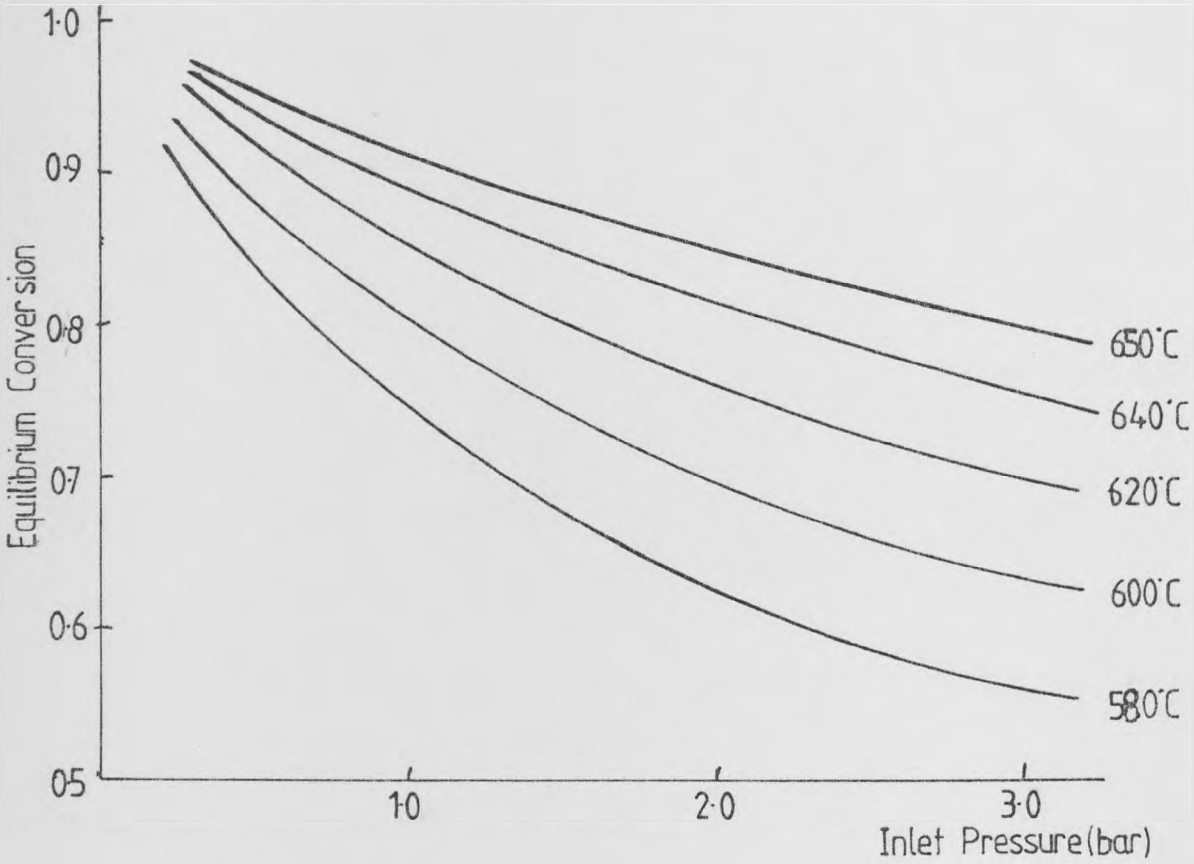

FIGURE 4.1: The Variation of the Equilibrium Conversion with Pressure and Temperature

The inlet pressure to the 1st bed is 1.68 bar and that to the 2nd bed is 1.35 bar. Pressure drop along the bed is neglected as the calculated and measured value is only 0.018 bar per foot of bed length. Section 4.3.2 shows that this is very small compared to the pressure drop for the rest of the inter-bed connecting equipment.

As the conversion along the bed length increases, the equilibrium conversion is approached. Thus the driving force of the reaction falls, resulting in less gain in conversion per unit increase in the reactor length and catalyst volume. Therefore the practical reactor size limit is governed by the falling rate of the increase in conversion.

Isothermal operation at 923 K would produce the most desirable conversions for a practical system of finite length. Yet, as Figure 4.3 shows, a bed of 0.4 m length represents the highest possible conversion possible for the styrene reaction. Further increase in bed length results in a small drop in conversion and an even greater drop in efficiency (Figure 4.4). Efficiences of less than 85% are regarded as undesirable for SSAR operation[24], and therefore it is already apparent that a bed of length greater than 0.4 m is uneconomical and undesirable. Table 4.1 shows the 2 stage SSAR conversions and efficiencies for varying bed lengths. The conversion limit is approached around bed length of 0.4 m and the fall in efficiency is quite apparent.

Figure 4.2 illustrates the temperature profiles for the SSAR tabulated in Table 4.1. The temperature fall is very small after 0.4 m for the first stage, and after about 0.35 m for the second stage. Figure 4.3 illustrates the conversion profiles for the same, and once again the fact that a bed length of more than 0.35 m has no advantages is borne out.

Industrial systems operate at efficiencies of 87 - 89% for the one stage SSAR and 86 - 88% for the two stage SSAR[20,21,24]. A 0.3 m bed shows efficiencies within this range (Table 4.1). The conversions shown

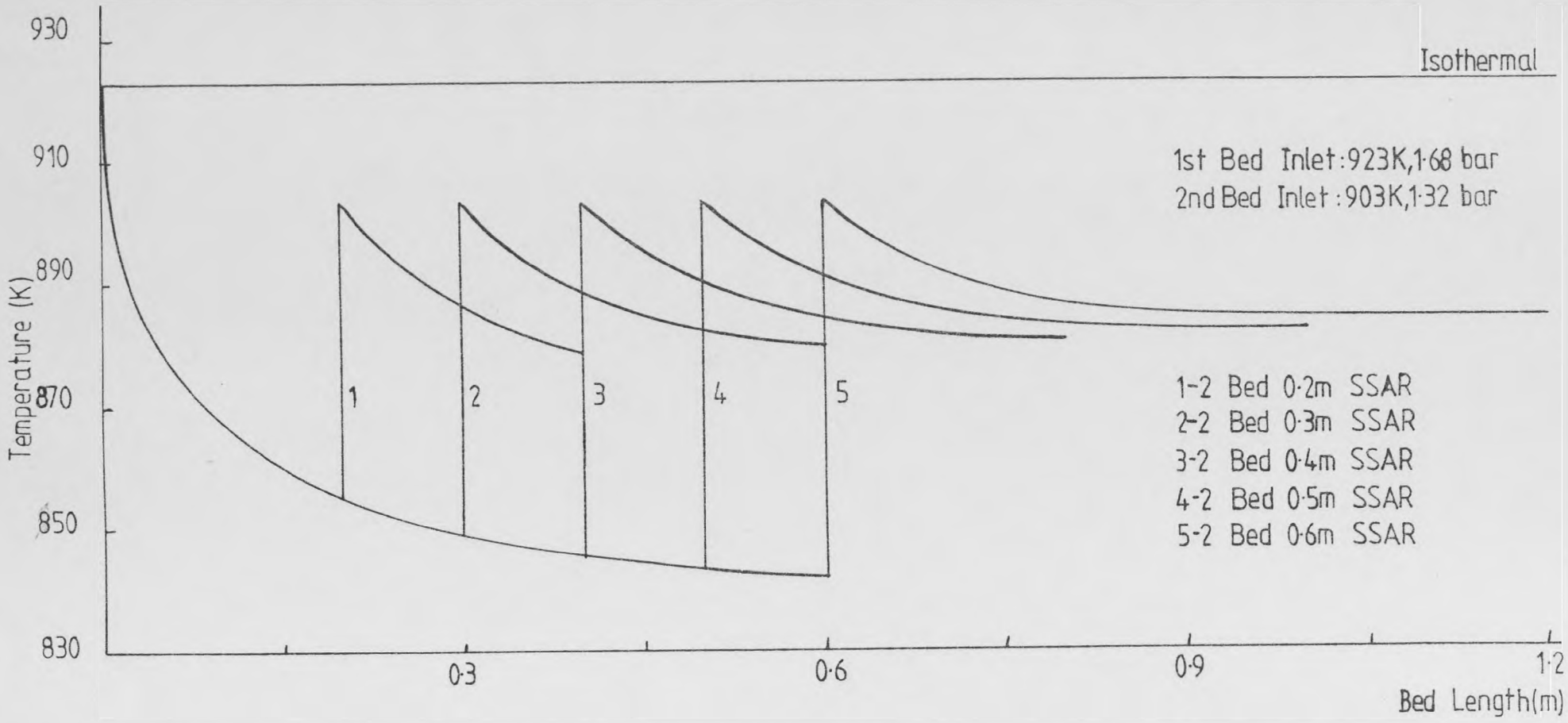

FIGURE 4.2: Effect of Increasing Bed Length on the Bed Temperature for a Two Stage SSAR

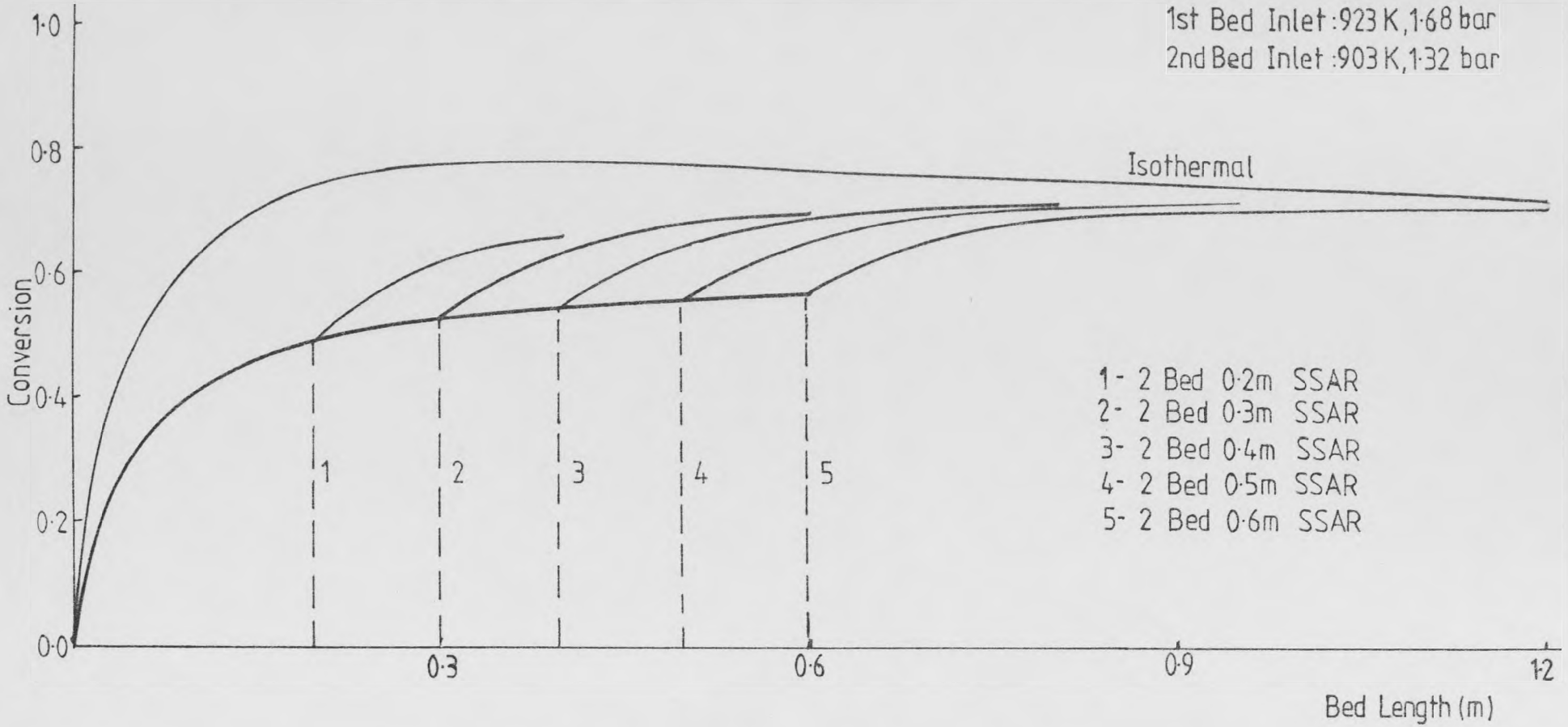

FIGURE 4.3: Effect of Increasing Bed Length on the Overall Conversion for a Two Stage SSAR

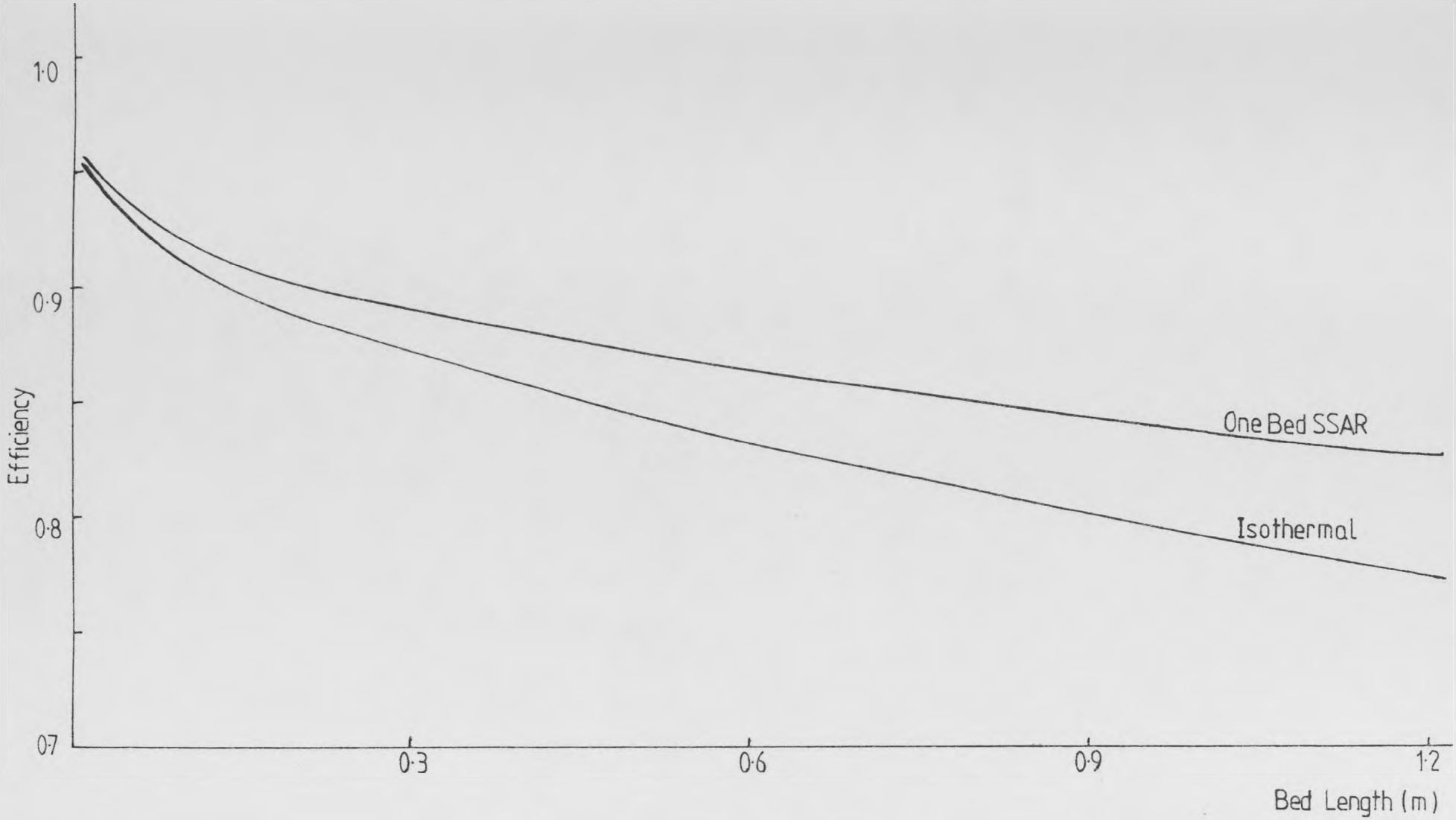

FIGURE 4.4: The Variation of Efficiency with Bed Length for a SSAR and an Isothermal Reactor

TABLE 4.1

Model Predicted Efficiencies and Conversions for a Two Stage SSAR of Varying Bed Length

Bed Length (m)	1st Bed		2nd Bed	
	Conversion (%)	Efficiency (%)	Conversion (%)	Efficiency (%)
0.2	48.7	90.2	66.2	88.2
0.3	52.4	88.9	69.6	86.5
0.4	54.6	87.9	71.1	85.1
0.5	56.1	87.0	71.6	83.8
0.6	57.1	86.2	71.6	82.6

by this bed length are higher than those claimed in patents[20,21,24], but these industrial reactors operate at greater pressures. Industrial reactors operate at around 60 - 66% two stage conversions. A 0.3 m bed would have its two stage conversion fall in this range if it operated at industrial pressures mentioned earlier (the two stage conversion is then 64.7%).

A 0.2 m bed gives efficiencies which are higher than these ranges for industrial systems. One factor that applies to this transient research is the need to have adequate differences in conversion and temperature drop between the isothermal and steady state cases so as to have an adequate working range for the transient runs that fall in between these extremes. This is best provided by a 0.3 m bed (Figure 4.3), and hence the case is overwhelmingly in favour of utilizing a reactor catalyst section of 0.3 m length (with the bed diameter as 10.2 cm).

Figure 4.5 shows the section of the actual system reactor, and

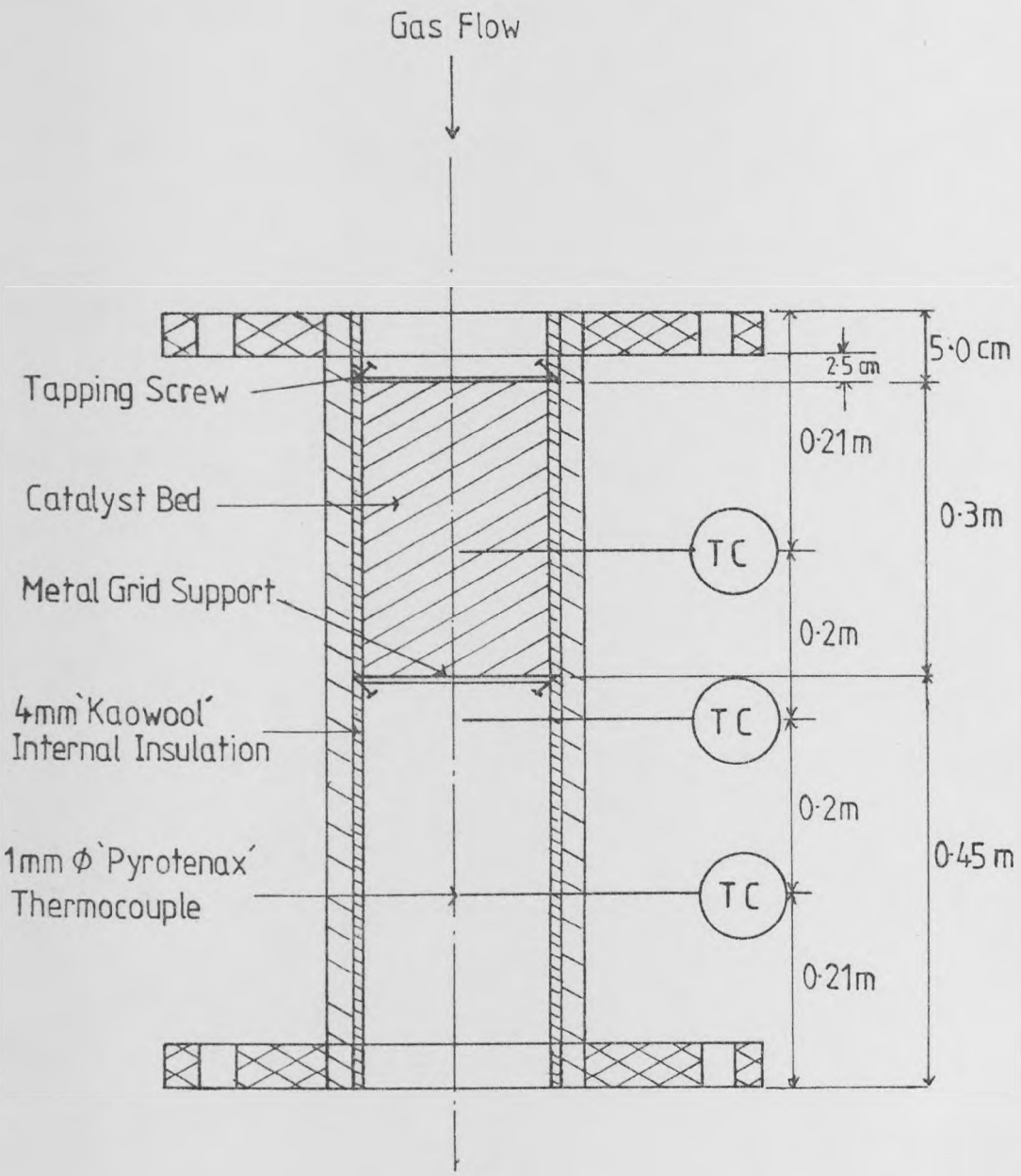

FIGURE 4.5: The Location of the Catalyst and the Thermocouples in the Reactor

includes the dimensions of the reactor, the catalyst bed and the temperature probe positioning. The reactor walls are internally insulated with 4 mm thick 'Kaowool' ceramic paper, held in place by 'Autostic' high temperature adhesive. The metal mesh catalyst supports are then screwed into the paper and onto the reactor wall to hold the catalyst in position.

Cockcroft[10] evaluated that the ceramic paper insulation drastically reduced the thermal inertia of the reactor wall and for a 4 mm thick lining, the reactor conversion and temperature profiles are only lower by 0.2% from the adiabatic wall results.

4.1.2 Transient run duration and model predictions

For this study, a 0.3 m bed is used, and the temperatures, conversions and efficiencies are generated every 15 seconds until steady state is achieved. Table 4.2 shows the falling outlet temperature and mean conversion and the rising efficiency for a set of transient runs of increasing duration. The variation in conversion and temperature with bed length, and variation of outlet efficiency and mean conversion for these run periods are illustrated in Figures 4.6, 4.7, 4.8 and 4.9 respectively.

It is difficult to estimate the total system residence time, as there are parts of the apparatus where two phase flow takes place (e.g. after the main condenser). Hence composite sampling is required. This means that the transient run should be of sufficient duration to allow the collection of at least 50 cc of organic sample for analysis purposes. At the same time, there should be sufficient changes in the temperatures (at least 3 Centigrade degrees) and mean conversion (at least 2%) to provide the temperature and analysis recorders reasonable difference in the measurements. Therefore, runs of less than 60 seconds are not considered adequate for sample purposes.

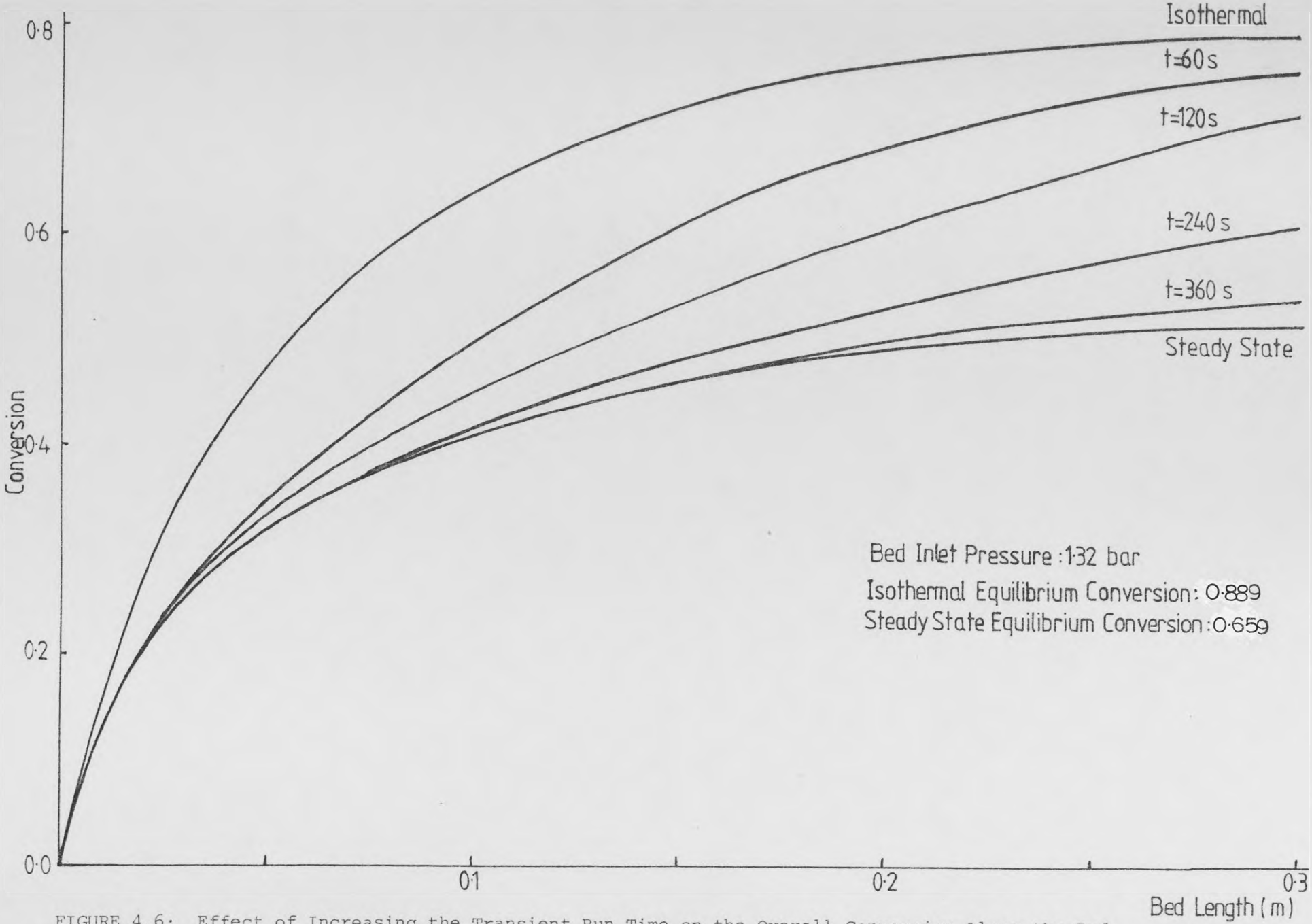

FIGURE 4.6: Effect of Increasing the Transient Run Time on the Overall Conversion Along the Bed

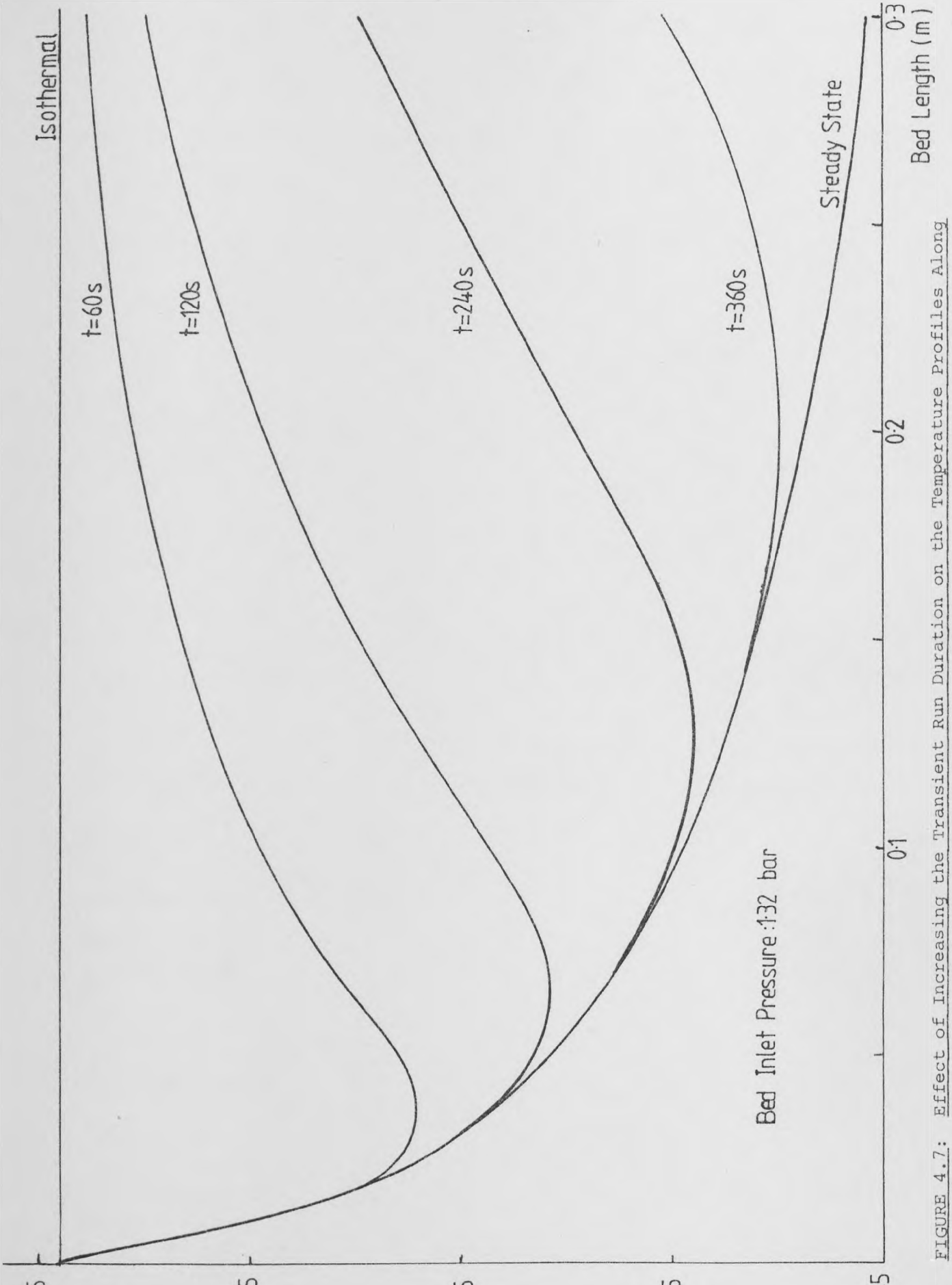

FIGURE 4.7: Effect of Increasing the Transient Run Duration on the Temperature Profiles Along the Bed

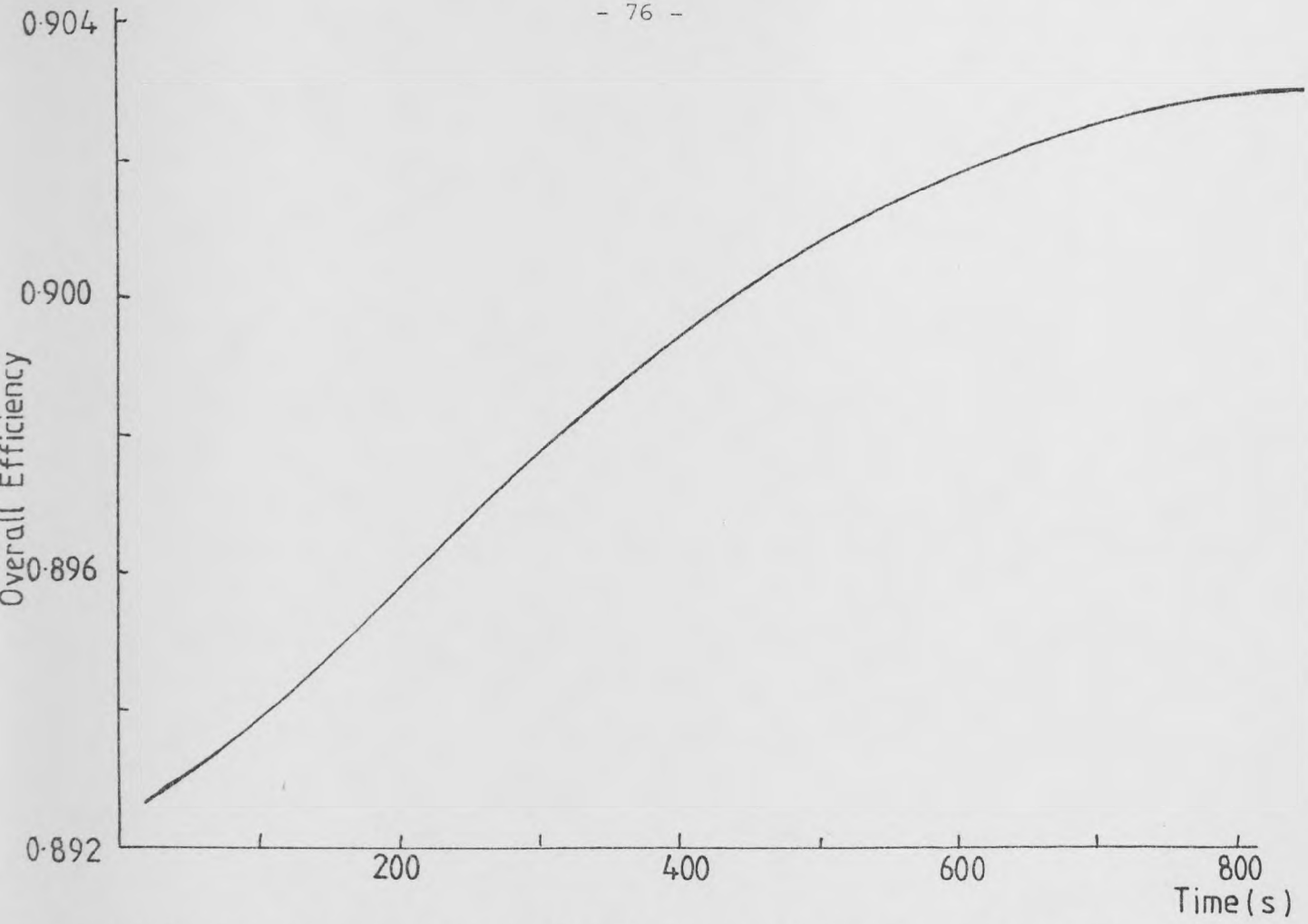

FIGURE 4.8: The Variation of Overall Efficiency with the Transient Run Time

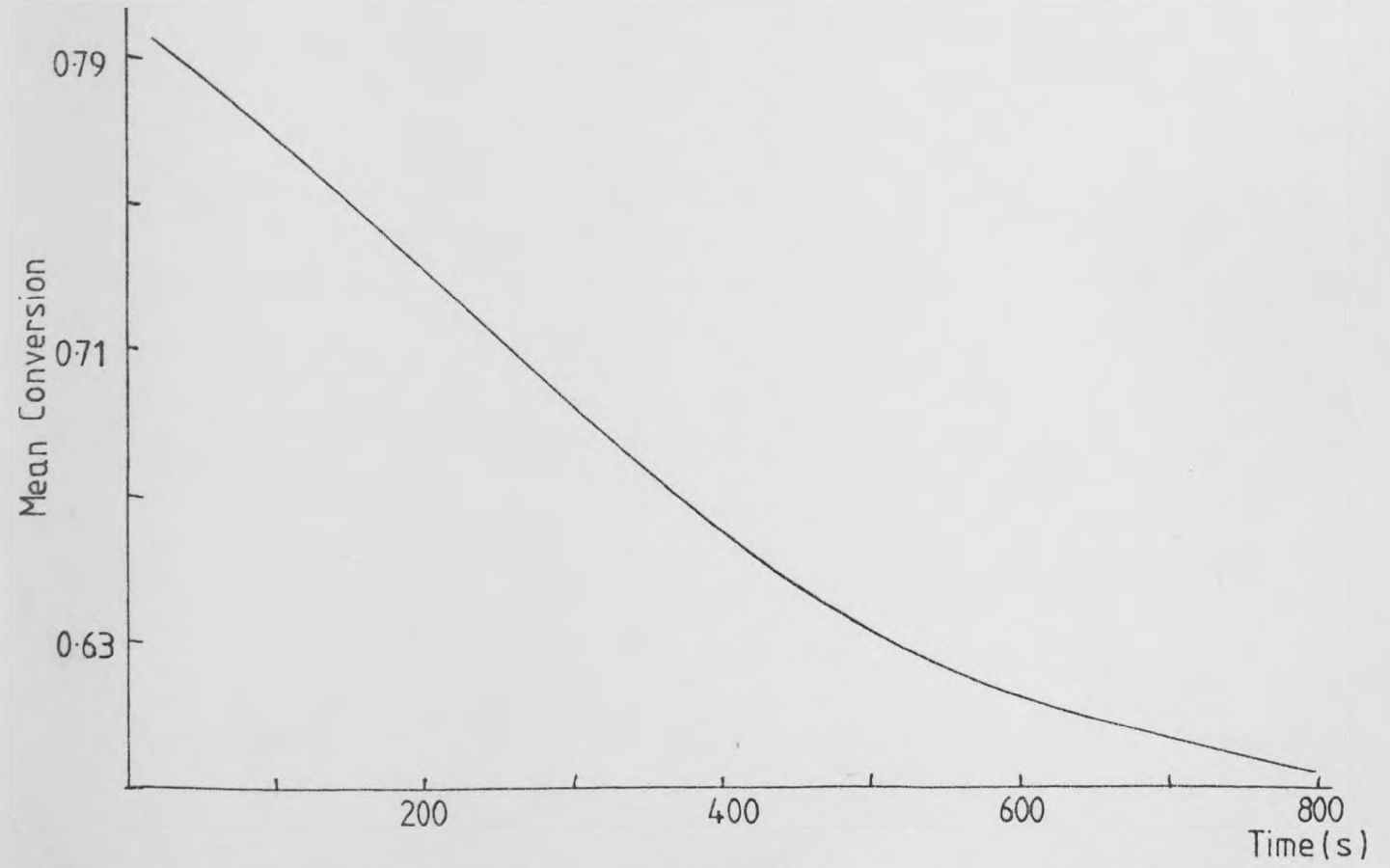

FIGURE 4.9: The Change in the Mean Overall Conversion with the Transient Run Time

With the organic/water separation time very small (less than 10 seconds after mixing or condensing), point liquid sampling is ruled out due to the difficulty in judging the flow patterns of the organic/water/gas mixture.

TABLE 4.2

The Outlet Temperature, Mean Conversion and Efficiency for Transient Runs of Varying Duration

Duration of Transient Run (s)	Outlet Temperature (K)	Mean Conversion (%)	Efficiency (%)
60	920.7	78.0	89.3
120	915.2	76.1	89.4
240	894.7	71.3	89.7
360	871.2	66.9	89.9
≥ 780 (s. state)	847.2	59.5	90.3

Figure 4.6 shows the predicted conversion profiles along the bed length. The isothermal profile, 4 transient runs, and the steady state profiles are shown. Figure 4.7 shows the predicted temperature profiles along the bed for the above mentioned cases. Figure 4.8 shows the overall change in efficiency with the duration of the transient run, and Figure 4.9 shows the change in mean conversion with time. The four transient runs selected are of duration t = 60 s, 120 s, 240 s and 360 s. These show enough differences in efficiency and mean conversion (fairly uniform change), and at the same time show enough temperature change for the temperature probes located 17.8 cm from the bed entrance and also enough temperature change at the outlet as well.

After 360 s, although the change in mean conversion is still quite

high, the actual change in conversion has slowed down considerably (Figure 4.6), and the temperature profile is beginning to approach the steady state profile (Figure 4.7). Therefore no runs are required here. Besides, at t = 150 s, the transient conversion (69.2%) is less than the 2 stage SSAR conversion (69.6%). Therefore the real interest is in the two transient runs of t = 60 s and t = 120 s. The other two serve as illustrations of the transient state as it approaches steady state.

The aim is to carry out four transient runs for a particular bed entry temperature, and one steady state run for the same conditions. The main investigations for the transient runs should centre around the first 3 - 4 minutes after commencement of the run, when there is the greatest advantage of the RCR system.

4.1.3 Transient Catalysis: literature survey and general discussion

The transient and steady state comparisons made are based on the steady state kinetics derived by Cockcroft[10]. Yet the behaviour of the catalyst under transient conditions has been ignored, simply due to lack of information in the literature for the styrene production catalysis. However, a good survey of catalysis and transient catalysis in particular emerges with a great number of points and questions that only extensive experimental work will confirm or answer.

Kobayashi and Kobayashi[72] mentioned that the reaction rate expressions present a particular model to describe the catalysis true mechanism for which there is no justification even at steady state. They utilized a method of temperature and concentration forcing to study the transient catalysis behaviour of N_2O decomposition over $NiO-SiO_2$ catalyst. Their studies concluded that different catalysts exhibited different kinetic sequences, unique in their own ways, at transient state.

Bennett[73] studied the same reaction and encouraged the thinking that the kinetic sequences occur in a series of steps, even at steady state. This is different from the current thinking, e.g. the steady state Langmuir-Hinshelwood equation which assumes that the rate of each step is the same, or a simple multiple of the others, and that there is no appreciable accumulation of the reaction intermediate. Bennett attempted to describe the variations in the rates at transient conditions as:-

$$\text{rate} = \text{fn}\ (T,\ P,\ c,\ \text{state of catalyst},\ \text{time},\ \text{steady state rates})$$

and had some success in correlating various dimensionless terms based on the above factors.

Scheintuch and Schmitz[74] studied N_2O decomposition, CO oxidation and H_2 oxidation over various catalysts in pulse reactors and concluded that the theoretical models that attempt to describe transient catalysis employing single step kinetic models, but accounting for chemical processes, generate results that have no bearing on the experimental results obtained. They had some success in correlating the kinetics and rates of reactions as:-

$$\text{rate} = \text{fn}\ (T,\ P,\ c,\ k,\ \text{activation energy},\ \text{chemisorption},\ \text{surface rate processes})$$

This modified the theoretical models to some degree of success.

Beusch et al[75] showed that under some experimental conditions, two different catalyst pellets from the same batch exhibit different periodic behaviour. They suggested that the reaction mechanism involved a slow periodic change in site activity, e.g. conditions blocking of sites followed by reactivation of sites.

Billimoria et al[76] investigated the hydrogenation of acetylene to ethylene and ethane over fresh and fouled Nickel catalyst. The reactor was subjected to change in steady state temperatures by hydrogen concentration forcing. They observed that the time to achieve steady state increased greatly as the levels of steady state were changed. The "fouling" (blocking and reactivation of catalyst sites, observed by photography) was affecting the progression to steady state and concluded that separate kinetics, using more complex modelling was required. They also observed "wrong way" concentration and temperature behaviour, though no data was presented.

Mehta et al[77] studied "wrong way" behaviour and showed by modelling that under certain conditions, a sudden drop in feed inlet temperature to a packed bed reactor lead to a transient temperature rise along the bed - the "wrong way" behaviour. They developed models to estimate the critical reactor lengths and maximum temperature positions for this behaviour. The steam/air shut down step for the styrene reactor does exhibit this phenomenon for a short time, and this could affect the catalyst site activity by air/steam mixtures during a shut down.

Unni et al[78] studied the effect of cycling and concentration forcing for SO_2 oxidation over V_2O_5 catalyst. Experimental work showed that the cycling significantly increased the rate of SO_2 oxidation. This was followed by a decaying period which eventually led to the steady state rate of reaction. Their studies showed that neither mass transfer, adsorption of reactants, surface reactions, nor the SO_2 desorption were rate controlling.

Schweich and Villermaux[79] investigated the dehydrogenation of cyclohexane to benzene over Pt/Al_2O_3 catalyst by high frequency periodic pulsing in a chromatograph reactor. They observed that for the first few pulses,

the rate of reaction was very much higher than that for a conventional steady state reactor. The rate then fell away to a constant value still much greater than the steady state value. The study concluded that the authors claiming steady state kinetics by the use of a chromatograph reactor ought to have a re-think.

Dale Wilson and Rinker[80] investigated a cyclic reactor system for the hydrogenation of nitrogen to ammonia over an iron-based catalyst, using both nitrogen and hydrogen in turn to force back the temperature profiles after the reaction period. They observed that the Temkin kinetics model, a reliable design base for years, completely failed to predict the transient high frequency cycling conversions. The values were also dependent on the regenerative gas used. They observed that periods of 30 seconds or less had mixing effects and flow fluctuations dominating the reaction mechanisms. The nitrogen desorption and hydrogenation of adsorbed nitrogen was essentially complete after 5 minutes, and therefore the steady state models could be used to predict the conversions for periods of 10 minutes or longer in duration. The major chemical processes also had to be regarded as interactive, transient and none of them controlling.

Abdul-Kareem et al[81,82,83] carried out a most extensive study into the catalytic oxidation of CO and investigated periodic concentration and temperature forcing for periods between 10 and 60 minutes. A great rise in the reaction rate between 10 and 25 minutes over that of normal steady state operation was observed. This tended to decay back to that of steady state after 50 minutes or so. An attempt to relate this rate to feed composition ratio, period duration, and temperature was made. At a low reaction temperature, the chemical adsorption-desorption could be explained by a three stage process. At higher temperatures, the mechanism could be modelled by a two stage process. However, the critical

periods of less than 10 minutes were not investigated.

Jain et al[84,85] carried out measurements on the reactant gases that are taken up at the catalyst surfaces. They utilized a stream of hydrogen to force out the nitrogen that gets taken up by the iron oxide catalyst used for the ammonia production process. The minute quantities of ammonia liberated after the end of the reaction stroke (c.f. Dale Wilson and Rinker[80]) were measured and the results showed that the nitrogen is not only chemisorbed at the catalyst surface, but is actually dissolved by the bulk phase of the catalyst. Calculations proved that the quantity of ammonia released was too great for only chemisorption of the nitrogen to occur. Seven times the expected ammonia released due to chemisorption was observed. The study went on to show that at the end of the reaction stroke, the initial nitrogen (reactant released as ammonia) liberated is that that has been chemisorbed, followed by the dissolved reactant from the catalyst bulk. Applied to the styrene transient reactor, the ethylbenzene participating in any combination of surface processes could affect the reaction rates and kinetics during subsequent reaction strokes after the initial reacting run.

This survey shows that the transient catalysis is a complex subject for even single reaction reactors. Work on competing reactions at transient conditions is not available in literature, as far as experimental data is concerned. The actual mechanisms for the styrene reactor can only be judged by experimentation. Nevertheless, the use of steady state kinetics does illustrate the potential for the implementation of a transient reactor.

4.1.3.1 The iron oxide catalysts for the dehydrogenation of ethylbenzene

Lee[86] carried out an extensive steady state experimentation on commercial styrene catalysts such as Shell 105, Shell 205 and Girdler G-64.

A summary of his work below gives an insight to possible theories on the transient catalysis in a styrene reactor.

(i) For alkali promoted iron oxide catalysts, the steam continuously removes carbonaceous residues, mainly as CO_2 (and maybe CO).

(ii) The steam, as an oxidant, equilibrates iron oxide catalysts to an oxidation state which is highly selective to styrene, reasons for which are not completely understood. After exposure to reaction, the catalyst turns black (Fe_3O_4) the normal state of the reacting catalyst. An equilibrium is created by the hydrogen and the steam:

$$FeO \underset{H_2}{\overset{H_2O}{\rightleftharpoons}} Fe_3O_4 \underset{H_2}{\overset{H_2O}{\rightleftharpoons}} Fe_2O_3$$

This implies that cut off of the reactant feed and introduction of the regenerative steam must shift the above equilibrium. The reduced catalyst is more selective than fresh catalyst, the improvement being very slow and taking place over hundreds of hours.

(iii) The potassium promoter, generally as K_2O or K_2CO_3, greatly increases the selectivity to styrene. Variations in porosity, pore distribution and pore size all affect the intraparticle diffusion and therefore the selectivity.

(iv) The potassium promoter migrates as the catalyst ages. The promoter has a slight vapour pressure that forces it to migrate to cooler parts of the reactor, as well

as the pellet. Therefore the promoter migrates to the centre of the pellet due to slightly lower temperatures in the centre (an endothermic reaction causes this gradient), and also towards the exit of the reactor (under steady state conditions). Therefore, the aged catalyst has a lower activity at the crucial part of the reactor, i.e. the entrance. The transient regeneration, especially by counter-current operation, should enable the retention of the catalyst activity due to the constant temperature forcing. Excessive amounts of potassium promoter at the centre of the pellets also leads to reduced activity. The loss of the promoter results in a 2 - 3 fold increase of specific area and porosity of the pellets.

(v) The promoter is very sensitive to chloride poisoning, and a content of 5 - 25 ppm of organic chlorides in the ethylbenzene feed is adequate to considerably reduce the catalyst activity by 60 - 70%.

4.2 Superheater Commissioning

The first commissioning problem is that of raising the superheater metal emissivity from 0.4 (for shiny stainless steel) to 0.95 (for furnace splotched stainless steel). Before being commissioned on the apparatus, the superheaters are treated in a furnace to 700^{o}C. Then the superheaters are insulated and run at high air flowrates (> 55 kg/hr) and very low power loads (≃ 100 W). Every hour the power load is increased by 100 Watts, until the heaters are running at their full loads (2 kW ratings). Once this has been achieved, the air flowrate is gradually reduced at the rate of 4.5 kg/hr every hour until the required air flowrate region (13.5 - 16 kg/hr) is reached. By now the superheaters are operating in the temperature ranges

required for the plant. SSH2 exit temperature of 650°C is achieved without any difficulty. Examination of the superheaters after the long runs shows that the surfaces are resembling those of furnace splotched metals (dark grey to black colouring). One problem that later commissioning showed is that there is a minimum rate of step up and step down for the superheaters. The first few runs after the emissivity commissioning showed that the firebar ceramic was prone to crumbling if the superheaters were stepped up to full power too soon. The firebar resistance wire did not burn out. Clearly this indicates that the ceramic is being put under stresses during the step up and especially the step down. A study to investigate the rate of temperature rise of the ceramic is required.

4.2.1 Firebar ceramic temperature distribution studies

A model is produced that looks at the rate of the temperature rise across the thickness of the ceramic, and the regime of the high temperature rise is located. A rate of temperature rise is then decided upon. This is then tried out in practice on the superheaters until a suitable step up and step down rate is found. Consider the firebar in Figure 4.10 enclosed in a steel pipe at a temperature T_{WI}. Assume the firebar to be infinitely long (l:r > 100:1). Applying the general equation for a long cylinder to the firebar,

$$\frac{C_p \rho}{k} \frac{\delta T}{\delta \theta} = \frac{\delta^2 T}{\delta r^2} - \frac{1}{r} \frac{\delta T}{\delta r} \qquad (4.2)$$

using the boundary conditions:

$$\text{At } r_I , \frac{\delta T}{\delta r} = 0 \qquad (4.3)$$

$$\text{and at } r_O , k A_x \frac{\delta T}{\delta r} = Q_T - h_r A_s (T - T_{WI}) \qquad (4.4)$$

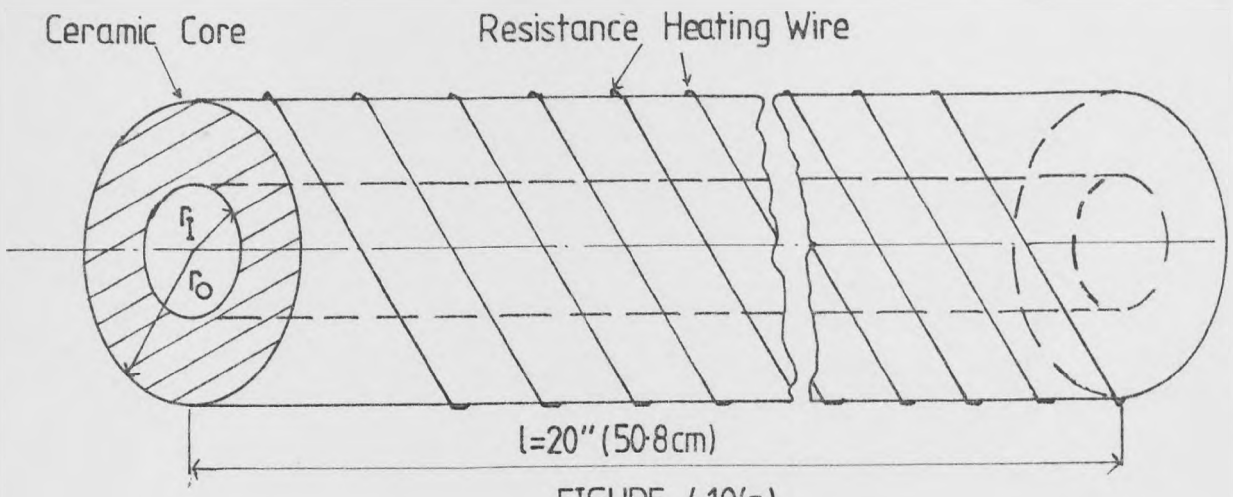

FIGURE 4·10(a)

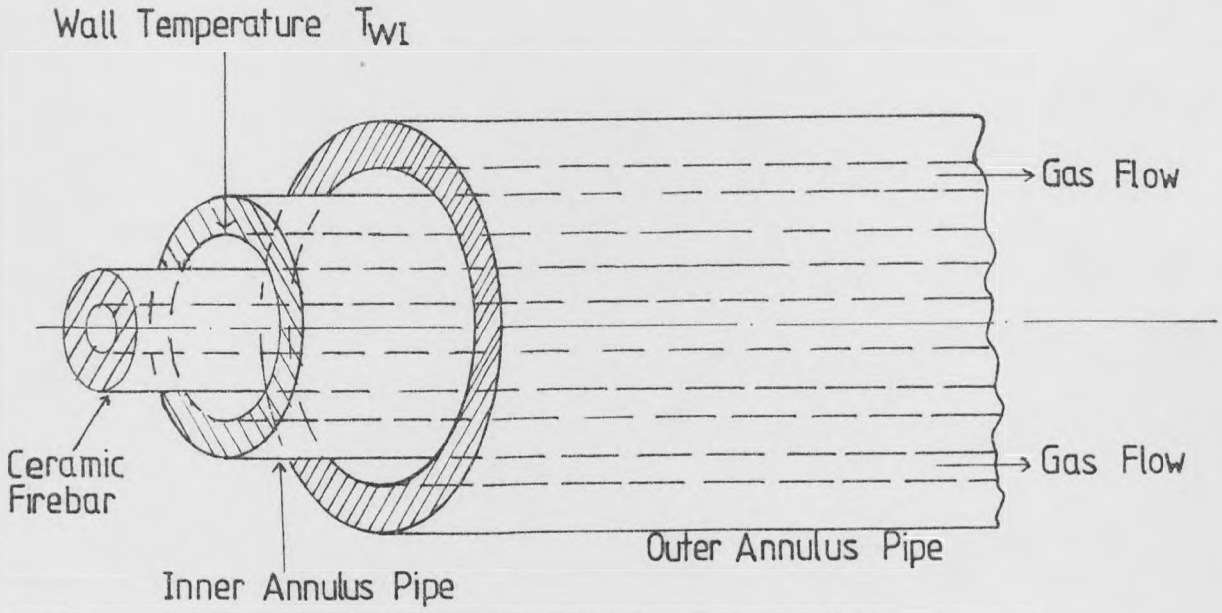

FIGURE 4·10(b)

FIGURE 4.10: The Ceramic Firebar Temperature Distribution Model Notation

with Q_T being the heat load on the firebar resistance wire, that is applied at r_o, along the length of the firebar.

h_R, the radiative heat transfer coefficient is given by:

$$h_R = \mathcal{F}_{FB \rightarrow WI} \frac{\sigma (T_{FB}^4 - T_{WI}^4)}{T_{FB} - T_{WI}} \qquad (4.5)$$

using the emissivities $\varepsilon_{SS} = 0.95$ (for splotched stainless steel) and $\varepsilon_{Ni/Cr} = 0.85$ (for splotched resistance wire).

Equations (4.2), (4.3), (4.4) and (4.5) are solved by Forward Difference Numerical Approximation Technique. The problem here is that as T_{FB} rises so does T_{WI} and hence h_R changes. The program uses the superheater design values in Table 3.6 for T_{WI} and assumes a linear rise in T_{WI} to the steady state value of the superheater design. This gives the "worst case" since the steady state value is not reached in the time it takes to raise the superheater to its full load. Initially, all temperatures are assumed to be at room temperature.

Observations

The highest gradients are observed between the load range 400 - 1200 Watts and the initial time for the complete step up and step down of ½ hour is found to be too large in practice (disintegration of the ceramic occurred). The rate of temperature rise or fall for this period averages to around 50 Centigrade degrees per minute, with a maximum of 150 Centigrade degrees at the inner wall of the ceramic around the 800 Watts region. Clearly, the step up/down time has to be of greater duration After trial runs, the maximum average rate of temperature rise/fall of the ceramic that did not result in a burn out was around 20 Centigrade degrees per minute with a maximum rate of around 60 Centigrade degrees per minute. This meant that the maximum step up time for a 1.5 kW firebar is 1 hour and that for a 2 kW firebar is around 1.3 hours. The step

down time is identical and in reverse method to the step up method. These step up and step down periods have worked successfully ever since without any burn outs, over more than 40 runs.

Note

Although the model showed near identical temperature rise and fall rates for a particular rate of loading or unloading, it is the step down period that really causes the stress on the ceramic, which is released during the next step up period. If the step down rate for any run is too great, then the crumbling of the ceramic is the result at the next loading session.

4.2.2 Run results and efficiencies for the superheater runs (steady state values)

Table 4.3 illustrates the sort of exit temperatures and efficiencies regularly observed for the superheaters. The results are for superheaters insulated with the 15.3 cm thick equivalent of Kaowool blanket (k_{av} = 0.082 W/m K over the range 0 - 750^{o}C). Figure 2.5 shows the positioning of the superheaters on the rig. The efficiency is the ratio of the heat supplied to the flow medium to the heat input to the superheaters, with the difference between the two being the heat lost to the ambient air, or being conducted away across the connecting pipework. The latter loss is the main reason for the lower efficiency of SSH2, compared with SSH1. These superheaters are connected by a short length of pipe (< 45 cm) and are insulated in a common box. Therefore the combined efficiency of the two is a more reliable guide to the overall efficiencies of such superheaters. Combined efficiencies in the range of 0.85 - 0.95 are regularly observed, even with SSH2 (the hotter of the main superheaters) operated at outlet temperatures exceeding 755^{o}C. Operating at such high outlet temperatures leads to a lower efficiency (as Table 4.3 shows for air and steam), but even then the overall efficiency is higher than that of good

TABLE 4.3

Steady State Temperature and Efficiency Results for the Three Major Superheaters

Superheater	Flow Medium	Flow kg/hr	Inlet Temp. °C	Outlet Temp. °C	Q_T Supplied Watts	Efficiency	Combined Efficiency
SSH1	Air	14.3	20°C	420°C	1583.8	0.999	0.901
SSH2	Air	14.3	420°C	660°C	1230.4	0.803	
SSH1	Steam	7.3	115°C	485°C	1583.8	0.992	0.878
SSH2	Steam	7.3	485°C	755°C	1652.1	0.776	
EBSH	Steam	4.0	115°C	560°C	1174.6	0.857	-

fuel gas burner-superheaters (with acceptable efficiencies of 0.8 - 0.85). The worthiness of the radiation superheater for small pilot plants is thus proven.

4.3 Ethylbenzene and Steam Lines Commissioning

4.3.1 Ethylbenzene vaporiser, condenser and pump commissioning

The initial commissioning is carried out using water, enabling the lines to be leak and pressure tested with a safe medium.

The Pump

The pump is calibrated using a 2 bar back pressure valve to substitute for the system pressure. Figure 4.11 shows the almost linear relationship of pump readings versus the volume delivered.

The vaporiser and condenser

These were commissioned with water, using a flow rate that would be equivalent in heat capacity to 2.95 kg/hr (55 cc/min) ethylbenzene for the temperature range of 10^{o}C to 160^{o}C. For water, 16 cc/min was required (Mark 15) and the heat duty required was 436 Watts as opposed to 340 Watts for the ideal case (no heat losses). The condenser flowrate used, 91 litres/hr handled the duty with a rise in coolant temperature of only 5 Centigrade degrees, as per the design. On successful commissioning with water, the Feedtank-Pump-Vaporiser-Condenser-Feedtank loop was successfully commissioned with ethylbenzene. The pump reading of 56 delivered the design flowrate of 55 cc/min. The vaporiser and the condenser produced identical readings, flowrates and duties to that when commissioned with water. Ethylbenzene boiled at 135^{o}C under atmospheric pressure.

4.3.2 Pressure drop calculations for the system

It is necessary to have an estimate of the complete system pressure drop so as to be able to aim for a certain range of settings when the

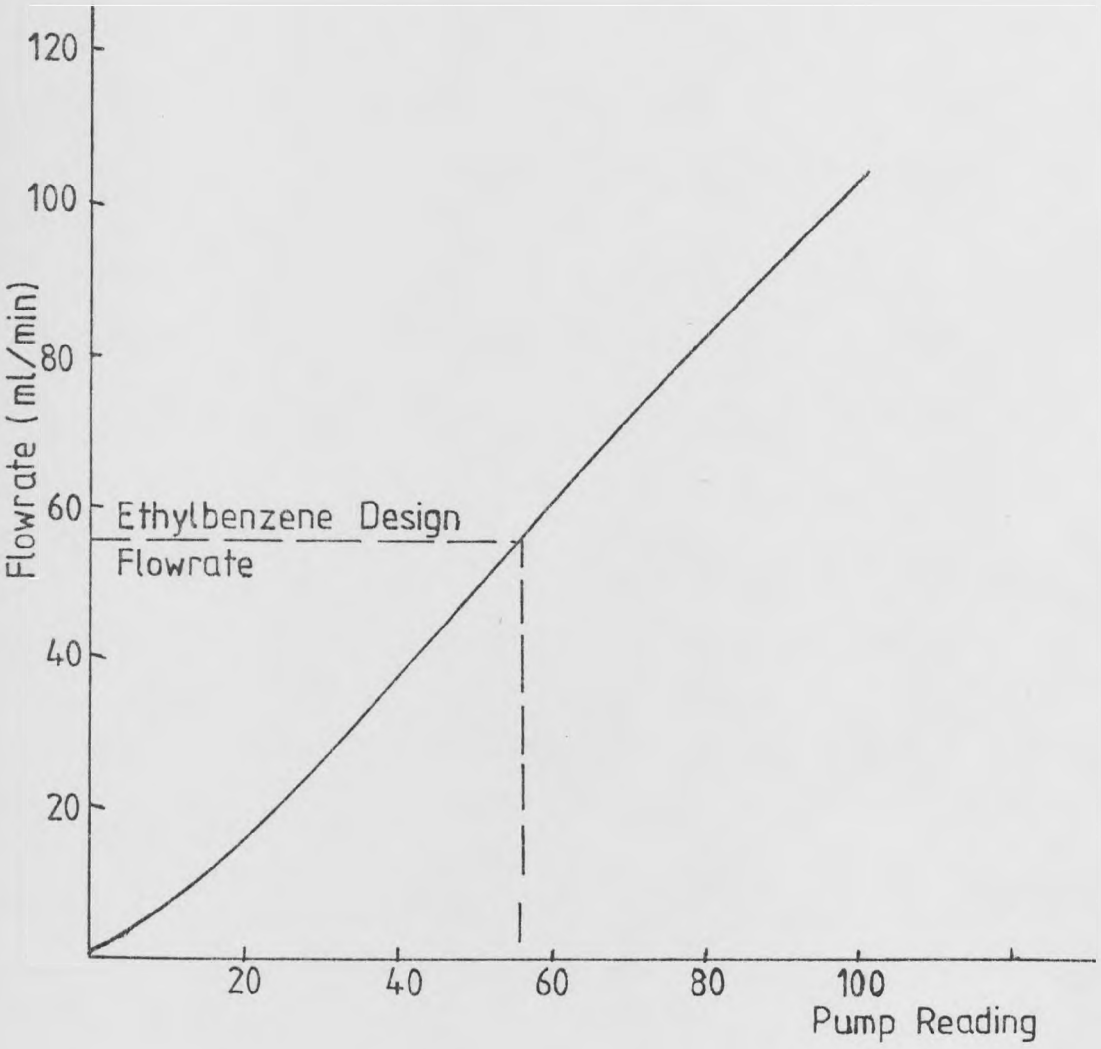

FIGURE 4.11: E-2 Type Metering Pump Calibration Chart

steam pressure regulator valves are being commissioned. Once the system has been built, the number of fittings, valves etc. is known and an exact figure of pipework lengths is known. The calculations assume that all lines carry steam, the medium that will give the highest pressure drop.

The pressure drop along pipes is calculated by the use of charts in Coulson and Richardson[58] which use the Equation (4.6) for various regimes of flow, with ΔP_f being the pressure difference.

$$\frac{F}{\rho u^2}\left(\frac{u d \rho}{\mu}\right)^{-1} = \frac{F}{\rho u^2} Re^{-1} = \frac{-\Delta P_f \mu}{4 \rho^2 u^3 l} \qquad (4.6)$$

The pressure drop along the packed reactor bed is calculated from the Modified Ergun equation of Heggs and Handley[69]:

$$\frac{\Delta P}{L} = \frac{2.63 (1 - e) G_M^2}{\rho e^3 d_p^2} + \frac{1093 (1 - e)^2 \mu G_M}{\rho e^2 d_p^2} \qquad (4.7)$$

For the fittings, e.g. elbows, tees, valves etc., the tables in Coulson and Richardson[58] relating the pressure drop across the fittings in equivalent pipe diameters are used.

The superheaters are modelled as an annulus with 90° elbows at each end. The main condenser is modelled as a straight pipe length, with one 90° elbow pressure drop value added for each complete turn of the condenser helix coil. The condensation traps, pipe reducers and enlargers, orifice plates, reactor cones, mixer nozzles and manifold etc. are all modelled to the venturi contraction and expansion pressure drop correlation from Coulson and Richardson[58]. For a sudden enlargement, the equation is:

$$-\Delta P_f = \frac{\rho u_1^2}{2}\left[1 - \left(\frac{A_{x1}}{A_{x2}}\right)\right]^2 \qquad (4.8)$$

where u_1 and A_{x1} apply to the narrower section.

For a sudden contraction, the Equation (4.8) is again used, but with u_1 and A_{x2} now applying to the wider section.

Tables 4.4, 4.5 and 4.6 tabulate the results of these calculations for the steam line 1 (SL1), steam line 2 (SL2) and the pressure head to be supplied by the metering pump during a reaction run, respectively. To get the maximum conversions, the system pressures should be as low as possible. Hence the steam pressure regulator valves have to be set at values just sufficient to overcome the system pressure losses. But the two steam lines need to be checked for choked flow in order to have a constant flow through both lines. The critical pressure is checked by Equation (4.9) by Kay[53] for steam with $\gamma = 1.3$, and P_* the supply pressure (SL1),

$$\frac{P}{P_*} = \left(\frac{2}{\gamma + 1} \right)^{\gamma/\gamma-1} \qquad (4.9)$$

If SL1 is set at 11.5 p.s.i.g. (1.78 bar) the throat pressure (SL2) works out at 6.3 p.s.i.g. (1.43 bar). Therefore, the two steam line regulator valves are set at the values in the range of those shown in Tables 4.4 and 4.5.

The calculation only aims to show the pressure losses that can be expected. During the actual commissioning, the inlet pressures set are rechecked for choked flow.

4.3.3 Steam line commissioning

The actual settings turn out to be remarkably close to those shown in the calculations, proving that the calculations are an accurate guide.

Pressure regulator valve setting for SL1	11.0 p.s.i.g. (1.75 bar)
Flowrate on SL1 (steam)	7.0 kg/hr
Manometer head (SL1)	9.3 cm Hg
Pressure regulator valve setting for SL2	6.5 p.s.i.g. (1.44 bar)

TABLE 4.4

Calculated Pressure Loss Across the Steam Line SL1

	(p.s.i.a.)	(bar)
Pressure drop across the two reactors	1.39	0.095
Pressure drop across SSH1, SSH2	2.33	0.159
Pressure drop across SSH3	0.52	0.035
Pressure drop across the mixer	1.68	0.114
Pressure drop across the main condenser	0.25	0.017
Pressure drop for all fittings (valves etc.) and pipes	1.53	0.104
Pressure drop across the reactor expansion cones	2.68	0.182
Pressure drop across the reactor contraction cones	0.95	0.065
Total pressure drop to be overcome by steam flow on SL1	11.33	0.771

TABLE 4.5

Calculated Pressure Loss Across the Steam Line SL2

	(p.s.i.a.)	(bar)
Pressure drop across the two reactors	0.75	0.051
Pressure drop across SSH3	0.27	0.018
Pressure drop across EBSH	0.52	0.035
Pressure drop across the main condenser	0.15	0.010
Pressure drop across the pipework and the fittings	1.68	0.114
Pressure drop across the reactor expansion cones	1.42	0.097
Pressure drop across the reactor contraction cones	0.51	0.035
Pressure drop across the mixer	1.30	0.088
Total pressure drop to be overcome by steam flow on SL2	6.60	0.448

TABLE 4.6

Calculated Pressure Head to be Overcome by the Metering Pump

	(p.s.i.a.)	(bar)
Metering pump back pressure valve losses	25.0	1.70
Feedtank cycle pipework and fittings losses	2.1	0.14
Pressure drop across the apparatus (identical formation to the losses on SL2, except the medium is ethylbenzene)	4.8	0.33
Pressure head to be delivered by the metering pump	31.9	2.17

Flowrate on SL2 (steam)	4.0 kg/hr
Manometer head (SL2)	4.1 cm Hg

Table 4.7 shows the flows for which the SL1 regulator has been accurately calibrated. Further flow control is achieved by the control valve downstream (see Appendix A2). The flow on SL2 is just about the smallest that can be controlled. Greater steam flowrates are not required on this line, and so this line is not commissioned for greater flowrates.

TABLE 4.7

Steam Line 1 (SL1) Calibration

Pressure		Pressure Head (cm Hg)	Steam Flowrate (kg hr^{-1})
(p.s.i.g.)	(bar)		
12.0	1.82	11.0	7.87
11.0	1.75	9.3	7.00
10.0	1.68	7.0	6.05
9.0	1.61	4.2	4.59

Steam Relief Valves

These are all set for 7.81 bar and the relief lines are vented to the PMA 6 extractor fan. No problems are encountered during the air/steam switchover once the condensate has cleared the regulator valves. The pressure regulator valves take about ½ hour to settle, mainly due to the small amounts of condensate clearing the valves as the lines warm up to the steam supply temperature. Nevertheless, the flows even during this stabilizing period can be judged to within ± 5% of the desired flowrates. The pressure heads indicated above are used as an initial guide during this stabilizing period.

4.4 Heat Loss Estimation, Calculations and Runs, and Compensation

Heat losses over the piping and the reactor lengths are relatively large and have to be compensated for. The small flowrates make it difficult to judge the extent of the losses through other leaks apart from the loss across the insulation, e.g. heat loss by conduction via metal supports, thermocouple probes, cold ends of the apparatus (acting as fins). Therefore a run is required to compare the calculated expected heat loss across the insulation with the observed heat loss.

The apparatus is set up for the two stage SSAR so as to check heat losses across the four superheaters, the two reactors, and the connecting pipework. Figure 4.12 shows the temperature measuring points for this run. Table 4.8 shows the steady state temperatures observed for the run. The run set out to achieve exit temperatures from SSH2 in excess of 650^{o}C. The calculations are split up into 5 zones for the heat loss estimation (see Figure 4.12):-

Zone 1: SSH2 Out to Reactor A Top

Zone 2: Reactor A Top to Reactor A Base

Zone 3: Reactor A Base to SSH3 In

Zone 4: SSH3 Out to Reactor B Top

Zone 5: Reactor B Top to Reactor B Base

4.4.1 Observed and calculated heat losses for the apparatus (see Figure 4.13)

The observed heat loss for each of the above zones can be calculated from:-

$$Q_{obs.} = M_G C_{PG} \Delta T \qquad (4.10)$$

The calculated heat loss is worked out from:-

$$Q_{calc.} = U A_S \Delta T_{ln} \qquad (4.11)$$

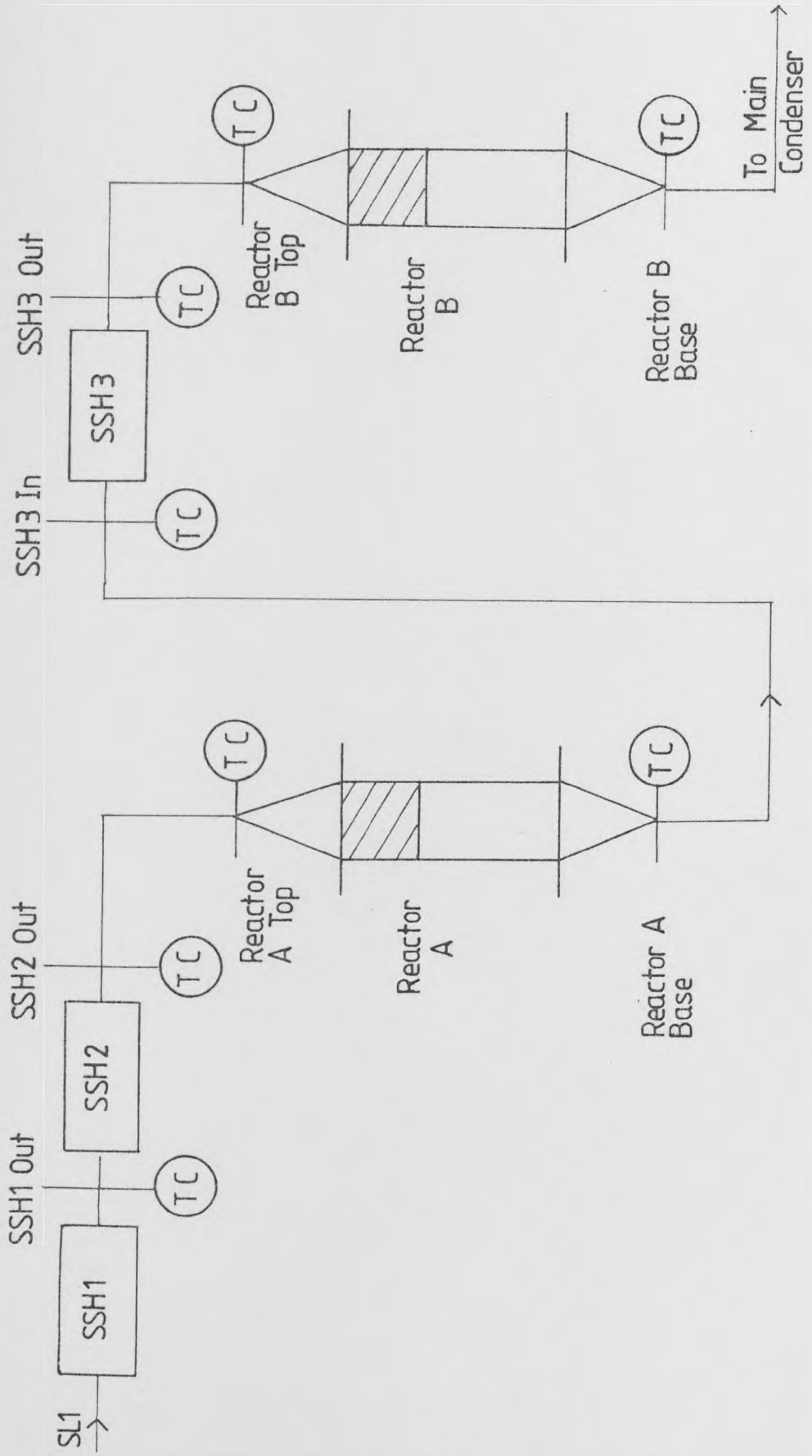

FIGURE 4.12: Location of the Temperature Probes for the Heat Loss Estimation Run

TABLE 4.8

Results for the Heat Loss Estimation Run

SSH1 Out (°C)	SSH2 Out (°C)	SSH3 In (°C)	SSH3 Out (°C)	Reactor A		Reactor B		Average Insulation Surface Temp.
				TOP (°C)	BASE (°C)	TOP (°C)	BASE (°C)	
395	670	640	295	450	300	510	340	40°C

where

$$\Delta T_{ln} = \frac{T_{OUT} - T_{IN}}{\ln\left(\frac{T_{OUT} - T_A}{T_{IN} - T_A}\right)} \qquad (4.12)$$

with air flowrate for the run = 14.6 kg/hr

average ambient temperature = $25^{\circ}C$ = T_A

average insulation surface temperature = $40^{\circ}C$ = T_S.

The overall heat transfer coefficient is calculated from (see Figure 4.13),

$$U = \frac{1}{\frac{r_3}{r_1 h_I} + \frac{r_3 \ln (r_2/r_1)}{k_w} + \frac{r_3 \ln (r_3/r_2)}{k_{Ins.}} + \frac{1}{h_o}} \qquad (4.13)$$

Calculation of outside heat transfer coefficient, h_o

This is the sum of the radiative, and the horizontal and vertical natural convection heat transfer coefficients:-

$$h_o = h_R + h_{NC}$$

where h_R is the radiation heat transfer coefficient,

$$h_R = \varepsilon_G \sigma \frac{(T_S^4 - T_A^4)}{(T_S - T_A)} \qquad (4.14)$$

(ε_G = Gray body emissivity for a small body in an enclosed atmosphere = 0.9).

and h_{NC} is the natural convection heat transfer coefficient. Depending on whether the pipes are vertical or horizontal, h_{NC} is calculated as below: h_{CV} is the natural convection heat transfer coefficient for the vertical section and is calculated from:-

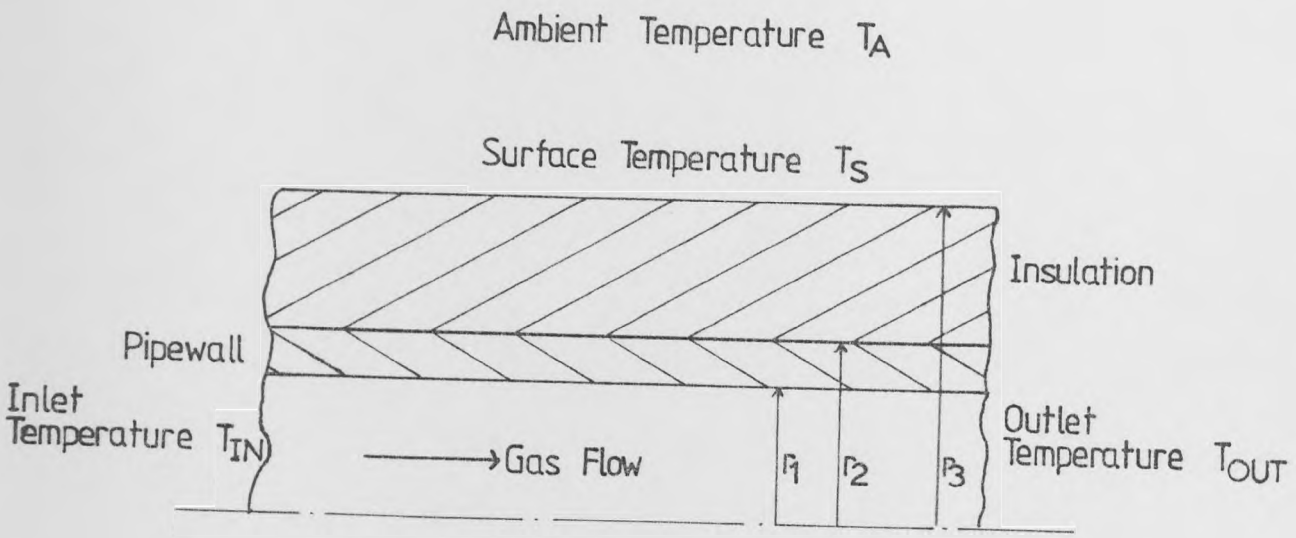

FIGURE 4.13: Model Notation for the Heat Loss Calculations Along the Various Apparatus Sections

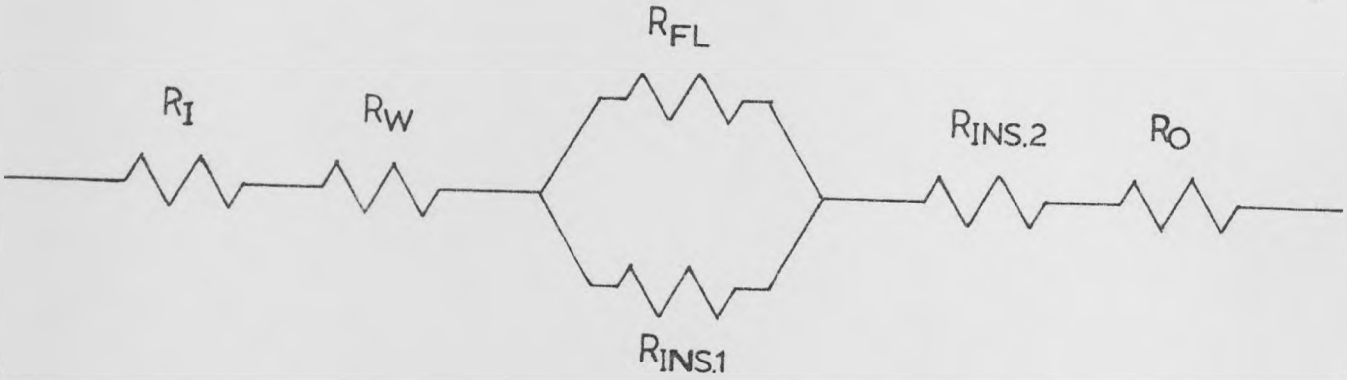

FIGURE 4.14: The Heat Transfer Resistance Network for the Reactor Bed, the Cones and the Flanges

$$\frac{h_{CV}\, L}{K} = Nu_L = 0.13\, [\text{Gr. Pr.}]^{0.33} \quad \text{for Gr} > 10^9 \qquad (4.15)$$

and $$Nu_L = 0.59\, [\text{Gr. Pr.}]^{0.75} \quad \text{for } 10^4 > \text{Gr} > 10^9 \qquad (4.16)$$

and h_{CH} is the natural convection heat transfer coefficient for the horizontal section and calculated from:-

$$Nu_D = \frac{h_{CH}\, D}{K} = 0.53\, [\text{Gr. Pr.}]^{0.25} \quad \text{for Gr} > 10^9 \qquad (4.17)$$

and $$Nu_D = \frac{h_{CH}\, D}{K} = 0.4\, [\text{Gr. Pr.}]^{0.25} \quad \text{for } 10^4 > \text{Gr} > 10^9 \qquad (4.18)$$

For pipe lengths which involve both horizontal and vertical piping use the smaller value of h_{CV} or h_{CH} as h_{NC}. Further details can be found in McAdams[65].

Calculation of the gas heat transfer coefficient, h_I

The Equation (4.19) from McAdams[65] is used for turbulent flow in pipes:

$$Nu = \frac{h_I\, D}{K} = 0.023\ Re^{0.8}\ Pr^{0.33} \qquad (4.19)$$

For packed reactor beds, the Heggs and Handley[69] correlation is used:-

$$St.\ Pr^{0.67}\ e = j_h\, e = 0.26\ Re_m^{-0.33} \qquad (4.20)$$

with the packed section having a modified Reynolds Number, Re_m, of 260.

Calculation of the heat transfer resistances for the reactor cones and flanges

As shown in Figure 4.15a the reactor cones and flanges create problems in evaluating the heat transfer resistances for the heat loss estimation calculations. Figure 4.15b shows how this model is simplified by assuming the cones as straight lengths of pipe (hence the worst case is assumed) Figure 4.14 shows the resistance network diagram from which Equation (4.21) is generated for working out the overall heat transfer coefficient:-

$$\frac{1}{U\,A_S} = \frac{1}{h_I\,A_{SI}} + \frac{\ln\,(r_2/r_1)}{2\pi\,k_W\,L} + \left\{\frac{R_{fl}\,R_{INSl}}{R_{fl}+R_{INSl}}\right\} + \frac{\ln\,(r_4/r_3)}{2\pi\,k_{INSl}\,L} + \frac{1}{h_o\,A_{SO}} \qquad (4.21)$$

where $R_{INSl} = \dfrac{\ln\,(r_3/r_1)}{2\pi\,k_{INS}\,(L-2l_o)}$ and $R_{fl} = \dfrac{\ln\,(r_3/r_2)}{2\pi\,k_{INS}\,2l_o}$

Table 4.9 shows the results of the observed and the calculated heat losses in accordance with Equation (4.10) and (4.11). Zones 2, 4 and 5 show that the calculated heat losses are close (within 10%) to the observed heat losses. The observed heat loss on Zone 1 is much greater than the calculated loss. This is found to be due to the "cold" zone, i.e. the EBSH to the mixer line that was not used for this run. Acting as a fin, this contributes to 0.2 kW of the heat loss observed. (Calculation as per Kreith[55] for infinitely long fins). The heat loss observed on Zone 3 is much smaller than the calculated loss. This can only be due to the heat transfer from the hotter superheaters SSH1 and SSH2 through to SSH3 as they are all enclosed in a common superheater box. The irregular shape and packing of the insulation makes it difficult to estimate this heat leak. Nevertheless, the calculation of the anticipated heat losses does give very good results, which are accurate enough for basing the

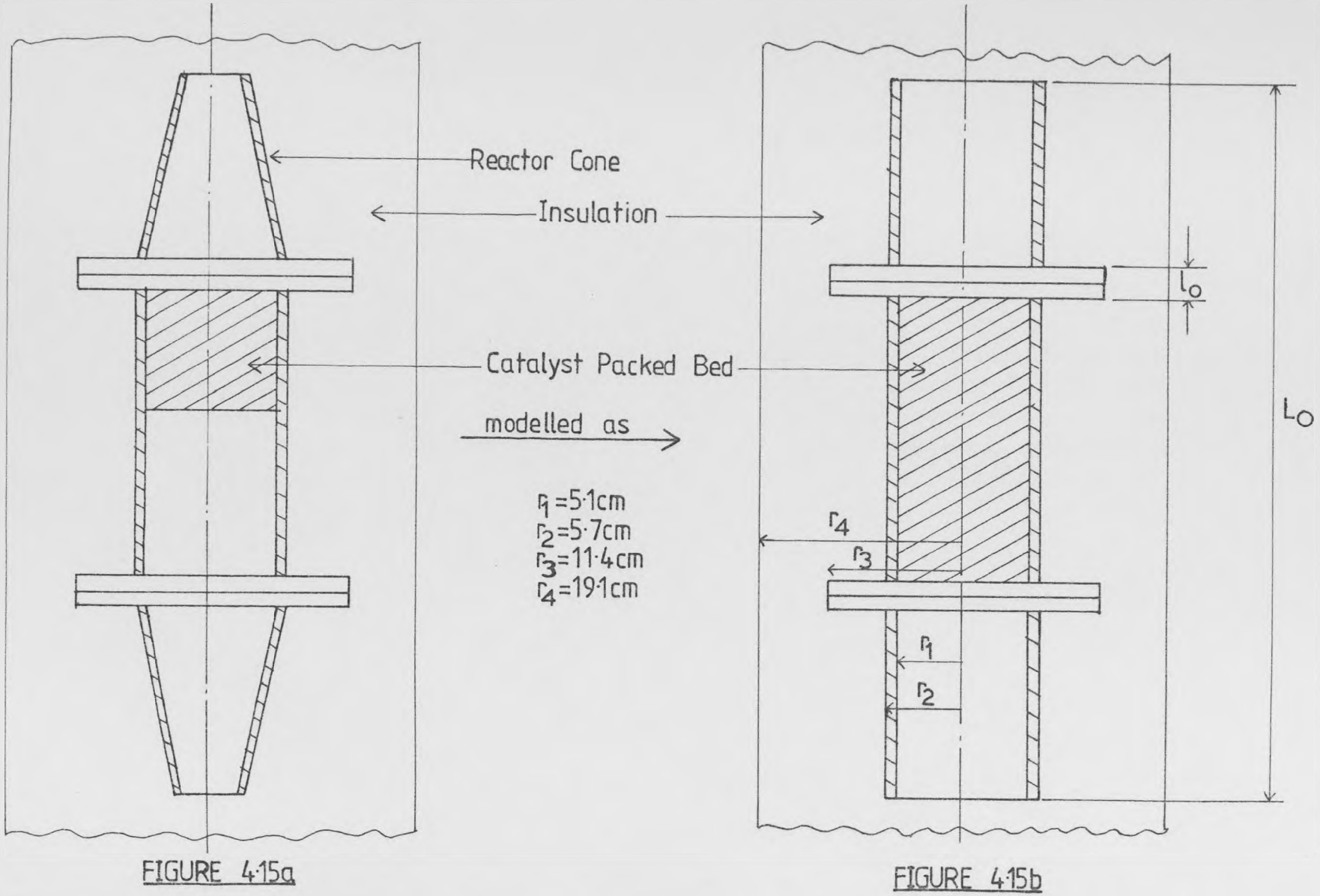

FIGURE 4·15a

FIGURE 4·15b

FIGURE 4.15: The Reactor Bed and Cone Models for the Heat Loss Calculations

TABLE 4.9

Calculated and Observed Heat Losses for the Various Sections of the Apparatus

Zone	U ($W/m^2\ ^oC$)	A_S (m^2)	Calculated Heat Loss ($U A_S \Delta T$) (kW)	Observed Heat Loss ($M C_p \Delta T$) (kW)
1	0.511	2.33	0.631	0.972
2	0.817	2.18	0.615	0.645
3	0.602	1.43	0.235	0.021
4	0.602	1.97	0.644	0.586
5	0.818	2.20	0.703	0.739

decisions of the compensation of the heat loss upon these calculations. The calculated heat losses in Table 4.9 need to be scaled up to the log mean temperatures that are to be maintained, in accordance with the initial design. Table 4.10 shows the heat duty that the compensation method will have to sustain.

Estimation of the losses on the EBSH to the mixer

The very long length of piping on this line (≃ 6 m), the low flow-rate (4.0 kg/hr steam, 2.95 kg/hr ethylbenzene) and the relatively lower superheater exit temperature (520 - 540°C) suggested that the use of this line for the heat loss estimation run would have resulted in lower reactor temperatures. This would make it difficult to estimate the heat loss for each individual zone. Hence the actual run did not incorporate gas flow on the EBSH → Mixer line. Nevertheless, the heat loss can be calculated from Equation (4.10), assuming that the full 6 m of piping has to be maintained at 540°C. The heat loss to be compensated works out at 0.651 kW.

The next section deals with the means and methods of the compensation of this heat loss on all six zones.

4.4.2 Method of compensation of the heat losses

A cheap and efficient method would be to wrap a length of ceramic 'fish' bead insulated resistance heater wire along the outside of the pipe walls and provide the heat duty across these windings. The use of such a winding between the metal walls and the insulation adds a resistance to heat transfer which cannot be easily estimated. Nevertheless, this resistance should lower the compensation duty required. The windings are designed to supply the duties calculated in the previous section, and the provision of voltage regulators to the heater circuits can manipulate the actual duty required. It is proposed to utilize three such windings as an initial study. No winding is necessary to compensate the heat loss

TABLE 4.10

Scaled Up Heat Losses Calculated for the Various Sections of the Apparatus

Zone	Calculated Heat Loss from Table 4.9 (kW)	Design Log Mean Temperature (^{o}C)	Scaled Up Heat Loss to be Compensated (kW)
1	0.631	725	0.755
2	0.615	625	1.121
3	0.235	605	0.521
4	0.644	605	0.743
5	0.703	625	1.121

on section 3 (Reactor A Base to Superheater SSH3) since there is more than adequate power (2 kW) capacity on SSH3 to supply the 0.651 kW duty for this section. It is proposed to use one winding (RAW) to cover the length of Zones 1 and 2, i.e. to cover from SSH2 Outlet to Reactor A Base (see Figure 4.16). Another such winding (RBW) covers the length of Zones 4 and 5, i.e. covers from the SSH3 Outlet to the Reactor B Base (see Figure 4.16). The third winding (EBW) will compensate the heat losses for the EBSH Outlet to the Mixer pipelength (see Figure 4.16).

Selection of the heating wire gauge and lengths

The heating wire length should be:-

(a) long enough to provide adequate coverage for the turns per metre that is considered desirable. Initially 15 turns per metre is used.

(b) capable of carrying the manufacturer's design recommendations for maximum surface loading of 5 - 6 W/cm^2 [49,52] for free air use, and capable of carrying the full compensation design load.

Surface loading of the resistance wire

According to the Kanthal Handbook[49], no reliable data is available but it recommends a maximum value of 5 - 6 W/cm^2 for use in free air.

An iterative calculation is needed to balance the surface loading possible versus the resistance required to produce the duty off the 240 V supply. (The resistance of the length must not exceed the resistance rating of 240 V). Table 4.11 shows the wire gauge, resistance, length and power rating for the three suggested windings. Note that for EBW, the winding will be used as a reheater rather than as a compensation heater because the pipe length to be covered is in excess of 6 m. A

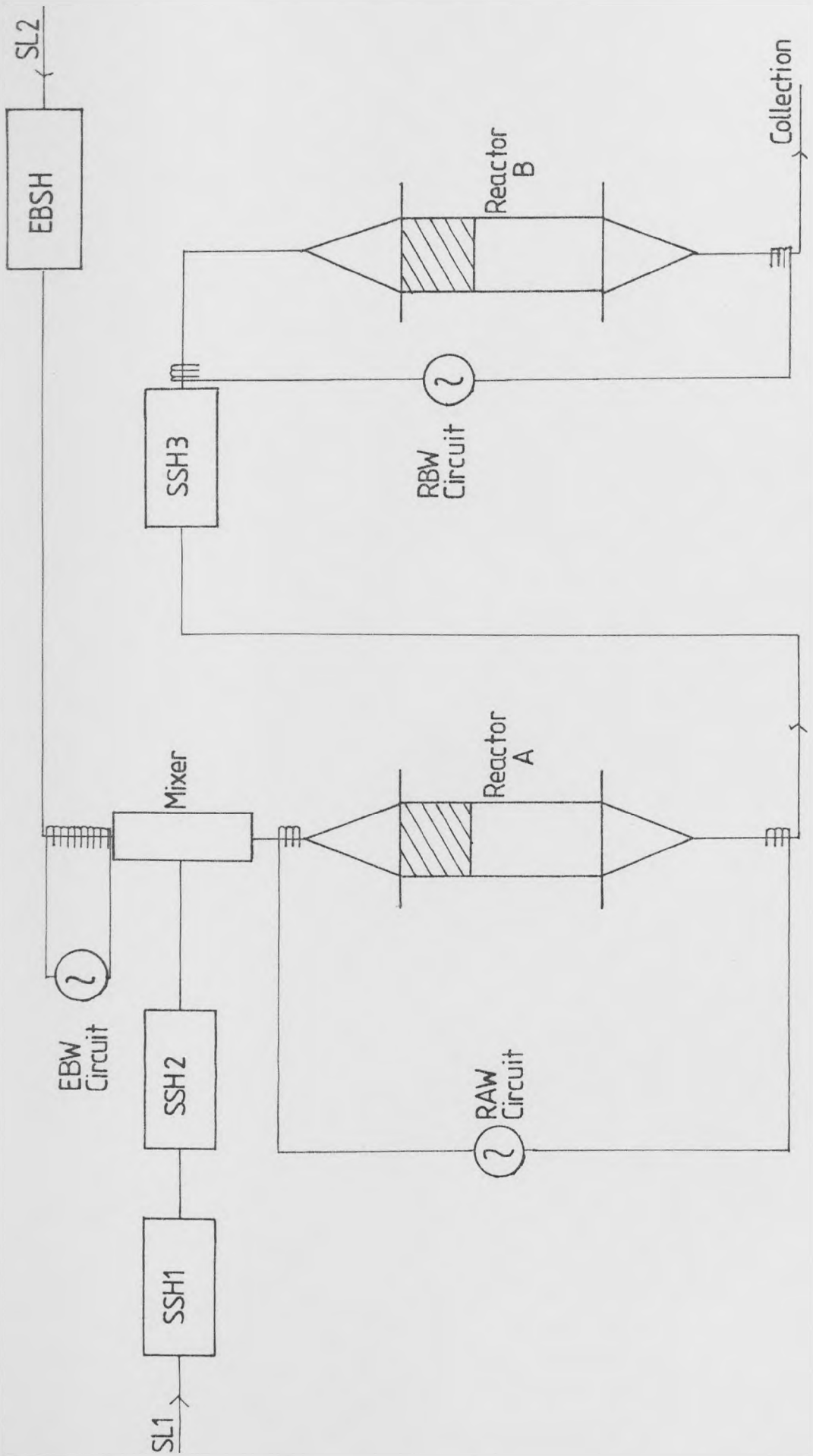

FIGURE 4.16: Location of the Three Heat Compensation Winding Heaters RAW, RBW and EBW

TABLE 4.11

Resistance Wire Ratings for the Heat Compensation Heaters

Winding	Maximum Power Rating (W)	Resistance (Ω)	Minimum Wire Gauge (Imperial)	Minimum Wire Diameter (cm)	Length of Wire (metres)	Wire Type (80/20 Nickel/Chromium)
RAW	2000	57.6	20 S.W.G.	0.091	14.0	Kanthal A-1 or Ghlom
RBW	2000	57.6	20 S.W.G.	0.091	14.0	Kanthal A-1 or Ghlom
EBW	1000	28.8	23 S.W.G.	0.061	10.0	Kanthal A-1 or Ghlom

compensation heater spread out over 6 m of piping would be difficult and very laborious to install, and difficult to re-wire in case of a burn out. The winding is to be spread out over the 2 metres before the mixer. Once installed, commissioning of the three windings can commence.

The next chapter deals with the achieving of the required temperature profiles along the pipework and the reactor beds.

CHAPTER 5

THE ACHIEVEMENT OF THE SYSTEM OPERATING TEMPERATURES

CHAPTER 5

THE ACHIEVEMENT OF THE SYSTEM OPERATING TEMPERATURES

Introduction

The suggested method (Section 4.4) for compensating for the heat losses by using ceramic bead insulated windings is unsuccessful due to the low system flowrates and low transfer areas. In addition, it is very difficult to determine the heat transfer resistances between the winding and the pipe wall. It is anticipated that these are relatively large and so the winding can only be operated at very low loads.

A novel heat shield sandwich method using a copper metal plate heated by the resistance wire and sandwiched between two layers of insulation is successful for operation of shields up to 620°C. Analytical studies are also carried out to examine the profiles produced by such heating methods.

Commercial heating tapes are commissioned for use on lines requiring temperatures greater than 620°C. These quartz based tapes are expensive and untried at such high temperatures using low flowrates and low transfer areas. A combination of the heating tapes and the copper shields succeeds in achieving reactor temperature of up to 635°C.

5.1 An Outline of the Methods Used to Achieve the System's Temperature Profiles

Most of the recent industrial process patents[24,91] tend to specify the temperature range 560° - 650°C as that for economical industrial operational zone. Therefore, the experimental apparatus must operate in this range. In particular, the range 580 - 630°C is important as Bogdanova's data[33], on which Cockcroft's 'derived kinetics'[10] are based, is confined to this temperature regime.

The method suggested in Section 4.4 turns out to be inadequate to

compensate the heat losses due to the high resistance between the ceramic insulating beads, the wire and the contacting surfaces. Amos et al[92] at Union Carbide indicate the difficulties of heat tracing on pilot plants. The low transfer areas and flowrates make it difficult to judge the limitations of industrial tracing tapes. Electrical heating of the reactor wall itself, as used by Amos et al[92] has not only sealing and electrical insulation problems as far as this apparatus is concerned, but is impractical as the supply lines cannot handle the current loads required (> 250 A). Therefore, a heat shield consisting of a bead insulated winding, covered by a copper plate, and sandwiched between insulation layers is mathematically modelled and tested out. It proves successful for operation up to 620°C. Therefore these shields can be implemented on the EBSH to the Mixer lines, where the maximum temperature is 540°C. A catalyst temperature of 560°C is achieved using copper shields on all lines that need heat shielding. This is only on the brink of the reacting zone.

After one unsuccessful attempt at utilizing industrial heating tapes, a maximum reactor temperature of 635°C is possible using a combination of tracing tapes on the hotter lines (SSH2 to the Mixer, and the Reactor itself) where there are comparative higher flows, and copper shields on the less hot, lower flow lines (EBSH to the Mixer).

Figure 5.1 summarises the results of Run 42, where RAW and S2MW are tracing tapes, and EBEW and EBCW are copper shields. The manufacturers claim a limit of 800°C for the expensive tracing tapes, but as no mention is made of the transfer resistances and areas, it is a matter of experimenting with them to check their claims. Since at present the study can proceed within the temperature range already achieved, no further experimentation and burn out risks need be taken. Perhaps a future study could aim for higher loads on these tapes, already checked for operation up to 710°C.

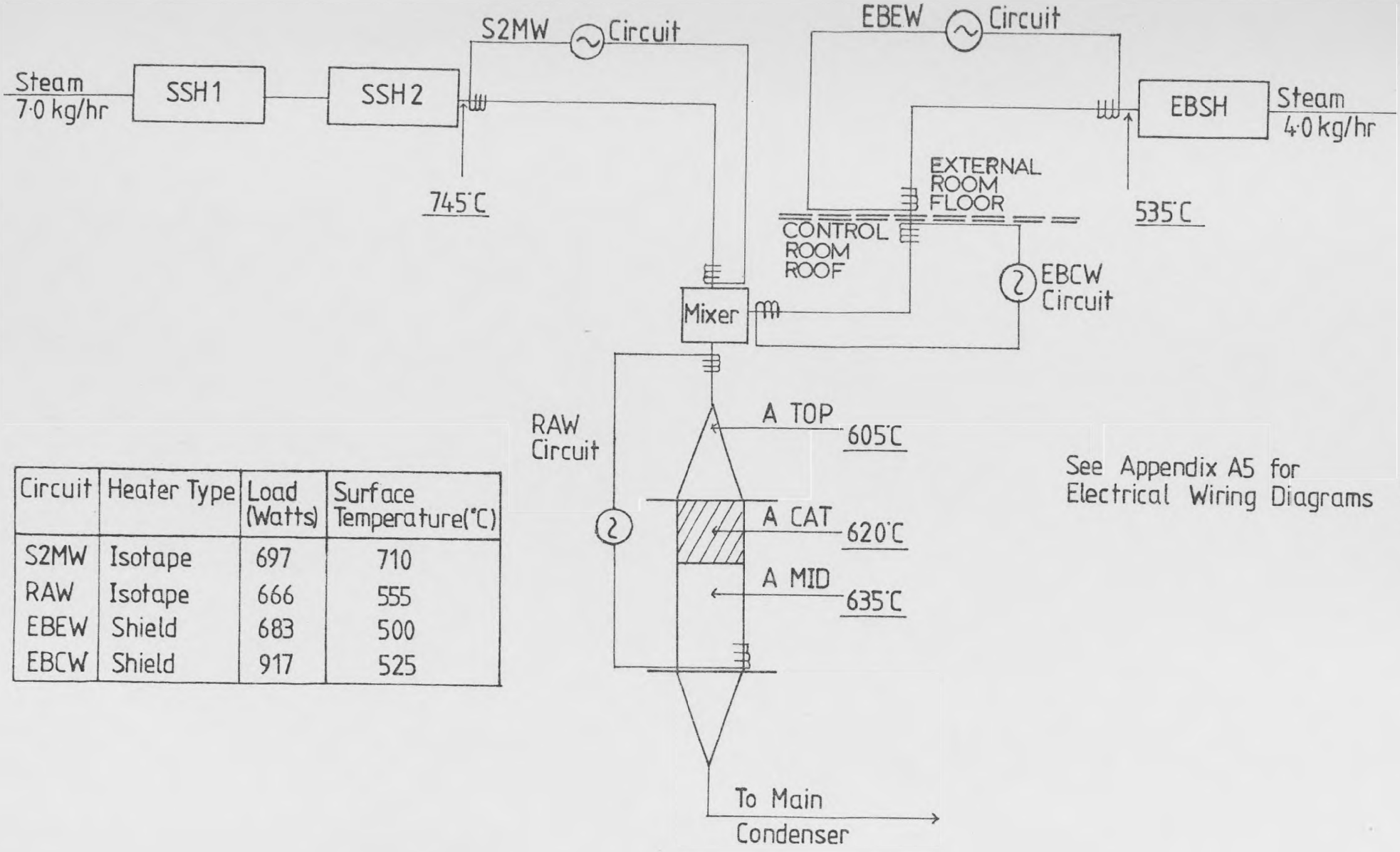

Circuit	Heater Type	Load (Watts)	Surface Temperature(°C)
S2MW	Isotape	697	710
RAW	Isotape	666	555
EBEW	Shield	683	500
EBCW	Shield	917	525

See Appendix A5 for Electrical Wiring Diagrams

FIGURE 5.1: Summary of Results for Run 42

Section 5.2 deals in detail with the numerous runs and mathematical studies carried out during the commissioning for achieving the system temperature levels. Tables 5.1 - 5.3 summarise these runs and their achievements.

5.2 Detailed Description of Experimental Runs and Studies for the Achieving of the System Temperature Levels

Tables 5.1, 5.2 and 5.3 are a summary of these runs and should be referred to for the corresponding runs.

5.2.1 Experimental runs using bead insulated resistance windings in contact with the pipe walls

Run 21

Two windings, RAW and EBW (see Figure 4.16) were used. RBW was not utilized as it duplicates the RAW situation. Air at 14.3 kg/hr on line SL1, and 8.05 kg/hr on line SL2 was used to achieve outlet temperatures of 710°C from SSH2 and 540°C from EBSH. The full apparatus was allowed to reach steady state. The catalyst temperature was 350°C. RAW and EBW were gradually loaded in steps of 50 W, ensuring that the catalyst temperature was rising by at least 5 Centigrade degrees every 15 minutes. EBW burnt out, but RAW was still operational. AT EBW burn out, the catalyst temperature was 475°C. The burn out was at a ceramic junction box (Both RAW and EBW were wound in 2 metre lengths to ease the replacement of any burnt out lengths). Both RAW and EBW were reinsulated as a single length winding of 12 metres. No. 3 'Quickline' ceramic insulating beads were used.

Run 22

The run procedure used was identical to Run 21. This time both RAW and EBW burnt out. The catalyst temperature had been raised to 490°C. The uneven transfer areas on the SSH2 to Reactor A pipework may have contributed to the uneven loading on RAW. It was decided to split RAW into

TABLE 5.1

Summary of the Highest Temperatures Achieved for Runs 21 - 26

Run No.	Medium	SSH2 Out Temp. (°C)	EBSH Out Temp. (°C)	RAW Load (W)	EBW Load (W)	S2MW Load (W)	Maximum Catalyst Temp. (°C)	Comments
21	Air	710	540	1218	180	-	475	EBW burn out at 180 W
22	Air	710	550	1099	545	-	490	EBW burn out at 545 W RAW burn out at 1099 W
23	Air	550	280	100	100	100	250	S2MW burn out at 100 W. Results are at burn out, not at steady state.
24	Air	570	-	-	-	55	350	S2MW burn out at 50 W
25	Air	710	-	-	-	25	345	S2MW burn out at 25 W
26	Air	720	-	-	-	800	450	S2MW, a 'copper shield sandwich', can sustain high duties.

TABLE 5.2

Maximum Temperatures Achieved Using Copper Shields on S2MW and RAW

Run No.	Medium	SSH2 Out Temp. (°C)	EBSH Out Temp. (°C)	S2MW SHIELD		RAW SHIELD		EBW Load (W)	Maximum Catalyst Temp. (°C)	Comments
				Load (W)	Temp. (°C)	Load (W)	Temp. (°C)			
27	Air	720	540	1065	620	-	-	200	450	S2MW shield compensating well enough. No burn outs.
29	Air	720	535	1080	610	1141	605	235	530	S2MW burn out at 1151 W and 630°C. The shields are showing significant effects.
30	Air	720	540	470	350	795	440	-	470	This run confirms the accuracy of the thermocouple readings
31	Air	720	545	1076	615	1218	615	545	550	S2MW burn out at 1100 W and 625°C. EBW burn out at 580 W.
32	Air	725	540	1132	620	1218	610	520	550	S2MW burn out at 1132 W and 620°C. Very little change fron the last run.

TABLE 5.3

Maximum Temperatures Achieved Using Copper Shields and Tracer Tapes

Run No.	Medium	SSH2 Out Temp. (°C)	EBSH Out Temp. (°C)	S2MW Shield/Tape		RAW Shield/Tape		EBEW Shield		EBCW Shield		Reactor A Temperatures (°C)			Comments
				Load (W)	Temp. (°C)	Load (W)	Temp. (°C)	Load (W)	Temp. (°C)	Load (W)	Temp. (°C)	TOP.	CAT.	MID.	
33	Steam	720	560	1129 (Tape)	640	1141	595	942	300	906	450	550	560	565	Sudden burn out on S2MW after operating at st. state for 5 hours.
34	Steam	710	550	1133	600	1067	600	906	300	945	540	545	550	565	'Double sandwich' method is no improvement.
37	Steam	735	540	738	605	1298	600	945	370	875	535	550	555	565	Heat sink still apparent around EBEW.
39	Steam	735	540	369 (Tape)	650	1089	575	683	485	945	525	560	560	560	RAW burn out due to shield oxidation and wire fatigue.
40	Steam	740	535	548 (Tape)	700	666 (Tape)	500	683	490	917	510	595	600	605	Isotapes and copper shield combination achieves reactor temperature range.
42	Steam	745	535	697 (Tape)	710	666 (Tape)	555	683	500	917	525	605	620	635	Apparatus run for 6 hours at this steady state without problems.

two windings, RAW (from the mixer to Reactor A Base) and S2MW (from SSH2 to the mixer). Both windings were designed as per Section 4.4 for 2 kW duties using 'Ghlom 80/20' alloy resistance wire[52]. Figure 5.1 shows the location of S2MW and RAW.

It was apparent at this stage that the commissioning was going to be a difficult and tricky process, and so it was decided to confine the commissioning to Reactor A only.

Run 23

Windings RAW, S2MW and EBW were loaded to around 100 W after SSH2 exit temperature had exceeded 350°C. S2MW burnt out with the SSH2 exit temperature having hardly achieved 550°C. Clearly if S2MW, the winding with the hottest surface cannot handle the low wattage, then this can hardly be a successful method for heat loss compensation. Experimental studies were thus limited to S2MW.

Run 24

Using a similar procedure to Run 23, the S2MW load was increased in steps of 25 W (the minimum load at switch on is around 25 W), allowing at least ½ hour between step ups. S2MW burnt out at a load of 50 W, with SSH2 outlet temperature around 570°C. For the next run, allow steady state to be reached in the complete system before using the smallest possible load on S2MW. This should check the theory that the transient state is contributing significantly to these low wattage burn outs. A different alloy, 'Kanthal A'[49] was used for the windings. 'Kanthal' has a maximum operation temperature of 1200 - 1250°C, as compared to 1100 - 1150°C for the 'Ghlom' alloy so far used[52].

Run 25

The full apparatus was allowed to reach steady state (SSH2 Outlet of 710°C, catalyst temperature of 345°C) before the minimum possible load

of 25 W was applied across S2MW; S2MW burnt out within 20 minutes. Since the best resistance alloy cannot sustain even a very low wattage, some mathematical models and solutions need to be developed to examine the transfer resistances in the system. Clearly the wire temperature must be exceeding 1200°C, whilst the maximum process temperature is not greater than 710°C. These high heat transfer resistances need to be reduced, or compensated for, if the system temperatures are to be raised to the required levels.

5.2.2 Mathematical solutions examining the transfer resistances

The first solution (Model 1, Appendix A4.1) is used to examine the effect of varying the heat transfer resistances on either side of the ceramic bead insulated resistance wire. The results show that the improvement in the heat load the wire can sustain is small relative to the heat duty required for loss compensation. This model shows that it is impossible to use a 12 m length of winding for this compensation.

However, the use of a copper plate to form a continuous metal shield on top of this resistance wire, shows the possibility of an effective heat shield. Model 2 (Appendix A4.2) examines the duty required for such a shield. The effect of varying the thickness of the copper plate, and the positioning of the heat shield is also checked, and the best positioning of the thinnest sheeting available is then checked for temperature peaks and troughs prior to the actual testing of the shields.

Model 3 (Appendix A4.3) examines the temperature peaks and troughs assuming a uniform distribution of the heat load along the resistance wire. The temperature troughs turn out to be small (less than 5 Centigrade degrees for a shield temperature of 700°C). Therefore the shield can prove an effective method of heat loss compensation.

Model 4, the 'Power Ring Model' (Appendix A4.4) looks at the case whereby the shield is heated by a set of circular power rings uniformly

spaced, with an equal heat load distribution. This model, the "worst case", shows the difference between the peaks and troughs to be no more than 8 Centigrade degrees around 700°C.

The copper shield method now needs practical testing to verify the conclusions of the numerical study.

5.2.3 Experimental runs using the copper shields, and tracer tapes

Run 26

This was a trial run using a copper shield on S2MW. The procedure was similar to that of Run 25. The shield was placed between two 5 cm Kaowool insulation layers, and the aim was to load at least 800 Watts on the shield. Continuous operation over a number of hours was possible and the catalyst temperature was lifted to 450°C. It was decided to install three thermocouples along the shield to check the temperature distribution along the shield. Care was taken to avoid any contact of the resistance wire with the thermocouples.

Run 27

Initially the SSH2 to the Mixer line was allowed to reach steady state (as per Run 25) with the S2MW shield non-operational. This would allow real values of the heat transfer coefficients to be calculated from the temperature readings and used in all modelling studies (Appendix A4). The heat shield was gradually heated up and an average shield temperature of 600 - 700°C was aimed for. Table 5.2 shows the results. The variation in the observed shield temperatures was no more than 10 Centigrade degrees. EBW was also stepped up to 200 W. The catalyst was lifted to 450°C this time with flow of air on the EBSH → Mixer line (not used in the previous run). For the next run, a copper shield was installed from the mixer to the base of Reactor A (RAW). The cones and flanges required special shapes to be cut out ensuring a 5 cm gap for the insulation. Thermocouples

were also installed to check the shield temperatures at four points. The wire was 'Ghlom' 80/20 alloy of 18 metres length, designed to handle up to 2 kW. The longer length was needed to keep to the spacing used in the modelling studies (Appendix A4) of one turn every 5 cm of pipework. The next run would operate S2MW and RAW shields around shield temperatures of 600 - 650°C. Higher temperatures are not to be attempted on S2MW until the accuracy of the thermocouple measurements is certain.

Run 29

The procedure used was standard, i.e. allow the full system to steady state before loading the shields. Once the shields had exceeded 550°C, the rate of the loading was reduced to around 25 W every 30 minutes so as to assess the approach to steady state. A catalyst temperature of 530°C was achieved with S2MW at 610°C, RAW at 605°C (average temperatures showed a spread of less than 15 Centigrade degrees), and EBW loaded to 235 W. S2MW burnt out at the next step up (630°C, 1151 W). The burn out could be due to the shield temperature being higher than indicated by the thermocouples (due to bad contact), or the heating wire to copper shield resistance. The next run checked the accuracy of the thermocouple readings, using lower shield temperatures than this run.

Run 30

The heat loss calculations in Section 4.4 served as a guide to the thermocouple effectiveness. Lower shield temperatures of 350 - 450°C were aimed for to check the heat loads being used, as compared to the calculated heat loss. The previous run was also used for this heat loss check (at higher temperatures). The run investigated steady state temperatures for S2MW at 350°C and RAW at 440°C. The calculated heat loss for both shields is around 1250 W, and 1650 W for the previous run. For the previous run, S2MW would account for around 990 W. The results showed

that the S2MW load for the last run was 1065 W, and the combined S2MW and RAW load for this run was 1265 W. This agreement between the observed and calculated heat loads and the consistency of the thermocouple measurements (less than 10 Centigrade degrees difference between four measurements) point to the high resistance between the wire and the shield as being the major determinant of the operational limits of the copper shield. This needs to be minimised. The next run attempted to investigate the limitations of EBW as a reheater, with S2MW and RAW operated near their limits. The run also attempts to estimate the value of the wire to shield resistance.

Run 31

The run procedure as per Runs 29 and 30. Both S2MW and RAW were maintained at 615°C. EBW was taken to 545 W, i.e. near its limit (Run 22). The catalyst was raised to 550°C. A further step up on S2MW resulted in a burn out at 625°C, and 1100 W. Heat balances across the mixer showed that the temperature at the exit of EBW could only be around 380°C, as compared to the design value of 540°C. The entry temperature, assuming 100% efficiency of EBW, turns out to be only 165°C. As EBW cannot handle higher loads, copper shields are the only solution. The long length of piping (≃ 6 m) means that two shields will be installed, one covering the piping in external room (EBEW) and the other covering the piping in the control room (EBCW). A further shield is installed on the mixer unit itself. This shield (MIXW) is a box of copper plate, covered by a resistance winding (the awkward shape of the mixer necessitates this). Figure 5.2 shows the five shields for the reactor system, and their various winding designs. As to the reducing of the wire to plate resistance, a trial run was conducted on S2MW using the thinnest and tightest fitting ceramic beads available (No. 1 'Quickline' beads). So far No. 3 were used due to the ease of threading the resistance wire.

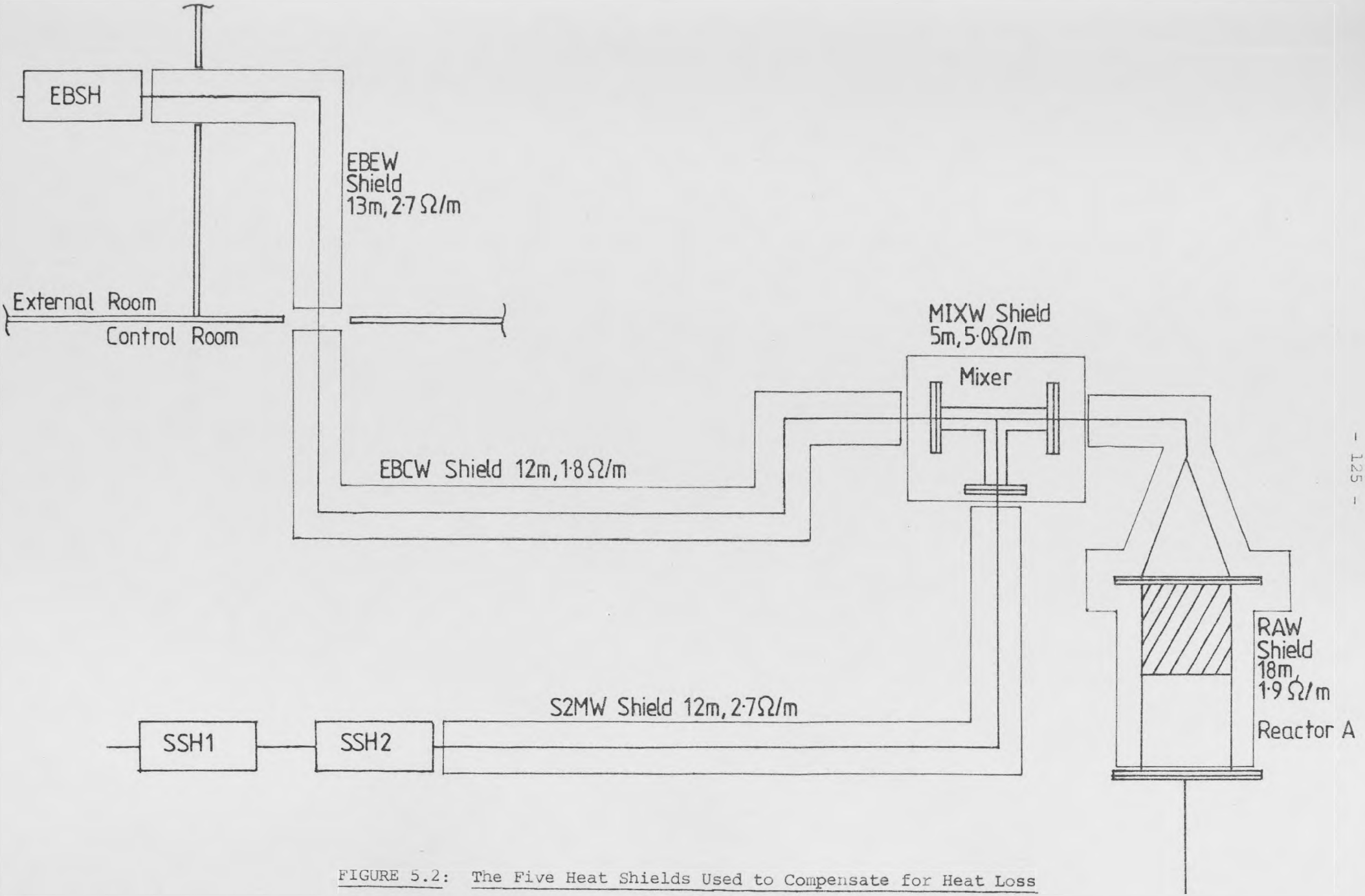

FIGURE 5.2: The Five Heat Shields Used to Compensate for Heat Loss

Run 32

Only S2MW was used, with flow only on the line SL1 (procedure as per Run 29). The result was that S2MW burnt out at 620°C, and 1132 Watts, showing very little improvement in the transfer resistances by the use of the tiny No. 1 beads. Having reached the conclusion that the copper shields cannot operate at temperatures greater than 620°C for the loads required, industrial tracer tapes were tried to boost the S2MW heat load capacity. These tapes are quartz cloth based using 'Ghlom' 80/20 alloy, and are very expensive. Therefore, experimentation is a difficult business, especially as no data is supplied as to their transfer resistance values at the operational limits claimed. An 'Isotape' ITQ-150-10.7 (87) was installed on the SSH2 → Mixer line (S2MW circuit), and on the copper plate to give a good tight contact on a greater transfer area than if wound on the pipe itself.

Run 33

The aim was to operate the EBEW and EBCW shields around 540°C, the 'Isotape' on S2MW around 650°C, and RAW around 600°C. MIXW would be used only upon approach of the above temperatures. The procedure used was as per Run 30, with a shield step up rate of around 50 W every 30 minutes. Experience of operating the RAW shield has shown that a load of 900 - 950 Watts should produce shield temperatures of around 540°C. However, as seen from Table 5.3, this was not the case with EBEW (300°C) and EBCW (450°C). No further boosts were applied on these shields as heat sinks that undoubtably exist need to be eradicated. The 'Isotape' operated perfectly at 640°C, but after 5 hours of steady state operation, it suddenly burnt out. The maximum catalyst temperature achieved was 560°C. The major heat sink for the EBEW and EBCW shields was the thick iron plate that formed the roof/floor for the two rooms. This plate was found to have become very hot during the run. Further examination showed that the

pipe, exerting its weight on the insulation, was compressing the insulation against the plate. The plate was cut away to avoid any contact with the insulation at its normal thickness. Faulty quartz braiding was found to be the cause of the 'Isotape' burn out. The braiding cord had disintegrated, causing the tape to slacken on the copper plate, and this additional resistance destroyed the tape effectiveness.

Run 34

This run was carried out in identical fashion to Run 33, except that S2MW now was a copper shield using Kanthal A-1 resistance wire (maximum operating temperature 1375°C), and a double copper plate was used (both sides of the resistance wire). The results showed that EBCW now worked perfectly at 540°C, but EBEW showed no improvement on 300°C. The double copper plate shield showed now improvement, and S2MW was changed back to a single plate shield for the next run. The smouldered fibreglass insulation covering on the EBEW line gave a clue to the problem on EBEW. It turned out that a heat exchanger network arose from the contacting of insulation on the EBSH → Mixer and Reactor A → Condenser lines (Figure 5.3). A large temperature drain must occur due to the much cooler condenser pipework. Although the contact was light, it was continuous over 4 m. The solution was to modify the pipework so as to have no contacting insulation around the external room, for the lines shown in Figure 5.3. Similar contacting in the control room is not crucial as both lines are of the same sort of temperature levels, as shown by the attainment of 540°C on EBCW.

Run 37

An identical run to Run 34 was carried out. This time there was some improvement on EBEW (70 Centigrade degrees) though not enough. MIXW was tried out but a very small load (< 100 W) caused a burn out because of the uneven and awkward shape of the box, resulting in varying

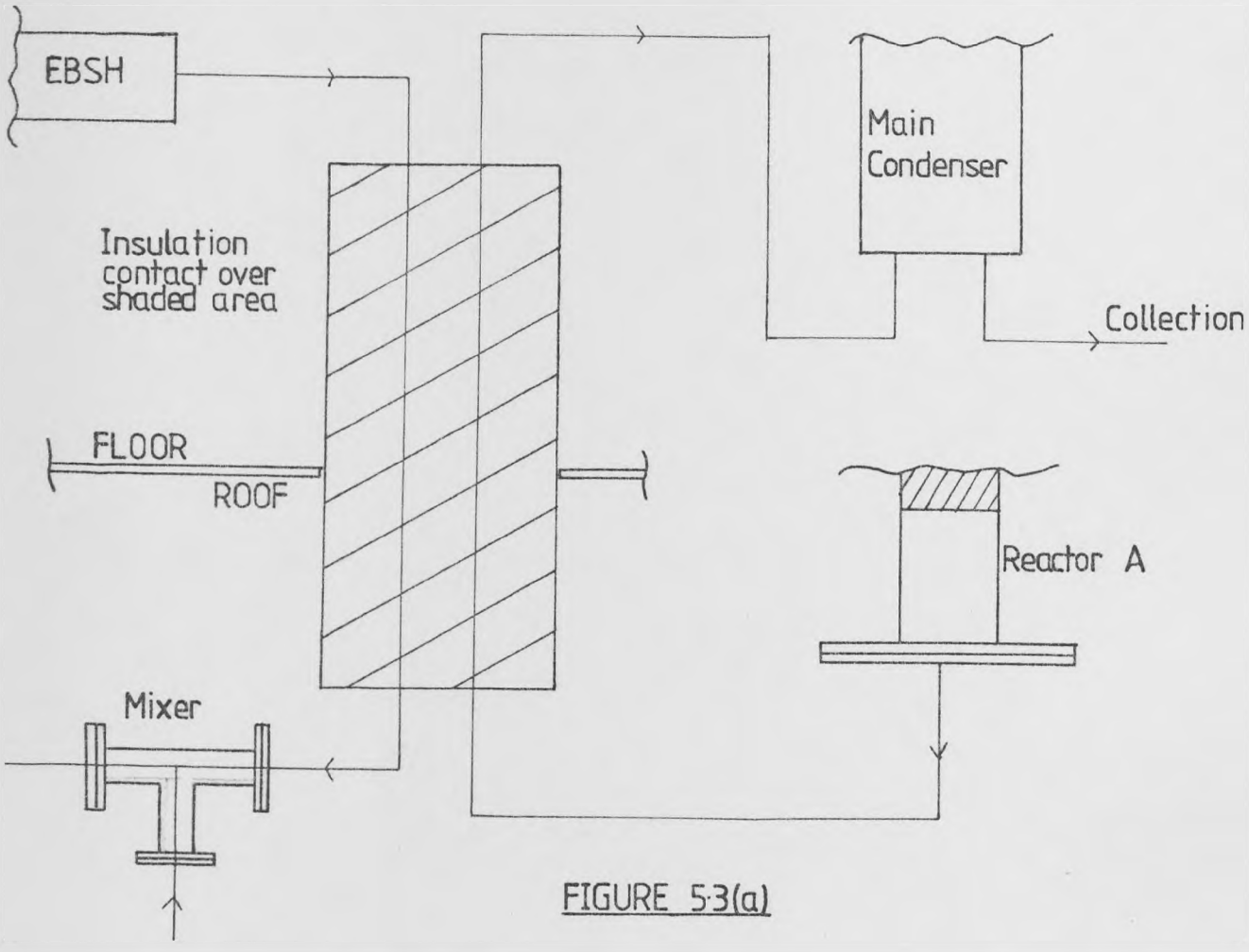

FIGURE 5.3(a)

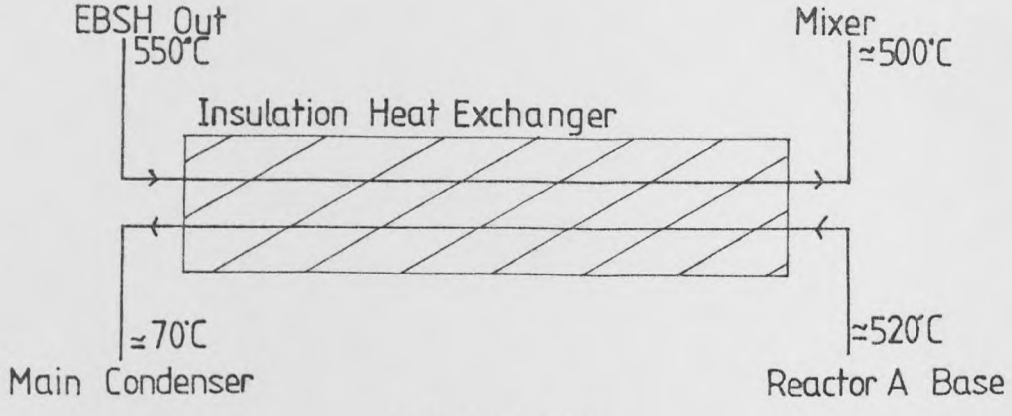

FIGURE 5.3(b)

FIGURE 5.3: Illustration of the Insulation Contact Causing a Heat Exchange Situation

resistances. Pipe supports were the main cause of the heat leak on EBEW, although a bad thermocouple contact also contributed to the false reading of the shield temperature. Extra insulation was installed on all system supports. The maximum catalyst temperature produced was 555°C, not sufficient to investigate the reaction substantially. Calculations needed to be carried out to estimate the maximum possible levels that can be attained using copper shields all round. Appendix A4.5 contains the calculations carried out. Assuming all four shields acted ideally, it should be possible to attain a catalyst temperature of around 620°C. Even if EBEW operated at 370°C, as for this run, 610°C should be possible. The losses across the mixer box, and the imperfect shields (e.g. at the bends on the pipework) must contribute to the lower catalyst temperature. S2MW, RAW, and EBCW shields were extended to the corresponding mixer flange, thereby removing the need for MIXW and the mixer box. Very little can be done about the problems of fitting the copper plate perfectly at bends without having edges acting as heat fins. For the next run, an 'Isotape' ITQ-150-10.7 was used on the S2MW circuit, but this time tightly wound on the metal pipework, ensuring no pipe length was left uncovered, and that the tape did not overlap. Special asbestos braiding was used to secure the tape, instead of the quartz braiding supplied by the manufacturer.

Run 39

The method and procedure was identical to Run 34. The run aimed at operating the 'Isotape' (S2MW) at around 650°C. If this was successful, then the 'Isotape' would be operated at higher temperatures. However, RAW burnt out before this could be done. The burn out was at the connecting terminal block and was very likely due to metal fatigue under the stress of the connection, and continuous operation. Nevertheless, the results tabulated in Table 5.3 are steady state ones obtained before RAW

burn out. A maximum catalyst temperature of 560°C was attained. The successful operation of the 'Isotape' at 650°C prompted the decision to install another 'Isotape' on the RAW circuit (Mixer to Reactor A Base). The ITQ-150-10.7 was the longest commercial length available. This gives a coverage of one turn every 10 cm. Once again, asbestos cord was used as the tape fastener. Three 5 cm 'Kaowool' insulation layers cover the full length of the Isotapes.

Run 40

The run procedure was as per Run 34, and the S2MW tape was gradually raised to a temperature of 700°C. The RAW tape temperature turned out to be unreliable, mainly due to the absence of a continuous quartz cloth shield as such. This meant that if the thermocouple had slipped off the tape, then the indicated temperature was unreliable. Instead, RAW was operated such that the three Reactor A temperatures were as close as possible, i.e. RAW was not adding any heat into the system. A catalyst bed temperature range of 595 - 605°C was achieved. Better voltage control was not possible due to fluctuations in the 3-phase voltage supply (limit is $\pm$ 3% - official Yorkshire Electricity Board figure). As manual voltage regulators cannot be continuously adjusted, some temperature gradient will result across the catalyst.

Run 42

This run operated S2MW at 710°C. This run is summarised in Section 5.1 and Figure 5.1. The study of the reactor system can now proceed. Therefore, no further experimentation on operating the S2MW 'Isotape' at even higher temperatures need be undertaken.

The reactor system can now be commissioned for ethylbenzene flow before the proper reaction runs are carried out.

CHAPTER 6

PRESENTATION OF THE RESULTS OF THE REACTION RUNS, AND GENERAL DISCUSSION

CHAPTER 6

PRESENTATION OF THE RESULTS OF THE REACTION RUNS, AND GENERAL DISCUSSION

Introduction

All runs carried out using ethylbenzene are examined individually. After the trial reaction and commissioning runs, the runs and the individual experiments performed are described. The results and analysis of all the samples is presented. Each experiment is individually discussed in relation to the temperature plots and the sample analysis. The transient and steady state experiments are compared, and the experimental parameters are used to generate model predictions from the programs used in Chapter 4. The final discussion centres around the theoretical predictions, the transient and the steady state experiments performed.

6.1 Summary of Actual Runs and Experiments Performed, Including Ethylbenzene Flow Commissioning

6.1.1 Run 45

This run followed the procedure as per Run 42, and steady state was reached after about 12 hours. The maximum temperatures shown in Table 6.1.

TABLE 6.1

Steady State Temperatures for Run 45

A TOP : 610°C	EBEW : 485°C	SSH2 OUT : 740°C
A CAT : 615°C	EBCW : 505°C	EBSH OUT : 525°C
A MID : 625°C	S2MW : 700°C	
	RAW : 505°C	

Once steady state was achieved, the ethylbenzene boiling was commenced. Solenoid valve SV5, returning the ethylbenzene to the feedtank was opened, as were the metering pump suction and delivery globe valves. The feedtank was pressurised to 5 p.s.i.g. (1.34 bar) with nitrogen, as all sample tanks were cleared with nitrogen. The feedtank was pressurised with nitrogen so as to have similar pressure heads for the metering pump on the feedtank return as that through the reactor route. Once the ethylbenzene was boiling (around 135^{o}C), a run was attempted to pass the ethylbenzene through the reactor. Continuous gas and liquid samples were also taken. The run was abandoned once the reactor temperatures, and the EBSH out temperatures started rising rapidly. The reactor temperatures soon exceeded 650^{o}C, whilst reduction of wattage on the EBSH heater did not result in any controllable temperatures. The liquid samples confirmed the suspicion that no ethylbenzene was passing through the reactor. The analysis of the gas samples showed that only nitrogen was present. Clearly a number of problems arose during this run, which were diagnosed as:-

(i) the ethylbenzene may not have been 100% vapour at the time of the steam cut off on SL2;

(ii) the solenoid valves were not seating firmly, allowing the ethylbenzene to be returned to the feedtank;

(iii) the metering pump may have been pumping more liquid through than the desired flowrates, thereby contributing to the ethylbenzene not being 100% vapour.

The solenoid valve seats were changed from 'PTFE' to 'Viton'. The manufacturer had found that although 'PTFE' is not attacked by ethylbenzene, it does not provide a good seal on surfaces that have had contact with organic liquids. This was also found to be the problem with the metering

pump where the ethylbenzene has slipped through the 'PTFE' diaphragm seal to attack the nitrile rubber behind it. Upon testing, the metering pump was found to be pumping 105 cc/min instead of 55 cc/min ethylbenzene due to the faulty diaphragm. The metering pump was changed from a 100 p.s.i.g. (7.81 bar) maximum head diaphragm type pump to a 1500 p.s.i.g. (103 bar) maximum head stainless steel plunger type with 'Viton' seals.

The ethylbenzene superheater EBSH was dismantled, to reveal a thin layering of coke on the transfer surfaces and a strong smell of ethylbenzene. The distribution holes on the flow areas (see Appendix A3.5) were found to be partially blocked with coke. Clearly the ethylbenzene was eventually pushed to the superheater to encounter a very hot transfer surface, resulting in the coking of the ethylbenzene. The distribution holes were enlarged from 0.04 cm diameter to 0.32 cm diameter to prevent complete blockage from occurring.

A ½" BSP (2.13 cm O.D.) 'Comanche' stainless steel 'Viton' seated ball valve was also installed after SV5 (EB Return) to allow manual shut off to the feedtank, in case of the SV5 valve failing to seat tightly again.

A run was required to test out the superheating of the ethylbenzene upon the exit from the vaporiser. 10 - 15 Centigrade degrees of superheat was aimed for above its boiling point of 138°C under 5 p.s.i.g. (1.34 bar) pressure. This would ensure that only vapour would be passed to the ethylbenzene superheater at the next full run.

6.1.2 Run 48: Ethylbenzene vaporisation and superheating

The metering pump was initially calibrated using water against a 20 p.s.i.g. (2.36 bar) head, and the required setting was found to be Mark 56 (see Figure 4.11 for the calibration chart) for the flowrate of 55 cc/min. The procedure for the ethylbenzene superheating was as follows:-

(i) open SV5, and the pump suction and delivery globe values;

(ii) pressurise the feedtank with nitrogen to 5 p.s.i.g. (1.34 bar) and switch on the pump. Turn on the ethylbenzene condenser water to around 90 - 100 litres/hr.

(iii) step up EBVI ('Isotape') and EBV (vaporiser winding) over 20 minutes to 550 W on EBV and 300 W on EBVI.

Figure 6.1 shows the heating up and the superheating of the ethylbenzene. After ½ hour, the ethylbenzene boiled at around 140°C, and after 1½ hours, the superheating commenced and settled at around 155°C. The superheating was maintained for 3 hours without any significant deviations.

After this, the power on EBVI and EBV was stepped down and cut off, and the cooling curve that emerged (Figure 6.1) showed the desuperheating, and then the subcooling of the liquid - the change in the temperature gradient around 140°C proved this. Therefore, this will be the procedure that will be followed for actual reaction runs for vaporising the ethylbenzene.

6.1.3 Run 50

This was the first run to successfully achieve ethylbenzene flow through the catalyst bed. The procedure for a successful start-up, reaction runs and shut-down is fully described in Appendix A7. Therefore, only the actual runs carried out will be described. Two transient experiments were carried out, and composite samples were collected, allowing at least 5 minutes flow after the end of the experiment so as to ensure the collection of all organic. The dead time of the liquid cannot be accurately measured, and therefore a "worst case" estimate of 5 minutes is adhered to for all experiments.

The duration of the first experiment, numbered 50-1, was 2 minutes. The short duration was to ensure that the ethylbenzene was flowing through.

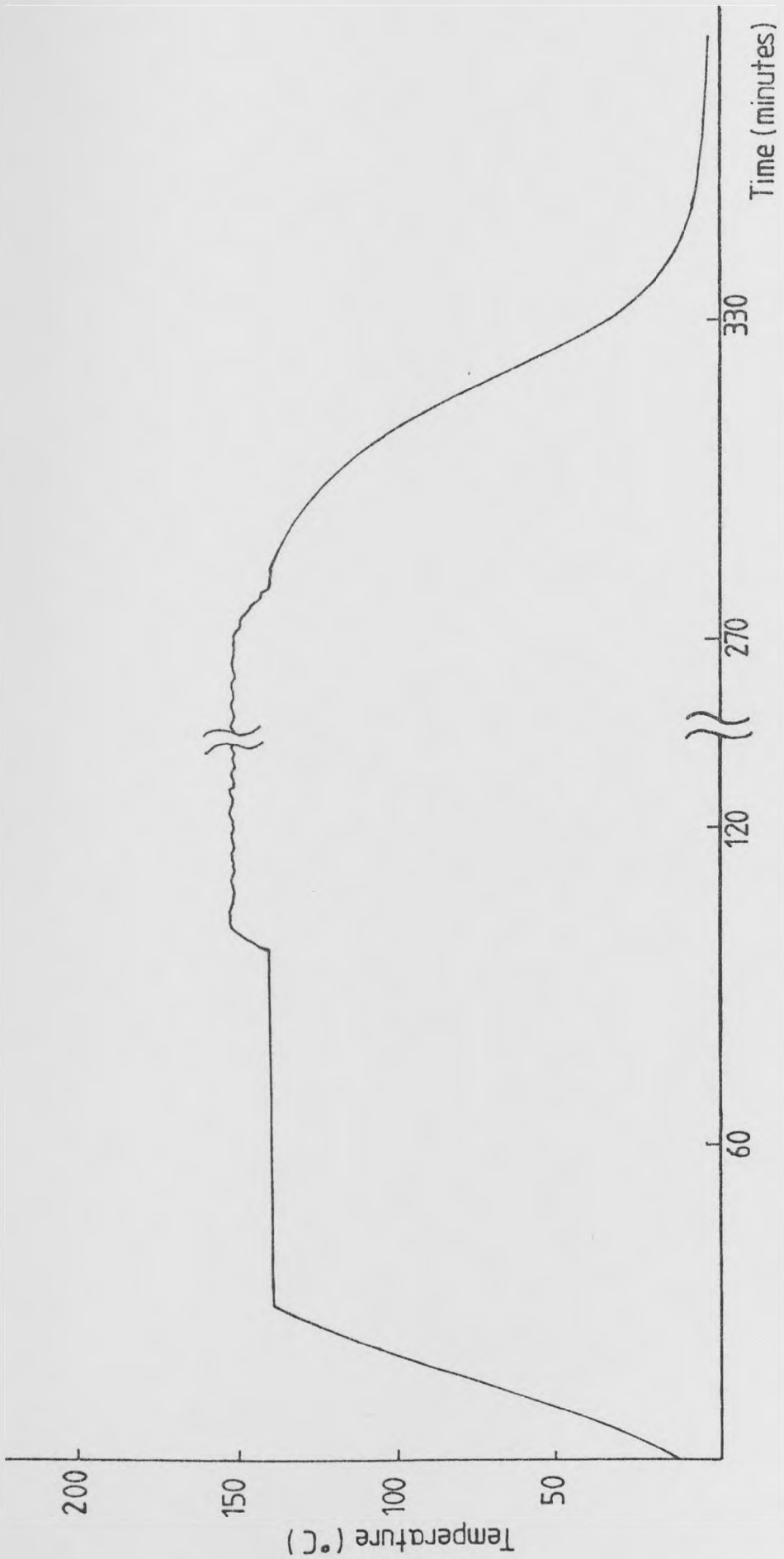

FIGURE 6.1: The Ethylbenzene Vaporisation, Superheating and Cooling Plot

Upon examination of the sample, some organic liquid was collected (35 cc), though not as much as one would expect (110 cc). Nevertheless, the temperatures (see Table 6.2) were regenerated by steam flow on both lines SL1 and SL2, and a longer run was attempted.

The duration of the second experiment, numbered 50-2 was seven minutes. The experiment was successful in as much that the organic flow-rate was close to that expected, i.e. 345 cc was collected as opposed to 385 cc that was desired. The anticipated fall in the catalyst bed temperature was observed much sooner for Experiment 50-2 than for 50-1, suggesting that the pump was not initially pushing the ethylbenzene through for Experiment 50-1.

Further experiments were not possible as at the end of Experiment 50-2, the ethylbenzene vaporiser temperature suddenly fell from 150°C down to 100°C, indicating water contamination. This was found to be the case, due to "dirt" keeping the solenoid valve slightly open upon switch off, and also bad seating in the non-return valve on the ethylbenzene feed line, enabling water to flow through into the ethylbenzene vaporiser.

The "dirt" from the vaporiser was actually the graphite based sealing compound which could explain why for Experiment 50-1, the pump did not displace the required amount of organic. A good clean up and drying of all valves and seals using nitrogen eliminated this problem. The analysis of the liquid samples can be found in Appendix A8, Table A8.1.

Full presentation of results of this and the experiments that followed, as well as discussion of these results follow in Sections 6.2 and 6.3.

6.1.4 Run 52

Upon start up of the run, the air inlet pressure to the bed gradually shot up to 65 p.s.i.g., and the supply pressure to 74 p.s.i.g., indicating

TABLE 6.2

Steady State Temperatures for Run 50

Temperature Point	Temperature for Experiment 50-1 (°C)	Temperature for Experiment 50-2 (°C)
EBVap	155	150
A Top	560	560
A Catalyst	570	570
SSH2 OUT	745	695
EBSH OUT	460	465
S2MW (shields)	695	700
RAW (shields)	460	460
EBEW (shields)	425	425
EBCW (shields)	430	430

that the catalyst bed had a blockage. The superheaters were not switched on. The catalyst support had collapsed forcing the catalyst into the contraction cone, and causing a blockage. The reactor was modified to include 4 pegs, welded into the reactor to allow the catalyst support mesh to rest on these pegs. Until now, the support mesh was screwed into the internal insulation (4 mm 'Kaowool' paper). This had gradually disintegrated over a period of two years causing the support to collapse. Three sets of pegs were welded in at 0.33 m, 0.48 m and 0.64 m from the top of the reactor. Girdler G-64C catalyst was now substituted for the Shell 105 catalyst. The catalyst bed length was maintained at 0.3 m.

6.1.5 Run 53

A set of six transient experiments (53-1 to 53-6) of duration from 1 minute to 3 minutes were carried out. Two long steady state experiments 53-7 and 53-8 were also carried out. The transient runs had their composite liquid samples collected, whilst with the steady state runs, a series of small liquid samples were taken as steady state was approached. Towards the end of the run, a gas sample was also taken. Table A8.1 in Appendix A8 contains all the liquid sample results and also tabulates the sample times for the steady state runs. Table A8.2 contains the gas sample analysis results for the steady state runs.

The duration of Experiment 53-7 was 26 minutes 37 seconds, whilst the duration of Experiment 53-8 was 30 minutes 50 seconds. The mean composite samples collected were also analysed.

Table 6.3 shows the bed inlet temperatures, and the superheater and shield temperatures at the start of each experiment.

Sections 6.2 and 6.3 contain the presentation and discussion of the results of Experiments 53-1 to 53-8. During the shut down, SSH2 lost its circuit supply due to the melting of hot end firebar support. This was found to be largely due to the high voltage 'live' contact of the hot end.

TABLE 6.3

Steady State Temperatures for Run 53

Temperature Point of Measurement	Temperatures for the Experiments of Run 53 (°C)							
	53-1	53-2	53-3	53-4	53-5	53-6	53-7	53-8
A TOP	575	570	568	565	565	565	575	570
A CATALYST	580	573	570	570	575	575	580	578
SSH2 OUT	745	748	755	753	753	750	748	753
EBSH OUT	485	485	500	535	520	543	510	490
S2MW	700	700	705	700	705	705	700	700
RAW	550	545	550	545	545	550	550	545
EBEW	440	440	445	440	445	445	440	445
EBCW	445	440	445	445	445	450	445	445

Continuous voltage and large temperature gradients across the support had caused the threaded rod to lose its taut connections onto the screwed rod. The solution was to make the hot end the 'neutral' supply. The firebar was also replaced and commissioned as per Section 4.2.

6.1.6 Run 55

A set of two transient experiments (55-1 and 55-2) each of duration 2 minutes, and two steady state experiments (55-3 and 55-4) were performed. More point liquid samples were collected for the steady state runs, and four gas samples were collected for Experiment 53-4. The transient sampling was as per Run 53. The analysis and sampling times of all liquid and gas samples are tabulated in Appendix A8, Tables A8.1 and A8.2 respectively.

The duration of Experiment 55-3 was 22 minutes 30 seconds, whilst that of Experiment 55-4 was 52 minutes 7 seconds. The mean composite samples collected were also analysed.

Table 6.4 tabulates the bed superheater and shield temperatures at the start of each experiment. The detailed analysis and discussion on all experiments follows in Sections 6.2 and 6.3.

TABLE 6.4

Steady State Temperatures for Run 55

Temperature Point of Measurement	Temperatures for the Experiments of Run 55 (°C)			
	55-1	55-2	55-3	55-4
A TOP	565	560	570	570
A CATALYST	575	570	580	580
A MID	580	575	585	585
SSH2 OUT	745	753	748	740
EBSH OUT	455	480	490	450
S2MW	695	700	700	695
RAW	550	545	545	550
EBEW	445	445	450	455
EBCW	445	445	450	455

6.2 Presentation of Results and Comments on Individual Experiments

6.2.1 Trial transient experiments 50-1 and 50-2

Experiment 50-1

The duration of this run was 2 minutes, with the aim of checking for ethylbenzene flow through the reactor. Figure 6.2 shows that initially hardly any temperature drop occurred along the catalyst bed. Towards the end of the run there was a small fall in catalyst temperature. The ethylbenzene was certainly flowing through, as shown by the 35 cc of organic collected in the composite sample, but nowhere near the 110 cc that ought to have been. Nevertheless, the sample analysis showed a conversion to styrene of 34.1% with an efficiency of 82.8%. The problems with joint sealing compound mentioned in Section 6.1.3 could have contributed to the small, or rather later delivery of the ethylbenzene. The next run confirmed the theory that the lines, once clear of the sealant, should enable a better flowrate to be delivered by the pump.

Experiment 50-2

Figure 6.3 shows the plots of the three major temperatures. The catalyst temperature does not begin to fall until around 4 minutes after commencing the ethylbenzene flow. The experiment was stopped after 7 minutes when the EBSH temperature dropped very suddenly. The sample collected was 345 cc of organic, which compares favourably with the desired flowrate of 385 cc. The high conversion (50.9%) is either an indication of late activity of the catalyst, i.e. the catalyst did not activate until after 4 - 5 minutes after the start, or that of an accumulation of ethylbenzene vapour and then a sudden larger than normal slug pushed through EBSH and onto the reactor. The latter could seem the more likely, as the drop in EBSH temperature would suggest. The lower conversion for Experiment 50-1 would suggest lower catalyst activity.

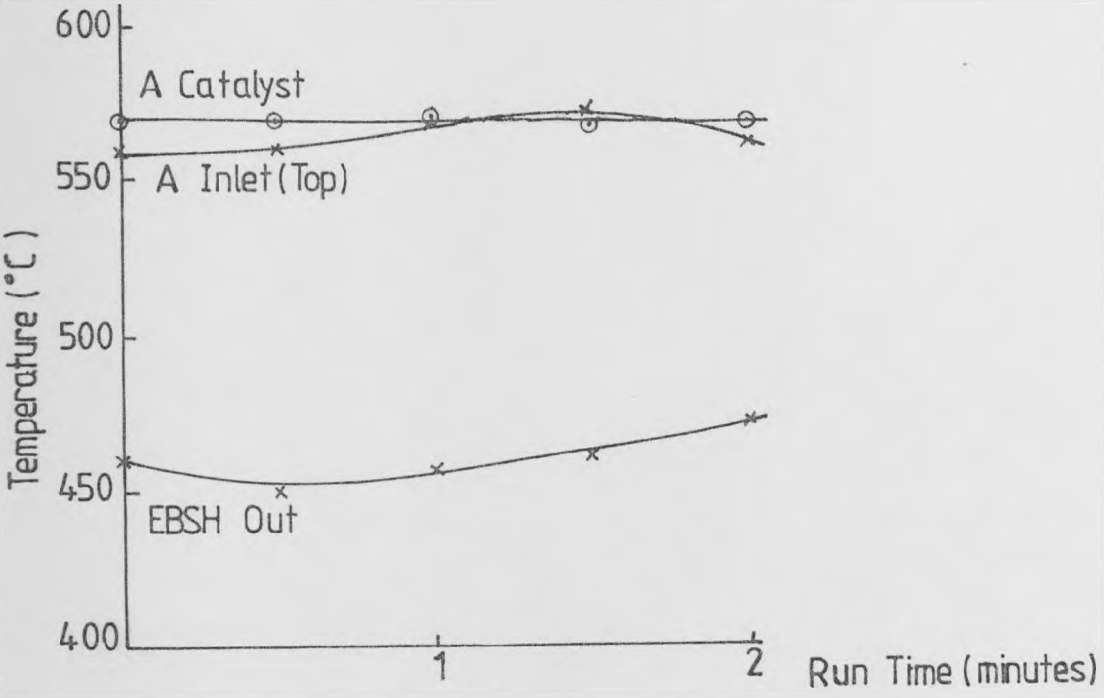

FIGURE 6.2: Temperature Profiles for Experiment 50-1

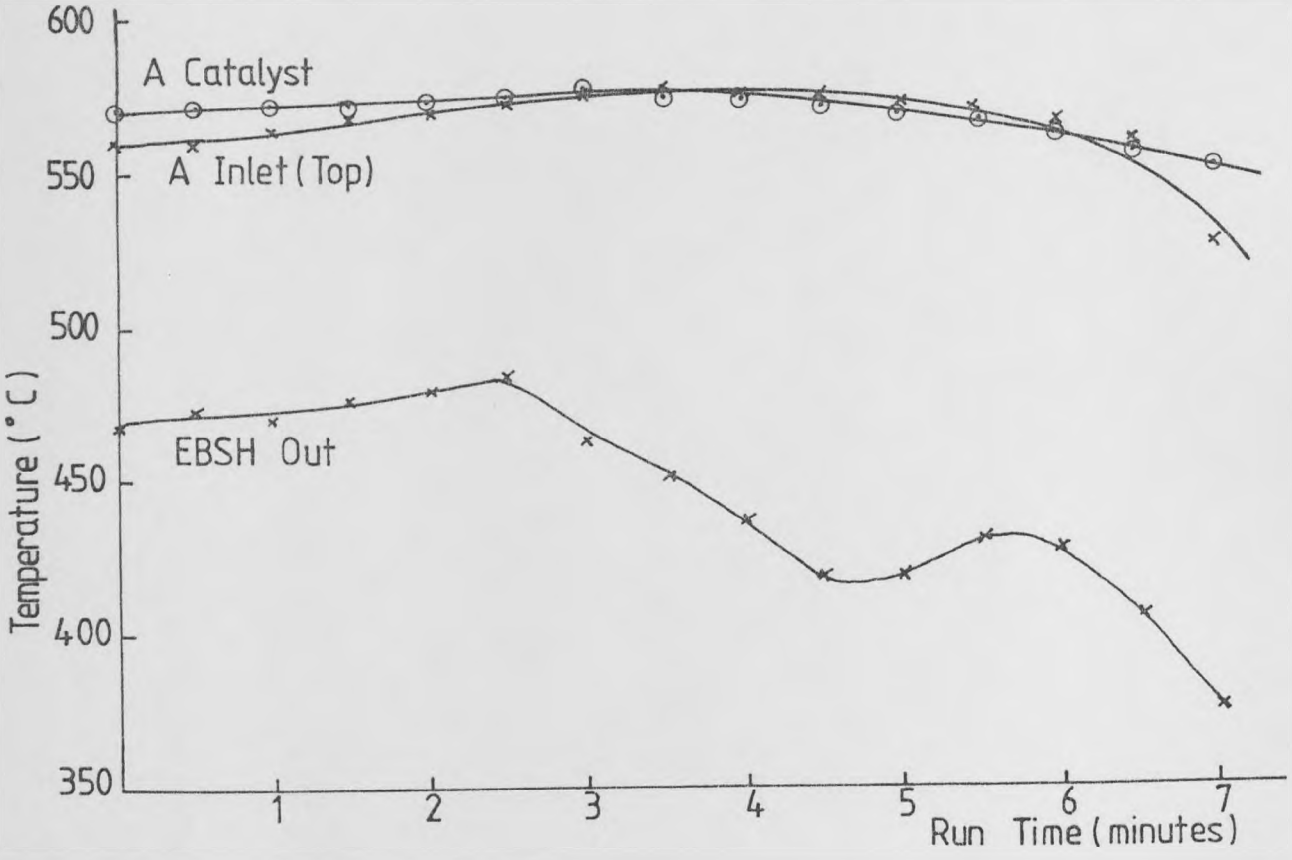

FIGURE 6.3: Temperature Profiles for Experiment 50-2

As indicated in Section 6.1.3, the run had to be stopped prematurely. Nevertheless, ethylbenzene flow is possible and the catalyst does activate rapidly. Experimental results 50-1 and 50-2 will not be used in any further discussion as they were trial runs on Shell 105 catalyst, compared to Girdler G-64C catalyst for the rest of this study.

6.2.2 Transient experiments 53-1 to 53-6

Experiment 53-1

Figure 6.4 shows the temperature profiles for the bed and EBSH out for the duration of this transient run, 3 minutes. A conversion of 48.1% with an efficiency of 85.0% is obtained for the composite sample. The fall in catalyst temperature begins within half a minute of the commencing of the run, thereby indicating the progress of the reaction along the bed. Total organic collected, after sample separation and filtration was 156 cc, compared to 165 cc to be expected. Thus the ethylbenzene delivery by the pump was found to be good.

Note on the ethylbenzene flowrate

For all experiments conducted over Runs 53 and 55, the amount of organic collected varied between 52 - 56 cc/min, i.e. 2.8 to 3.0 kg/hr as compared to the design flowrate of 2.96 kg/hr. Considering the small losses due to collection, separation, filtration and the density changes between the ethylbenzene feed and the organic product, the error in the ethylbenzene flowrate is not greater than $\pm$ 5%. The majority of the samples averaged around 52 - 54 cc/min.

Experiment 53-2

This transient run was of duration 3 minutes, at a lower bed inlet temperature than Experiment 53-1. The conversion was 43.0% with an efficiency of 84.7%. Figure 6.5 shows the temperature profiles for the experiment. Note the similar drops in EBSH out temperature, and the

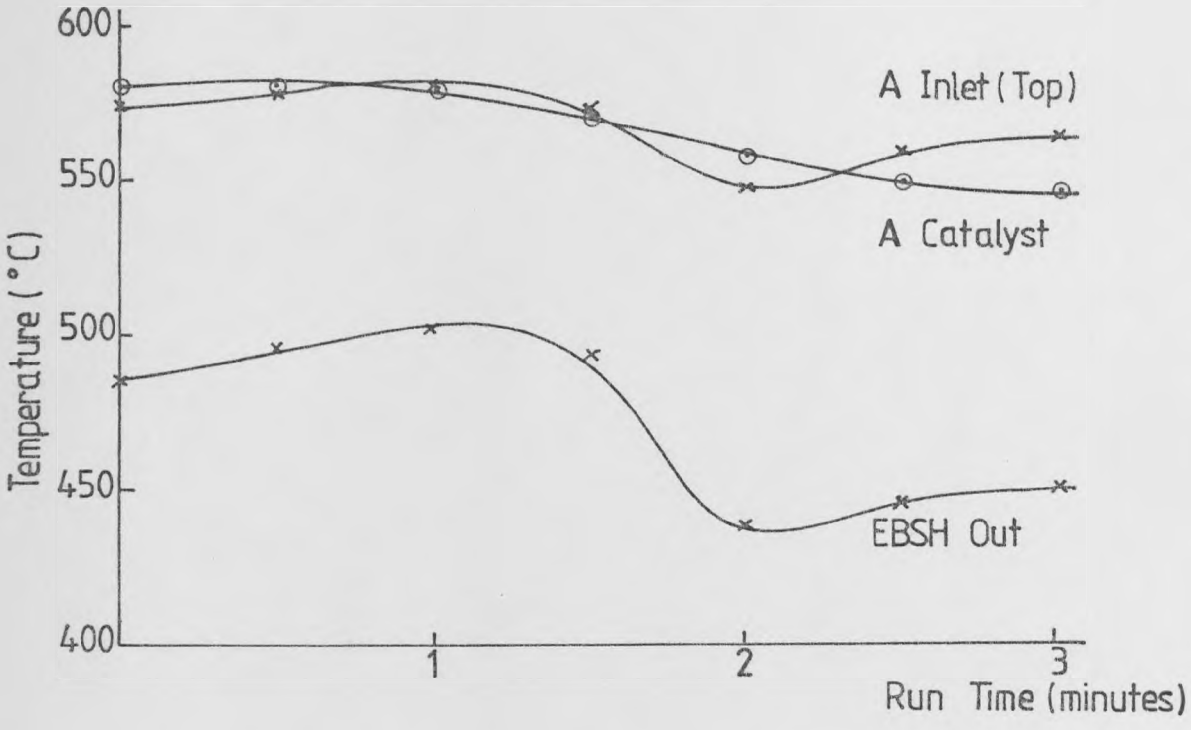

FIGURE 6.4: Temperature-Time Plot for Experiment 53-1

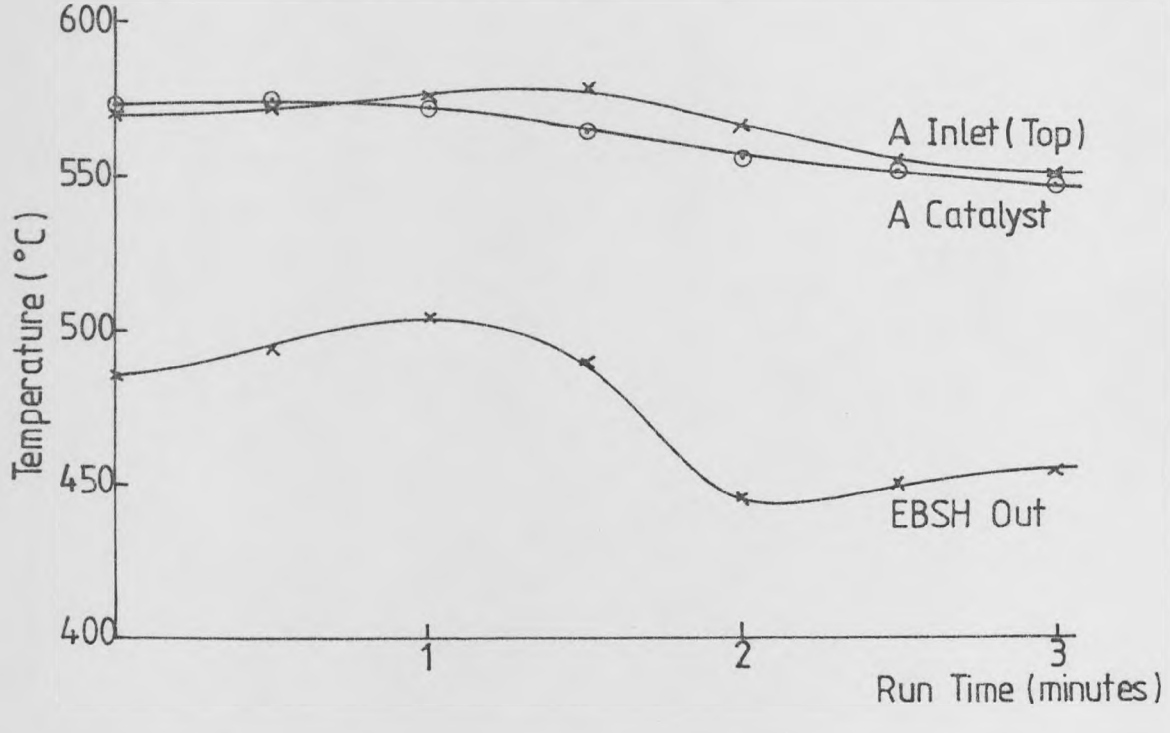

FIGURE 6.5: Temperature-Time Plot for Experiment 53-2

similar trough as well. The likely cause is the sudden switchover from steam to ethylbenzene causes the ethylbenzene to lose some of its heat to the relatively cooler piping and valves before the entry to EBSH (155^{o}C ethylbenzene temperature, 115^{o}C steam temperature).

Experiment 53-3

The duration was once again 3 minutes, at a lower inlet temperature than Experiment 53-2, but a slightly higher EBSH out temperature. The conversion obtained was 39.3% with an efficiency of 81.1%. Figure 6.6 shows the three major temperature plots for the run. Notice the very shallow EBSH trough, an indication that the solenoid valve, non-return valve and the short length of piping are probably warmer after two ethylbenzene runs, than before any reaction run switchover. The lower conversion is also represented by the smaller drop in the catalyst temperature.

Experiment 53-4

The transient run was conducted for a period of 1 minute, and Figure 6.7 shows the temperature changes that occurred. The short period, and the small number of temperature points makes precise judgement rather difficult, but the EBSH out trough appears rather small. The conversion obtained was 39.0% with an efficiency of 81.1%. Note that the EBSH out temperature was the highest used thus far for transient runs - basically to enable one to judge the effect of pyrolysis of ethylbenzene with increasing temperature.

Experiment 53-5

A conversion of 32.2% and an efficiency of 77.8% was obtained for this run of 2 minutes in duration. The temperature plot is shown in Figure 6.8. The drop in catalyst temperature is reflecting the lower conversion. These transient runs have varying inlet and average inlet temperatures, and the emerging trends are traced and discussed in Section 6.3.

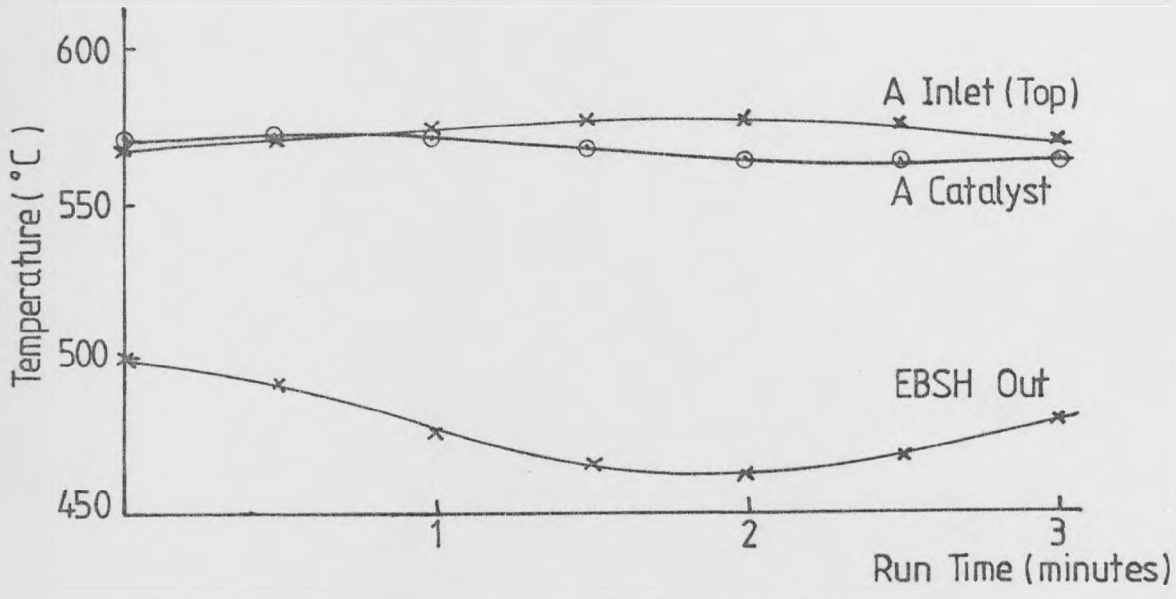

FIGURE 6.6: Temperature-Time Plot for Experiment 53-3

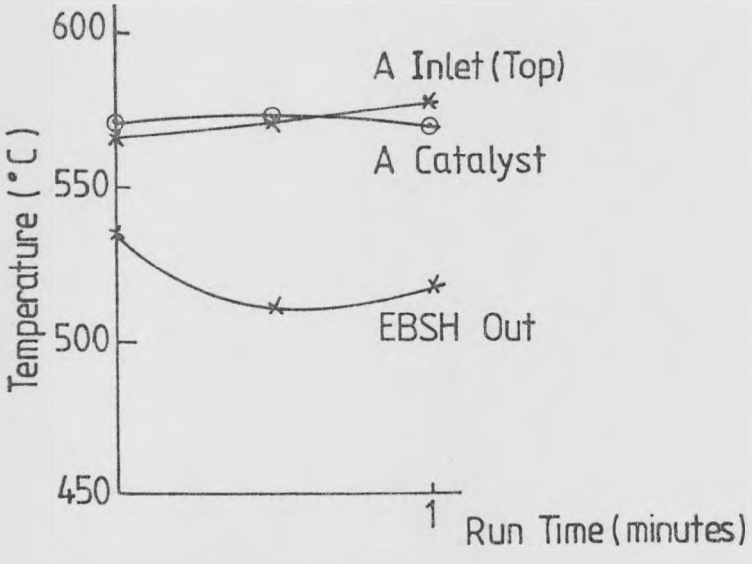

FIGURE 6.7: Temperature-Time Plot for Experiment 53-4

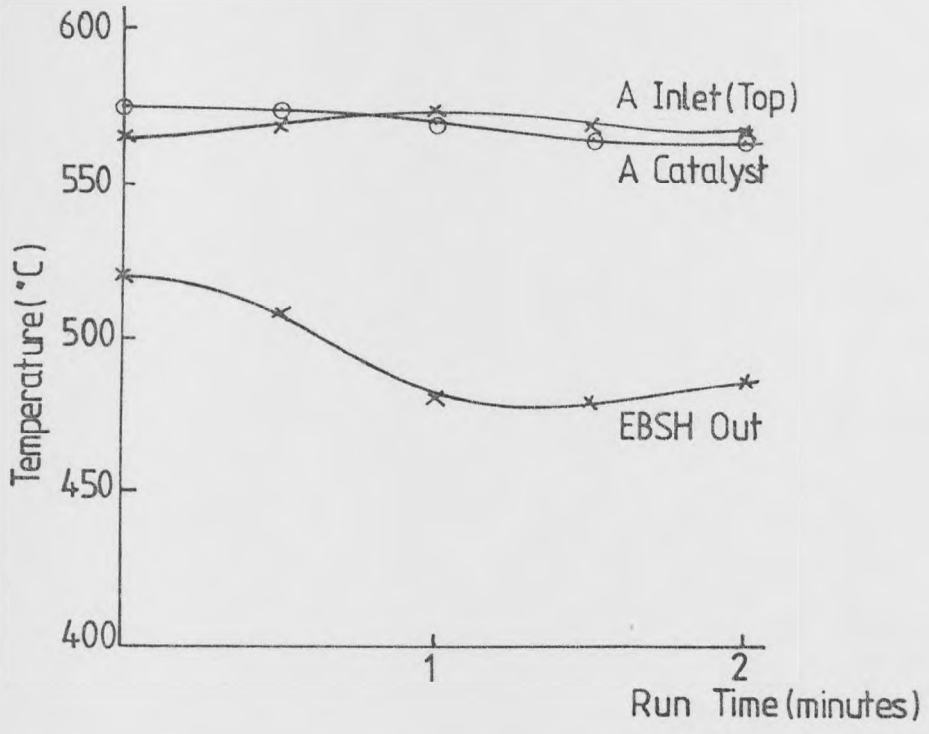

FIGURE 6.8: Temperature-Time Plot for Experiment 53-5

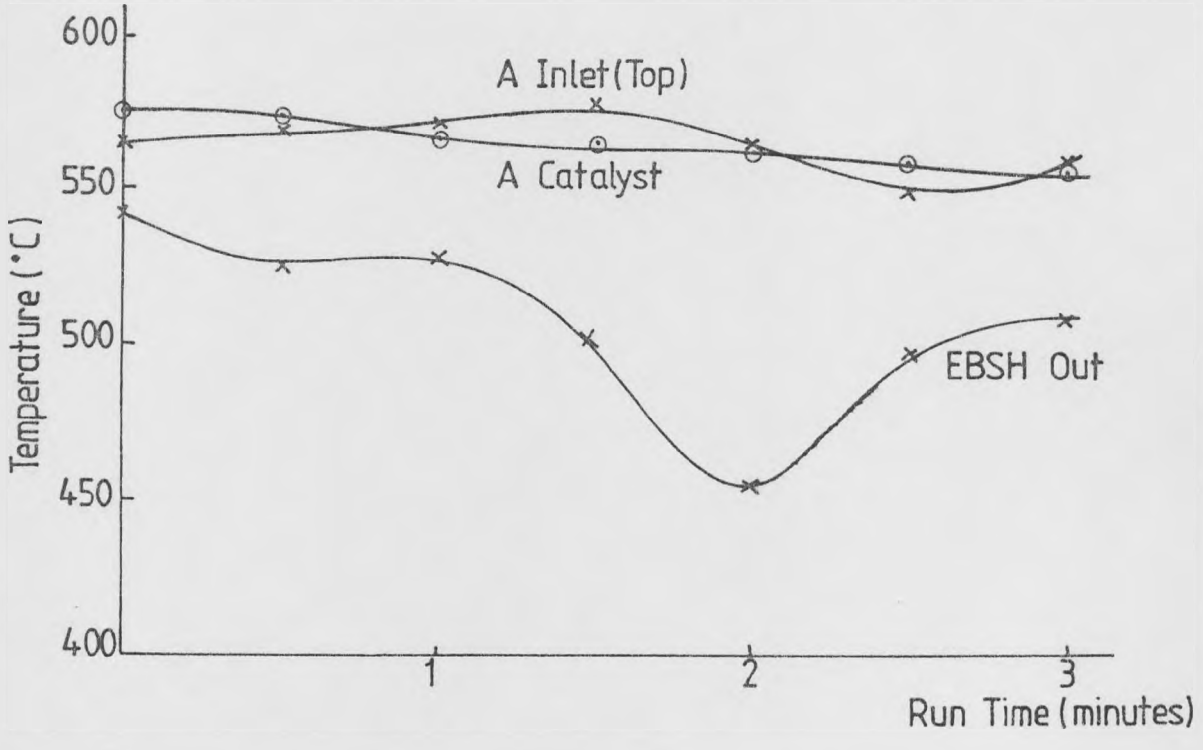

FIGURE 6.9: Temperature-Time Plot for Experiment 53-6

Experiment 53-6

After two experiments of shorter duration, a 3 minute reaction period is carried out by this run so as to check the validity of the Experiments 53-1, 53-2 and 53-3, all of which were of duration 3 minutes. Figure 6.9 shows the relevant temperature plots. The conversion was 31.3% and the efficiency 73.8%. Note the high EBSH out temperature.

6.2.3 Steady state experiments 53-7 and 53-8

Experiment 53-7

This being the first steady state run attempted, the intention was to let the run progress as long as possible, with small liquid samples taken at intervals once near steady state conditions have been established in the reactor bed. After about 6 minutes, the catalyst temperature has stopped falling, and so samples were taken at various intervals after the run had progressed for 7 minutes. Appendix A8, Table A8.1 carries the sampling times and the analysis of the liquid samples for this experiment as well as Experiment 53-8. An analysis of the mean composite sample is also included. A gas sample was also taken towards the end of the experiment, the analysis of which is tabulated in Table A8.2. Figure 6.10 presents the four relevant temperature profiles for the run. Figure 6.11 shows the change in conversion and efficiency with sampling time, and Figure 6.12 shows the variations in concentration of the four components, i.e. ethylbenzene, styrene, benzene and toluene for the experiment.

The run was stopped after 26 minutes and 37 seconds as the EBSH temperature which had stopped oscillating and had steadied for a while, rose very sharply past 580^{o}C. No attempt was made to control this so as to observe the effect of pyrolysis of the ethylbenzene, as well as the result of increasing pyrolysis. This continuous rise in EBSH temperature results in the gradual rise of the inlet temperature to the bed, and correspondingly a rise in conversion, and a significant drop in the efficiency,

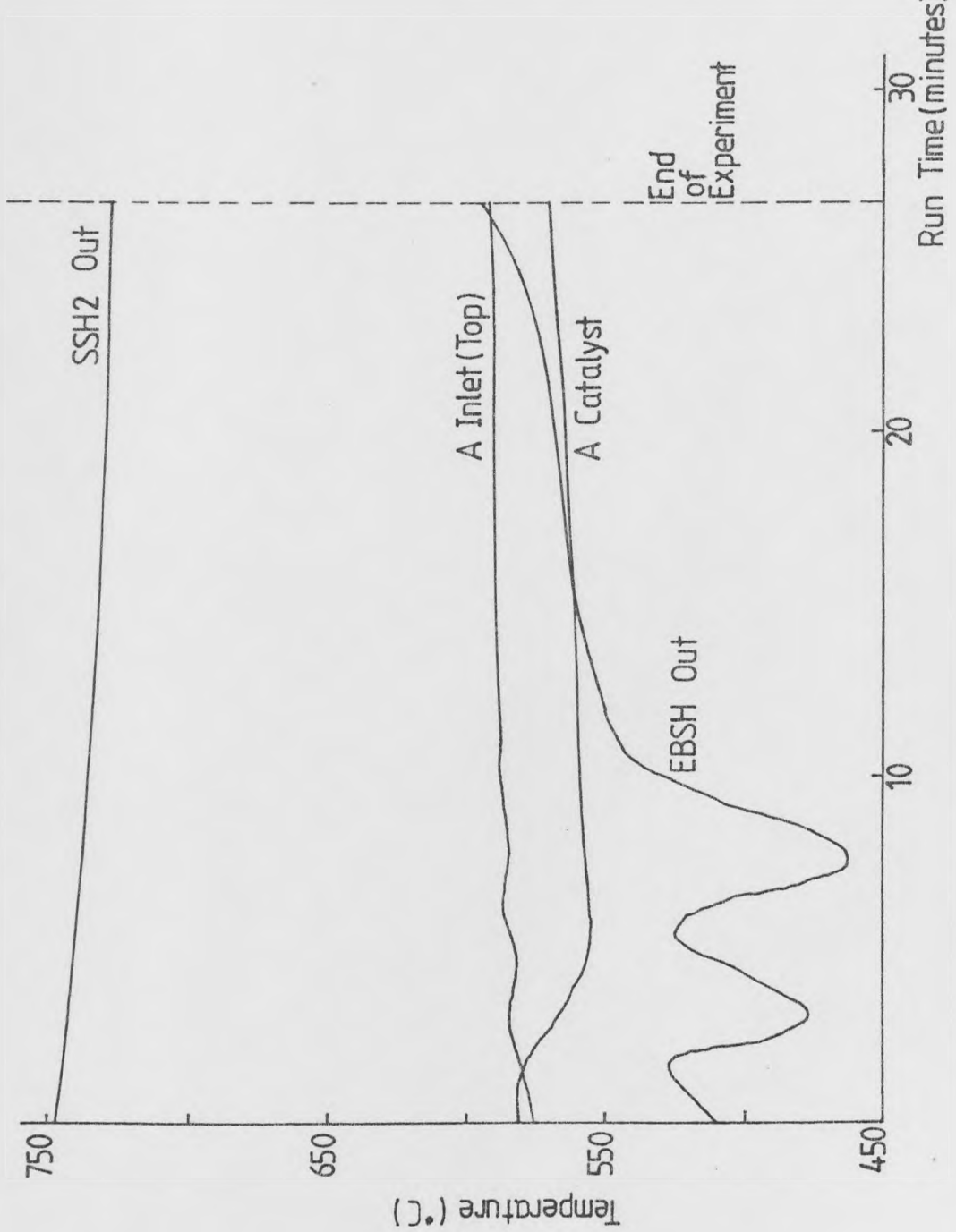

FIGURE 6.10: Temperature-Time Plot for Experiment 53-7

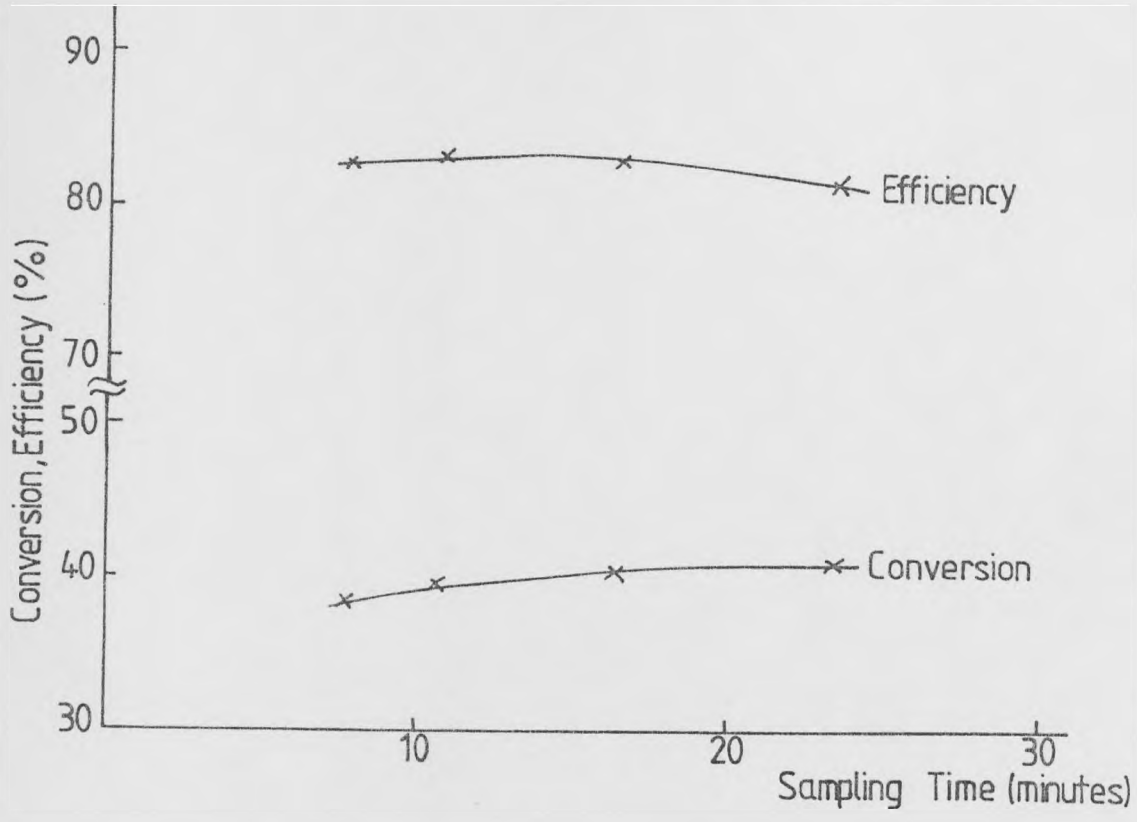

FIGURE 6.11: Conversion, Efficiency Plot for Experiment 53-7

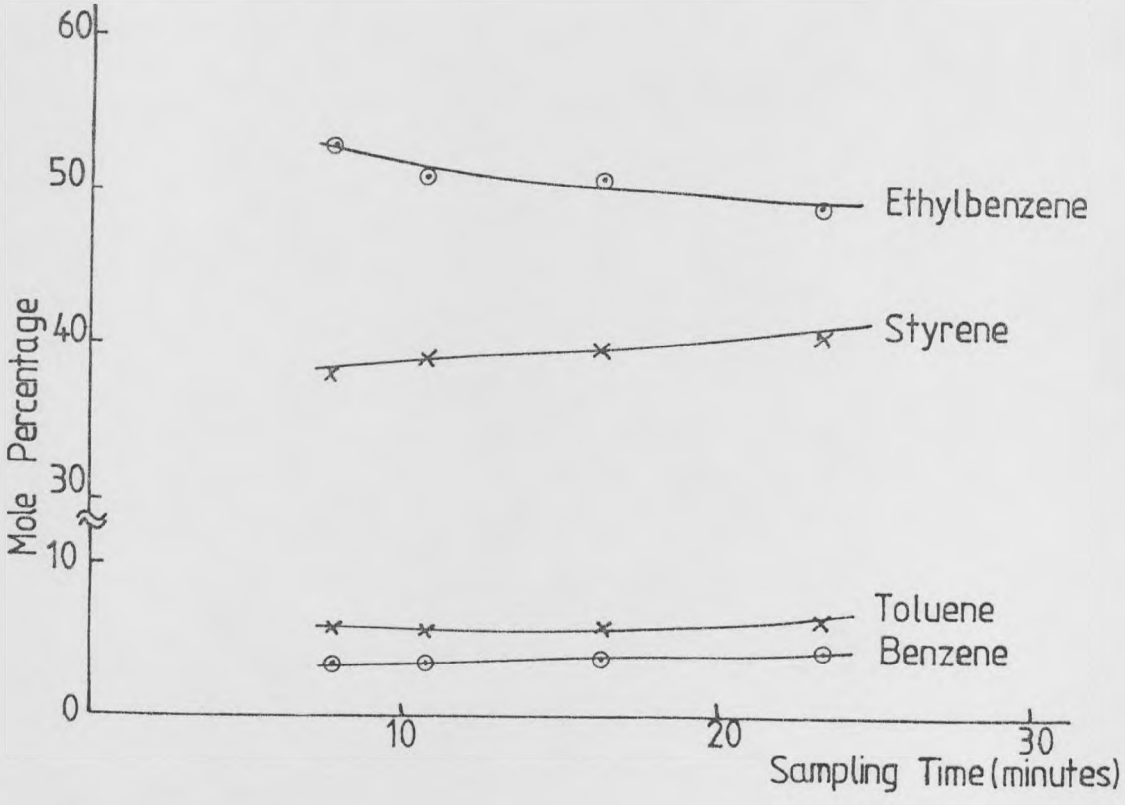

FIGURE 6.12: Component Content Plot for Experiment 53-7

especially towards the end of the run. The catalyst temperature also shows the gradual rise in temperature. A slight increase was observed in the steam flow on line SL1, which is estimated by two methods:-

(a) Fall in SSH2 temperature - the temperature falls from 755°C to 728°C. With a steam inlet temperature of 115°C, this implies a rise in the flowrate from 7.0 kg/hr to 7.3 kg/hr, an increase of 4.4% (new steam: ethylbenzene molar ratio 14.6:1 instead of 14:1).

(b) Collection of liquid - the duration of the experiment was 26 minutes 37 seconds. The complete sample was collected for 36 minutes 5 seconds. The total water layer was 5010 cc, of which 1733 cc was collected during the time steam only was flowing through the system at 183 cc/min. This implied a flowrate of 7.4 kg/hr (steam : EB :: 14.8:1, increase of 5.3%).

The actual steam flowrate will be taken as 7.4 kg/hr for all studies. The above calculation also applied to Experiments 53-8, 55-3 and 53-4.

Experiment 53-8

After Experiment 53-7, the power to EBSH was cut from 1300 W to 1170 W. This resulted in a lower EBSH temperature than for Experiment 53-7 (see Figure 6.13 for temperature plots). As a result, Experiment 53-8 turned out the best possible steady state profiles, and the steady inlet and catalyst temperatures reflect the slow rise in EBSH temperature. However, once past 540°C, this rise began to quicken, at which point the run was stopped (run duration 30 minutes, 30 seconds). The conversion and efficiency plots in Figure 6.14 show perfectly the expected trends. The

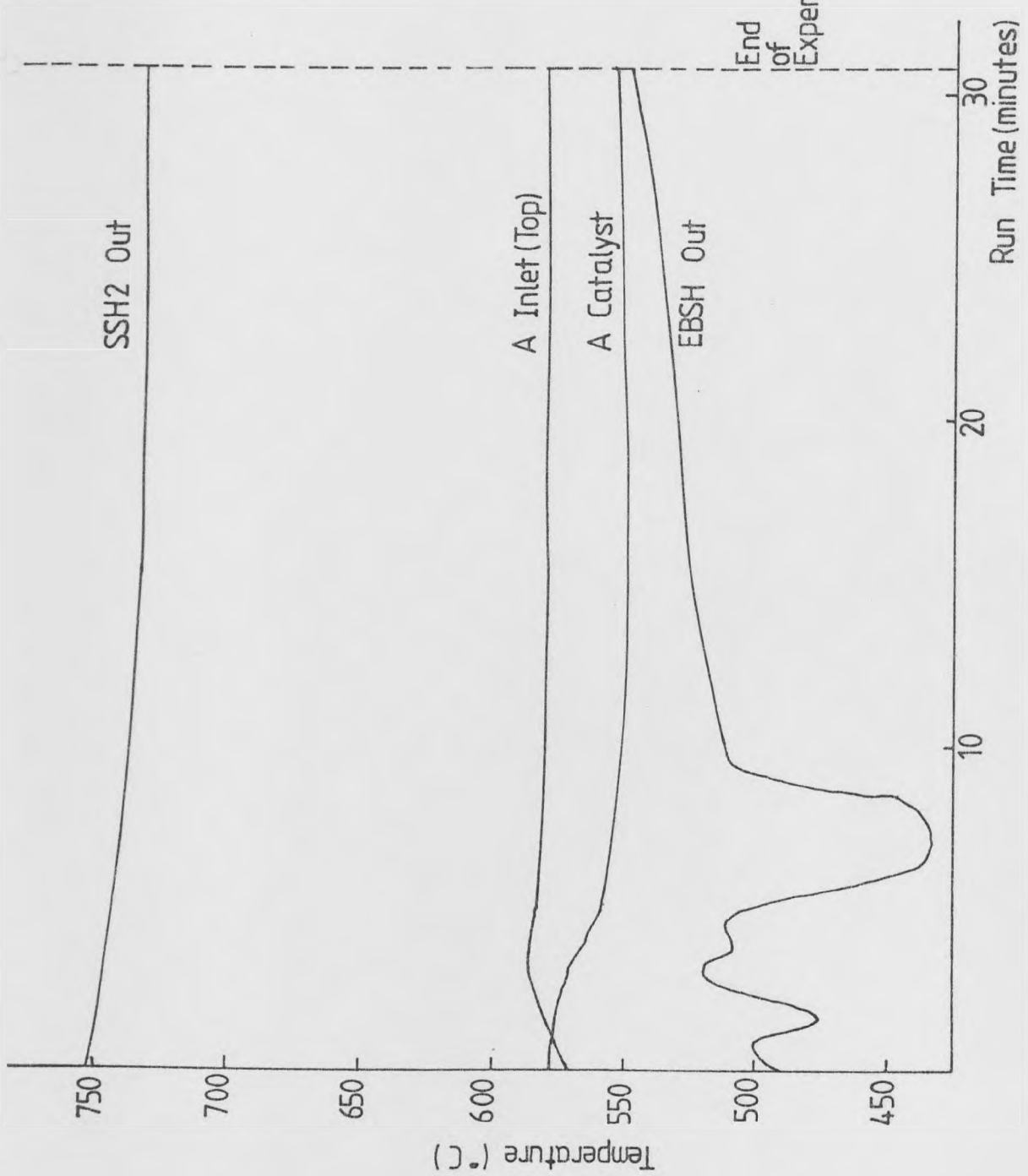

FIGURE 6.13: Temperature-Time Plot for Experiment 53-8

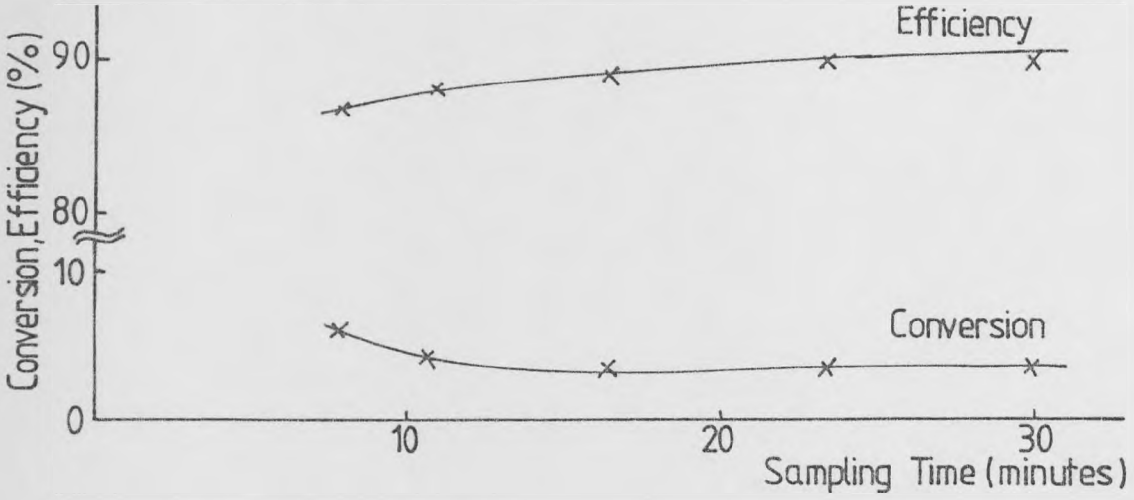

FIGURE 6.14: Conversion, Efficiency Plot for Experiment 53-8

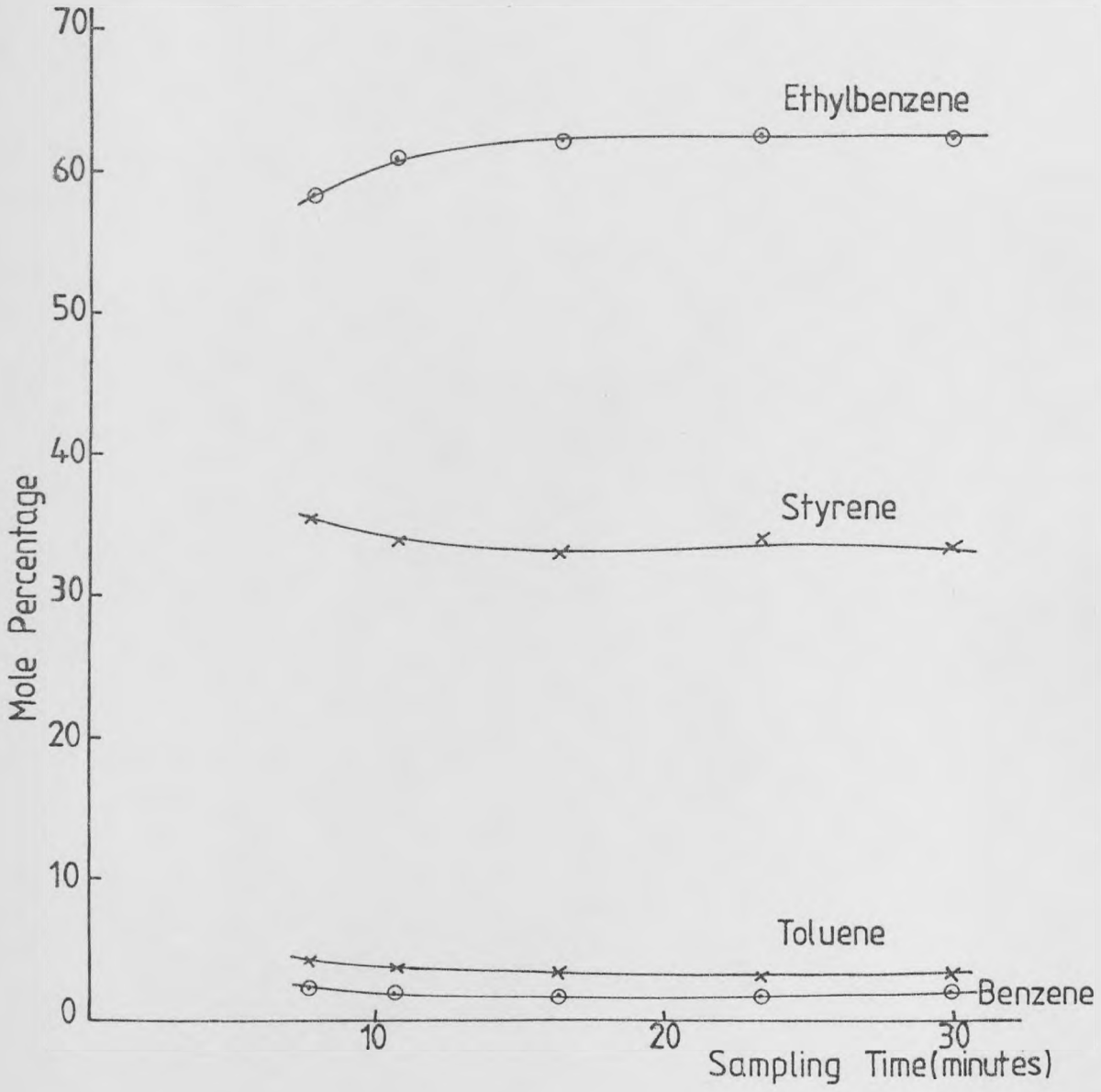

FIGURE 6.15: Component Content Plot for Experiment 53-8

efficiency rises as steady state is approached, then evens out, whilst the conversion falls as steady state is approached and then flattens out. Figure 6.15 shows the concentration of the four aromatics stabilising as well. All this reflects a catalyst of uniform activity.

6.2.4 Transient experiments 55-1 and 55-2

Experiment 55-1

Figure 6.16 shows the unexpected temperature profiles for this transient experiment of 2 minutes duration whilst the bed inlet temperature showed no abnormalities, both the bed catalyst and outlet temperatures rose rapidly. All this points towards a highly exothermic reaction domination. Yet the conversion to styrene was 40.4%, though at a low efficiency (69.4%). The only major exothermic reaction is the toluene producing reaction. Yet the toluene content in the sample though slightly higher than 'normal' experiments, is not that significant to account for the tremendous increase in bed temperature. Since this was a new run, catalyst activation and possibly the 'dormant' effect of transient catalysis may have something to do with this. Section 6.3 will discuss further the transient catalysis effects. After temperature regeneration with steam, the experiment was repeated.

Experiment 55-2

A reaction period of 2 minutes was repeated, at slightly lower temperatures (see Figure 6.17). This time, however, the reaction along the bed showed the anticipated drop in both the catalyst and bed outlet temperatures. The conversion was 35.8% for an efficiency 79.6%. The EBSH temperature this time showed the slight trough towards the end of the run, not observed for Experiment 55-1. The EBSH out temperature for Experiment 55-2 was higher than for 55-1 at the commencing of the experiments. The organic collected for both runs was 56 cc/min, slightly

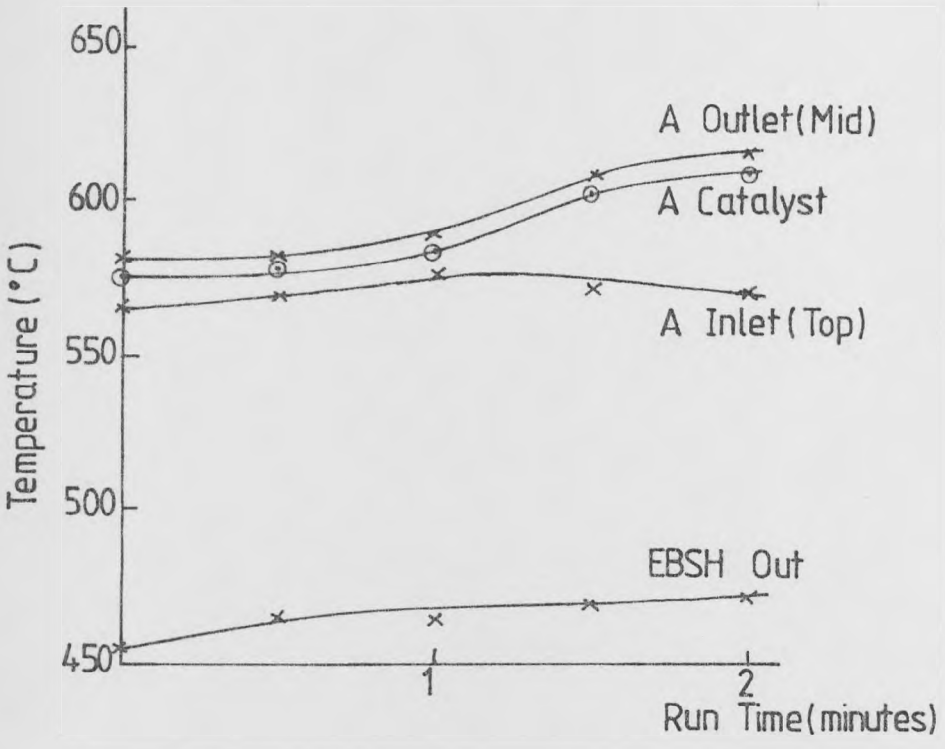

FIGURE 6.16: Temperature-Time Plot for Experiment 55-1

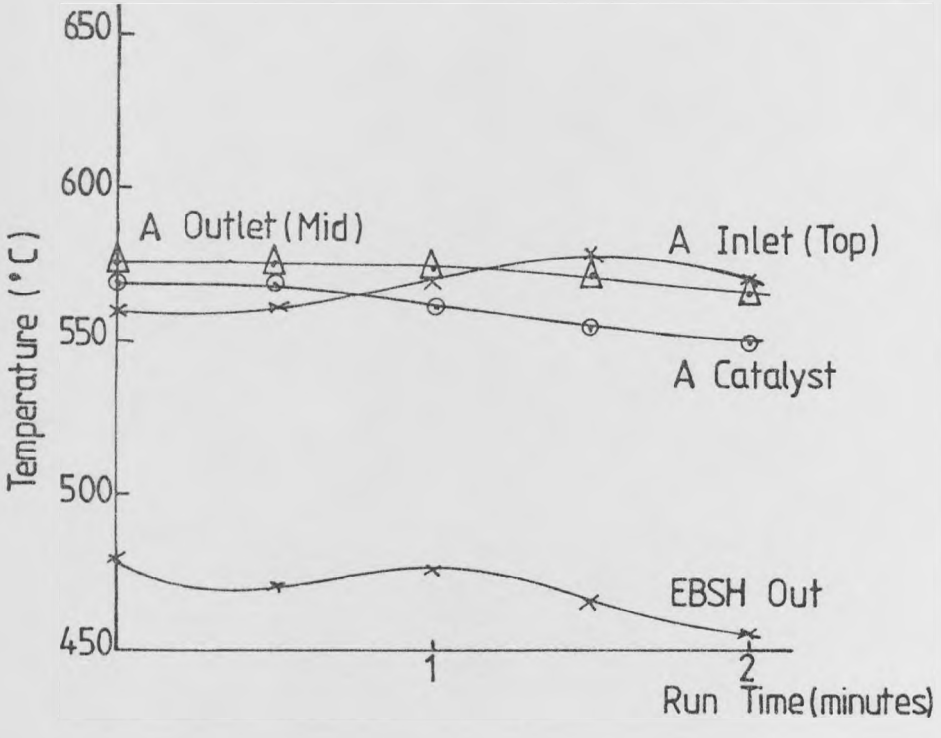

FIGURE 6.17: Temperature-Time Plot for Experiment 55-2

more than the desired flowrate of 55 cc/min.

6.2.5 Steady state experiments 55-3 and 55-4

Experiment 55-3

Having observed the peculiarities in Experiment 55-1, a steady state run was carried out for a duration of 22 minutes 30 seconds. None of the strange patterns of 55-1 were noticed (see Figure 6.18 for the temperature profiles). The experiment showed the characteristics of Experiment 53-7 whereby the EBSH temperature showed similar oscillations before settling to a gradual rise. More liquid samples were taken than for previous steady state experiments and one gas sample was taken (all results in Appendix A8). Figure 6.19 shows the variation of the conversion and efficiency, whilst Figure 6.20 shows the component content change for the four aromatics. The conversion shows the small fall to steady state and then the gradual rise as the bed inlet temperature increases. The efficiency shows the small rise to steady state, and then a fall as EBSH out temperature rises. However, a closer examination of the conversion for a particular bed inlet temperature shows a significantly higher value compared with Experiments 53-7 and 53-8. Section 6.3 will deal with this in detail. The next experiment showed even greater variations in the conversions obtained.

Experiment 55-4

This experiment was the longest of all the steady state experiments (duration 52 minutes 7 seconds), and as the profiles in Figure 6.21 show, steady temperatures were maintained for almost half an hour. Twelve liquid samples and five gas samples were taken. Table A8.1 in Appendix A8 has the analysis of the liquid samples, whilst Table A8.2 has the analysis of four gas samples. The last two of the five gas samples taken were within 2 minutes and 3 minutes of the end of the run. The final

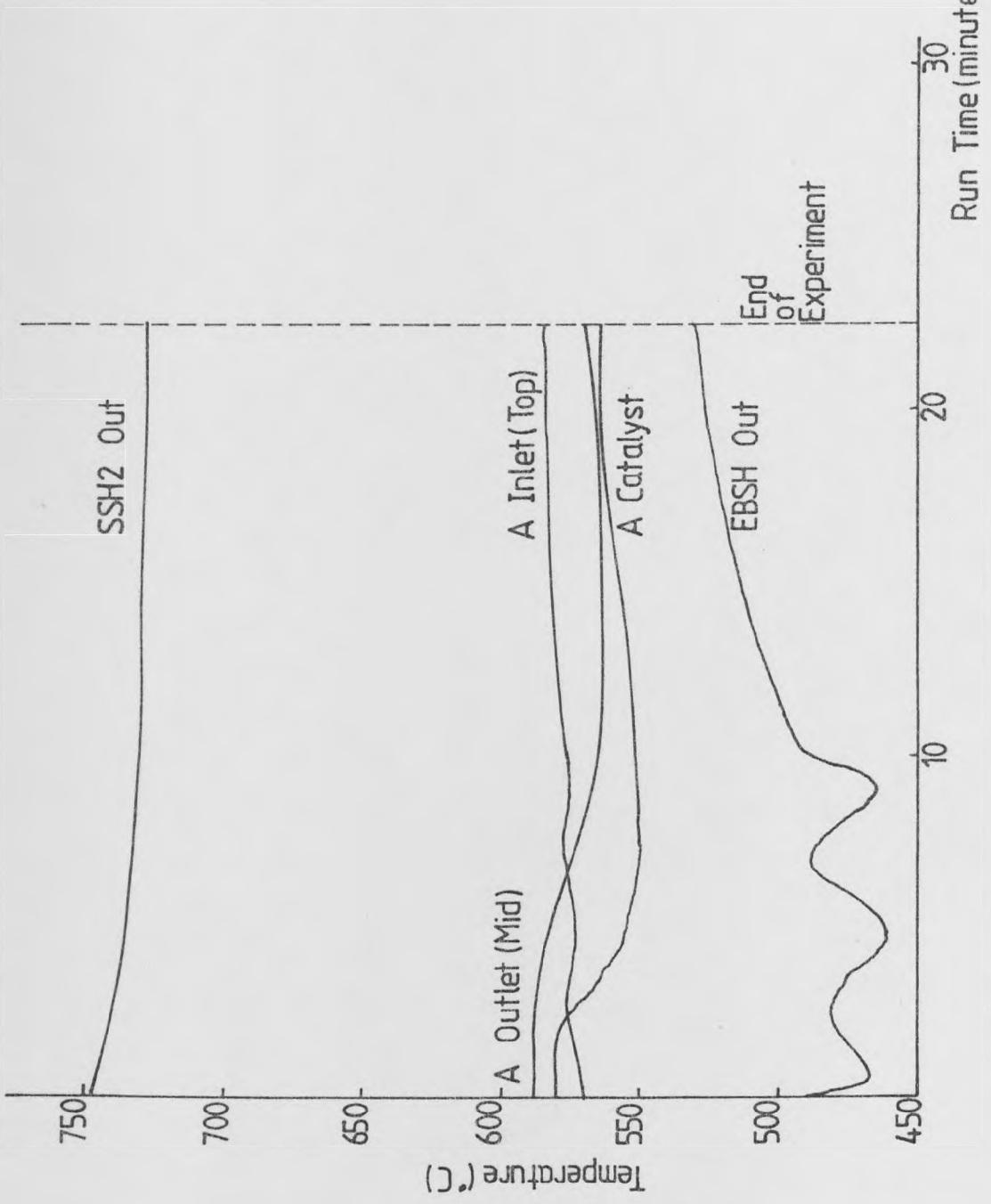

FIGURE 6.18: Temperature-Time Plot for Experiment 55-3

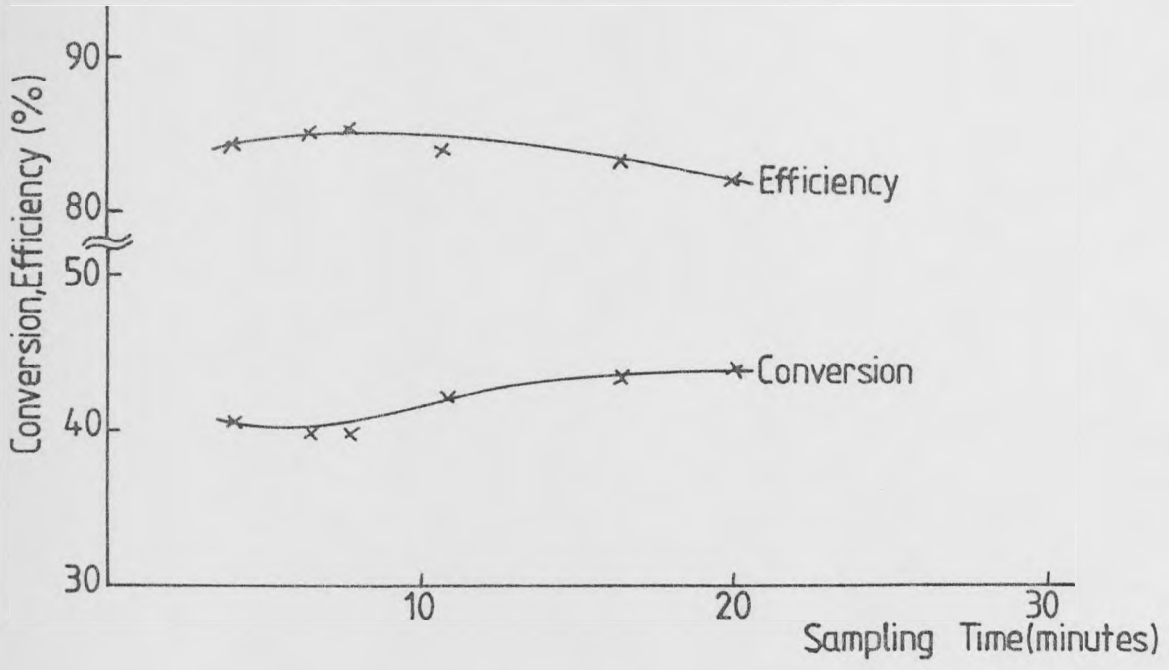

FIGURE 6.19: Conversion, Efficiency Plot for Experiment 55-3

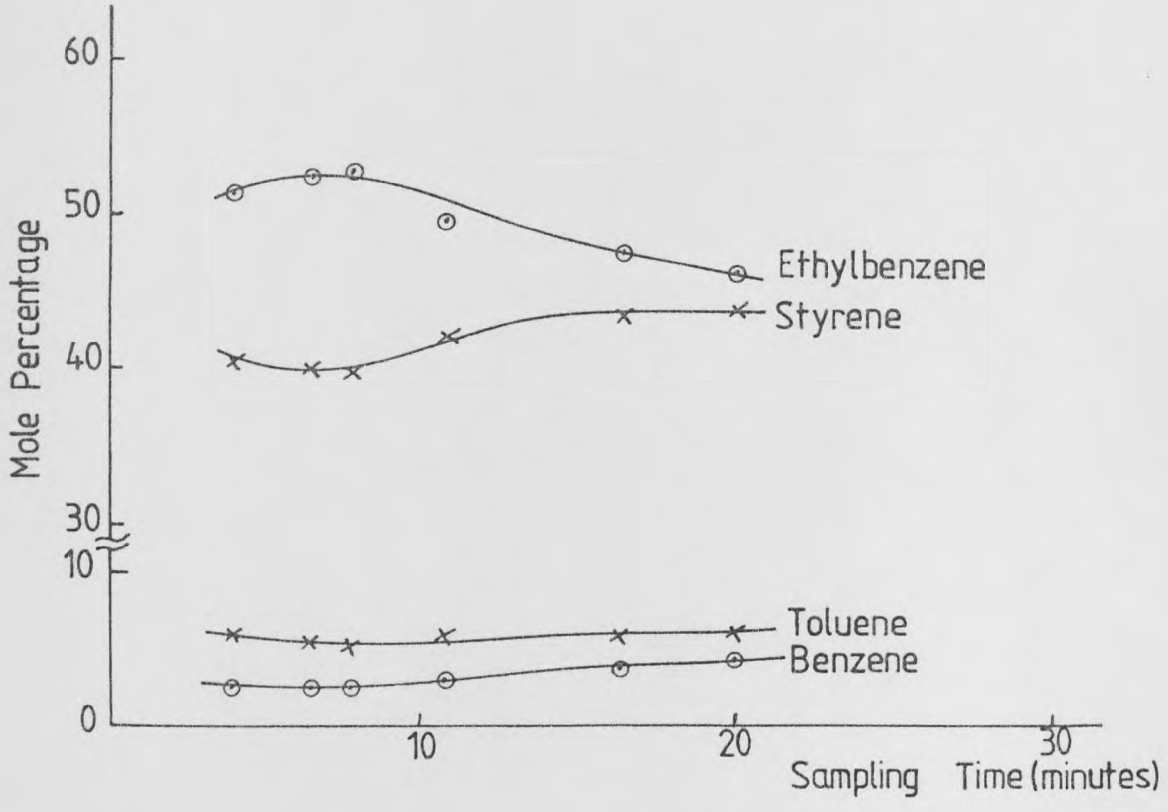

FIGURE 6.20: Component Content Plot for Experiment 55-3

sample only contained oxygen and nitrogen and is therefore ignored. The reason for taking gas samples after the end of the experiment was to investigate the possibilities of any oxides of carbon, that may indicate if any coking or decoking of the catalyst has occurred. The non-existence of any such gases discounts the carbon formation theory.

Nevertheless, the activity of the catalyst has certainly changed dramatically as Figure 6.22 shows. The conversion falls all along the duration of the run, completely against all other steady state experiments that showed that the conversion levels out after 7 minutes. The efficiency also shows a gradual rise. The conversion eventually shows signs of levelling off towards the end of the run. Figure 6.23 shows the changes in concentration of the aromatics and the most obvious observation is a continuous fall in the toluene and benzene levels even though the EBSH temperature has settled to a value higher than at the start of the run. The levels are in fact far lower than those for other steady state experiments. Figures 6.24 and 6.25 attempt to shed some light on this observation by showing the changing concentrations of various gases in the four gas samples taken during and after the experiment.

Clearly, there are many interesting observations raised by these runs, besides the expected results and observations. The next section discusses all the results in greater detail and examines the theory as well as considering the transient experimental results and the steady state experimental results, interlinking all three wherever definite conclusions can be drawn.

6.3 Discussion of Overall Results and Comparisons to Model Predictions

6.3.1 Discussion of transient experiments

Table 6.5 presents the conversions, efficiencies and relevant averaged temperatures for the eight transient experiments carried out.

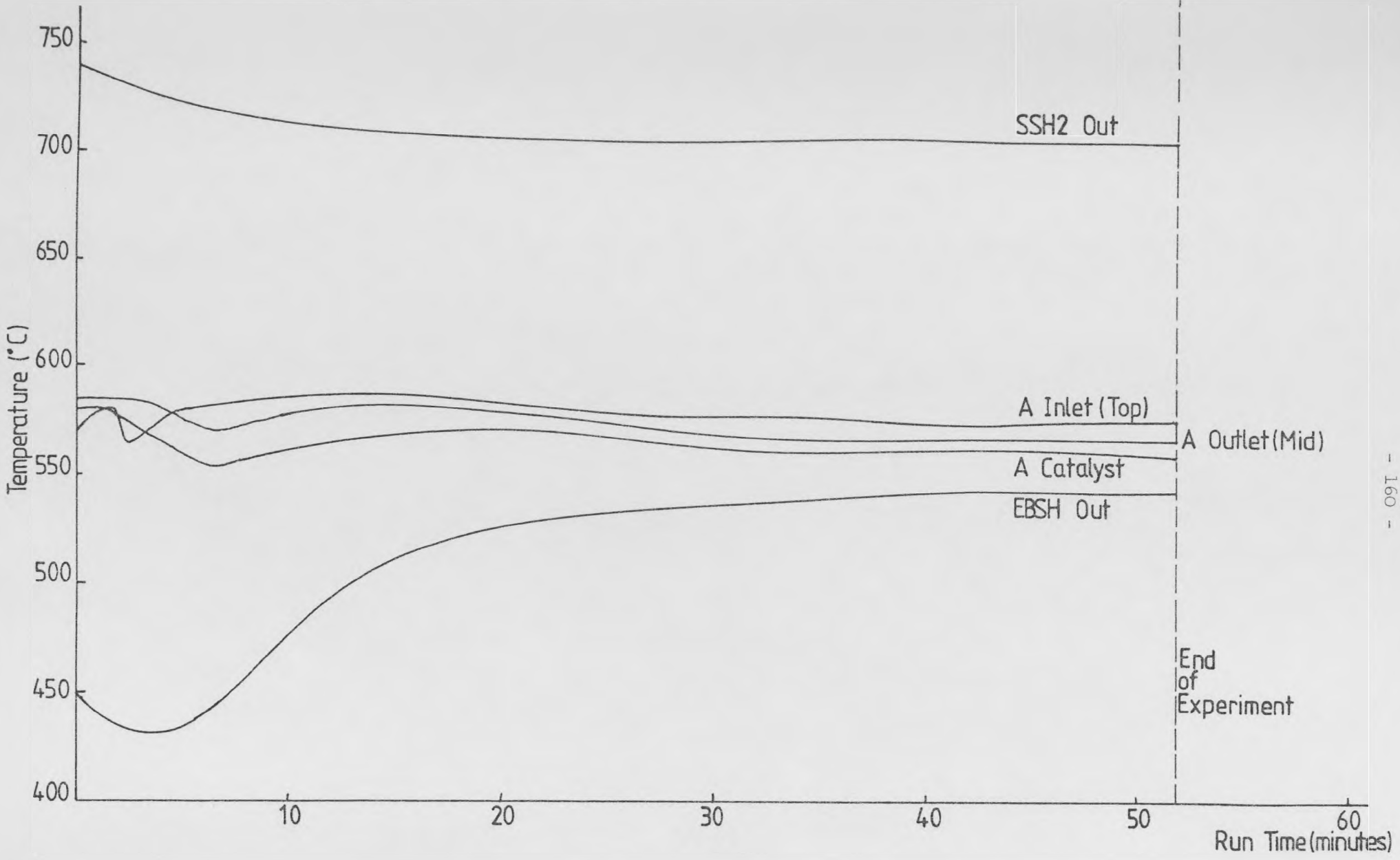

FIGURE 6.21: Temperature-Time Plot for Experiment 55-4

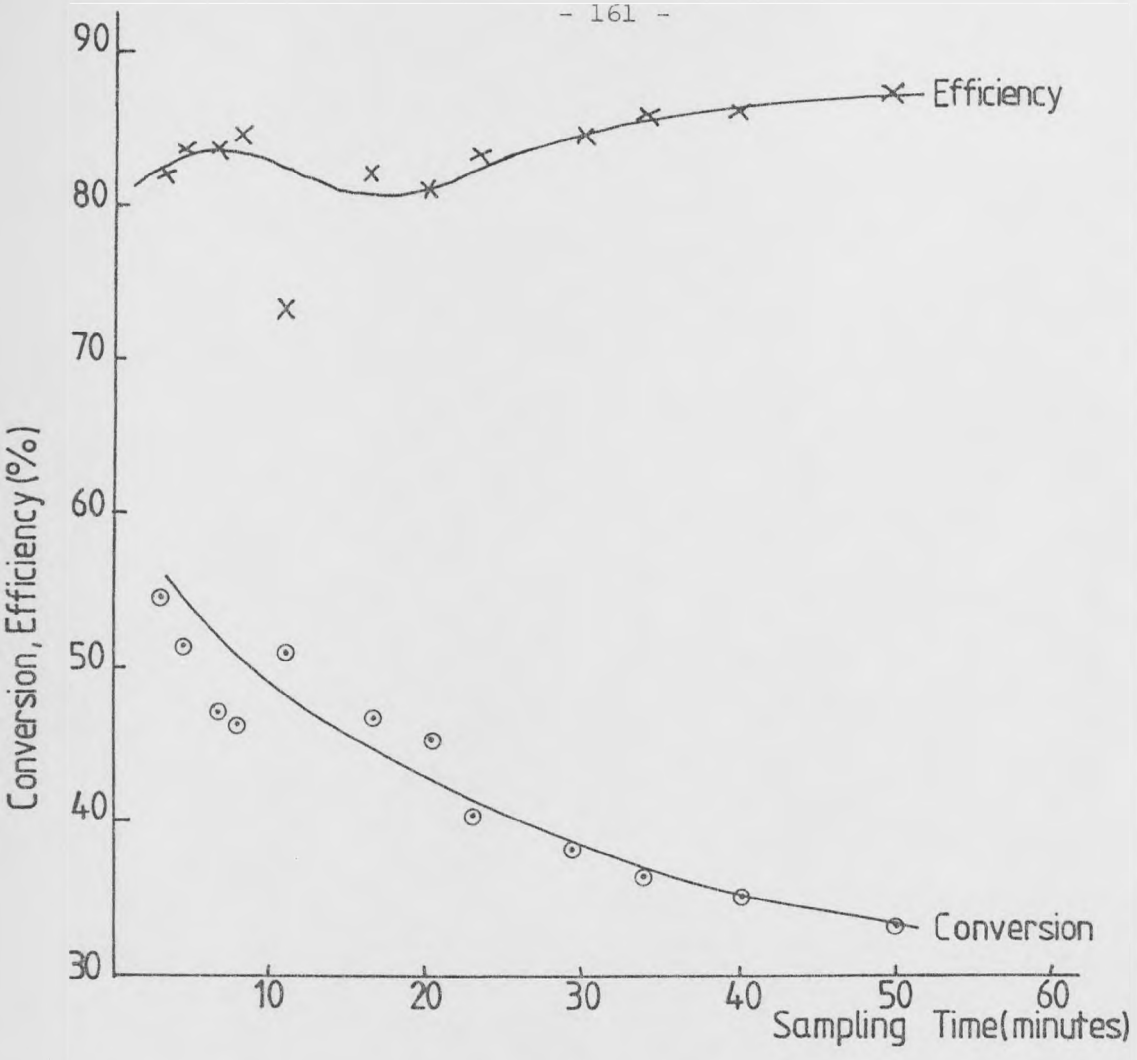

FIGURE 6.22: Conversion, Efficiency Plot for Experiment 55-4

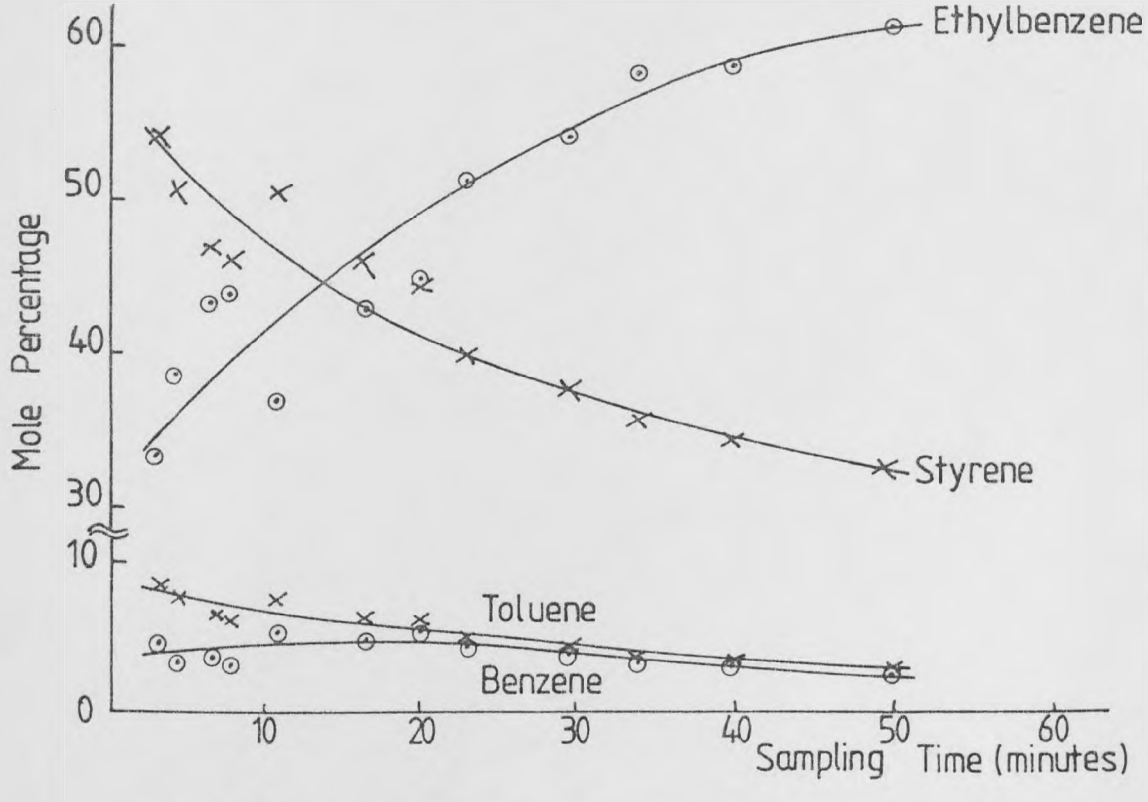

FIGURE 6.23: Component Content Plot for Experiment 55-4

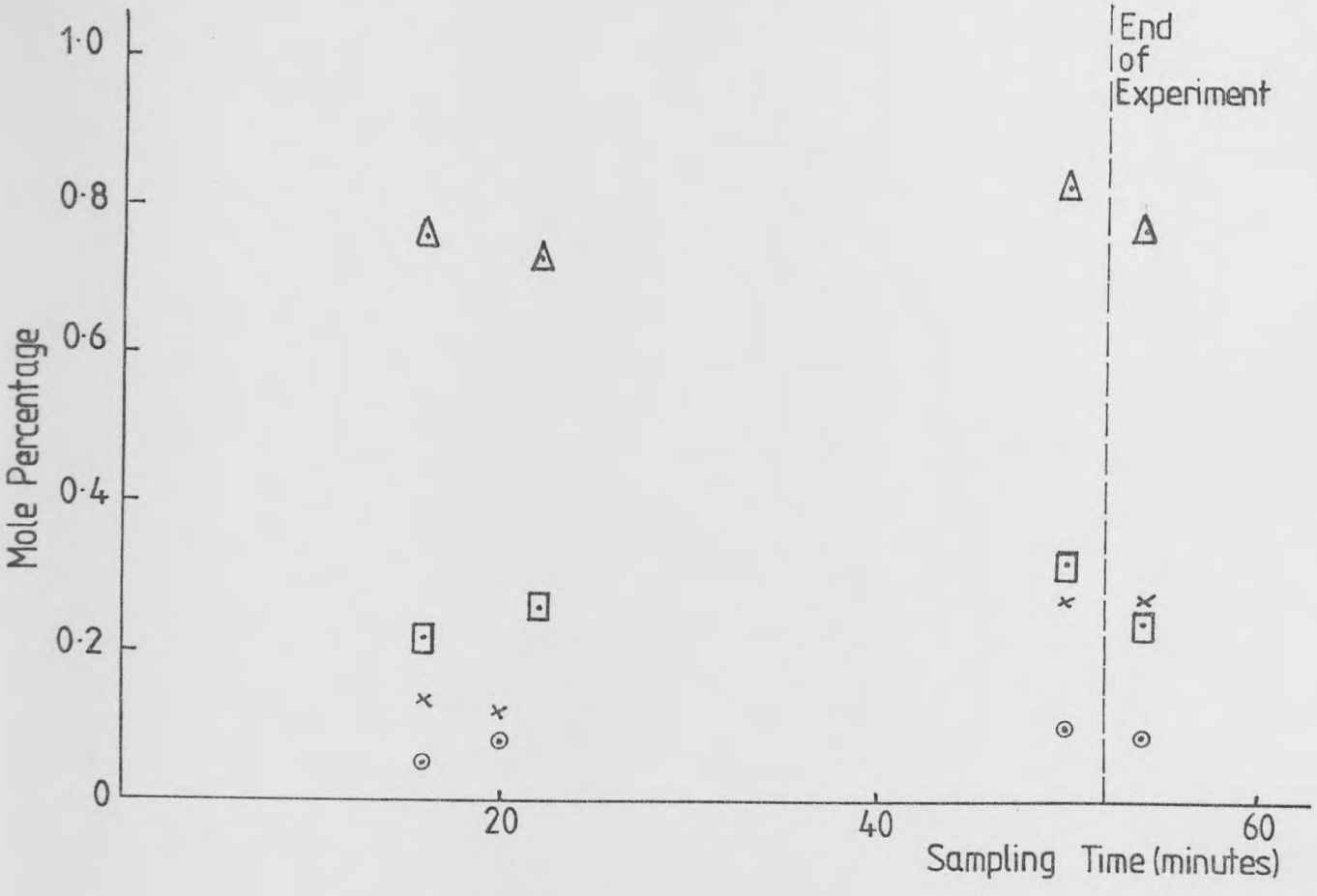

FIGURE 6.24: Gas Content Plot for Experiment 55-4

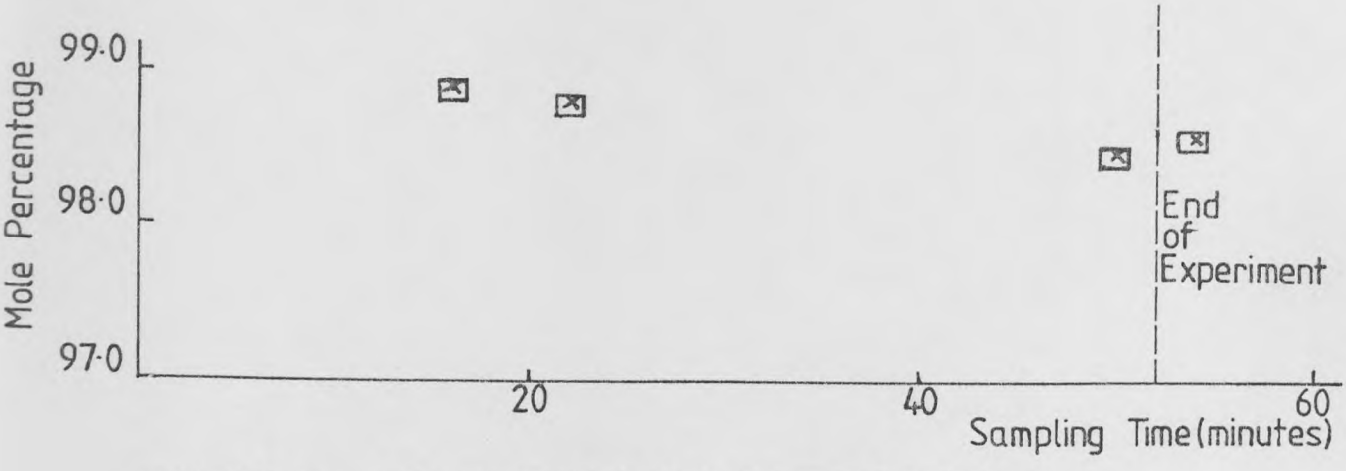

FIGURE 6.25: Hydrogen Content Plot for Experiment 55-4

KEY FOR FIGURES 6.24 AND 6.25

- Methane
- Ethylene
- Ethane
- Hydrogen
- Carbon Dioxide

TABLE 6.5

Comparison of the Eight Transient Experiments

Experiment Number	Duration (minutes)	Conversion (%)	Efficiency (%)	$T_{BED\ INLET}$ (averaged) (^{o}C)	$T_{EBSH\ OUT}$ (averaged) (^{o}C)
53-1	3	48.1	85.0	575	473
53-2	3	43.0	84.7	572	475
53-3	3	39.3	81.1	570	477
53-6	3	31.3	73.8	565	509
53-4	1	39.0	81.1	565	520
53-5	2	32.2	77.8	565	496
55-1	2	40.4	69.4	570	465
55-2	2	35.8	79.6	568	472

The following points are of importance:-

(a) Experiments 53-1, 53-2, 53-3 and 53-6 - these experiments have the same duration of 3 minutes. The conversion to styrene falls from 48.1% at 575°C to 31.3% at 565°C. At the same time, the efficiency falls from 85.0% for an averaged EBSH out temperature of 473°C, to 73.8% for an averaged EBSH out temperature of 509°C, the fall being greater after 500°C.

(b) Experiments 55-1, 55-2 and 53-5 - these experiments have the same duration of 2 minutes. The conversion falls from 40.4% for an averaged bed inlet temperature of 570°C to 32.2% for 565°C. The efficiency of Experiment 55-2 is 79.6% at an EBSH out of 472°C, whilst that of Experiment 53-5 is 77.8% at 496°C. The efficiency falls with increasing EBSH out temperature. Experiment 55-1 exhibited certain unusual aspects discussed in Section 6.2.4 which does not allow its efficiency to be a "normal" result.

(c) Experiments 53-4, 53-5 and 53-6 - these experiments have the same averaged bed inlet temperatures and the conversion falls from 39.0% for a duration of 1 minute to 31.3% for a duration of 3 minutes. The 1 minute experiment exhibits a greater efficiency than one would expect, considering the high EBSH out temperature, and the short duration of the run. The efficiency for the 2 minute duration is greater than that of the 3 minute duration experiment due to the far higher EBSH out temperature.

A study of ethylbenzene pyrolysis at transient and steady states for varying temperatures should provide some more insight into transient behaviour. The surface temperature of the superheater for a particular EBSH outlet temperature could be the crucial factor as well.

6.3.2 Discussion of the steady state experiments

Figures 6.18, 6.13 and 6.10 show that temperature wise, steady state is reached for experiments 55-3, 53-8 and 53-7 within 10 minutes. The conversion profiles for the same experiments also show this, particularly for Experiment 53-8 in Figure 6.14. But although Experiments 55-3 and 55-4 have their temperature profiles indicating the achievement of steady temperatures within this time period, the conversion profiles show a slower decay to steady state for Experiments 55-3 and 55-4 (Figures 6.19 and 6.22), than those of Experiments 53-7 and 53-8 (Figures 6.11 and 6.14). This point is further illustrated in Table 6.6 where the temperatures at the bed inlet as well as the conversions are tabulated for various reaction times for the four experiments. The catalyst activity seems to be affected for Experiment 55-3, and to an even greater extent for Experiment 55-4. This can be seen by comparing the conversions at 576°C and 578°C for Experiments 55-4 and 55-3 with those of Experiment 53-8. Experiments 55-3 and 55-4 show the observations of Billimoria[76] discussed in Section 4.1.3. The equilibrium of the Fe_2O_3 catalyst mentioned in Section 4.1.3 is certainly affected by prolonged regeneration by steam. Both Experiments 55-3 and 55-4 had black Fe_3O_4 particles washed out in the samples (this was proved by oxidation to red Fe_2O_3 in a furnace at 850°C). Experiments 53-7 and 53-8 had very few such particles washed out. This seems to indicate a change in the surface composition during steam regeneration, which could explain the higher catalyst activity.

Another point of note is the high toluene and benzene content during the earlier stages of Experiment 55-4. This then tends to fall

TABLE 6.6

Comparison of the Four Steady State Experiments

Experiment Number	Time = 10 minutes		Time = 20 minutes		Time = 25 minutes	
	Bed Inlet Temperature (°C)	Conversion (%)	Bed Inlet Temperature (°C)	Conversion (%)	Bed Inlet Temperature (°C)	Conversion (%)
53-7	588	39.0	590	40.6	592	41.0
53-8	580	34.6	580	33.3	578	33.2
55-3	576	41.7	583	44.0	-	-
55-4	585	48.5	582	44.0	580	41.7

continued .....

TABLE 6.6 continued .....

Experiment Number	Time = 30 minutes		Time = 40 minutes		Time = 50 minutes	
	Bed Inlet Temperature (°C)	Conversion (%)	Bed Inlet Temperature (°C)	Conversion (%)	Bed Inlet Temperature (°C)	Conversion (%)
53-7	-	-	-	-	-	-
53-8	578	33.2	-	-	-	-
55-3	-	-	-	-	-	-
55-4	578	39.2	576	35.6	576	33.3

dramatically as the run progresses, outweighing the effect of EBSH Out rise. This feature is not exhibited by Experiment 53-7, 53-8 and 55-3 (see Figures 6.12 (for 53-7); 6.15 (for 53-8); 6.20 (for 55-3); and 6.23 (for 55-4)). This can be explained by examining the gas sample analysis (Table A8.2 in Appendix A8, and Figures 6.24 and 6.25).

Comments on the gas sample results

The first point of importance is the significant quantity of ethane present. None of the six reactions presented and used in Section 2.1 produce ethane. Sheel and Crowe[25]*** suggest two ethane producing reactions, but then proceed to ignore their significance.

$$C_2H_6 \rightleftharpoons C_2H_4 + H_2 \qquad (6.1)$$

$$C_6H_5C_2H_5 + H_2 \rightarrow C_6H_6 + C_2H_6 \qquad (6.2)$$

The sheer quantity of ethylbenzene and hydrogen present during reaction in the reactor, and the similar mechanism of reaction 6.2 to reaction 2.3, the toluene producing reaction, question of the validity of reaction 6.2. No other data in literature on reaction 6.2 can be traced. Thereby one can assume that the ethane producing reaction is reaction 6.2.

*** Note:- Sheel and Crowe[25] are mistaken in assuming Reaction 6.1 as being:

$$C_2H_6 \rightarrow C_2H_4 + H_2 \qquad (6.3)$$

Smith[93] and others verify that this is in fact an equilibrium reaction, and is assumed as such as reaction 6.1.

The fact that the amount of ethane produced is shown to increase with EBSH Out temperature (i.e. greater pyrolysis, therefore more benzene and ethylene) shows the validity of reaction 6.1. Reaction 6.1 cannot be ignored for mass and heat balances for this system and the G-64C catalyst.

Figures 6.24 and 6.25 show a drop in H_2, no change in CH_4 and C_2H_4 as Experiment 55-4 proceeds, and a large increase in CO_2. This certainly points to a changing activity of the catalyst since the last sample had no oxides of carbon at the end of run, and steam regeneration rules out carbon deposits accounting for the CO_2. Sheel and Crowe[25] mention the possibility of the following reactions:-

$$C_2H_4 + 2H_2O \rightarrow 2CO + 4H_2 \qquad (2.4)$$

$$CH_4 + H_2O \rightarrow CO + 3H_2 \qquad (2.5)$$

$$CO + H_2O \rightarrow CO_2 + H_2 \qquad (2.6)$$

The evidence seems to indicate that whilst the steam regeneration produces greater catalyst activity, the decaying period leads to more production of the oxides of carbon, and finally the high content of CO_2.

6.3.3 The comparison of transient and steady state experiments

Due to small changes in reactor bed inlet conditions before steady state is reached (10 - 15 Centigrade degrees), the reactor steady state results are generally at higher temperatures than those for the transient runs. But the advantages of the transient system over the steady state system are apparent. Tables 6.5 and 6.6 can be compared to show the greater conversions possible for a transient system over that of a steady state system. An example is the steady state conversion for a bed-inlet temperature of 575^{o}C is 33.2% (Experiment 53-8) whilst that for a transient experiment of duration 3 minutes (Experiment 53-1) is 48.1%. A steady state system with an inlet temperature of 592^{o}C has a conversion

of 41.0%. Therefore a two way improvement is possible by a transient reactor system:-

(i) higher conversions at a fixed inlet temperature,

or

(ii) lower operational temperatures for a fixed conversion. This has the added advantage of better efficiencies.

The conversion profiles of the result of catalyst superactivation show the further advantage of regeneration by steam, which can result in prolonging the duration of the transient run to obtain a particular conversion as the catalyst is exposed to longer periods of steam regeneration.

Kaeding[94] showed that a 1% increase in styrene yield in a 250,000 tonne/year styrene plant represents a $300,000 annual saving (1973 figure, $780,000 present day value). This shows the value of aiming for an understanding of the transient reactor.

6.3.4 The application of the reactor models to the experimental conditions

The computer programs used in Sections 4.1 and 4.2 are now used to generate their predictions for the conversions, efficiencies and the bed temperature profiles for the experimental conditions. The bed temperatures used range from 560°C for the lowest inlet temperature for a transient run, to 592°C for the highest bed inlet temperature used for a steady state run. Tables 6.7 and 6.8 tabulate the two-stage adiabatic reactor system predictions using both beds at the same inlet temperature shown. The pressure at the entry to the first bed is 1.67 bar, and to the second bed is 1.32 bar, the actual observed pressures for the experimental apparatus. The flowrates for the Table 6.7 are 7.0 kg/hr steam and 2.95 kg/hr ethylbenzene, the system design flowrates, whilst for Table 6.8 the flowrates are 7.4 kg/hr steam and 2.95 kg/hr ethylbenzene, the flowrates during an actual reaction run.

TABLE 6.7

Model Results for a 2 Bed SSAR with Same Inlet Temperatures to Both Beds (using 7.0 kg/hr steam and 2.95 kg/hr ethylbenzene)

Bed Inlet Temperature (^{o}C)	1st BED OUTLET		2nd BED OUTLET	
	Conversion (%)	Efficiency (%)	Conversion (%)	Efficiency (%)
560	22.7	92.0	36.2	90.2
565	24.3	91.8	38.6	89.9
570	25.8	91.7	40.8	89.7
575	27.5	91.5	43.2	89.5
580	29.1	91.3	45.5	89.2
585	30.7	91.1	47.8	89.0
590	32.3	90.9	50.2	88.8

TABLE 6.8

Model Results for a 2 Bed SSAR with Same Inlet Temperatures to Both Beds (using 7.4 kg/hr steam and 2.95 kg/hr ethylbenzene)

Bed Inlet Temperature (°C)	1st BED OUTLET		2nd BED OUTLET	
	Conversion (%)	Efficiency (%)	Conversion (%)	Efficiency (%)
560	23.0	92.2	36.6	90.5
565	24.6	92.0	38.9	90.2
570	26.1	91.9	41.2	90.0
575	27.8	91.7	43.6	89.8
580	29.4	91.5	46.0	89.6
585	31.1	91.3	48.3	89.3
590	32.8	91.1	50.7	89.1

Table 6.9 shows the mean conversions, efficiencies and point temperatures predicted for transient runs of varying duration from 1 minute to 3 minutes and bed inlet temperatures varying from 560°C to 590°C. The bed inlet pressure used is 1.27 bar, the actual experimental reading during a reaction run. The next section uses this data, derived from kinetics by Bogdanova[33] and Cockcroft[10] as a comparison with the actual results obtained.

6.3.5 The composition of the model results with the experimental transient and steady state results

(a) The transient runs

Table 6.10 shows the actual observed conversions, and the model conversions (from Table 6.9) for various averaged inlet temperatures. At lower temperatures, 565 - 568°C, Cockcroft's models show underestimates for the conversions obtained though not to a large level. As the bed inlet temperature increases, the model completely fails especially at around 575°C and 572°C, giving rise to the suspicion that the kinetics are in fact functions of time and temperature, as well as chemical surface processes. At around 565°C, the model predictions are slightly higher than those observed.

Efficiency comparisons are not advisable since the pyrolysis of ethylbenzene is not a factor in Bogdanova's experimental data. The ethylbenzene was only preheated to 300°C before being mixed with steam at the bed entrance and passed through a heated bath-type reactor. Therefore, one would expect slightly higher conversion predictions from this data since more ethylbenzene is available for the reaction. This clearly is not the case.

(b) The steady state runs

Table 6.11 illustrates the various conversions (predicted and

TABLE 6.9

Model Results for a Single Bed Transient Reactor (using 7.4 kg/hr steam and 2.95 kg/hr ethylbenzene)

Bed Inlet Temperature (°C)	Transient t = 1 minute				Transient t = 2 minutes			
	Mean Conversion (%)	Efficiency (%)	T_{CAT} (°C)	T_{OUT} (°C)	Mean Conversion (%)	Efficiency (%)	T_{CAT} (°C)	T_{OUT} (°C)
560	32.9	92.6	554.3	556.6	31.5	92.6	548.1	552.8
565	35.6	92.4	558.9	561.5	34.1	92.5	552.1	557.5
570	38.3	92.2	563.5	566.3	36.7	92.3	556.3	562.1
575	41.1	92.0	568.0	571.2	39.3	92.1	560.3	566.7
580	44.0	91.8	572.7	576.1	42.0	91.9	564.3	571.4
585	46.9	91.6	577.2	581.0	44.7	91.7	568.4	576.0
590	49.7	91.4	581.8	585.9	47.5	91.6	572.4	580.7

continued .....

TABLE 6.9 continued .....

Bed Inlet Temperature (°C)	Transient t = 3 minutes				Steady State			
	Mean Conversion (%)	Efficiency (%)	T_{CAT} (°C)	T_{OUT} (°C)	Mean Conversion (%)	Efficiency (%)	T_{CAT} (°C)	T_{OUT} (°C)
560	30.3	92.7	544.1	548.6	23.1	93.1	534.9	526.4
565	32.7	92.6	545.6	553.1	24.7	92.9	537.9	529.2
570	35.9	92.3	549.1	557.5	26.3	92.8	540.9	532.0
575	37.7	92.2	552.6	561.7	27.9	92.7	543.8	534.6
580	40.2	92.1	556.2	566.1	29.6	92.5	546.8	537.4
585	42.8	91.9	559.6	570.5	31.3	92.4	549.7	540.2
590	45.4	91.7	563.0	574.8	32.9	92.3	552.4	542.8

TABLE 6.10

Actual and Predicted Conversions for the Transient Experiments

Experiment Number	Duration (minutes)	Averaged Bed Inlet Temperature (^{o}C)	Model Predicted Conversion (%)	Observed Conversion (%)
53-1	3	575	37.7	48.1
53-2	3	572	36.4	43.0
53-3	3	570	35.9	39.3
53-6	3	565	32.7	31.3
53-4	1	565	35.6	39.0
53-5	2	565	34.1	32.2
55-1	2	570	36.7	40.4
55-2	2	568	35.7	35.8

TABLE 6.11

Actual and Predicted Conversions for the Steady State Experiments

Experiment Number	Averaged Bed Inlet Temperature (°C)	Model Predicted Conversion (%)	Observed Conversion (%)
53-7	588	32.3	39.0
	590	32.9	40.6
	592	33.6	41.0
53-8	578	28.9	33.2
	580	29.6	34.6
55-3	576	28.2	41.7
	583	30.6	44.0
55-4	576	28.2	33.3
	576	28.2	35.6
	578	28.9	39.2
	580	29.6	41.7
	582	30.3	44.0
	585	31.3	48.5

observed) for a range of steady state bed inlet conditions, similar to the data extracted for Table 6.6, i.e. for steady state temperature conditions. The efficiency comparisons are not used, for the reasons mentioned above. The major point of note is the tremendous increase in catalyst activity for Experiments 55-3 and 55-4. Experiments 53-7 and 53-8 show the difference between the predicted conversion and the observed conversion for a fresh catalyst to be around 15 - 22% over the temperature range 578 - 592°C. However, this is forced up to 55% for Experiment 55-4 at 585°C, and later this decays to 18% at the last value observed, i.e. at 576°C. Similarly, the difference is of the order of 44% for Experiment 55-3.

Finally, a point of note on the ethylbenzene pyrolysis. There is no data available in literature on this subject. Various patents[21,24,91] mention that ethylbenzene pyrolysis becomes significant after 540°C. However, these observations are based on industrial gas fired superheaters, operating at high flowrates and transfer coefficients. Table 6.12 shows the superheater surface temperatures predicted by the model in Section 3.7.2. The right criterion, on which any deductions on the extent of ethylbenzene pyrolysis are made, should be the temperatures of the transfer surfaces, and not the outlet temperature of the ethylbenzene. The model predictions in Table 6.12 show that the pipe surface temperatures are significantly higher than the ethylbenzene superheater exit temperatures. The discussion has avoided any comparison of efficiency results due to the unknown effect of this pyrolysis. However, any such study of pyrolysis undertaken, whether for transient state, or for steady state flow conditions, must attempt to correlate the degree and levels of pyrolysis with the superheater heat transfer surface temperatures, especially the maximum temperature of the inner annulus tube. An initial guess at the critical temperature after which the pyrolysis is significant

TABLE 6.12

Superheater Temperatures for Varying EBSH Outlet Temperatures

(Inlet temperature 155°C, flowrate 2.95 kg/hr)

Maximum Firebar Temperature $T_{M.FB}$ (°C)	Maximum Inner Annulus Pipe Temperature $T_{M.WI}$ (°C)	EBSH Outlet Temperature $T_{EB.OUT}$ (°C)	Maximum Outer Annulus Pipe Temperature $T_{M.WO}$ (°C)
691.1	532.2	450.0	510.0
713.6	555.3	470.0	533.4
735.8	578.3	490.0	556.7
768.5	612.5	510.0	591.4
790.0	635.1	530.0	614.4
811.2	657.6	550.0	637.3
836.4	685.5	570.0	667.2
863.2	713.0	590.0	693.8

would be a temperature of 600°C for the inner tube, but this could vary greatly for transient and steady state experiments.

Concluding, the advantages of a transient reactor system for the dehydrogenation of ethylbenzene over an iron oxide catalyst exist in the higher conversions (greater than any model predictions) possible as well as the strong regeneration the steam cycle provides to the catalyst. This study also gives rise to a number of questions on the transient behaviour of the catalyst. Certainly the evidence indicates complex and competing mechanisms during the transient runs. The catalysis survey in Section 4.1.3 shows some general directions in which this relatively modern subject is being pursued. The competing benzene and toluene producing reactions make this a far more complex investigation than others so far pursued (most of them single reactions, observing 2 to 3 stages of progression). A study of ethylbenzene pyrolysis at transient and steady state should lead to more clarity on the subject of the competing reactions, and the actual conversion of these reactions over the catalyst itself during the transient run. The pyrolysis study needs to be linked to the actual superheater surface temperature as well.

A study of ethylbenzene pyrolysis ought to allow the development of reliable kinetics, both at transient and steady states. Unfortunately, the necessity to keep lower temperatures on the EBSH → Reactor line has meant that the present set up cannot pursue studies at any higher temperatures.

The provision of an additional superheater would allow greater steam flow at greater temperatures and should enable this study to be pursued at temperatures in excess of 600°C, where the advantages of a transient system will be even more apparent.

Certainly, the generation of catalytic kinetics for transient and steady state conditions for fresh and fouled (and superactive) catalysts,

as well as the use of different catalysts should contribute greatly to the sparse research in the field of transient catalysis, and the viability of a transient regenerative reactor system should be even more certain.

CHAPTER 7

SUMMARY OF THE RESEARCH ACHIEVEMENTS AND SUGGESTIONS FOR FUTURE STUDIES

CHAPTER 7

SUMMARY OF THE RESEARCH ACHIEVEMENTS AND SUGGESTIONS FOR FUTURE STUDIES

7.1 Summary of the Project Conclusions

Adiabatic or multitubular steady state reactors do not give the optimum temperature profiles for heterogeneous catalytic reactions, especially if the reactions have a high heat of reaction and are equilibrium controlled. This project is aimed at developing a pilot plant for the investigation of the regenerative catalytic reactor (RCR). The RCR utilizes the inherent characteristics of the thermal regenerator to provide better control of the temperature profiles along the bed resulting in better conversions. A RCR system must have at least two reactors to ensure continuous production. At any one time, one bed carries out the reaction stroke whilst the temperature levels of the other are being regenerated.

The investigation has centred round the dehydrogenation of ethylbenzene to styrene; a strongly endothermic, equilibrium controlled reaction which is carried out over alkali promoted iron oxide catalysts. The reaction utilizes steam as a diluent. Steam can also be used as the heat transfer medium for the RCR system.

The pilot plant has been designed to accommodate several reactor configurations: one bed and two bed SSAR arrangements, as well as a single bed RCR system. The design also allows for variations in the steam to ethylbenzene ratio, the system pressure, as well as the transient run duration. Safety considerations dictated that the pilot plant must be housed on two levels of the laboratory with the majority of the inflammable isolated outside the main laboratory building. This created problems in maintaining the required temperature levels due to heat loss

from the long delivery pipelines.

The high temperatures to which the feed streams have to be heated (up to 750°C) posed a considerable design problem since only electrical heating capacity was available. A novel design of radiation superheaters was implemented. Mathematical models for the steady state operations of such firebar source heaters were developed. Successful operation predictions allowed the commissioning to be carried out. This involved problems in raising the transfer surface emissivities and the successful power step up and step down of the heaters without excessive stress on the brittle ceramic firebar cores. These were overcome by the use of mathematical solutions predicting the high temperature gradient zones, and by means of actual trials of the rates of power step ups and step downs. The superheaters were found to work to very high heat transfer efficiencies, long operation without firebar replacement, and provide good, stable temperature control.

The heat loss compensation along the system pipework and reactors called for extensive modelling of the transfer resistances that caused failings of the bead insulated resistance wires. Novel heat shields utilizing copper plates and bead insulated resistance wires were developed and successfully utilized for operation up to 620°C. Models for their temperature distribution were also developed. A combination of the copper shields and heat tracing tapes enabled the reactor temperatures to reach the required reaction range of 560 - 650°C. The high power loads needed for the heat loss compensation forced this study to be limited to investigations with a single reactor subjected to steady state and transient operating conditions.

A series of transient runs of varying duration and steady state runs were carried out and the results were compared to the reactor model solutions based on the only set of reliable kinetics available in literature.

The transient runs yielded conversions far higher than those of the steady state runs (e.g. for a bed inlet temperature of 575°C, a transient run of 3 minutes duration showed a conversion of 48.1%, as to 33.2% for the steady state run). The trends in conversions expected were more in evidence than those in efficiencies largely due to the uncertainty over the transient and steady state pyrolysis of the ethylbenzene before the entrance to the catalyst bed. This needs further investigation.

The steady state results showed a good agreement with the model predictions, especially at the lower ranges of the temperatures investigated. However, the transient results were much higher than the predictions, giving rise to doubts over the validity of the use of steady state kinetics to predict transient operation. Observations showed that steam regeneration superactivates the catalyst and raises reaction rates before prolonged reaction operation causes the rate to gradually decay towards its steady state level.

Data in the literature is scarce and limited to single reaction processes. However, observations suggest a dependence of the transient reaction rates on reactant chemisorption, reactant dissolution into the catalyst bulk and other chemical surface processes, the duration of the run, the temperature levels, steady state reaction rates etc.

The potential of a transient catalytic reactor for styrene manufacture is in no doubt. However, there are uncertainties over the catalysis and the pyrolysis of the ethylbenzene at transient states that need to be greatly examined. The study certainly emphasised the advantages of the periodic operation over the steady state operation even in the relatively small range of investigation.

7.2 Suggestions for Future Work

(a) Ethylbenzene pyrolysis

The first important study should aim to investigate the transient and steady state pyrolysis of ethylbenzene, over the temperature range 450 - 550°C, and correlate this to the superheater surface temperatures as suggested in Section 6.3.5. The study would then enable steady state and transient kinetics to be derived, taking the effect of pyrolysis into account.

(b) Catalysis and reaction runs

The initial studies should be limited to the present range investigated, i.e. bed inlet temperatures of 560°- 590°C. The effects of transient and steady state reaction runs, as well as steam regeneration should be carried out on:-

(i) fresh catalysts - alkali based Fe_2O_3 catalysts;

(ii) fouled (superactive) catalysts - after a couple of shut-downs;

(iii) various commercial catalysts including the more recent nickel/cobalt based silver catalysts[96].

The studies should centre around achieving cyclic steady state for a particular bed inlet temperature and transient run duration. The effect of surface processes should become more apparent here. Steady state runs as well can be repeated at particular temperature levels so as to assess the catalyst superactivation, the change in the reaction rates, and the decay of these rates to their original level. Better sampling, e.g. immediately after the bed exit should help the transient studies in particular. Since the safety of the plant is now proven, the very latest manual 3-way valves[97] that can operate at 650°C can be utilized in the control room.

(c) Two bed SSAR studies

The provision of new power supply lines should enable these studies to proceed without much difficulty especially as the interstage superheater (SSH3) has already been commissioned, and the methods for heat loss compensation have been examined in detail.

(d) Better temperature read-outs

The present 16 point Kent temperature recorder leaves much to be desired in recording the temperatures during the first and crucial three minutes of the reaction runs. Even the present arrangement of monitoring reactor bed temperatures twice during a 16 point cycle is not adequate. An e.m.f. measurement read-out every 5 - 10 seconds would be desirable for the four major temperatures, i.e. EBSH out and the three bed readings. A small micro would be advisable.

(e) Studies at higher temperatures

The need to maintain the EBSH out temperature around 500^{o}C has meant that the present investigations have been carried out at the highest possible temperature levels for this apparatus. The circuit control resistances and the variation in firebar resistance means that the maximum, a so-called 2 kW firebar can supply during operation is 1.8 kW. Therefore, it is suggested to utilize an additional superheater, SSHX, thereby providing a total capacity of 5.4 kW. There is room in the superheater box to accommodate another heater. The limit that the three superheaters can heat the steam to should be set at 800^{o}C (limitation temperature of gaskets, seals, seats, 'Isotapes').

To obtain a maximum temperature of 650^{o}C in the catalyst bed therefore necessitates an increase in the steam/ethylbenzene molar ratio. Assuming a combined superheater efficiency of 0.8, the maximum possible steam flowrate is 9.9 kg/hr (a ratio of 19.9:1). At present the heat

shields operate to a combined efficiency of 0.95 (refer to Appendix A4.5). For a shield efficiency of 0.9, only 8.8 kg/hr steam (ratio 17.4:1) need be heated to 800°C, to enable the bed temperatures to be raised to 650°C. All the ratios are still within industrial range (12 - 20:1). Table 7.1 shows the predicted superheater firebar and wall temperatures for the three superheaters.

These temperatures, especially those of the firebar are well within the maximum allowable limits detailed in Section 3.7. The table shows that with SSH1 operated at full power, the other two heaters SSH2 and SSHX can be manipulated to share the task of heating 8.8 kg/hr of steam to 800°C. Two different methods are shown in Table 7.1. The first shows SSH2 carrying out the higher duty, and working to almost full power (as has already been tested in this research). The second shows SSHX carrying out the duty with the greatest stress, i.e. highest firebar temperature. This shows that with careful manipulation of loads and temperatures, the three heater system should enable investigations to be carried out over the full industrial operational temperature range at lower firebar temperatures than the present two heater arrangement.

(f) "Wrong way" behaviour

This is very briefly exhibited during the steam/air switchover during shut down. Temperatures of 500°C have been recorded even though the superheater and bed temperatures have been below 400°C. A detailed study at transient state, based on the studies of Mehta[77] should serve as a useful guide to the effect of shut down on the styrene catalysis. Since lower temperatures for the switchover cannot be used, the rate at which the switchover occurs must be investigated.

TABLE 7.1

Superheater Temperatures for a Three Heater Arrangement

Heater	Inlet Temperature (°C)	Outlet Temperature (°C)	Maximum Firebar Temperature (°C)	Maximum Inner Wall Temperature (°C)	Maximum Outer Wall Temperature (°C)
SSH1	115	458	888	565	510
SSH2	458	728	968	774	751
SSHX	728	800	878	811	805
SSH2	458	665	887	704	682
SSHX	665	800	930	822	811

APPENDIX A1

ISOMETRIC PROJECTIONS OF THE APPARATUS ARRANGEMENT

APPENDIX A1

ISOMETRIC PROJECTIONS OF THE APPARATUS ARRANGEMENT

Figure A1.1 is the initial isometric drawing of the control room pipework and equipment skeleton. The control panel and all supports are deliberately left out of the drawing. The drawing is to scale.

Figure A1.2 is the initial isometric drawing of the external room equipment and connecting pipework skeleton. Once again the supports and secondary piping is left out, for construction simplicity. Full details of the revised pipework can be found in Figure A3.8.

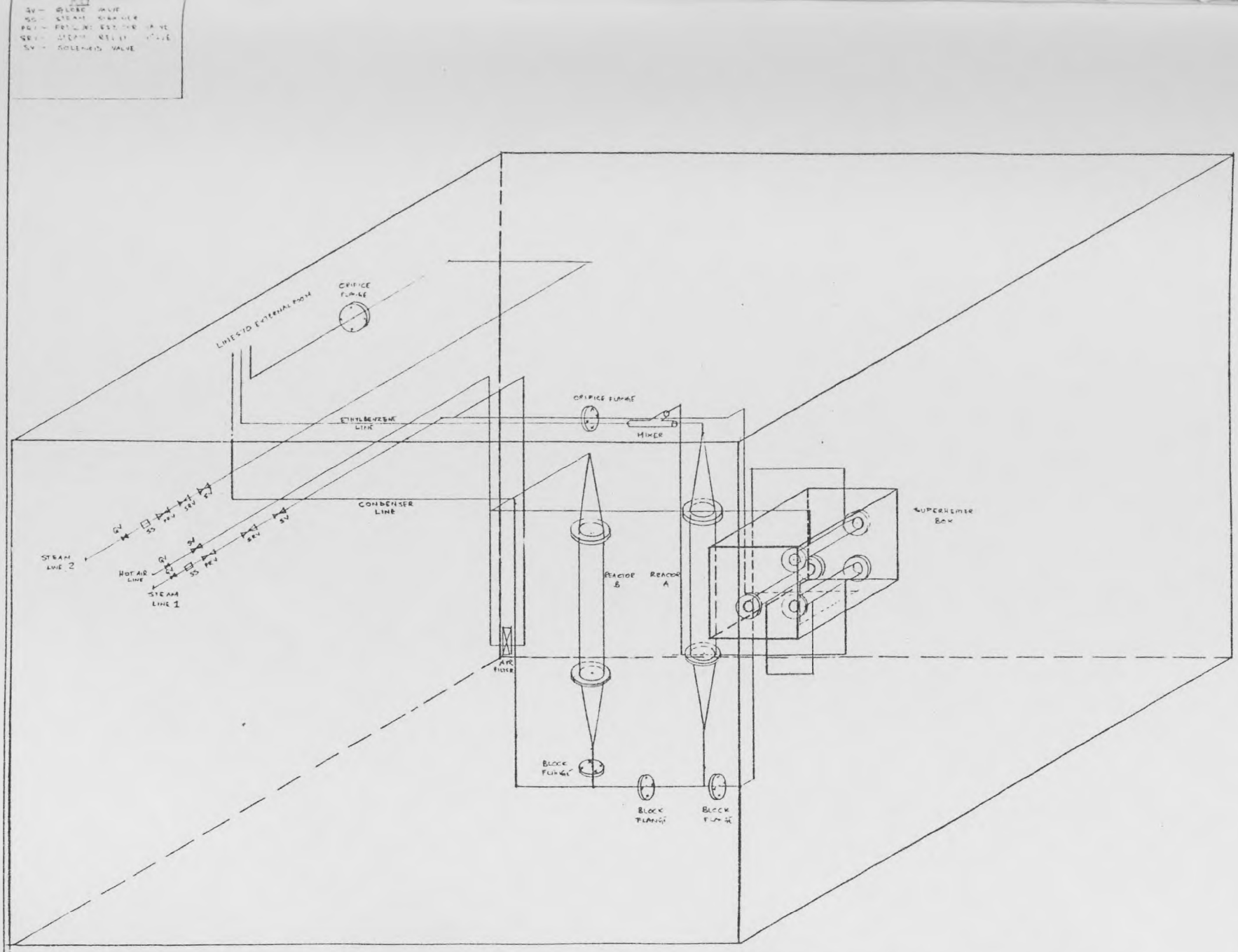

DO NOT SCALE IF IN DOUBT ASK

WELD AT
MACHINE AT
BREAK ALL SHARP EDGES

MACHINING TOLERANCES

GENERAL SPECIFIED TO BS 1916 1953

DECIMALS ± .010" 0.25 mm
FRACTIONS ± 1/64" 1/4 mm

PROJECTION: ISOMETRIC 30°
DIMENSIONS: INCHES

UNIVERSITY OF LEEDS
DEPARTMENT OF CHEMICAL ENGINEERING

SCALE 1/10

TITLE ISOMETRIC PROJECTION OF PROPOSED SET UP OF CONTROL ROOM

CHECKED BY
DRAWN BY
DRAWING No M.A.T

DATE
DATE

FIGURE A1.1: Isometric Projection of the Control Room Arrangement

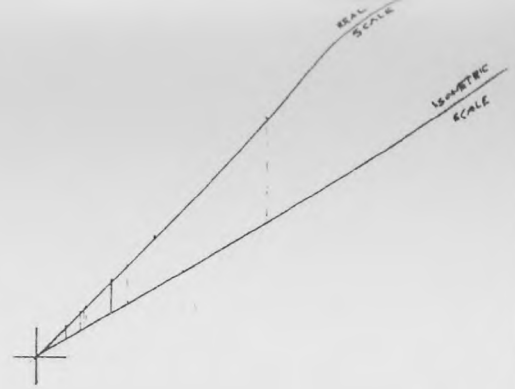

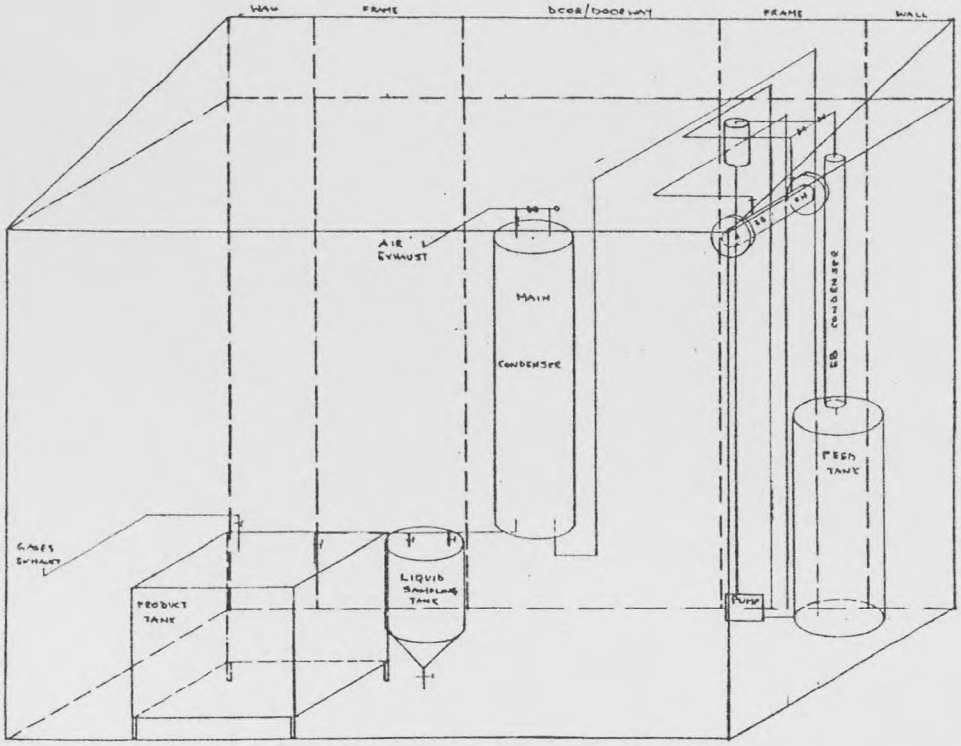

DO NOT SCALE IF IN DOUBT ASK	WELD AT ⊥ MACHINE AT ✓ BREAK ALL SHARP EDGES	MACHINING TOLERANCES	GENERAL SPECIFIED TO BS 1916 : 1953	DECIMALS ± .010" 0·25 mm FRACTIONS ± 1/64" 1/4 mm	PROJECTION: ISOMETRIC 30 DIMENSIONS: INCHES	UNIVERSITY OF LEEDS DEPARTMENT OF CHEMICAL ENGINEERING	SCALE 1/10	TITLE ISOMETRIC PROJECTION OF PROPOSED SET-UP OF EXTERNAL ROOM	CHECKED BY DRAWN BY DRAWING No

FIGURE A1·2 : Isometric Projection of the External Room Arrangement

APPENDIX A2

STEAM AND AIR LINE CONTROL AND SAFETY INSTRUMENTATION

APPENDIX A2

STEAM AND AIR LINE CONTROL AND SAFETY INSTRUMENTATION

Figure A2.1 shows the major control valves and meters on the supply lines SL1 and SL2. Both lines are of ½" BSP (2.13 cm O.D.) SS316 pipework. The following notation has been used:-

GV	Gate Valve
Gl.V	Globe Valve
SV	'ALCON' ACP-4X Solenoid Valve, 24 V D.C.
SS	1/32" 'Bailey's' Steam Strainer
PRV	'Bailey's' 5-100 psig (1.34 - 7.81 bar) Pressure Regulator Valve
SRV	'Bailey's' Steam Relief Valve, 100 psig (7.81 bar)
PG	0-100 psig (0 - 7.81 bar) Pressure Gauge
COF	'Deltech' Coarse Oil Filter (5 μm)
FF	'Deltech' Cartridge E Type Fine Filter
OM	Orifice Meter and Assembly
MSR	Metric Series Rotameter, size as indicated.

Air Rotameter Calibration

The SL2 air flow rotameter is a Metric Series Size 14 utilizing a standard duralumin float. The calibration of this is standard, and can be found in the GEC-Elliot manual[67]. The SL1 air flow rotameter is a Metric Series Size 18 using a specially weighted float. The calibration of this rotameter is presented below:-

Float material	:	Duralumin weight by a stainless steel ball
Weight of float	:	9.96 g
Mean density of float	:	4.634 g/cc

The calibration is then carried out as per the manual[67] with the constants K_1 = 0.57 and K_2 = 1.754. For a normal air inlet pressure of 2.3 bar full flow the variation of air flowrate with float position is shown in Table A2.1.

TABLE A2.1

Air Line SL1 Rotameter Calibration

Float Position Scale (cm)	Air Flowrate litres/min	Air Flowrate kg/hr
3.4	22.4	3.3
6.6	33.5	4.9
9.7	44.8	6.6
12.6	55.9	8.3
15.3	67.1	9.9
18.1	78.6	11.6
20.6	89.5	13.2
23.2	100.6	14.9
25.6	111.8	16.5

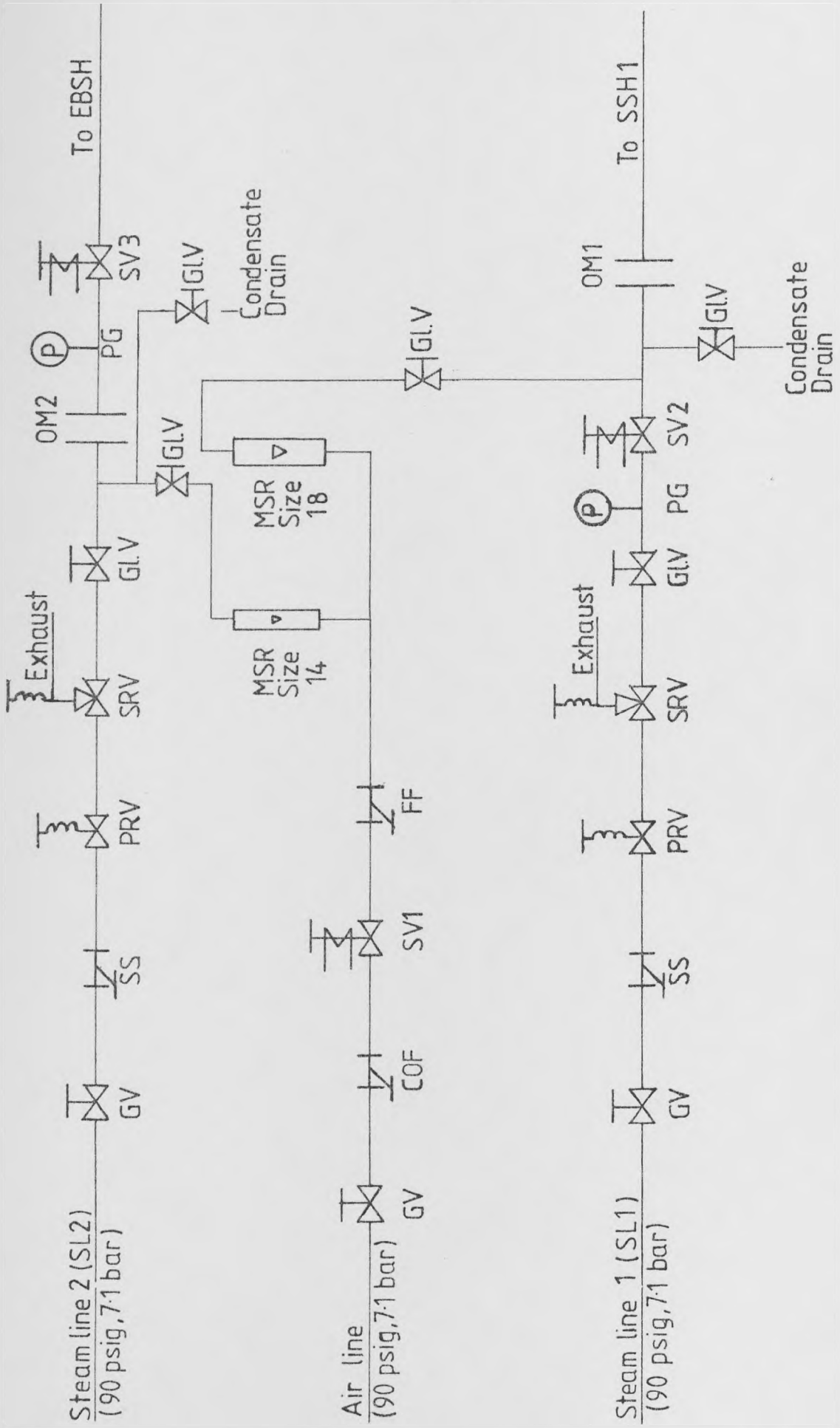

FIGURE A2.1: Control Instrumentation of the Steam and Air Supply Lines

APPENDIX A3

DESIGNS AND DRAWINGS OF APPARATUS EQUIPMENT

APPENDIX A3

DESIGNS AND DRAWINGS OF APPARATUS EQUIPMENT

A3.1 Orifice Plate and Assembly Designs

As mentioned in Section 3.3, these designs use the calculation methods of Spink, and the mechanical design conforms to BS 1042[48] for a D x D assembly. A 15% allowance factor is made for the design flow-rate, and a water-on-mercury head of around 5 cm Hg is aimed for (BS 1042 recommendation).

Spink's correlation:-

$$S = \frac{8.04 \times 10^{-9} W_m}{359 D^2 F_a F_m F_c Y \sqrt{\gamma_f} \sqrt{h_m}} \qquad (3.2)$$

is used for this design. The constants F_a, F_m, F_c are worked out from charts by Spink[47] ($F_a = 1.006$, $F_m = 0.962$, $F_c = 1.003$). This is an iterative calculation which involves the working out of S and Y until the successive iteration values of S and Y show a difference of less than 1%. Spink carries charts for S and Y. For the 1st iteration, Y is assumed as equal to one. A value of S corresponding to Y = 1 is worked out. From the charts of S and Y for varying diameter ratios (d/D), a new value of Y is read. The process is repeated to the final convergence.

The design results for lines SL1 and SL2 are tabulated in Table A3.1.

The mechanical design is shown in full detail in Figure A3.1 and meets all the specifications of BS 1042 for a D x D Carrier Ring mounted orifice plate assembly.

TABLE A3.1

Orifice Plate Design Results

Steam Line	Design Flowrate (kg/hr)	Re	Y_1	S	Y_2	h_m (cm Hg)	Pipe Inside Diameter (cm)	Orifice Diameter (cm)
1	7.95	14405	1.000	0.04852	0.997	11.0	1.27	0.452
2	4.23	7691	1.000	0.02499	0.997	5.0	1.27	0.328

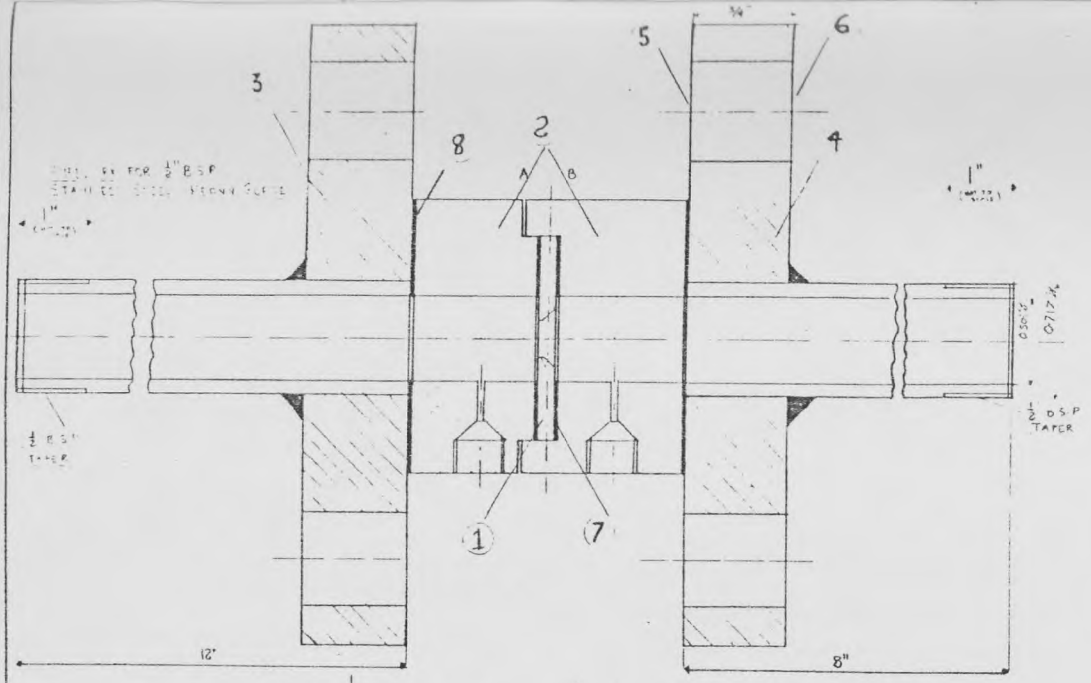

ASSEMBLED METER : 2 OFF

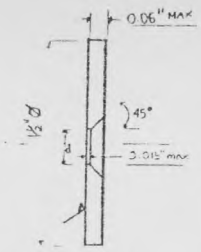

ORIFICE PLATE

BORE EDGE TO BE SQUARE, FREE FROM BURS AND ROUNDING
UPSTREAM FACE TO BE FLAT WITHIN 0.005"
d = 0.178" ± 0.0005" , 1 OFF
d = 0.129" ± 0.0005" , 1 OFF

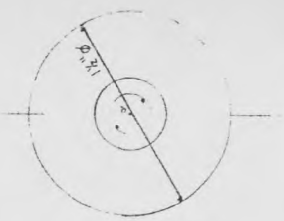

ORIFICE PLATE 1½ Ø

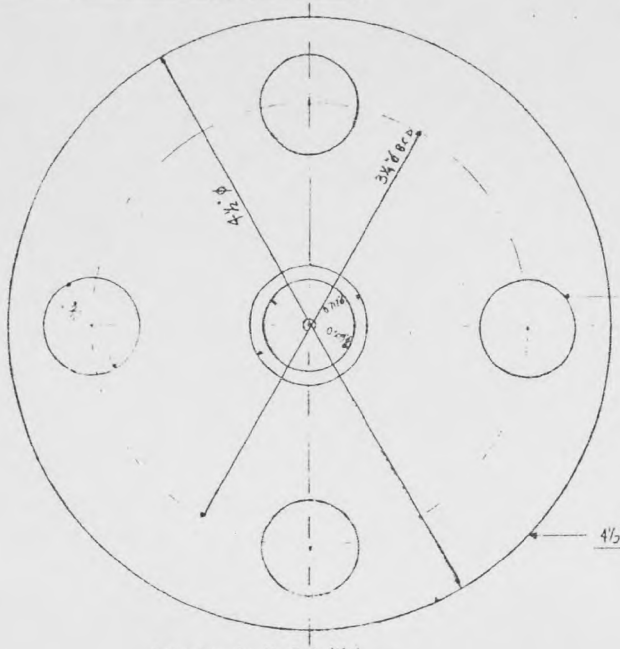

BOLT AND FLANGE ENDS TO BE DRILLED BY BS 10 TABLE F NOM BORE

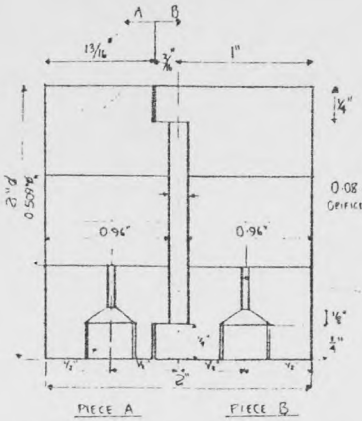

ASSEMBLED CARRIER RING 2" Ø

PIECES A & B

PARTS LIST

No.	NAME	NUMBER REQUIRED	MATERIAL	REMARKS
1	ORIFICE PLATE	2	S. STEEL	d = 0.178" 1 OFF d = 0.129" 1 OFF
2	CARRIER RING	2	S. STEEL	PRESSURE TAPS ⅛" B.S.P TAPER PRESSURE HOLES 0.05" MAX
3	UPSTREAM BODY & FLANGE	2	S. STEEL	½" B.S.P TAPER AT END
4	DOWNSTREAM BODY & FLANGE	2	S. STEEL	½" B.S.P TAPER AT END
5	STUD-BOLTS	8	CARBON STEEL	⅝" B.S.W. LENGTH 4" MIN
6	NUTS	8	CARBON STEEL	⅝" B.S.W TO FIT STUD BOLTS
7	ORIFICE GASKET	4	KLINGERITE	I.D TO FIT PIPE; O.D 1½" MAX
8	CARRIER RING GASKET	4	KLINGERITE	I.D TO FIT PIPE; O.D 2" MAX

ALL STAINLESS STEEL PIECES, TYPE 316 USED

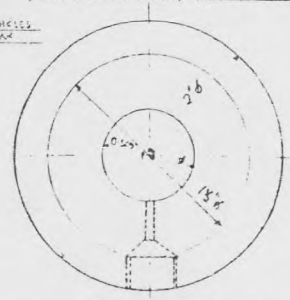

CARRIER RING: PIECE A

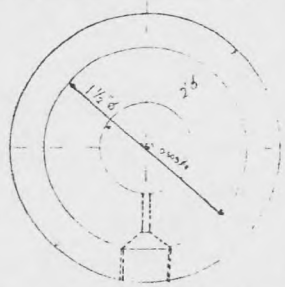

CARRIER RING: PIECE B

DO NOT SCALE IF IN DOUBT ASK	WELD AT MACHINE AT BREAK ALL SHARP EDGES	MACHINING TOLERANCES	GENERAL SPECIFIED	DECIMALS ± .010" 0.25 mm FRACTIONS ± 1/64" 1/4 mm TO BS 1916 : 1953	PROJECTION: DIMENSIONS: INCHES	UNIVERSITY OF LEEDS DEPARTMENT OF CHEMICAL ENGINEERING	SCALE 2/1	TITLE ORIFICE METER ASSEMBLY FOR STEAM SUPPLY LINE	CHECKED BY / DRAWN BY N.A. / DRAWING No N.H. 1 — DATE / DATE 11-7

FIGURE A3.1: Drawing of the Orifice Assembly

A3.2 Ethylbenzene Vaporiser Design

The ethylbenzene vaporiser is designed to vaporise 2.95 kg/hr of ethylbenzene from liquid at 10°C to saturated vapour under a pressure of 2 bar (164°C). A rising film evaporator of 1.27 cm I.D. (⅜" BSP (1.71 cm O.D.) fittings onto the rest of the equipment) is designed in accordance with the procedure by Lord et al[51] for vertical nucleate boiling. The equation for stainless steel surfaces is:-

$$\frac{h_{NB}}{C_p \, M_{EB}} = 2.412 \, Re^{-0.3} \, Pr^{-0.6} \left(\frac{\rho_{EB} \, \tau_{EB}}{P^2} \right)^{-0.425} \qquad (A3.1)$$

Equation (A3.1) enables the heat transfer coefficient for boiling, h_{NB}, to be calculated and has a value of 3520 W/m^2 K.

The maximum length available for the vaporiser is 0.92 m. Thus the design is first checked for a vaporiser of 0.92 m length and of ⅜" BSP (1.25 cm I.D.) diameter. It also has to be able to accommodate a resistance wire of 6 m in length. The evaporator wire covering possible works out at around 9 m per foot. Therefore there is adequate length available for the winding of the ceramic bead insulated heater wire.

The duty of the heater wire is worked out as:-

$$Q = M \, C_p \, \Delta T = 493.8 \text{ Watts} = U \, A_S \, \Delta T_{ln} = h_{NB} \, A_S \, \Delta T_{ln} \qquad (A3.2)$$

(ignoring the metal wall resistance).

Equation (A3.2) demands a minimum length of 0.86 m for the vaporiser. Therefore, a 0.92 m vaporiser would fit this design. A more detailed design need not be performed. The top of the vaporiser is also provided with a 7.6 cm diameter condensate trap of 15.3 cm length. There is sufficient room for the addition of any thermocouple or pressure gauge fittings that may be required (see Figure A3.2).

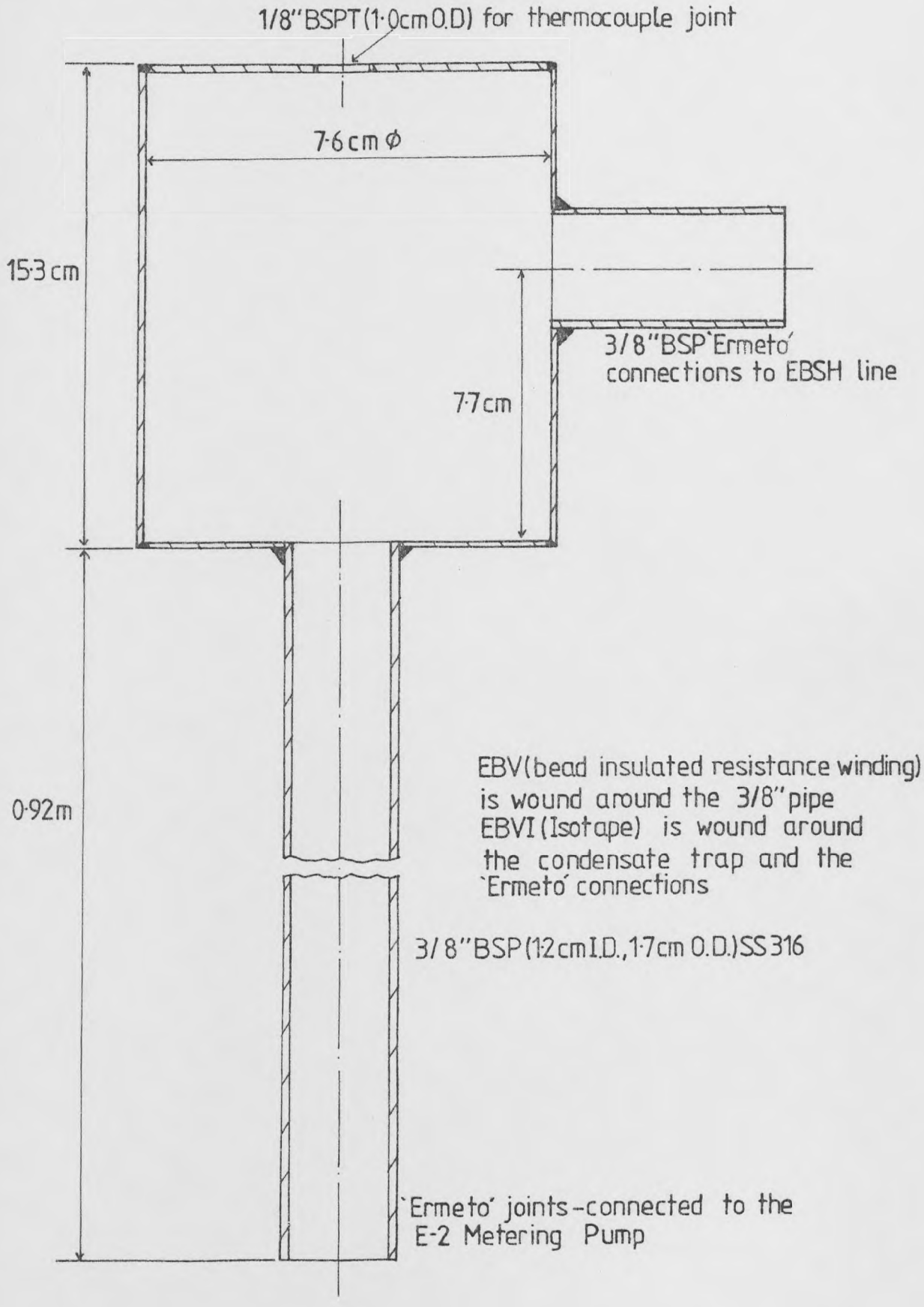

FIGURE A3.2: The Ethylbenzene Vaporiser

The vaporiser heater circuit power requirement is at least 500 Watts and the resistance wire is designed for 1000 W capacity (37.3 Ω resistance) and 6 cm length. An 'Isotape' ITH-250-1.3 m is also provided for the connecting fittings and pipework on and after the condensation chamber so as to be able to provide for any heat losses. The maximum power for the tape is 330 W.

A3.3 The Design of the Mixer

An in depth guide to this design is presented in Section 3.5, and so only the detailed design of the penetration and venturi section is given here.

Design of the penetration section

This consists of the design of the penetration nozzles enclosed in the manifold (see Figure A3.3). Firstly, the nozzles are designed for choked flow so as to ensure a constant flowrate regardless of back pressure fluctuations. This is as per carried out in Kay[53], and the choked throat area can be calculated from Equation A3.3.

$$M = \left(\frac{2}{\gamma + 1}\right)^{\frac{1}{\gamma-1}} \sqrt{\left(\frac{2\gamma}{\gamma + 1}\right) P_{IN}\, \rho_{IN}\, A_{xt}} \qquad \text{(A3.3)}$$

where for saturated steam at 1.68 bar $\gamma = 1.3$, then Equation (A3.3) becomes:

$$A_{xt} = \frac{M}{0.668 \sqrt{P_{IN}\, \rho_{IN}}} \qquad \text{(A3.4)}$$

For a back pressure of 1.68 bar (P_{IN}), and a mass flowrate of 7.0 kg/hr of steam, gives a choked flow diameter of 0.211 cm. Therefore, any size of diameter below 0.21 cm will give choked flow. Hence the nozzles vary in diameter from $^{1}/_{64}$" (0.04 cm), the smallest workshop drill size, to

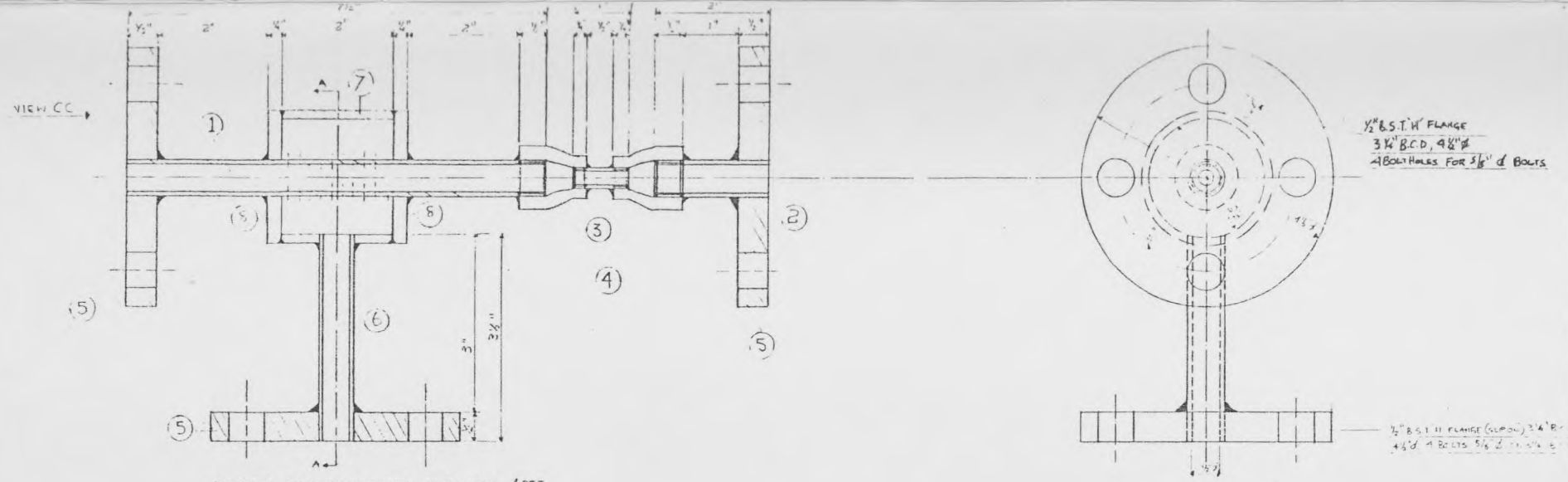

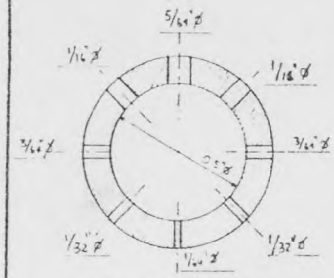

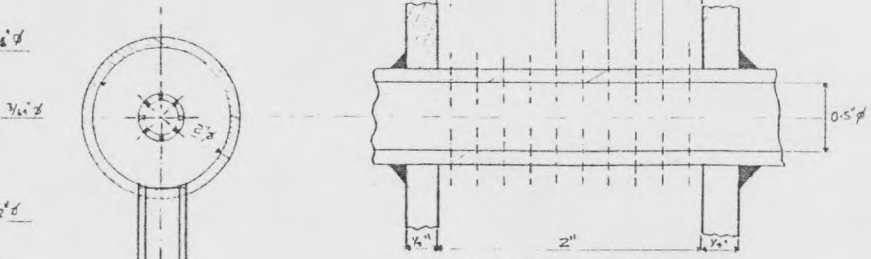

PARTS LIST

ITEM Nº	Nº REQD.	MAIN	MATERIAL	G	REMARKS
1	1	DRILLED PIPE	S.S. 316	12	7½" LENGTH, ½" B.S.P. TAPER AS SHOWN
2	2	MIXED LINE PIPE	S.S. 316	2	2" LENGTH ½ B.S.P. TAPER AS SHOWN
3	1	VENTURI PIPE	S.S. 316	12	1" LENGTH ½" B.S.P. TAPER AS SHOWN
4	2	FERRULES	S.S. 316	–	½"x¼" WELD WHEN ASSEMBLED
5	3	FLANGES	S.S. 316	–	SLIP ON B.S.T. 'H' ½"
6	2	STEAM LINE PIPE	S.S. 316	12	3" LENGTH ½" B.S.P.
7	1	MANIFOLD PIPE	S.S. 316	12	2" LENGTH 2" B.S.P.
8	2	MANIFOLD COVERS	S.S. 316	–	¼" THICK, O.D. TO FIT MANIFOLD PIPE

NOTE ALL PIPE GUAGES SHOWN ARE THE MINIMUM RECOMMENDED LARGER THICKNESS MAY BE USED

ASSEMBLY TO BE SUPPLIED WITH 3 x 4 BSW BOLTS AND NUTS FOR THE FLANGES SIZE 5/8" ϕ

DO NOT SCALE IF IN DOUBT ASK | WELD AT | MACHINE AT | BREAK ALL SHARP EDGES | MACHINING TOLERANCES | GENERAL DECIMALS ± .010" 0.25 mm FRACTIONS ± 1/64" 1/4 mm | SPECIFIED TO BS 1916 : 1953 | PROJECTION: | DIMENSIONS: INCHES | UNIVERSITY OF LEEDS DEPARTMENT OF CHEMICAL ENGINEERING | SCALE 1/1 | TITLE STEAM-ETHYL BENZENE MIXER UNIT | CHECKED BY | DRAWN BY M.A | DRAWING No N & 15 | DATE | DATE 21/7/71

FIGURE A3.3: Drawing of the Mixer

5/64" (0.20 cm) with the smallest nozzles being nearest to the penetrating stream inlet point.

The depth of the penetration is checked from charts by Patrick[54]. Although these charts are for gas penetration around room temperature, they give a good estimate of the penetration possible. For a steam against steam penetration, the distance to which 90% of the penetrating medium reaches is 3.05 cm for a nozzle of 0.203 cm diameter. This is more than adequate a distance for a pipe of radius 0.635 cm.

Design of the venturi section

The venturi section aims to aid the thorough mixing of the streams by increasing the turbulence of the mixed streams. This is done by doubling the Reynolds number over the venturi section. The Reynolds number is increased from Re = 19,704 to Re = 39,408 by reducing the pipe diameter from 1.27 cm to 0.635 cm over the venturi section.

Pressure drop check

The pressure drop over the mixer unit should not exceed 15 - 20 kN/m^2 so as to have adequate driving force for the rest of the system. The greatest pressure drop possible across the mixer is 11.4 kN/m^2 (see Tables 4.4 and 4.5). Therefore the design has an acceptable pressure drop.

A3.4 System Condenser Designs

A3.4.1 Ethylbenzene condenser design

The small flowrate handled means that this condenser can be a single tube, single pass condenser. It is designed to cool ethylbenzene vapour at 180°C to liquid at 20°C. The design of the three sections of the condenser (see Section 3.6.1) are detailed here, starting with the heat transfer coefficient evaluation.

(i) The desuperheating section - the heat transfer coefficient, h_{DS}, is calculated from Equation (3.3)(for laminar flow as Re = 220)

$$Nu = \frac{h_{DS} D_H}{k} = 1.86 \left[Re\ Pr \frac{L}{D_H} \right]^{0.33} \left(\frac{\mu_b}{\mu_s} \right)^{0.14} \qquad (3.3)$$

With a small change in temperature, viscosity effects are neglected, i.e. $\mu_b = \mu_s$. The pass tube hydraulic mean diameter D_H is 1.27 cm. The heat transfer coefficient is calculated to be 55.08 W/m^2 K, assuming L = 0.3 m.

(ii) The condensing section - the heat transfer coefficient, h_C is calculated from Equation (3.4)(for laminar flow as Re = 30)

$$h_C = \left(\frac{\mu_f^2}{k^3 \rho^2 g} \right)^{1/3} = 1.47 \left(\frac{4\Gamma}{\mu_f} \right)^{-1/3} \qquad (3.4)$$

The value of h_C is calculated to be 1008.9 W/m^2 K.

(iii) The subcooling section - that heat transfer coefficient, h_{SC} is calculated from Equation (3.5)(for laminar flow as Re = 30)

$$Nu = \frac{h_{SC} D_H}{k} = 1.86 \left[Re\ Pr \frac{L}{D_H} \right]^{0.33} \left(\frac{\mu_b}{\mu_s} \right)^{0.14} \qquad (3.3)$$

The viscosity effects are neglected, i.e. $\mu_b = \mu_s$. Assuming the length of the section, 1 metre, the heat transfer coefficient h_{SC} is calculated to be 381.0 W/m^2 K.

Coolant heat transfer

Water is used as the coolant and a maximum rise in temperature of 5 Centigrade degrees is designed for. The outside diameter of the condenser

is 5.1 cm. The heat duty to be carried out by the water is worked out from Equation (A3.5):-

$$Q = M (C_p \Delta T + \lambda) \qquad (A3.5)$$

The coolant duty is 1755.6 Watts, implying a water flow rate of 84.3 kg/hr. The Reynolds number, Re, is 130 hence Equation (3.3) is used to calculate the heat transfer coefficient, h_f, on the coolant side, estimating a full condenser length of 1.6 m.

A counter-current mode of operation is designed for. An iterative procedure needs to be used to evaluate the heat transfer areas from the heat transfer coefficients estimated, by evaluating the log mean temperatures and the heat duties for each of the above sections. The overall heat transfer coefficients are calculated using the above estimated heat transfer coefficients, and revaluated using the new estimates of the transfer areas. The process is repeated to convergence. Equation (A3.6) is used for the evaluation of the overall heat transfer coefficient. Equation (A3.7) then gives the new estimate of the transfer area using the log mean temperatures in Table A3.2.

$$\frac{1}{U} = \frac{1}{h_o} + \frac{x_w}{k_w} + R_i + \frac{1}{h_I} \qquad (A3.6)$$

where R_i = 0.0008 for organic scaling resistance

$$Q = UA_S \Delta T_{ln} \qquad (A3.7)$$

Table A3.2 shows the first estimates of the heat transfer coefficients and the transfer areas for the heat loads and log mean temperatures shown. Table A3.3 shows the final values for the same after convergence of the iterative calculation.

TABLE A3.2

First Estimates of the Transfer Variables for the Ethylbenzene Condenser Design

Section	ΔT_{ln} (^{o}C)	Q (Watts)	h_o' ($W/m^2\ ^{o}C$)	h_i' ($W/m^2\ ^{o}C$)	U_o' ($W/m^2\ ^{o}C$)	A' (m^2)	L' (cm)
Condensing	150.5	265.1	1980.5	1009.0	417.3	4.185×10^{-3}	30
Subcooling	49.0	223.7	1980.5	332.2	226.6	0.0201	100
Desuperheating	156.9	21.7	1980.5	47.7	44.9	3.069×10^{-3}	30

TABLE A3.3

Final Values of the Ethylbenzene Condenser Design Variables

Section	h_o ($W/m^2\ ^oC$)	h_I ($W/m^2\ ^oC$)	U ($W/m^2\ ^oC$)	A_S (m^2)	L (cm)
Condensing	1583.0	946.5	396.9	4.465×10^{-3}	5.57
Subcooling	1583.0	264.0	187.9	0.0243	30.41
Desuperheating	1583.0	41.4	38.2	3.534×10^{-3}	4.42
				Total Length of Condenser:	40.40
				Safety allowance 20%:	48.48

The minimum length of the condenser has to be 0.49 m. A length 0.61 m is to be used, and Figure A3.4 illustrates the design of the ethylbenzene condenser.

A3.4.2 The design of the main condenser

The three main sections of the condenser are designed as such:-

(i) the desuperheating section: using Equation (3.5), the heat transfer is calculated, the flow being turbulent (Re = 13290).

$$\frac{h_{DS}\, D_H}{k} = 0.023\, Re^{0.8}\, Pr^{0.33} \qquad (3.5)$$

This section cools the steam (product gas assumed to be 100% steam) from 650°C to 115°C.

(ii) the condensing section: using Equation (3.4), the heat transfer coefficient is calculated, the flow being laminar (Re = 1019)

$$h_C \left(\frac{\mu_f^2}{k^3\, \rho^2 g} \right)^{0.33} = 1.47 \left(\frac{4\,\Gamma}{\mu_f} \right)^{-0.33} \qquad (3.4)$$

(iii) the subcooling section: using Equation (3.3), the heat transfer coefficient is calculated, the flow being laminar (Re = 1019)

$$\frac{h_{SC}\, D_H}{k} = 1.86 \left[Re\, Pr\, \frac{L}{D_H} \right]^{0.33} \left(\frac{\mu_b}{\mu_s} \right)^{0.14} \qquad (3.3)$$

The subcooling lowers the temperature to around 70°C.

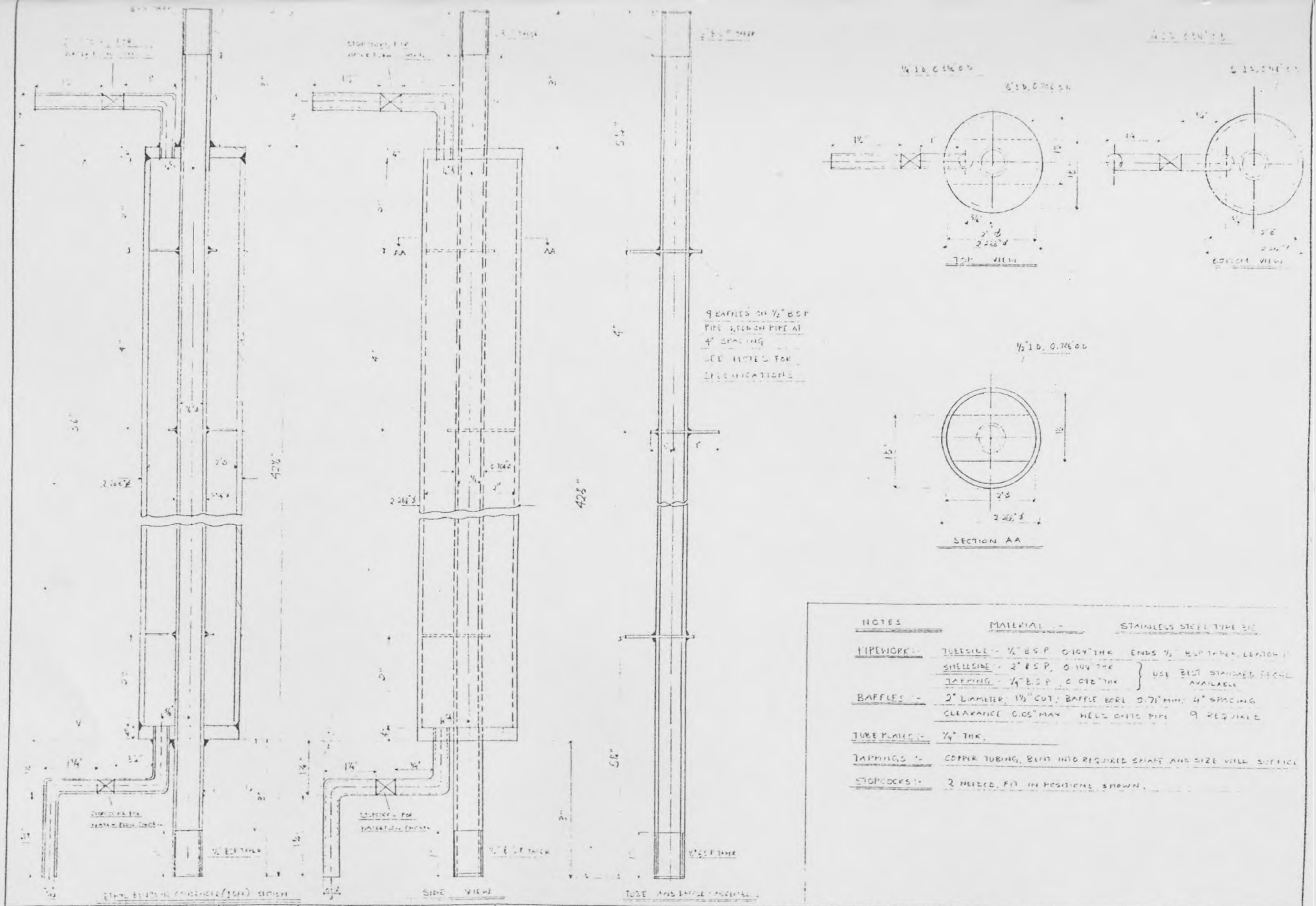

FIGURE A3.4: Drawing of the Ethylbenzene Condenser

The total coolant duty is 9100 Watts and the rise in temperature allowed for is 30 Centigrade degrees. This means, using Equation (A3.5) that the flowrate of the coolant is 250 kg/hr.

$$Q = M (C_p \Delta T + \lambda) \qquad (A3.5)$$

The coolant heat transfer coefficient is calculated from Equation (3.3) as the flow is laminar (Re = 1507). An iterative procedure, similar to that for the design of the ethylbenzene condenser in the previous section is carried out. Table A3.4 tabulates the final values of the variables including the converged length of the three condenser sections.

The condenser is designed for two cooling coils, one for the desuperheating duty, the other for the condensing and subcooling duties. The desuperheating coil is wound on a core of 19 cm diameter at an angle of 20°C. The cores are determined by the best mechanical designs possible, i.e. the tubes are coiled such that they can be individually dismantled, yet there should be adequate room for the tools required to assembly the condenser to work in. The condenser must also make allowance for various elbows, tees and threads (see Figure A3.5 for the drawing of the main condenser). The subcooling and condensing coil is wound on a core of 15.2 cm at an angle of 45°C. The angle is kept above 15° as this simplifies the design, and it also simplifies the mechanical coiling of the tube. The two coils are separated by stainless steel metal sheets, isolating the coil from one another.

A3.5 The Radiation Superheater

Figure A3.7 shows the mechanical design of the body of the radiation superheater. The firebar used for the heating is the standard 20" 'pencil-type' firebar, serial number 33555, available from Heating Elements Ltd., Leicester[64] for 1250 W, 1500 W and 2000 W power capacities. These

TABLE A3.4

Final Values of the Main Condenser Design Variables

Section	Q_T (W)	Re	h_o ($W/m^2 K$)	h_I ($W/m^2 K$)	U ($W/m^2 K$)	A_S (m^2)	L (m)
Desuperheating	3419	13290	1893	182.6	164.5	4.69×10^{-4}	3.7
Condensing	4923	1019	1893	4952	2046.5	7.61×10^{-5}	0.6
Subcooling	760	1019	1893	6242	4257.8	1.40×10^{-4}	1.1

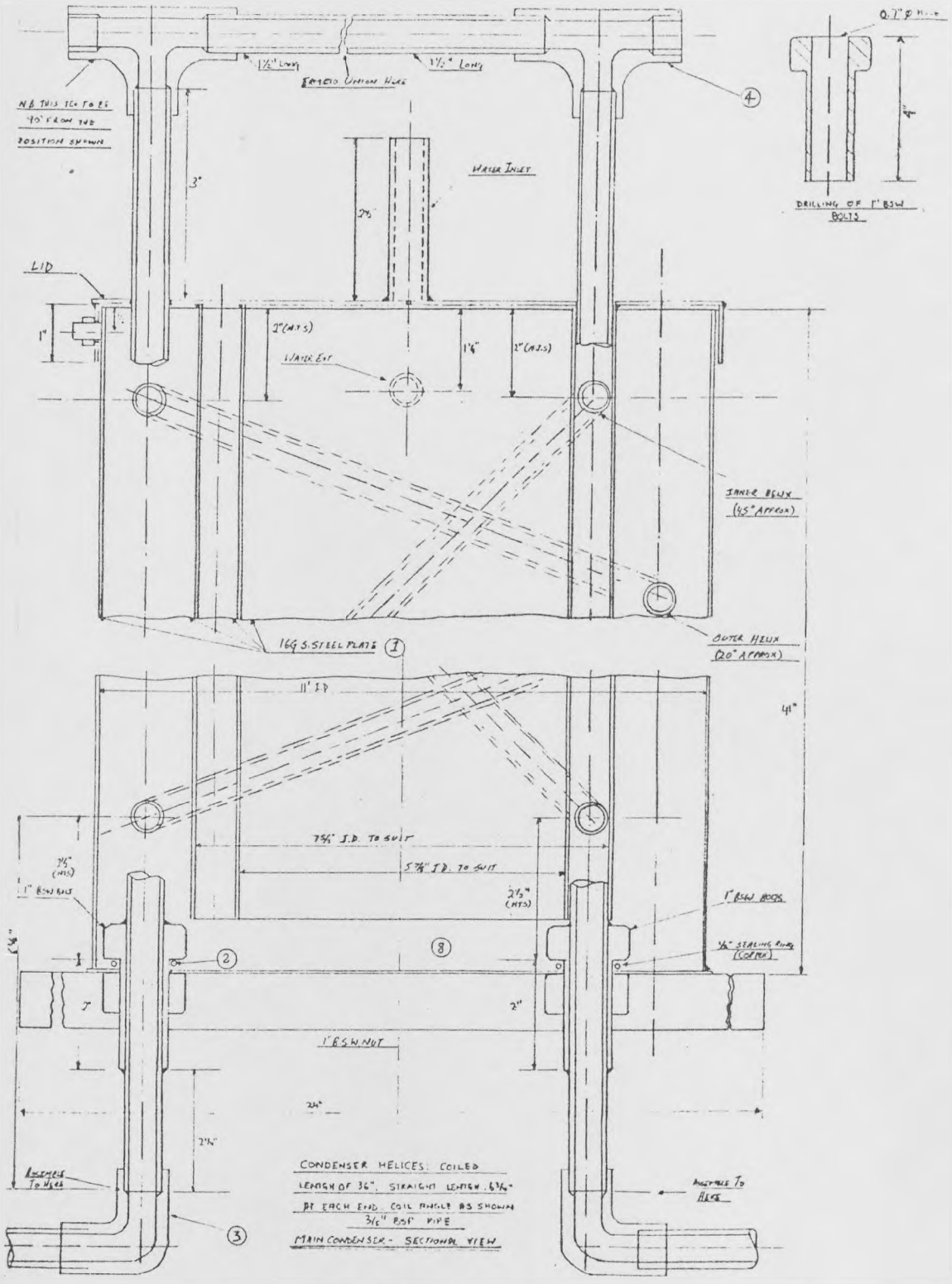

FIGURE A35(a)

FIGURE A3.5: Drawing of the System's Main Condenser (Side Section)

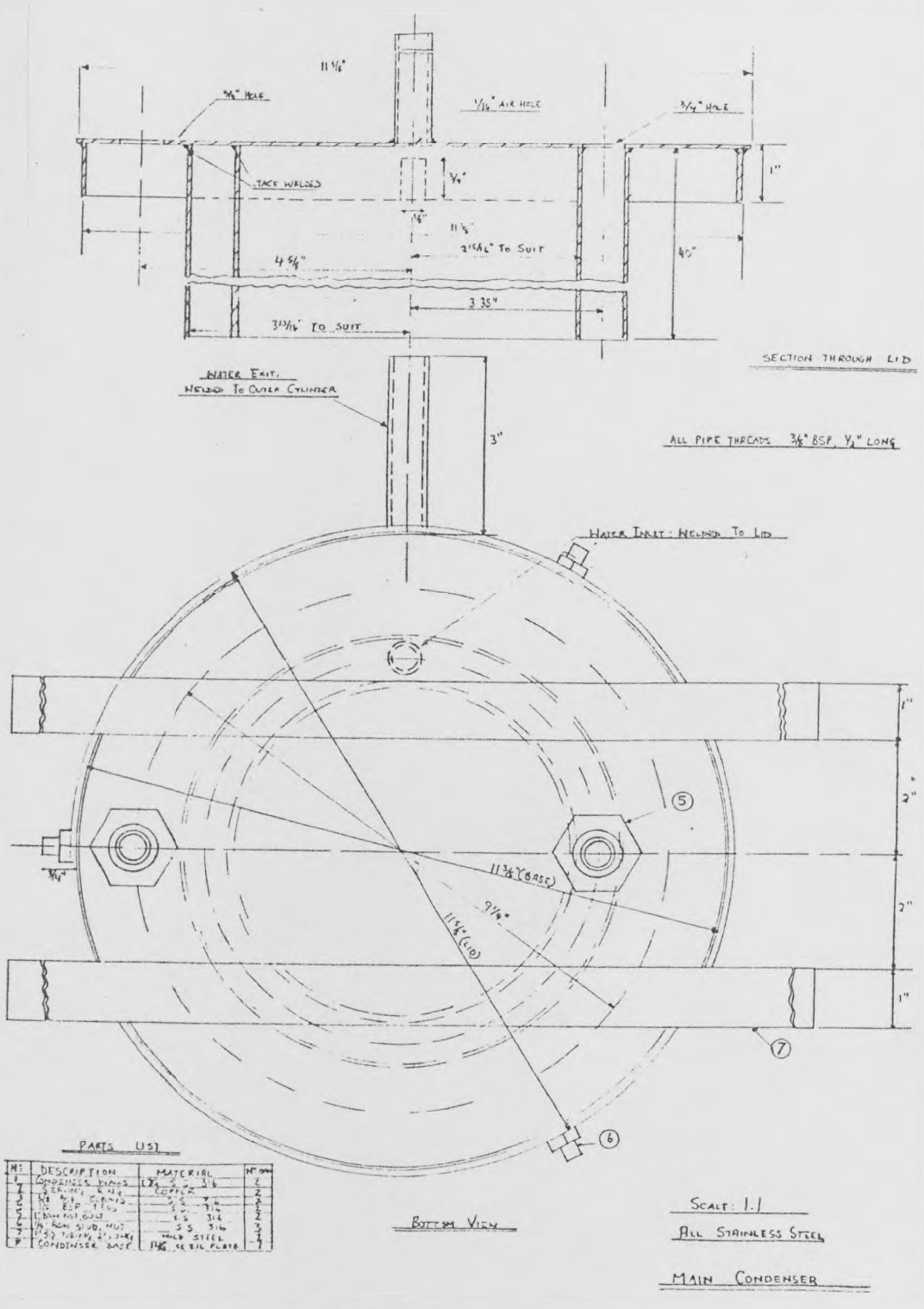

FIGURE A3.5(b)

FIGURE A3.5: Drawing of the System's Main Condenser

(Top View and Lid)

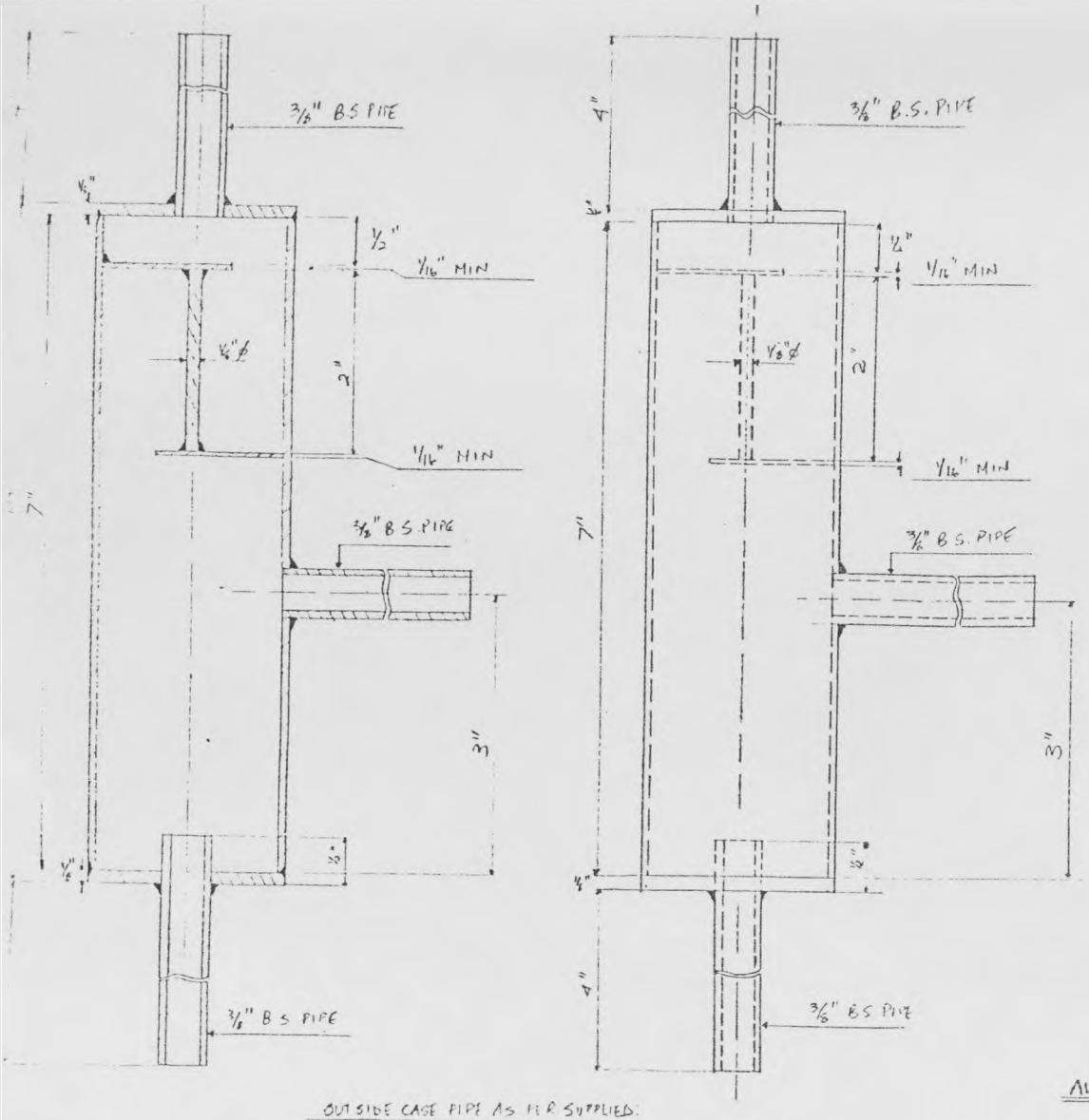

OUT SIDE CASE PIPE AS PER SUPPLIED:
I.D: 1 15/16", O.D 2 1/8"

SIDE-SECTIONAL VIEW

OUT-SIDE VIEW

ALL STAINLESS STEEL 316

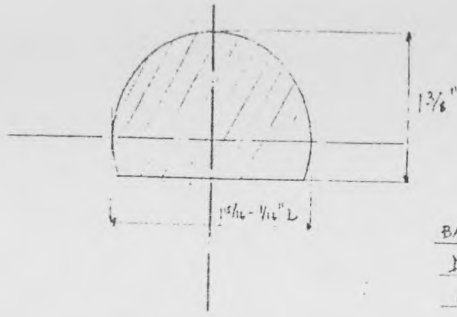

BAFFLE THICKNESS 1/16" MIN
DIAMETER 1 15/16" - 1/16"
LENGTH 1 3/8"

BAFFLE : 2 OFF

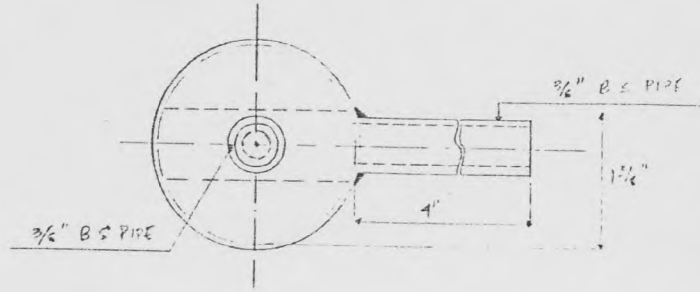

TOP VIEW

NOTES

1/ PLATE MINIMUM THICKNESS 1/8", DIAMETER 2 1/8"
2/ MAIN 3" PIPE SUPPLIED (AMS 264 - 7210) I.D 1 15/16"
3/ 3/8" PIPES AS PER MY STOCK IN LAB.
4/ BAFFLES & TIE ROD ASSEMBLY TO BE WELDED AT THE TOP END
5/ TIE ROD 1/8" ϕ MINIMUM. LARGER USABLE

ERAL	DECIMALS ± .010" 0.25 mm FRACTIONS ± 1/64" 1/4 mm	PROJECTION :-	UNIVERSITY OF LEEDS DEPARTMENT OF CHEMICAL ENGINEERING	SCALE	TITLE VAPOUR-LIQUID SEPARATOR FOR DEHYDRATION RIG	CHECKED BY / DATE
CIFIED	TO BS 1916 : 1953	DIMENSIONS :- INCHES		1/1		DRAWN BY / DATE DRAWING No.

FIGURE A3.6: Drawing of the Gas-Liquid Separator

firebars need to have their ends slightly modified, and this change, together with the means by which electrical insulation is provided is shown in Figure A3.8.

A3.6 Sample Collection, Air Exhaust and Water Drainage Set Up

Figure A3.9 shows the collecting tanks, the sampling points, the nitrogen blanketing lines, the air and gas exhaust lines, and the condensed steam drainage lines. Three-way valves can divert the liquid from the gas-liquid separator (GLS) to any one of the three collection tanks, or to the 'steam' drain line:-

CT1 : Copper Tank No. 1, capacity 10 litres

SST2 : Stainless Steel Tank No. 2, capacity 30 litres

MST3 : Mild Steel Tank No. 3, capacity 57 litres.

Two gas sampling points (GSP) are provided with replaceable septa seals for needle injection.

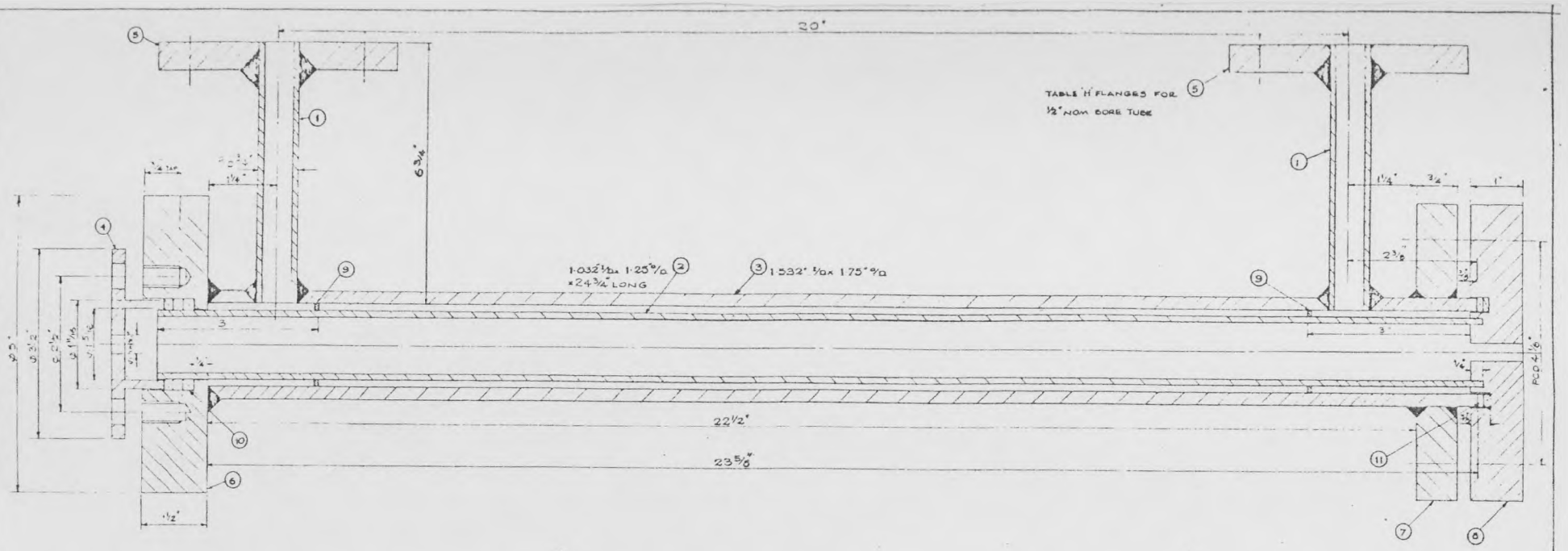

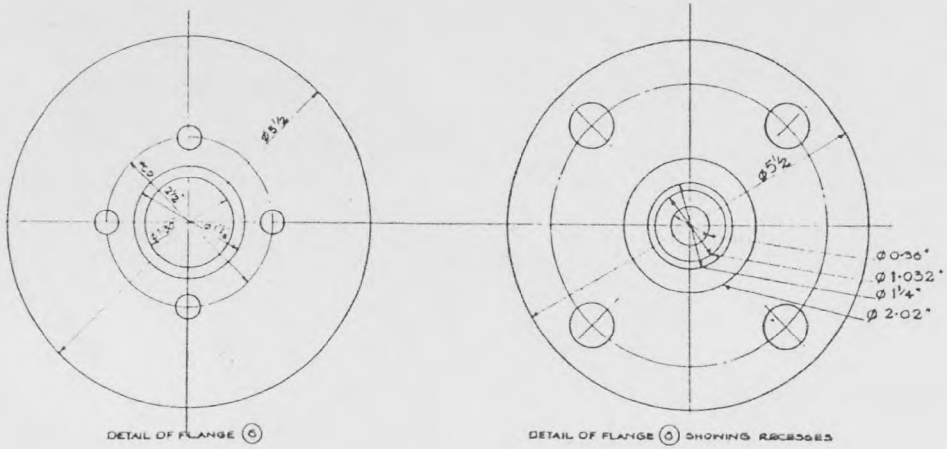

DETAIL OF FLANGE ⑥

DETAIL OF FLANGE ⑥ SHOWING RECESSES

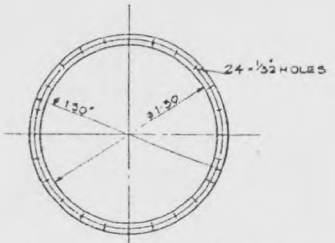

DISTRIBUTOR ⑨ 1/16 THICK SCALE 2/1
TACK WELDED TO INNER TUBE

ITEM NO	DESCRIPTION	MATERIAL	NO OFF
14	3/8 NUT & WASHER	-	4
13	3/8 BSN STUD 2" LONG	-	4
12	3/8 BSN NUT, BOLT & WASHER	STEEL	4
11	1/8 PACKING	KLINGERIT	2
10	3/16 GLAND PACKING	VALVASCA TYPE 65	3
9	DISTRIBUTOR	TROPIC FD OR STAINLESS STEEL	2
8	FLANGE	TROPIC FD	1
7	FLANGE	-	1
6	FLANGE	-	1
5	FLANGE	-	2
4	GLAND RING	-	1
3	OUTER TUBE	-	1
2	INNER TUBE	-	1
1	½" STEAM PIPE	TROPIC FD	2

ALL WELDS TO BS 1515
WORKING TEMPERATURE 700°C: PRESSURE 2½ ATMS
HYDRAULIC TEST 5 ATMS

RADIATION SUPERHEATER
3 OFF

SCALE 1/1

FIGURE A3·7: Drawing of the Radiation Superheater

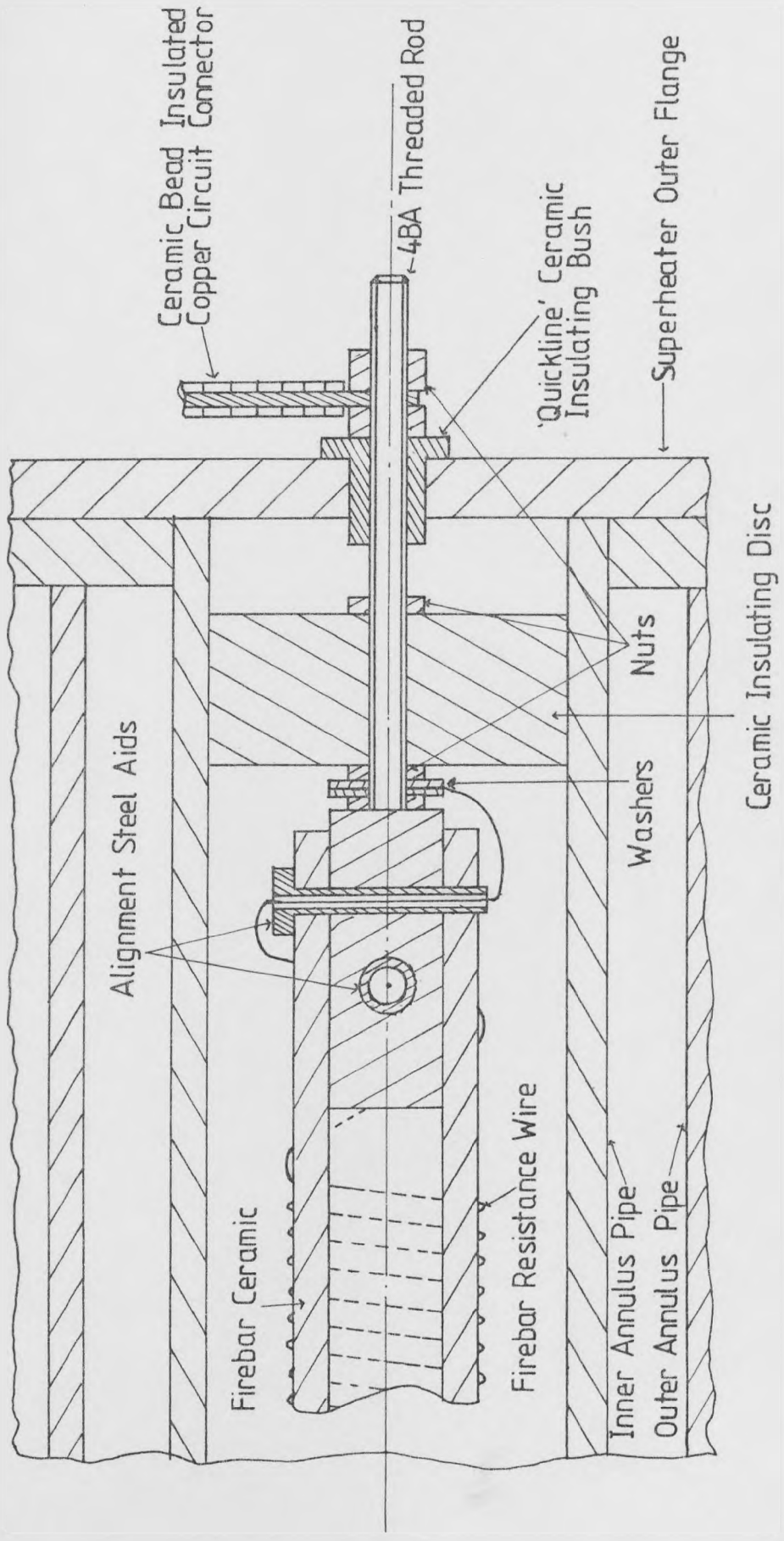

FIGURE A3.8: Radiation Superheater Firebar Support Assembly

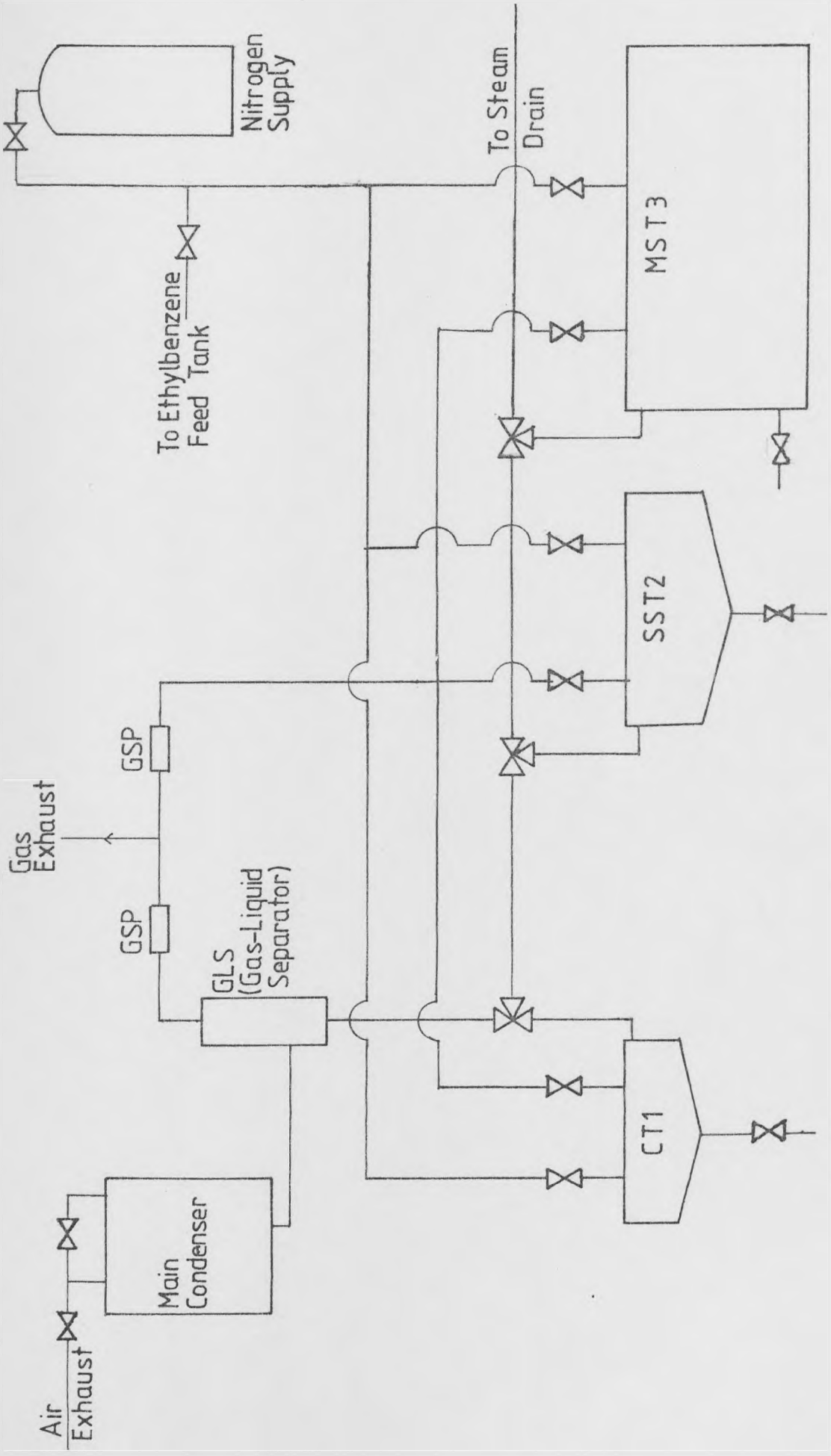

FIGURE A3.9: The Sample Collection, Gas Exhaust, and Water Drainage Arrangement

APPENDIX A4

MATHEMATICAL MODELS AND SOLUTIONS FOR THE HEAT LOSS COMPENSATION METHODS

APPENDIX A4

MATHEMATICAL MODELS AND SOLUTIONS FOR THE HEAT LOSS COMPENSATION METHODS

The ceramic bead insulated wire wound on the metal pipe was shown to have high heat transfer resistances which caused burn outs at very low wattages. A model is required to examine the heat transfer resistances and attempt to check the effect of varying the various resistances in order to provide a suitable location of the winding so as to be able to sustain wattages of around 1500 W without burn outs.

A4.1 Model 1

Consider a length of wire placed adjacent to the pipe wall with insulation covering it (Figure A4.1a). The ceramic beads (Figures A4.1b and A4.1c) only have point contact with the metal pipe. This causes a number of transfer resistances (Figure A4.2) of which only the pipe and insulation resistances can be accurately determined. The total resistance due to the winding, R_{TBW}, can be estimated from the burn out data in Table 5.1. Assuming a surface temperature of 710^{o}C, and a wire melting temperature of 1400^{o}C, the heat transfer coefficient due to the wire h_{WIRE}, is estimated to have a value of 0.977 W/m^{2} ^{o}C. Run 24 power values are used for this estimation.

Consider the arrangement in Figure A4.1. A heat balance over a length element dx of the wire, at steady state reads:-

$$q_x - q_{x+dx} + \dot{Q} A_x \, dx - U_I \, A_{SI} \, dx \, (T - T_I) - U_O \, A_{SO} \, dx \, (T - T_A) = 0 \quad (A4.1)$$

where $\dot{Q}$ is the heat load per unit volume of the wire;

U_I is the heat transfer coefficient on the inside of the resistance wire ($R_I + R_W + R_{TBW}$);

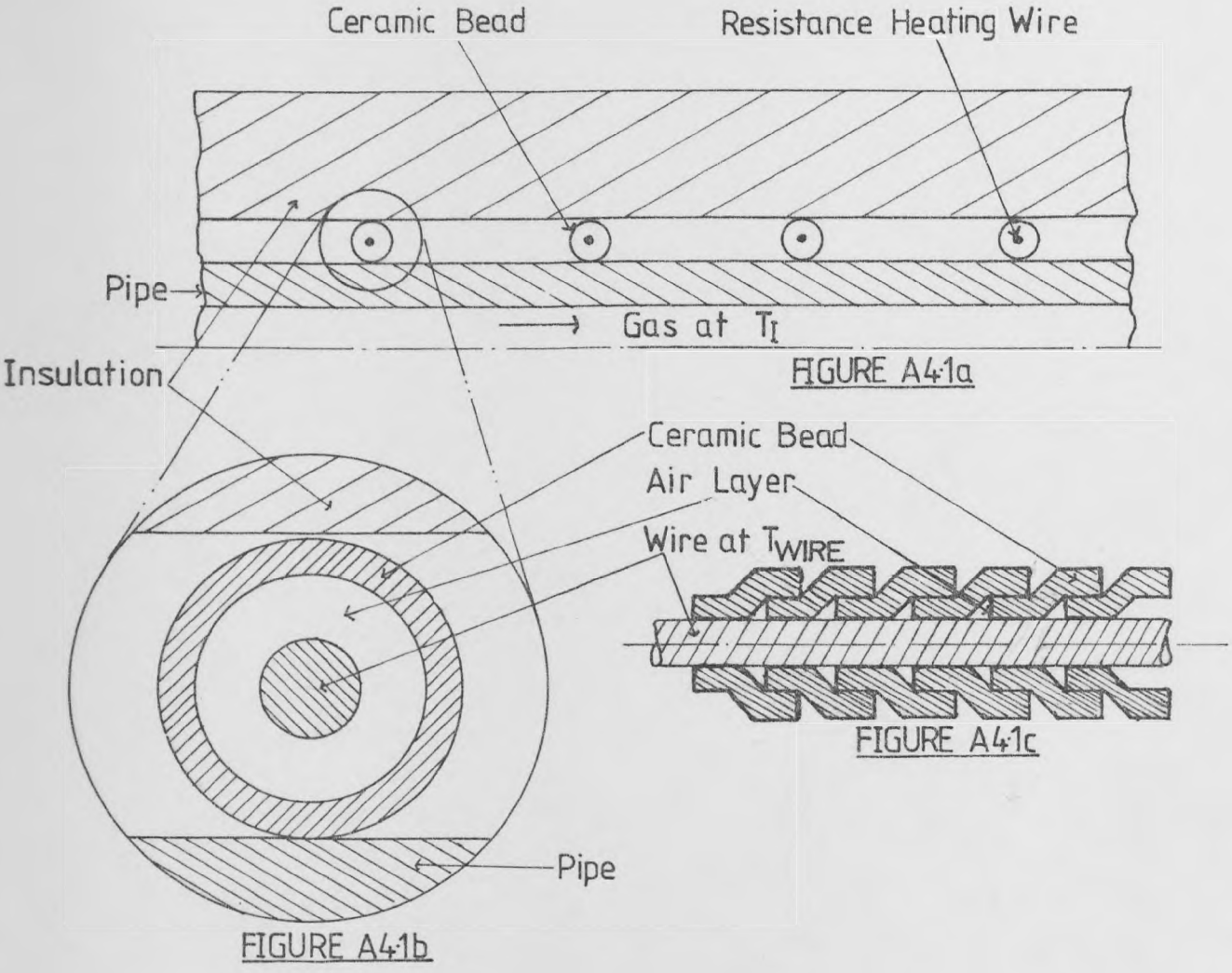

FIGURE A4.1: The Position of the Ceramic Bead Insulated Wire Relative to the Full System and the Resistance Wire

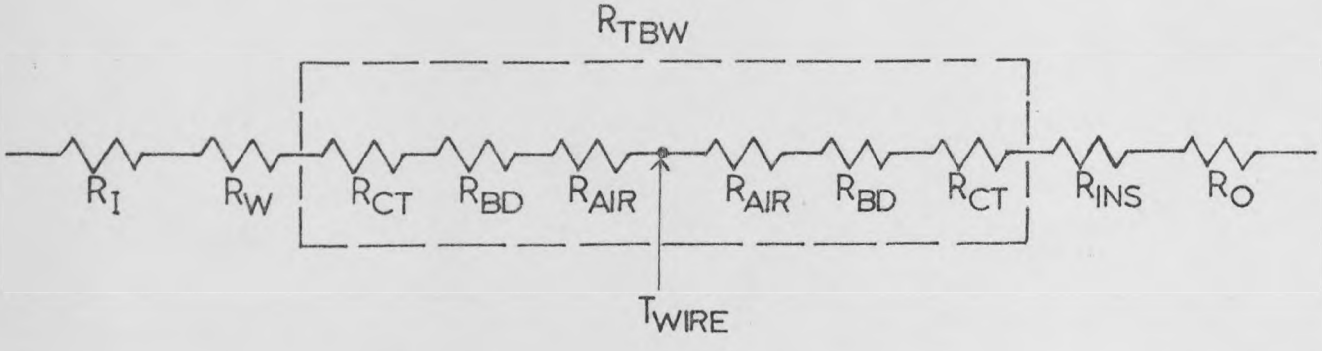

FIGURE A4.2: The Heat Transfer Resistances for the Compensating Winding Wound on the Hot Pipe

U_O is the heat transfer coefficient on the outside of the resistance wire ($R_{INS} + R_O$).

T_I is the gas temperature and

T_A is the ambient temperature.

By Taylor's approximation, if $q_x = - k A_x \frac{dT}{dx}$, then:-

$$q_{x+dx} = - k A_x \frac{dT}{dx} - k A_x \frac{d^2T}{dx^2} dx \qquad (A4.2)$$

Substituting Equation (A4.2) into Equation (A4.1):-

$$k A_x \frac{d^2T}{dx^2} + Q^{\cdot} A_x - U_I A_{SI} (T - T_I) - U_O A_{SO} (T - T_A) = O \qquad (A4.3)$$

T_O is constant, therefore an analytical solution is possible if $T_I = f(x)$. Assuming a linear variation of T_I, i.e.

$$T_I = Mx + N \qquad (A4.4)$$

Equation (A4.3) can be rearranged to read, assuming $A_{SI} = A_{SO}$,

$$\frac{d^2T}{dx^2} - \frac{A_S T}{A_x k} \left[U_I + U_O \right] = \frac{U_I A_S Mx}{A_x k} - \frac{(Q^{\cdot} A_x + U_O A_S T_A + U_I A_S N)}{k A_x} \qquad (A4.5)$$

which is an equation of the form:-

$$\frac{d^2T}{dx^2} - AT = Bx + C \qquad (A4.6)$$

where $$A = \frac{A_S}{k A_x} \left[U_I + U_O \right] \qquad (A4.7)$$

$$B = - \frac{U_I A_S M}{A_x k} \qquad (A4.8)$$

and $$C = - \frac{\dot{Q} A_x + A_S (U_O T_A + U_I N)}{k A_x} \qquad (A4.9)$$

The boundary conditions for Equation (A4.6) are:-

$$\text{At } x = 0, \quad \frac{dT}{dx} = 0 \quad \text{and}$$

$$\text{At } x = L, \quad \frac{dT}{dx} = 0$$

Using a complimentary function and particular integral solution, the full solution of Equation (A4.6) is:-

$$T = \frac{B}{A\sqrt{A}} (1 - e^{-\sqrt{AL}}) \frac{\text{Sinh } \sqrt{Ax}}{\text{Sinh } \sqrt{AL}} - \frac{B}{A} \left(x - \frac{e^{-\sqrt{Ax}}}{\sqrt{A}} \right) - \frac{C}{A} \qquad (A4.10)$$

The solution can be simplified by assuming:-

(i) $\exp(-\sqrt{AL}) \rightarrow 0$ as $L > 10$ metres and

(ii) it is the maximum wire temperature that is of interest, and this occurs at $x = 0$. Equation (A4.10) simplifies to:-

$$T_{WIRE} \Big|_{x=0} = - \frac{C}{A} \qquad (A4.11)$$

Table A4.1 carries the data for the ceramic bead wire on pipe situation. This data is used in Equation (A4.11).

TABLE A4.1

Data for Model 1 and Run 24 Solutions

Wire diameter	0.081 cm
Wire length	12 m
Total heat load	25 Watts
U_O (three Kaowool layers)	0.29 W/m^2 K
U_I (without h_{WIRE})	14.97 W/m^2 K

For a heat load os 24 W (as per Run 24) without the wire thermal resistance, the wire temperature works out at 783°C for a gas temperature of 710°C. Therefore, the high value of h_{WIRE} is causing the burn outs. This was not foreseen in the original intention to implement the winding for heat loss compensation. A balancing of U_I and U_O may aid the situation. The resistance between the pipe and the wire can be increased by an insulation layer. Assuming one 2" Kaowool layer between the pipe and the wire, and two layers on the outside of the wire, the wire can only sustain 81 Watts. With two layers on the inside of the windings, the duty possible rises to 95 W. Any more insulation is impractical due to the weight and the covering area required. Nevertheless, it appears that it is unlikely that a 12 metre wire will carry out the compensation.

The solution seems to be to have a length of wire of around 150 metres! Clearly this is impracticable. However, this does give rise to an idea that if a continuous metal layer could be maintained at 700°C, then this might be a way of compensating for the heat loss. The only practical method is to utilize a 'heat shield sandwich', i.e. a continuous metal plate is placed on the resistance winding helping to distribute the heat. Copper, with a melting point of 1080°C and a thermal conductivity of 359 W/m K is ideal, and is available in thin sheeting.

A model needs to be developed to examine the effect of such a shield on the wire duty, as well as the best location of such a shield.

A4.2 Model 2

Assuming instantaneous heat conduction from the wire to the copper plate, then the solution identical to that of Model 1, T_I, the gas temperature is assumed constant, as well as applying those assumptions for Model 1. The gas temperature value used is the highest required that the shield has to maintain. The general solution is Equation (A4.10) and also simplifies to Equation (A4.11):-

$$T_{PLATE} = -\frac{C}{A} \qquad (A4.11)$$

with C and A worked out for the copper plate from Equations (A4.9) and (A4.7) respectively.

Figure A4.3 shows the various positions where the heat shield can be located. Position 4 can be ruled out due to the high load required to maintain a heat shield at 700°C radiating to ambient conditions. Position 1 has been shown to have very high contact resistances, which are only complicated by the difficulties in folding a sheet of copper over a narrow pipe diameter.

Therefore, positions 2 and 3 need to be examined for the heat duties required, assuming only heat loss to the outside, i.e. $T_{PLATE} = T_{GAS}$ in Equations (A4.10) and (A4.11). Position 2 has a heat loss of 1280 W compared to position 3 which has a heat loss of 2475 W. The wire has been designed to carry only a maximum of 2 kW, and the duties of implement 2-3 shields as per position 3 will stretch the power capacity of the 3-phase supply. Therefore, a 12 metre wire will be used in position 2 with a thin copper layer covering the entire length of the pipework being compensated for the heat loss. The thinnest sheeting available is 26 G

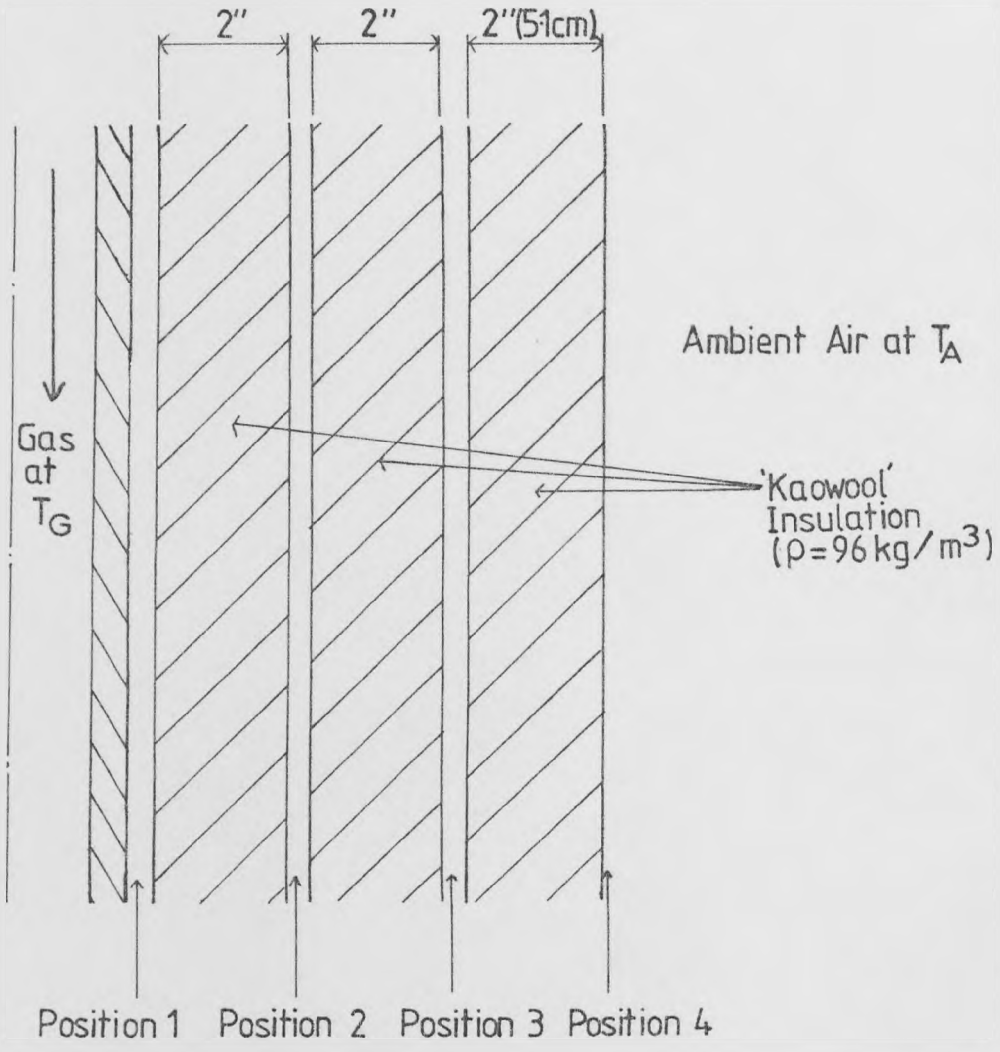

FIGURE A4.3: The Positions Possible for the Use of Heat Shields

(0.046 cm thick). For a shield of 2.8 m length (SSH2 → Mixer length) at 700°C, Equation (A4.11) is checked for the effect of a thicker copper plate, say 21 G (0.082 cm). The load falls to 1275 W making very little difference. Further addition of insulation on the inside of the shield, yet maintaining a 4" layer on the outside makes little difference (< 5%) to the loading possible on the shield. If the value of h_{WIRE} of 0.977 W/m^2 K is integrated into the solution, the duty required rises to 1560 W, still within the wire capacity. These calculations show the duties required for maintaining a heat shield sandwich at 700°C. Experimental runs are required to estimate what sort of limitations are posed by the wire to copper plate resistance. Before then, a model needs to be developed to investigate the troughs and peaks along the copper shield.

A4.3 Model 3

Consider the copper plate and bead insulated wire arrangement shown in Figure A4.4. At steady state:-

$$q_x - q_{x+dx} + \dot{Q} A_x \, dx - U_I A_{SI} (T_{PL} - T_I) \, dx - U_O A_{SO} (T_{PL} - T_A) \, dx = 0 \qquad (A4.12)$$

The boundary conditions are:-

$$\left.\frac{dT}{dx}\right|_{x=L} = 0 \quad \text{and} \quad \left. T_{PL} \right|_{x=0} = \text{constant} = T_{CP} \qquad (A4.13)$$

and assume that $A_{SI} = A_{SO}$.

Solving Equation (A4.12) after substitution of Equations (A4.2, A4.6, A4.7, A4.8 and A4.13) into (A4.5)

$$T = \left[\frac{B}{A\sqrt{A}} + e^{-\sqrt{AL}} \left(T_{CP} + \frac{C}{A}\right) \right] \frac{\text{Sinh } \sqrt{Ax}}{\text{Cosh } \sqrt{AL}} + \left(T_{CP} + \frac{C}{A}\right) e^{-\sqrt{Ax}} - \frac{Bx}{A} - \frac{C}{A} \qquad (A4.14)$$

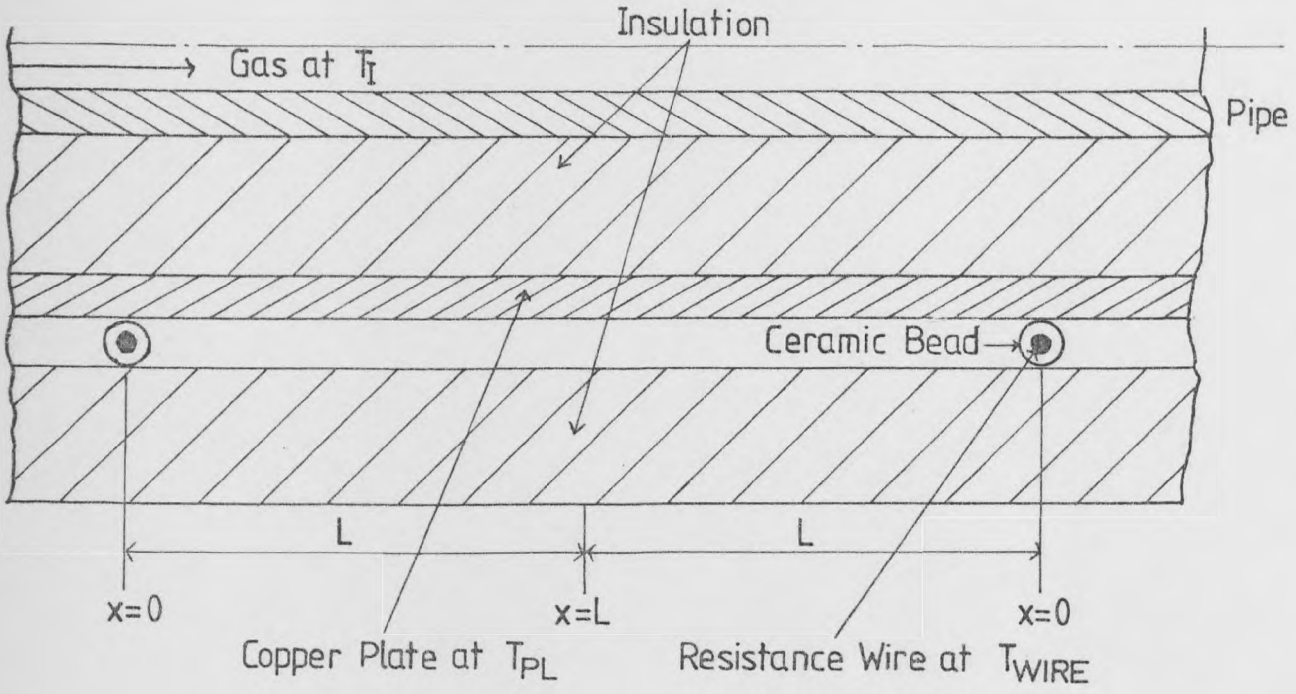

FIGURE A4.4: Heat Shield Positioning for Model 3

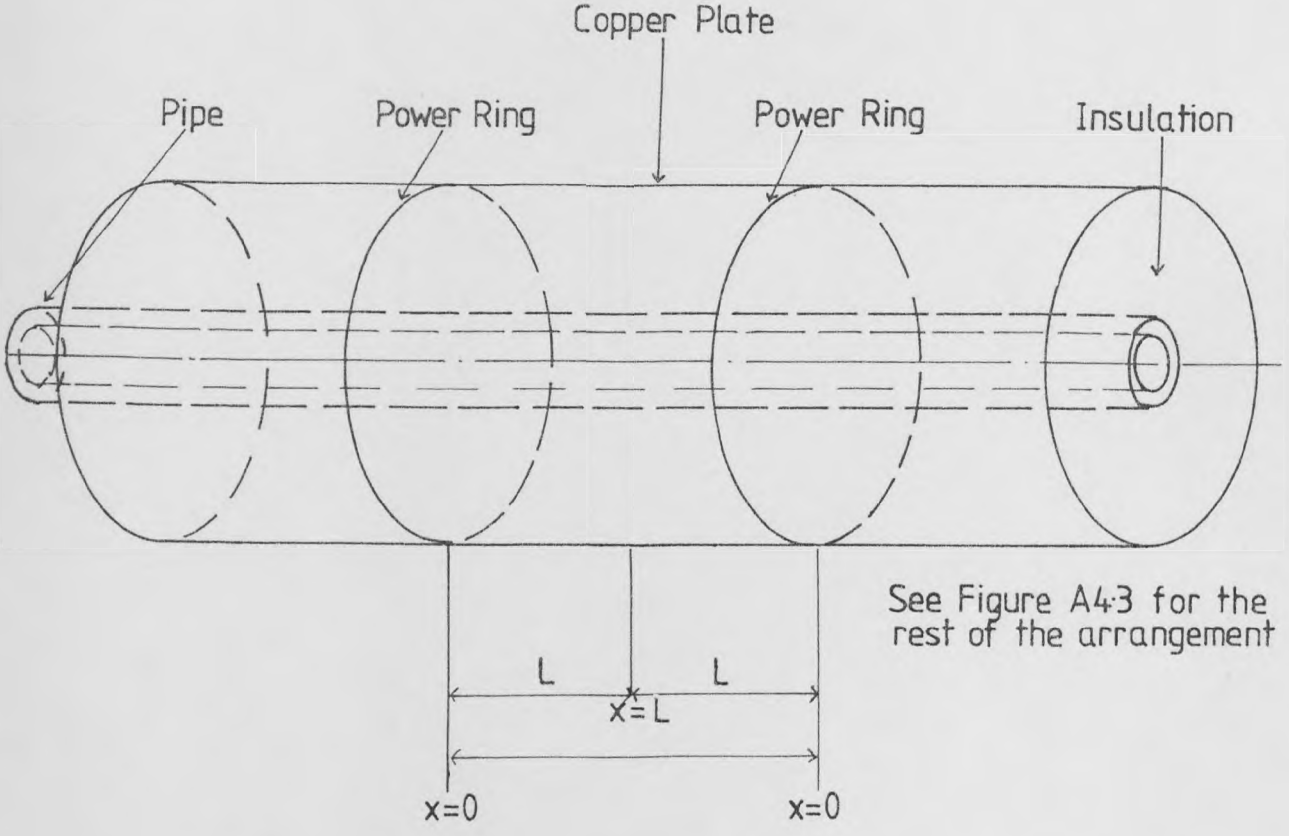

FIGURE A4.5: Heat Shield Positioning for Model 4: The 'Power Ring'

Assuming that T_I is constant (this may not be so if the plate turns out to have large temperature troughs and peaks), and that B = 0, the solution simplifies to:-

$$T = (T_{CP} + \frac{C}{A}) \left[e^{-\sqrt{AL}} \frac{\text{Sinh } \sqrt{Ax}}{\text{Cosh } \sqrt{AL}} + e^{-\sqrt{Ax}} \right] - \frac{C}{A} \qquad \text{(A4.15)}$$

For a 26 G (0.046 cm thick) copper plate, with L = 6.1 cm (distance between adjacent wire turns), Equation (A4.15) works out that if $T_{MAX} = T_{x=O} = 700^{o}C$, $T_{MIN} = T \Big|_{x=L} = 695.5^{o}C$, showing that the troughs are small, and the model need not be expanded to consider the effect of the variation in T_I (less than 0.6% variation in T_I). If the trough had been significant then an iterative method for solving the coefficient B at x = O and x = L would be necessary, to account for $T_I = f(x)$.

This model does, however, assume a uniform distribution of the heat load along the wire. A more accurate model would be Model 4 (the 'Power Ring' model) which assumes the shield to have a series of loading rings of wire, each a distance 2 L apart through which the power is equally distributed (see Figure A4.5).

A4.4 Model 4: The 'Power Ring'

Each ring (Figure A4.5) distributes a head load of Q_R Watts. The general equation at steady state

$$q_x - q_{x+dx} - U_I A_S (T - T_I) dx - U_O A_S (T - T_A) dx = O \qquad \text{(A4.16)}$$

is solved (similar method to Model 3) using the boundary conditions:-

$$\frac{dT}{dx}\Big|_{x=O} = \frac{-Q_R}{k A_x} \quad \text{and} \quad \frac{dT}{dx}\Big|_{x=L} = O \qquad \text{(A4.17)}$$

The full analytical solutions emerge as:-

$$T = \left[\frac{B}{A\sqrt{A}} - \left(\frac{B}{A\sqrt{A}} - \frac{Q_R/k}{A_x \sqrt{A}} \right) e^{-\sqrt{AL}} \right] \frac{\text{Cosh } \sqrt{A}x}{\text{Cosh } \sqrt{AL}} - \left(\frac{B}{A\sqrt{A}} - \frac{Q_R/k}{A_x \sqrt{A}} \right) e^{-\sqrt{A}x} - \frac{Bx}{A} - \frac{D}{A} \quad \text{(A4.18)}$$

where $$D = - \frac{A_S}{k A_x} \left[U_O T_A + U_I N \right] \quad \text{(A4.19)}$$

A and B are as per Equations (A4.7) and (A4.8) respectively. Once again, as per Model 3, if T_I is initially assumed constant, Equation (A4.18) simplifies to:-

$$T = \frac{Q_R}{k A_x \sqrt{A}} \left[e^{-\sqrt{AL}} \frac{\text{Sinh } \sqrt{A}x}{\text{Cosh } \sqrt{AL}} + e^{-\sqrt{A}x} \right] - \frac{D}{A} \quad \text{(A4.20)}$$

For a 26 G copper plate, using Q_T = 1583 W (evaluated in Section A4.3),

$$T\Big|_{x=L} = T_{MIN} = 694.9^{\circ}C$$

and $$T\Big|_{x=O} = T_{MAX} = 701.3^{\circ}C$$

Once again the troughs are small, and there is no need to reassess the model. The results for Models 3 and 4 are consistent. Runs 26-32 carry out the experimental work required to confirm this modelling, and the limitations of the shield.

Note:- The value of h_{WIRE} of 0.977 W/m^2 K was obtained from Run 24. This value was initially used in the study, until Runs 26-32 confirmed the success of the copper shields. At the same time, a more accurate value of h_{WIRE} was available from these later runs. Assuming that the wire burnt out at 620°C for the S2MW shield, and the melting point of the resistance wire is 1400°C, the value of h_{WIRE} works out to be 0.926 W/m^2 K.

This value has been used in the calculations in Models 3 and 4. Equation (A4.20) can be used to check the experimental value. 1100 Watts gave a shield of 620°C. Using Equation (A4.20) with Q_R = 23.5 Watts for a 12 metre wire on S2MW, the shield temperature is calculated to be 642°C, confirming the experimental work, and the validity of this model.

A4.5 Calculation of Catalyst Temperature for the Arrangement Using Four Copper Shields

Consider a shield between two points X and Y (Figure A4.6) with a shield at temperature T_{SD} covering the length of pipe which has the gas flow at temperatures T_I at X, and T_O at Y. The temperature T_O can be worked out using Equation (A4.22):-

$$q_l = UA_S\theta_m = M\,C_p\,\Delta T = UA\left[\frac{\theta_1 - \theta_2}{\ln(\theta_1/\theta_2)}\right] = M\,C_p\,(T_I - T_O)$$

$$\rightarrow\ q_l = \frac{U\,A_S\,(T_I - T_O)}{\ln\left(\dfrac{T_I - T_{SD}}{T_O - T_{SD}}\right)} = M\,C_p\,(T_I - T_O) \qquad \text{(A4.21)}$$

$$\therefore\ T_O = (T_I - T_{SD})\exp(-UA_S/M\,C_p) \qquad \text{(A4.22)}$$

Four copper shields can be used on the apparatus (Figure A4.7). S2MW and RAW have operating limits of 605°C and 600°C. EBEW and EBCW would be maintained at 540°C for the best case, and 370°C and 540°C for Run 37. The maximum catalyst temperature possible, assuming perfect shield operation, for the two situations is tabulated, along with other temperatures, in Table A4.2.

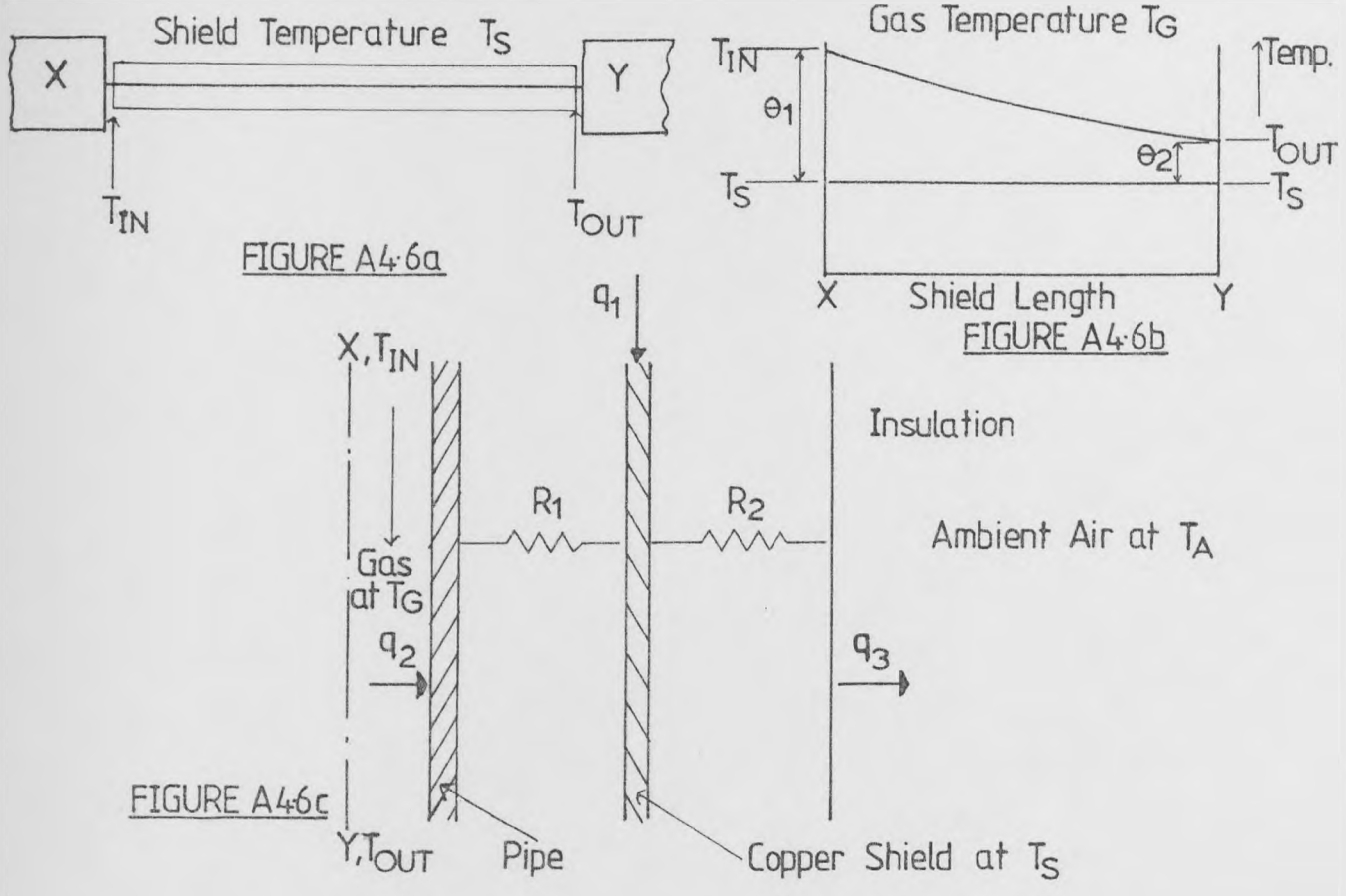

FIGURE A4.6: Copper Shield Calculation Notation

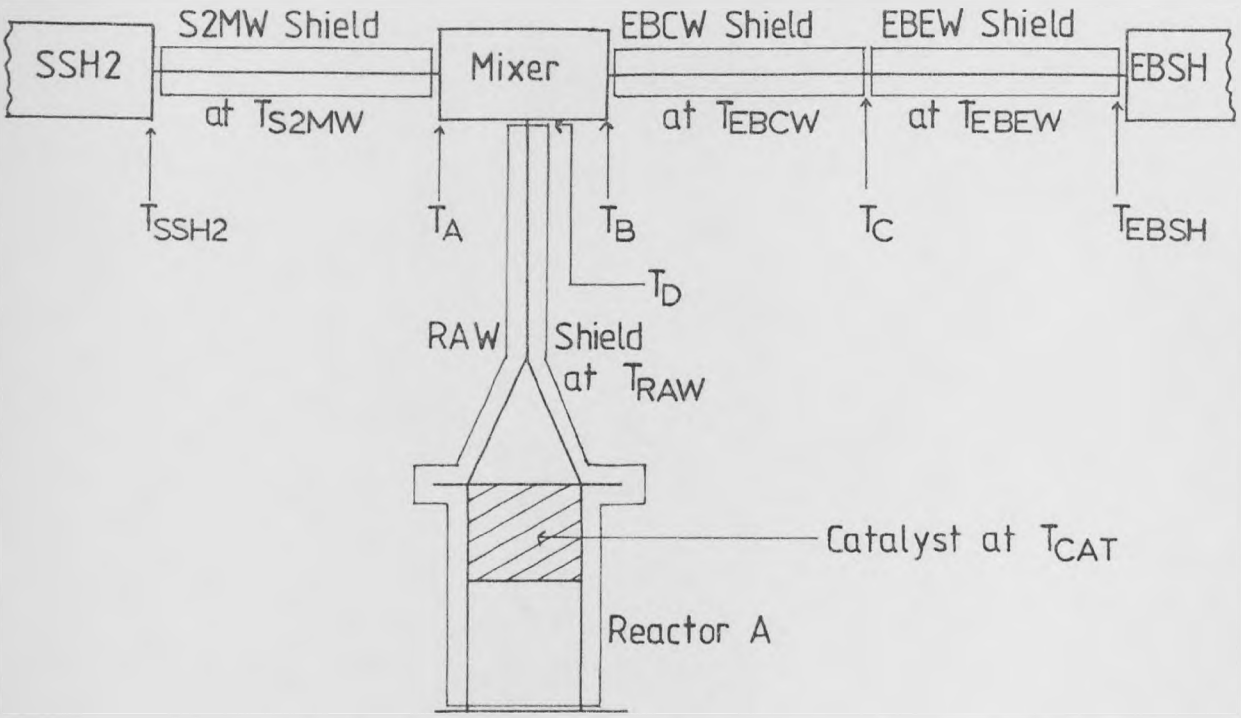

FIGURE A4.7: Temperature Notation of Copper Shield Calculations for the Apparatus

TABLE A4.2

Results for the Catalyst Temperature Calculations

Run	T_{SSH2} °C	T_{EBSH} °C	T_{S2MW} °C	T_{RAW} °C	T_{EBEW} °C	T_{EBCW} °C	T_A °C	T_B °C	T_C °C	T_D °C	T_{CAT} °C
Ideal	720	540	605	600	540	540	675	540	540	627	621
37	720	540	605	600	370	540	675	497	436	612	609

APPENDIX A5

ELECTRICAL CIRCUITS AND TEMPERATURE RECORDER WIRING

APPENDIX A5

ELECTRICAL CIRCUITS AND TEMPERATURE RECORDER WIRING

Notes on the Electrical Circuits

The circuits are supplied by three phase (415 V, 240 V single phase) mains. Each phase has a distribution load limit of 25 A (Yorkshire Electricity Board requirement) and is fused for 30 A. Each phase in turn has 4 mains circuits, all individually fused for 15 A. Figures A5.1 and A5.2 show the secondary 'Live' wiring for all electrical circuits that utilize the main power supply. Figures A5.3 - A5.6 show the complete wiring for the electrical heating circuits. Figure A5.7 shows the solenoid valve step-down transformer wiring, from 240 V A.C. supply to 24 V D.C. output, as two 12 V secondary coils, each rated at 2:5 A. Each transformer (of three) can supply two solenoid valves (0.96 A, 24 V D.C.). The rectifier and transformers are all housed together in a black box at the back of the control panel. Table 5.1 shows the power capacities of all the heater circuits. The transformer has two 12 V secondary coils, and is rated at 2.5 A. The solenoid valve coil is rated at 0.96 A/24 V D.C. Three transformers are all housed together with the rectifiers and the fuses, in the 'Transformer Box' at the back of the control panel.

Notes on the Temperature Recorder Wiring

Table A5.2 shows the temperature recording connections to the 16 point Kent recorder for two positions of a 4 pole wafer switch. Point 16 is also shorted to indicate the zero reading on the recorder scale.

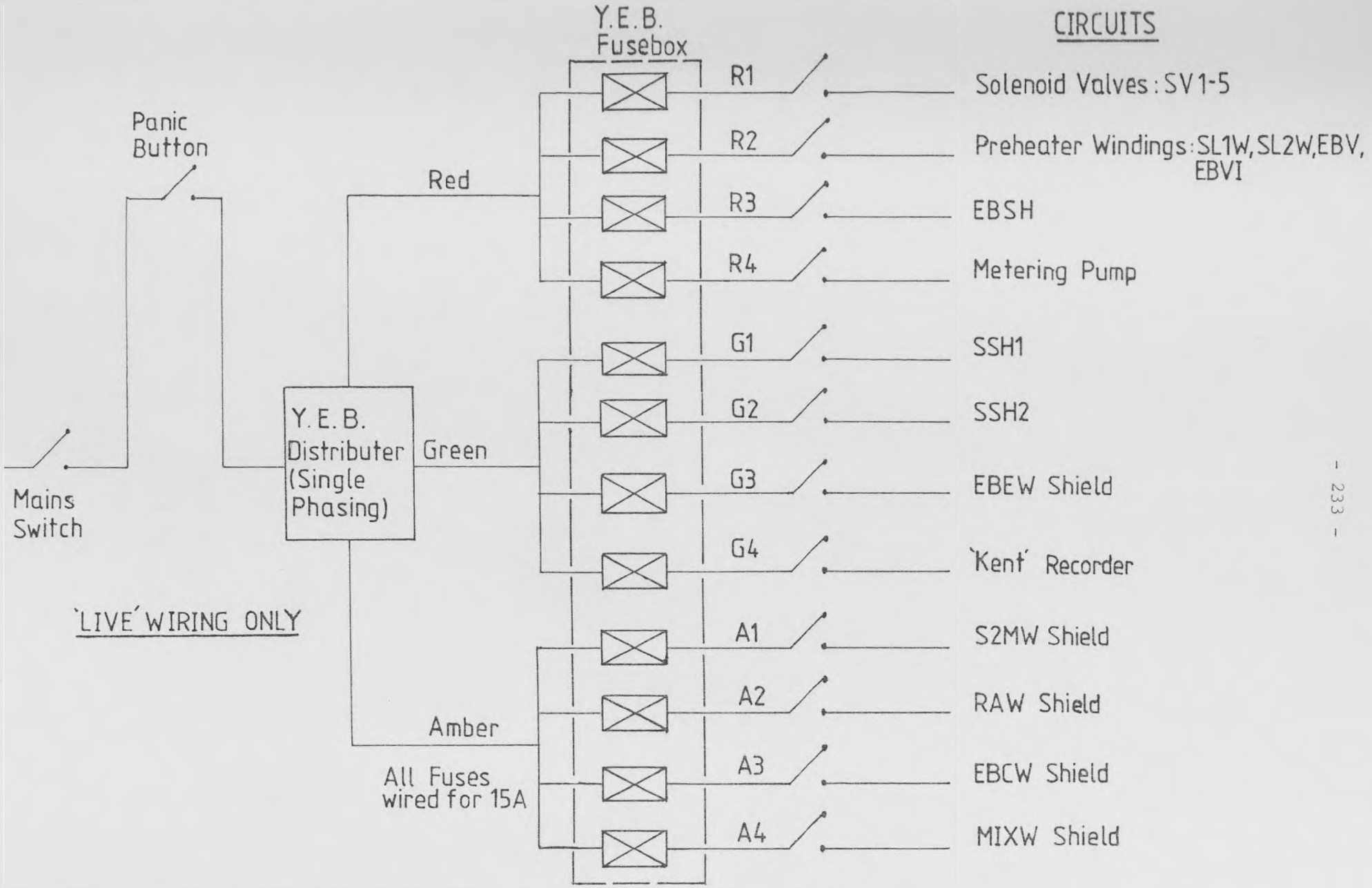

FIGURE A5.1: The 3 Phase Mains Distribution to the Individual Circuits

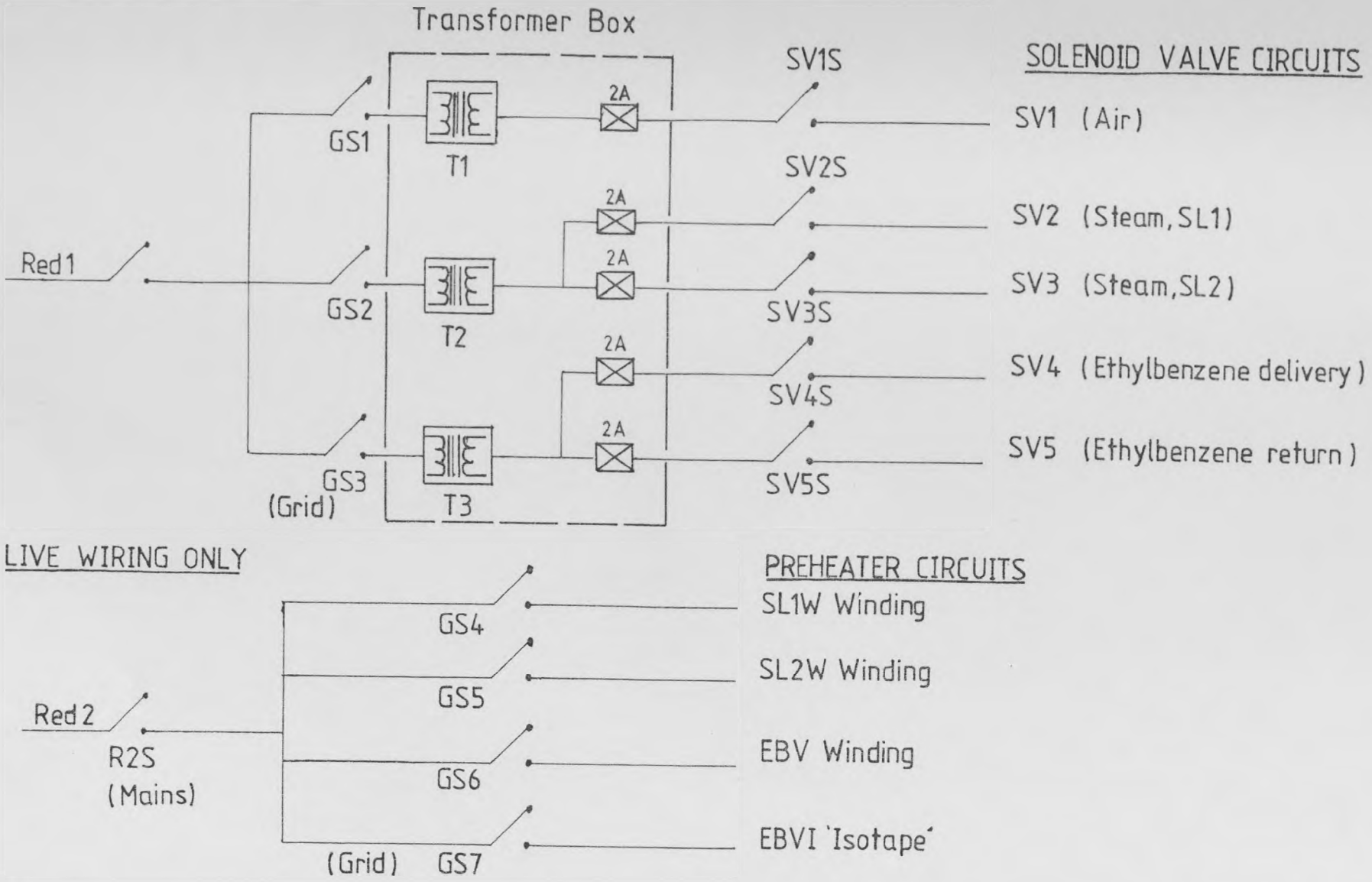

FIGURE A5.2: The Solenoid Valves and Low Wattage Winding Circuits

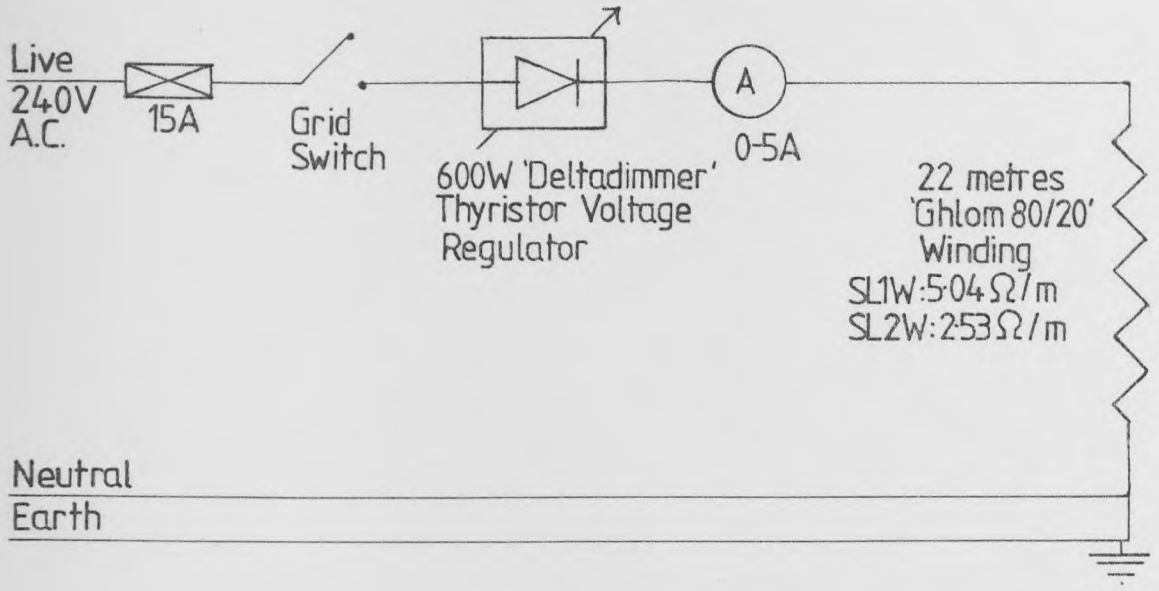

FIGURE A5.3: Preheater Circuits for the Steam Supply Lines SL1 and SL2

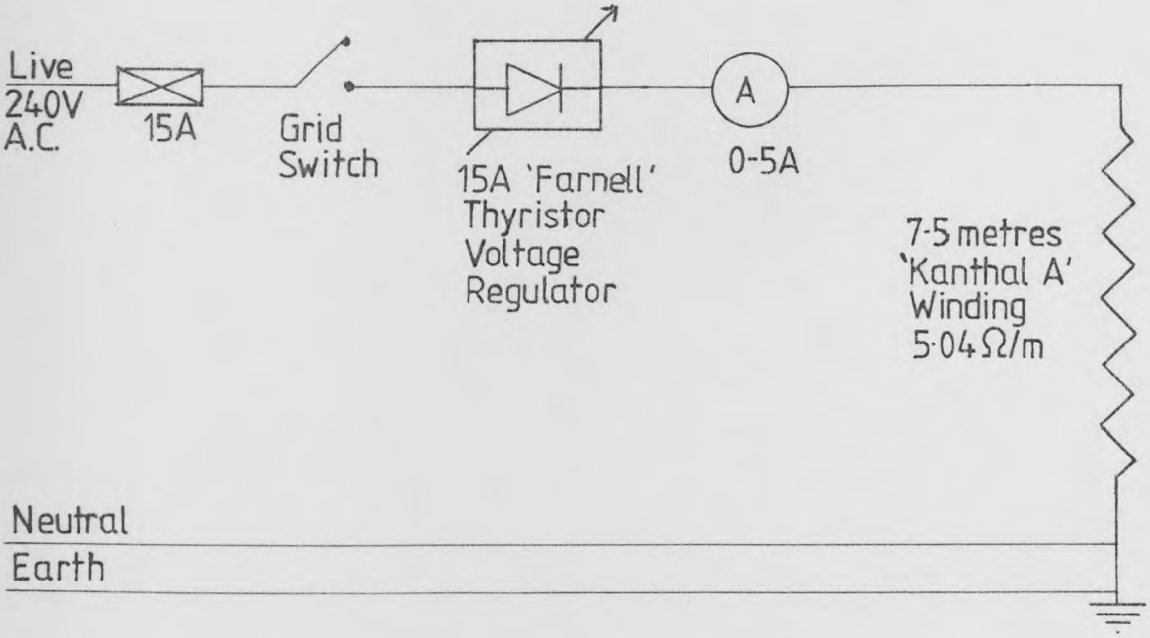

FIGURE A5.4: The Ethylbenzene Vaporiser Circuit

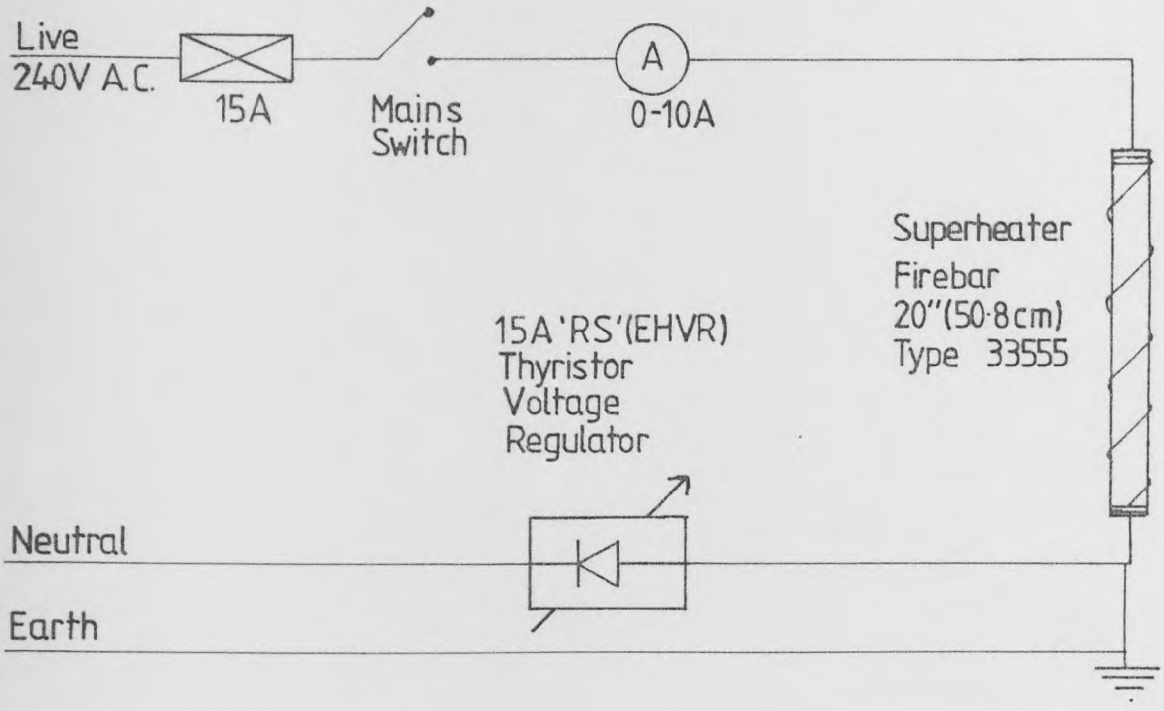

FIGURE A5.5: Superheater Circuits for SSH1, SSH2, SSH3 and EBSH

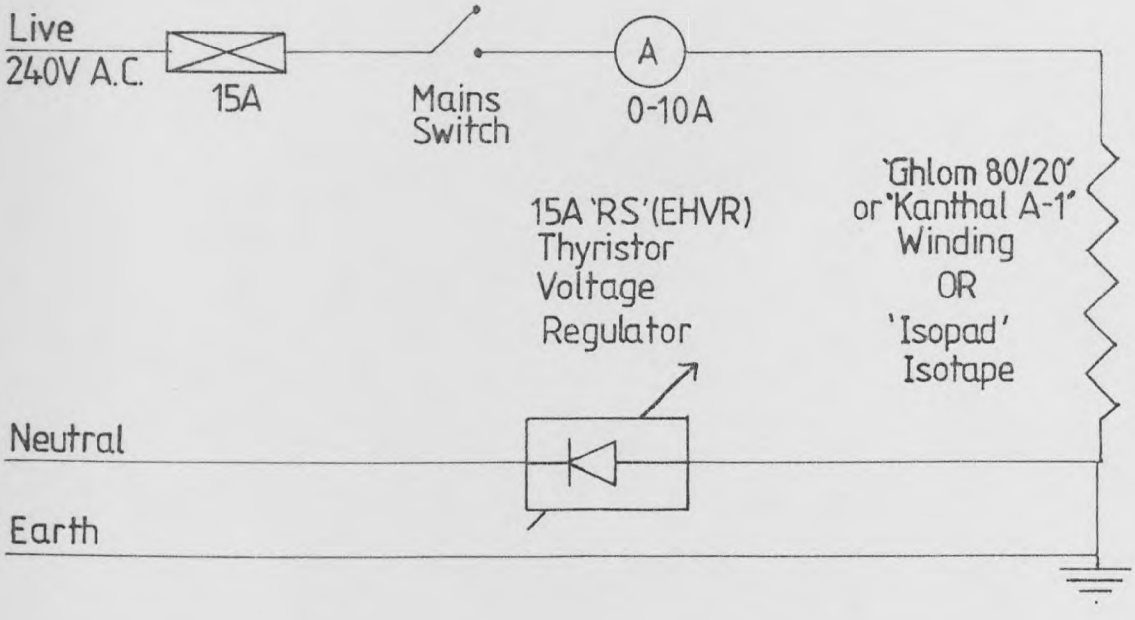

FIGURE A5.6: Circuits for the Heat Loss Compensation Tapes and Shields

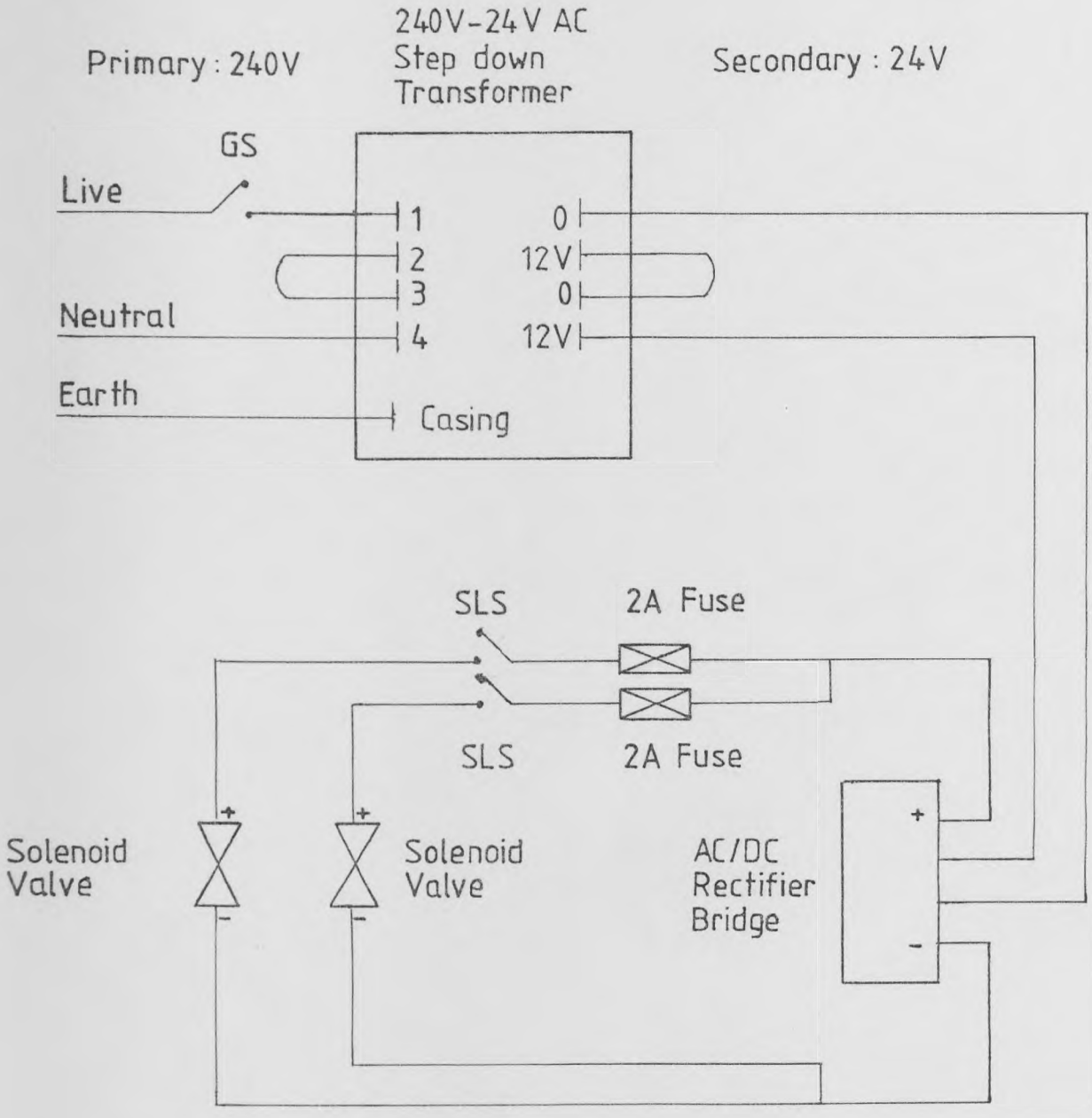

FIGURE A5.7: The Solenoid Valve Circuits and Wiring to the Step Down Transformer

TABLE A5.1

Power Ratings of all Heater Circuits

Heating Circuit	Maximum Power (W)	Maximum Current (A)	Type of Heater	Resistivity (Ω m^{-1})	Circuit Resistance (Ω)
SSH1	1800	7.5	Firebar	2.68	32.0
SSH2	1800	7.5	Firebar	2.68	32.0
SSH3	1800	7.5	Firebar	2.68	32.0
EBSH	1500	6.2	Firebar	3.27	39.0
RAW	1570	6.5	'Isotape'	1.78	37.1
S2MW	1570	6.5	'Isotape'	1.78	37.1
EBEW	1545	6.5	Winding	2.68	36.6
EBCW	2730	11.4	Winding	1.75	21.0
SL1W	1000	4.2	Winding	2.53	56.7
SL2W	500	2.1	Winding	5.04	113.4
EBV	1500	6.2	Winding	5.04	39.0
EBVI	330	1.4	'Isotape'	42.1	168.4

TABLE A5.2

Kent Recorder Temperature Indicator Locations

Recorder Circuit and Pen Number	Temperature Indicator Location	
	Wafer Switch Position 1	Wafer Switch Position 2
1, 9	Reactor A TOP (Inlet)	A TOP
2, 10	Reactor A MID (Outlet)	A MID
3, 11	Reactor A CAT (Catalyst)	A CAT
4, 12	Reactor A BASE	A BASE
5	EBCW Shield	SSH1 In
6	S2MW Shield	EBSH In
7	EBEW Shield	SSH1 Out
8	SSH2 Out	SSH2 Out
13	EBSH Out	EBSH Out
14	EBV (Vaporiser)	EBVap
15	RAW Shield	RAW Shield
16	Zero Point	Condenser Mid Point

APPENDIX A6

THE REACTOR DATA, CATALYST PROPERTIES AND THE 'DERIVED' KINETICS

APPENDIX A6

THE REACTOR DATA, CATALYST PROPERTIES AND THE 'DERIVED' KINETICS

A6.1 The Reactor Modelling Data and Catalyst Properties

The compositions of the Girdler G-64 C/D and Shell 105 are very similar and is basically Fe_2O_3 (85 - 90%), Cr_2O_3 (2 - 4%) and K_2CO_3 (6 - 10%) or KOH (1 - 2%). The data of Girdler G-64 catalyst is used for all modelling studies. Data used for computer models is presented below:-

Reactor Diameter	:	10.2 cm
Bed Specific Heat	:	1.051 kJ kg^{-1} K^{-1}
Ethylbenzene Flowrate	:	2.95 kg hr^{-1}
Steam Flowrate	:	7.0 kg hr^{-1}
First Bed Inlet Pressure (for 2 bed SSAR)	:	1.67 bar
Second Bed Inlet Pressure (for 2 bed SSAR)	:	1.35 bar
Bed Inlet Pressure for one bed system	:	1.27 bar
Catalyst particle size (actual)	:	3.2 mm dia., 6.4 mm length
Catalyst particle size (spherical for model studies)	:	4.2 mm dia.
Catalyst packed density	:	1747.2 kg m^{-3}
Voidage of catalyst	:	0.31
Catalyst specific area per unit volume	:	13231.1 m^2 m^{-3}

A6.2 The 'Derived' Reaction Kinetics

These steady state kinetics were derived by Cockcroft[10] from experimental data by Bogdanova et al[33]. Only the three ethylbenzene consuming reactions are considered.

Reaction 1 $C_6H_5C_2H_5 \rightleftharpoons C_6H_5C_2H_3 + H_2$

$$K_p = \exp (16.12 - 15350/T)$$

$$rr_1 = \frac{K_1 (p_{EB} - p_{ST}\, p_{H2}/K_p)}{0.093 + p_{EB} + 8.03\, p_{ST}}$$

where $K_1 = 3.032 \times 10^6 \exp (-23050/T)$

Reaction 2 $C_6H_5C_2H_5 \rightarrow C_6H_6 + C_2H_4$

$$rr_2 = \frac{K_2\, p_{EB}}{0.093 + p_{EB} + 8.03\, p_{ST}}$$

where $K_2 = \exp (8.132 - 20336/T)$

Reaction 3 $C_6H_5C_2H_5 + H_2 \rightarrow C_6H_5CH_3 + CH_4$

$$rr_3 = \frac{K_3\, p_{EB}\, p_{H2}}{0.093 + p_{EB} + 8.03\, p_{ST}}$$

where $K_3 = \exp (11.109 - 18820/T)$

APPENDIX A7

FULL START-UP, RUN AND SHUT-DOWN PROCEDURE

APPENDIX A7

FULL START-UP, RUN AND SHUT-DOWN PROCEDURE

A7.1 Start-Up and Run Procedure

Ensure air compressor is on before start-up:-

1. Open solenoid valves SV1 and SV3. Open air rotameter to the following settings: Line SL1: Series 18 Rotameter Mark 22-23 (14.3 kg/hr, 20 psig (2.36 bar)). Line SL2: Series 14 Rotameter Mark 18-19 (8.1 kg/hr, 10 psig (1.68 bar)). Ensure air is exhausting to the atmosphere via the exhaust line at the top of the main condenser. Switch on superheaters SSH1, SSH2 and EBSH. Step up to full power over a period of 1 hour and 45 minutes, with load step ups of around 50 W. Turn on Main Condenser to Mark 16 on Series 18 Rotameter. Switch on Kent Recorder after ice has been packed for the zero indicator. (Time elapsed: 1¾ hours)

2. Switch on heat compensation windings S2MW, RAW, EBEW and EBCW. Turn up the power to around 1/3 of anticipated full load over the next 15 minutes. (Time elapsed: 2 hours)

3. Step up the compensation windings by 50 W or so every 25-30 minutes for about 2 hours since the superheaters were fully loaded. By now, the catalyst temperature should be in the range 400 - 420°C. Ensure all reactor temperatures are in the range 375 - 450°C (manufacturer's recommended range for air/steam switchover). (Time elapsed: 3¾ hours)

4. The system is ready for the air/steam switchover. The following stages have to be performed in rapid succession:-

   (i) shut off the globe valves on SL1 and SL2 at which the air enters the steam lines (this prevents any condensate from entering the rotameters).

(ii) drain condensate off the mains steam line and fully open the mains steam gate valves to lines SL1 and SL2.

(iii) shut solenoid valve SV1. Open solenoid valves SV2 and SV3 (remember SV2 is reverse acting).

(iv) gradually open downstream globe valves on lines SL1 and SL2 (downstream of the pressure regulator valves). Initially use the pressure gauges on SL1 and SL2 as a guide to the steam flow, as some condensate has to clear the lines and the 'cold' instruments and control devices. The required settings on the lines are:

Line SL1: P = 11 psig (1.75 bar), h_m = 9.5 cm Hg,
M = 7.0 kg/hr.

Line SL2: P = 7 psig (1.48 bar), h_m = 4.0 cm Hg,
M = 4.0 kg/hr.

Two or three minutes after the steam is brought on, the orifice meters can be used as a more accurate guide to the steam flowrate.

(v) divert the flow on the main condenser from the air exhaust line to the water drain.

(vi) Switch on the steam preheater windings SL1W and SL2W and turn up to 230 W and 115 W respectively. (Time elapsed: 4¼ hours)

5. Continue the step up of the compensation windings from around 20 minutes after the steam has come on, maintaining the rate of 50 W every 20 minutes, on EBCW and EBEW, whilst halving this rate on RAW and S2MW. The pressure regulator valves will hammer for 30 - 40 minutes after the steam/air switchover until the flows settle down.

The flowrates can be adjusted accurately using the orifice meters. (Time elapsed: 5 hours).

6. Cut down the power on SSH2 and EBSH as steady state is approached. The exit temperatures should be kept around 740 - 750°C on SSH2, and 500°C on EBSH.

7. The compensation windings EBCW, EBEW, RAW and S2MW should be up to their required loads around 2½ hours after the steam/air switchover. Cut down the power on SSH2 and EBSH as required. (Time elapsed: 6½ hours)

8. Around 11 hours after start-up, the reactor bed temperatures, as well as the shield temperatures should be pretty close to steady state. The bed temperature rise should not be greater than 5 Centigrade degrees every hour. The ethylbenzene vaporisation can now commence. (Time elapsed: 11 hours)

9. Open the pump section and delivery valves, as well as solenoid valve SV5 (EBReturn). Pressurise the ethylbenzene tank to at least 5 psig (1.34 bar) with nitrogen. Switch on pump at Mark 56. Turn on the ethylbenzene condenser to Mark 30. Switch on EBV and EBVI circuits and load them over the next 20 minutes to 550 W on EBV and 300 W on EBVI. (Time elapsed: 11½ hours)

10. Half an hour after the EBV and EBVI circuits were switched on, the ethylbenzene should be boiling around 140°C. About an hour later, the ethylbenzene should begin to superheat. Control EBVI and EBV to ensure around 10 - 15 Centigrade degrees of superheat. The settings above should produce an ethylbenzene vapour temperature of around 155 - 160°C. Once the temperature has stabilized, the reactor system is ready to perform runs in accordance with the procedures and require-

ments of Section 2.2. Before the runs can commence, clear all sampling tanks with nitrogen for 3 minutes or so. Flows can be diverted to these tanks by the use of the various 3-way valves positioned before each tank. (Time elapsed: 13 hours)

Note:- The time elapsed figures apply to an eventual catalyst temperature of 580 - 590°C.

A7.2 System Shut-Down Procedure

After the reaction runs have been completed, and steam is flowing through both lines SL1 and SL2, allow at least an hour for the "steaming" before commencing shut-down.

1. Start by gradually reducing power loads on ethylbenzene vaporiser circuits EBV and EBVI, and preheater windings SL1W and SL2W. A period of 10 minutes should be sufficient. Switch off SL1W, SL2W, EBVI and EBV circuits.

2. Simultaneously keep reducing power loads on the compensation circuits S2MW, RAW, EBEW and EBCW, and step these down over 15 minutes. Switch off S2MW, RAW, EBEW, EBCW circuits. (Time elapsed: 15 minutes)

3. Start step down of SSH1, SSH2 and EBSH superheater loads. Initially the step down is carried out the same rate as the step up, but when the power loads are about ½ of those at the start of the step down, the fall in the catalyst temperature has to be taken into account. In general, ensure that EBSH Out does not fall below 250°C before the system is ready for the steam/air switchover, and that SSH2 does not fall below 300°C. When all reactor temperatures are within the range 375 - 400°C, the system is ready for the switchover.

4. Ensure the air compressor is on. Divert flow at the top of the main condenser from the drain to the air exhaust line. (Time elapsed: 1½ hours)

5. The following steps should be carried out in rapid succession:-

   (i) open SV1, open both air rotameter on SL1 and SL2.

   (ii) shut steam control globe valves downstream of the pressure regulator valves on both SL1 and SL2.

   (iii) fully open the globe valves controlling the air entry to the steam lines on SL1 and SL2. Adjust the rotameters to the desired air flowrates as mentioned for the start-up. Shut solenoid valve SV2 (reverse acting). Shut gate valves for SL1 and SL2 on the mains steam lines.

6. Continue step down of the superheaters SSH1, SSH2 and EBSH 5 - 10 minutes from the steam/air switchover at the rate of around 50 Watts every 2 - 3 minutes. Switch off SSH1, SSH2 and EBSH circuits when step down is completed. (Time elapsed: 2¼ hours)

7. Switch off the pump. Close SV5. Close pump suction and delivery line globe valves. Shut off nitrogen supply. Keep air running for ½ hour to allow system to cool to temperatures of less than 250^{o}C. Shut off air rotameters and solenoid valve SV1. Turn off water to the main and ethylbenzene condensers. Switch off the Kent Recorder and the solenoid valve transformer circuits. The mains switch directly cuts off the power to the extractor fans. (Time elapsed: 2¾ hours)

APPENDIX A8

GAS AND LIQUID CHROMATOGRAPHY SYSTEMS, AND THE RESULTS OF SAMPLE ANALYSIS

APPENDIX A8

GAS AND LIQUID CHROMATOGRAPHY SYSTEMS, AND THE RESULTS OF SAMPLE ANALYSIS

A8.1 Gas and Liquid Chromatography Systems

A8.1.1 Liquid chromatography

Spencer[90] compared various packings and columns for the separation of ethylbenzene from o-m-p xylenes, and Clough[88,89] utilized these packings for the ethylbenzene-styrene separation. The following particular column was found to be the most reliable, giving well separated peaks (see Figure A8.1) within a reasonable analysis time of 8 minutes.

Column packing	:	Apiezon-L on Celite-545
Column length	:	¼" O.D. (0.64 cm) SS316 of 2 metre length
Column temperature	:	120°C
Carrier gas	:	Helium at 30 - 40 ml/min
Detector	:	Katharometer
Detector temperature	:	120°C
Sample volume	:	1 µl minimum

Elution order of peaks

(i) Benzene after 1.8 minutes
(ii), Toluene after 3.1 minutes
(iii) Ethylbenzene after 5.3 minutes
(iv) Styrene after 6.8 minutes.

A8.1.2 Gas chromatography

No problems were encountered in separating the gases. However, the water vapour peak interfered with the carbon monoxide peak, and therefore

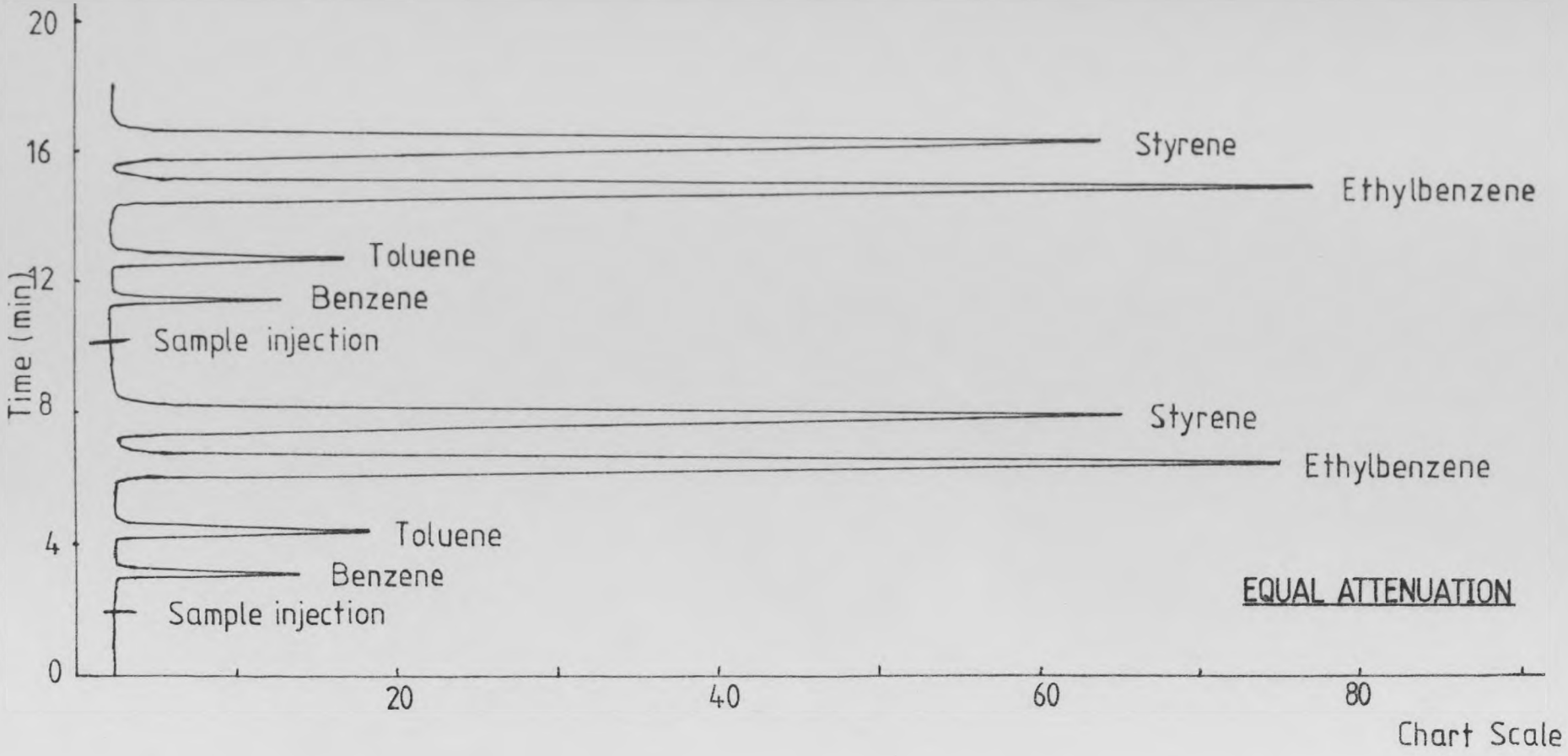

FIGURE A8.1: Liquid Chromatography Component Separation

a molecular sieve was used to separate the two. The sieve also separated the oxygen and nitrogen peaks, though this is not crucial for this separation. Figure A8.2 shows the column separation, followed by the sieve separation.

Column packing	:	Porapak Q, 80 - 100 mesh
Column dimensions	:	¼" O.D. (0.64 cm), SS316, 2 metres long
Sample size	:	10 ml minimum
Sieve	:	Molecular sieve 5A
Sieve column dimensions	:	¼" O.D. (0.64 cm), SS316, 1.5 metres long
Carrier gas	:	Helium at 30 ml/min
Column temperature	:	90°C

Elution order of peaks

(a) Porapak Q packing

(i)	Hydrogen	after 1.0 minutes
(ii)	Air (nitrogen and oxygen)	after 3.2 minutes
(iii)	Methane	after 3.7 minutes
(iv)	Carbon Dioxide	after 5.0 minutes
(v)	Ethylene	after 7.1 minutes
(vi)	Ethane	after 9.2 minutes
(vii)	Carbon Monoxide and water vapour	after 15.2 minutes

(b) Molecular Sieve 5A

(i)	Hydrogen	after 0.9 minutes
(ii)	Oxygen	after 2.0 minutes
(iii)	Nitrogen	after 4.8 minutes
(iv)	Methane	after 7.4 minutes
(v)	Carbon Monoxide	after 14.8 minutes

Total separation time:- 40 minutes.

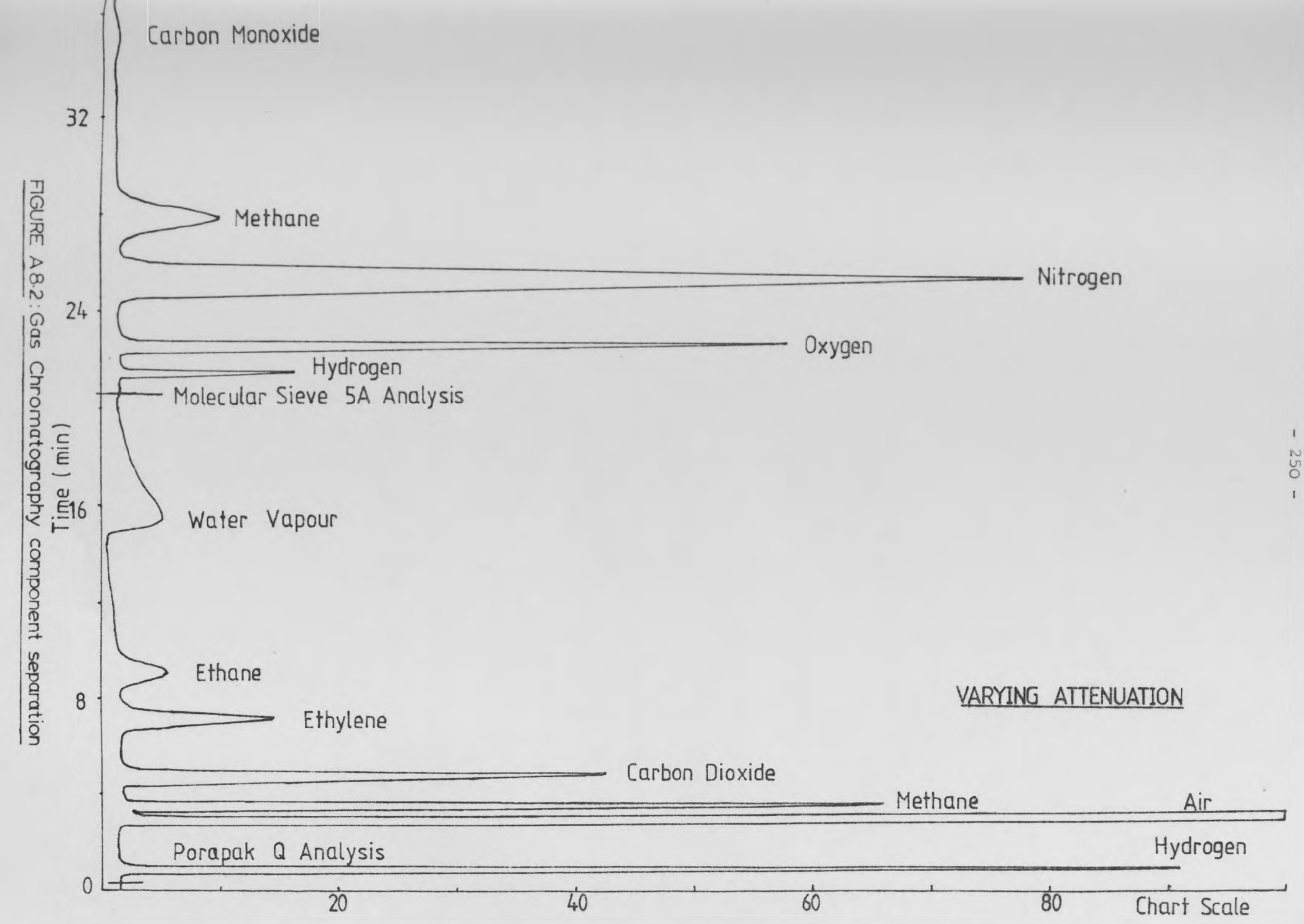

FIGURE A8.2: Gas Chromatography component separation

A8.2: Results of Liquid and Gas Sample Analysis

TABLE A8.1

Liquid Sample Analysis Results

Run No.	Experiment Type	Sample Number	Sampling Time	Benzene (mole %)	Toluene (mole %)	Ethylbenzene (mole %)	Styrene (mole %)	Conversion (%)	Efficiency (%)
50	Transient	50-1-1	Composite - 2 min	7.14	0.82	58.26	33.78	34.1	82.8
50	Transient	50-2-1	Composite - 7 min	4.24	4.15	41.16	50.44	50.9	87.0
53	Transient	53-1-1	Composite - 3 min	4.32	4.99	43.00	47.68	48.1	85.0
53	Transient	53-2-1	Composite - 3 min	3.81	4.80	48.79	42.60	43.0	84.7
53	Transient	53-3-1	Composite - 3 min	4.41	5.59	51.04	39.96	39.3	81.1
53	Transient	53-4-1	Composite - 1 min	4.01	5.88	51.42	39.69	39.0	81.1
53	Transient	53-5-1	Composite - 2 min	4.26	5.97	57.87	31.90	32.2	77.8
53	Transient	53-6-1	Composite - 3 min	5.24	6.69	57.05	31.02	31.3	73.8
53	Steady State	53-7-1	7 min 45 sec	3.31	5.65	53.04	37.99	38.3	82.5
53	Steady State	53-7-2	10 min 45 sec	3.31	5.59	51.99	39.11	39.5	83.0
53	Steady State	53-7-3	16 min 20 sec	3.59	5.10	50.93	39.79	40.2	82.6
53	Steady State	53-7-4	23 min 25 sec	4.29	6.11	49.06	40.55	40.9	81.0
53	Steady State	53-7-MC	Mean Composite	3.92	6.01	50.41	39.65	40.0	81.4
53	Steady State	53-8-1	7 min 45 sec	2.19	4.18	58.29	35.34	35.7	86.6
53	Steady State	53-8-2	10 min 45 sec	1.88	3.65	60.76	33.72	34.0	87.9
53	Steady State	53-8-3	16 min 20 sec	1.71	3.31	62.12	32.86	33.2	88.8
53	Steady State	53-8-4	23 min 25 sec	1.64	3.08	62.38	33.90	33.2	89.6

continued .....

Run No.	Experiment Type	Sample Number	Sampling Time	Benzene (mole %)	Toluene (mole %)	Ethylbenzene (mole %)	Styrene (mole %)	Conversion (%)	Efficiency (%)
53	Steady State	53-8-5	29 min 30 sec	1.72	3.02	62.15	33.01	33.3	89.6
53	Steady State	53-8-MC	Mean Composite	1.78	3.60	60.81	33.81	34.1	88.3
55	Transient	55-1-1	Composite - 2 min	9.95	8.57	41.44	40.04	40.4	69.4
55	Transient	55-2-1	Composite - 2 min	3.93	6.06	54.57	35.45	35.8	79.6
55	Steady State	55-3-1	4 min 15 sec	2.61	5.90	51.26	40.24	40.6	84.1
55	Steady State	55-3-2	6 min 30 sec	2.57	5.34	52.44	39.65	40.0	85.0
55	Steady State	55-3-3	7 min 45 sec	2.48	5.18	52.76	39.58	39.9	85.4
55	Steady State	55-3-4	10 min 45 sec	3.13	5.89	49.29	42.00	42.4	83.8
55	Steady State	55-3-5	16 min 20 sec	3.88	5.84	47.13	43.15	43.5	83.0
55	Steady State	55-3-6	20 min 05 sec	4.51	6.10	45.81	43.58	44.0	81.8
55	Steady State	55-3-MC	Mean Composite	3.54	5.73	49.82	40.91	41.3	83.0
55	Steady State	55-4-1	3 min 00 sec	4.30	8.34	33.39	53.98	54.5	82.1
55	Steady State	55-4-2	4 min 15 sec	3.31	7.46	38.63	50.60	51.1	83.7
55	Steady State	55-4-3	6 min 30 sec	3.55	6.49	43.36	46.61	47.0	83.6
55	Steady State	55-4-4	7 min 45 sec	3.31	5.97	44.85	45.87	46.3	84.5
55	Steady State	55-4-5	10 min 45 sec	5.21	7.33	37.08	50.38	50.8	72.9
55	Steady State	55-4-6	16 min 20 sec	4.73	6.19	43.11	45.96	46.4	82.1

continued .....

TABLE A8.1 (continued)

Liquid Sample Analysis Results

Run No.	Experiment Type	Sample Number	Sampling Time	Benzene (mole %)	Toluene (mole %)	Ethylbenzene (mole %)	Styrene (mole %)	Conversion (%)	Efficiency (%)
55	Steady State	55-4-7	20 min 05 sec	5.20	6.08	44.26	44.46	44.9	81.1
55	Steady State	55-4-8	23 min 25 sec	4.07	4.82	51.17	39.94	40.3	83.3
55	Steady State	55-4-9	29 min 30 sec	3.82	4.21	54.25	37.73	38.1	84.9
55	Steady State	55-4-10	34 min 00 sec	3.31	3.58	57.16	35.95	36.3	85.7
55	Steady State	55-4-11	40 min 00 sec	3.31	3.28	58.79	34.61	34.9	85.9
55	Steady State	55-4-12	50 min 00 sec	2.85	2.86	61.45	32.84	33.1	87.2
55	Steady State	55-4-MC	Mean Composite	3.71	4.23	54.8	37.26	37.6	84.1

Ethylbenzene Feed Analysis

Ethylbenzene	99.11 mole %
o-m-p xylenes	0.50 mole %
Toluene	0.32 mole %
Benzene	0.07 mole %

TABLE A8.2

Gas Sample Analysis Results

Run No.	Experiment Type	Sample Number	Sampling Time	Hydrogen (mole %)	Methane (mole %)	Ethane (mole %)	Ethylene (mole %)	Carbon Monoxide (mole %)	Carbon Dioxide (mole %)
53	Steady State	53-7-G	19 min	99.06	0.62	0.06	0.16	0.02	0.08
53	Steady State	53-8-G	19 min	99.48	0.39	0.01	0.03	0.02	0.07
55	Steady State	55-3-G	20 min	99.00	0.65	0.07	0.21	-	0.08
55	Steady State	55-4-G1	16 min	98.91	0.76	0.05	0.22	-	0.14
55	Steady State	55-4-G2	22 min	98.81	0.73	0.08	0.26	-	0.12
55	Steady State	55-4-G3	50 min	98.48	0.83	0.10	0.32	-	0.27
55	Steady State	55-4-G4	54 min	98.61	0.77	0.09	0.24	-	0.27

APPENDIX A9

PAPER BY COCKCROFT, AS A SUMMARY OF HIS WORK

A THERMAL REGENERATIVE CATALYTIC REACTOR SYSTEM FOR THE DEHYDROGENATION OF ETHYLBENZENE TO STYRENE

P.J.Heggs[1]
C.S.Cockcroft[2]

1. University of Leeds, Leeds, LS2 9JT., U.K.
2. Simsci, Simulation Science Inc., Regent House, Heaton Lane, Stockport, SK4 1BS.

ABSTRACT

This paper discusses the use of thermal regenerators as catalytic fixed bed reactors and investigates the possible design variables for the dehydrogenation of ethylbenzene to styrene. The values of the design variables are predicted by a simplified design approach and then used in a detailed mathematical model of the regenerative-catalytic-reactor system. The latter calculations validate the excellent predictions of the proposed simple method. In addition, the regenerative-catalytic-reactor system is predicted to produce higher conversions to styrene at better efficiences than the normally employed two stage adiabatic reactor system.

INTRODUCTION

A previous paper by the authors[1] described the use of thermal regenerators as catalytic fixed bed reactors. These systems appear to have distinct advantages over existing commercial reactor arrangements for reversible catalytic reactions. However, the regenerative-catalytic-reactor (RCR) system operates in a cyclic mode, whereby the reactor alternately experiences reaction and then is either heated or cooled to regenerate favourable temperature conditions. The operation during reaction and regeneration is transient. The catalyst support material is used either as a heat sink or source depending upon the thermicity of the reaction. A suitable heat transfer medium must be employed during the regeneration stroke, because process

stream contamination will occur at the switch-over between the two strokes. In addition, for continuous operation, two reactor beds are necessary. This paper extends the initial suggestions of the authors and presents a detailed investigation of the RCR system for the dehydrogenation of ethylbenzene to styrene.

MATHEMATICAL MODEL OF THE RCR

It has been shown that the pseudohomogeneous representation of transient adiabatic reactors and heat transfer in packed beds is invalid[2]. Gavalas[3,4] has used this assumption when considering thermal regenerators for the exothermic catalytic-oxidation of hydrocarbons. However, he did not present how the RCR could be designed from scratch. A heterogeneous film resistance representation[2] is used in this work and includes the following assumptions; plug flow, no intra-transfer effects, no axial dispersion, ideal gas behaviour, constant physical properties and adiabatic reactor walls.

The reactor mass and heat balances for the fluid phase are

$$\frac{\partial c_i}{\partial t} = -\frac{G}{\rho_g e}\frac{\partial c_i}{\partial z} - \frac{S_v k_g}{e}(c_i - c_{si}) \qquad (1)$$

$$\frac{\partial T}{\partial t} = -\frac{G\partial T}{\rho_g e \partial z} - \frac{S_v h}{e\rho_g C_{pg}}(T - T_s) \qquad (2)$$

and for the solid phase are

$$\frac{\partial c_{si}}{\partial t} = \frac{S_v k_g}{(1-e)e_p}(c_i - c_{si}) + \frac{\rho_s}{e_p}\sum_j a_{i,j} r_j \qquad (3)$$

$$\frac{\partial T_s}{\partial t} = \frac{S_v h}{(1-e)\rho_s C_{ps}}(T - T_s) - \frac{1}{C_{ps}}\sum_j \Delta H_j r_j \qquad (4)$$

where r_j is the rate of the j^{th} reaction and $a_{i,j}$ is the stoichiometric coefficient of the i^{th} component in the j^{th} reaction (negative for reactants and positive for products).

The regenerator heat balances for the fluid and solid phases are respectively

$$\frac{\partial \bar{T}}{\partial t} = -\frac{\bar{G}}{\bar{\rho}_g e}\frac{\partial \bar{T}}{\partial z} - \frac{S_v \bar{h}}{\bar{e}\bar{\rho}_g \bar{C}_{pg}}(\bar{T} - \bar{T}_s) \qquad (5)$$

$$\frac{\partial \bar{T}_s}{\partial t} = \frac{S_v \bar{h}}{(1-e)\rho_s C_{ps}}(\bar{T} - \bar{T}_s) \qquad (6)$$

The parameters with the bar are particular to the regenerator and need not have the same value as the corresponding reactor parameters. The reactor and regenerator strokes are coupled by the boundary conditions representing the periodic switching operation of the RCR.

For the reactor stroke, the boundary conditions are

$$T = T_o \quad c_i = c_{is} \quad \text{at} \quad z = 0 \quad \text{for} \quad n\tau < t < n\tau + t_1 \qquad (7)$$

and for the regenerator stroke is

$$\bar{T} = \bar{T}_o \quad \text{at} \quad z = 0 \text{ or } z = Z \quad \text{for} \quad n\tau + t_1 < t < (n+1)\tau \qquad (8)$$

where τ is a total cycle comprising the reactor stroke duration, t_1, and the regenerator stroke duration, t_2, and n represents a large number of cycles. A cyclic steady state will be achieved after a number of cycles has passed and this is mathematically defined as follows:

$$T_s = f(z) \quad \text{for} \quad 0 < z < Z \quad \text{at} \quad n\tau \text{ and } (n+1)\tau \qquad (9)$$

The solution for the equations (1) to (9) has been obtained by numerically using backward and central difference approximations for the time and length derivatives respectively. The stability and convergence of the numerical solution were substantiated in an earlier paper[2].

DESIGN VARIABLES FOR THE RCR SYSTEM

In addition to the reactor space time, i.e. catalyst volume and flowrate, the formulation of the mathematical model provides the extra design variables for a RCR system.

1. Cycle time

The cycle time is the major design variable. Each stroke is of identical duration, $t_1 = t_2$, if only two vessels are employed. The reactor stroke duration must be long enough for practical purposes, but short enough so that the average conversion is considerably greater than steady state conversion. On the other hand, the regenerator stroke duration must be long enough so that the favourable temperature conditions within the reactor are regenerated.

2. Catalyst Temperature for the Reactor Stroke

The cyclic steady state condition equation (9) represents the initial catalyst temperature for the reactor stroke and this profile is critical because of the transients that follow. For an endothermic reaction, it should be the optimum temperature profile for maximum conversion, whereas for an exothermic reaction, it must result in the optimum temperature profile occurring at the end of the reactor stroke.

3. Regeneration flowrate

The regeneration flowrate must be great enough so that sufficient heat is carried into or out of the catalyst bed, so that the favour-

able temperature conditions are restored for the following reactor stroke.

4. Inlet temperatures for each stroke

The inlet reactant and heat transfer medium temperatures must be determined, so that the temperature levels do not exceed the maximum permitted catalyst temperatures either during reaction or regeneration.

To search for the best combination of all these variables for any reaction system using the mathematical model equations (1) to (9) would be a monumental task, if at all possible. Thus a simpler approach is proposed whereby the total system is decoupled and the reactor and heat transfer regenerator are considered separately.

SIMPLIFIED DESIGN APPROACH FOR AN ENDOTHERMIC REACTION

The reactor is considered in the steady state, where the optimum reactor temperature profile for endothermic reversible system is isothermal at the maximum operating catalyst temperature. Hence the volume of catalyst required for a given conversion c_{if} at this profile with the reactants entering at the same level is simply given by

$$V(1 - e) = F\int_{c_{is}}^{c_{if}} \frac{dc_i}{r_i} \qquad (10)$$

where V is the reactor volume and F is the flowrate. The rate of fall of the catalyst support temperature depends upon its heat capacity and the endothermic heat of reaction. If the heat of reaction is uniformly distributed along the reactor, the maximum rate is given by

$$\delta T = \frac{F(c_{if} - c_{io})\,\Delta H}{V(1 - e)\,\rho_s C_{ps}} \qquad (11)$$

where ΔH is the reaction heat. The time t_1, taken for a specified fall in catalyst support temperature is obtained directly from equation (11) and the conversion at this lower temperature level evaluated by equation (10). The average conversion over the time interval represents the predicted process value.

For a two bed system this time is also the time for the regeneration. Assuming that the temperature profile is isothermal at the end of the reaction stroke and that the fluid-to-particle heat transfer coefficient is very large, the fluid mass velocity, $\bar{G}$, required to regenerate the optimum reactor temperature profile is

$$G = \frac{(1 - e)\,\rho_s C_{ps} Z}{\bar{C}_{pg} t_1} \qquad (12)$$

Excessive temperature levels in the catalyst are avoided by assuming the inlet temperature is fixed at the maximum catalyst value and this is included in equation (12).

Hence this simplified approach provides estimates of all the design variables of a RCR system for an endothermic catalytic reaction.

THE DEHYDROGENATION REACTION

The catalytic dehydrogenation of ethylbenzene

$$C_6H_5CH_2 - CH_3 \rightleftharpoons C_6H_5CH = CH_2 + H_2 \qquad (13)$$

is the major commercial process used for the production of styrene[5]. The overall process has been described by several authors[6-19] and considerable utility savings can be made by improved reactor performance[10]. High performance plants[8] presently employ two adiabatic reactors in series with interstage heating as illustrated in Figure 1.

The reaction is reversible, endothermic and accompanied by an increase in volume. Hence a high equilibrium conversion is favoured by a high reaction temperature and a low ethylbenzene partial pressure. A large number of possible side-reactions have been proposed[11,12], but the important ethylbenzene side-reactions are those producing benzene and toluene

$$C_6H_5C_2H_5 \rightarrow C_6H_6 + C_2H_4 \qquad (14)$$

$$C_6H_5C_2H_5 + H_2 \rightarrow C_6H_5CH_3 + CH_4 \qquad (15)$$

Steam is used as a diluent which produces a low ethylbenzene partial pressure without the expensive use of vacuum operation[5],[13]. The steam to ethylbenzene molar ratio (SR) is typically 12-20, and the steam cleanses the iron oxide of any carbon depositation. The overall molar efficiency of styrene produced to ethylbenzene consumed can be as high as 94%[5], and the molar conversion to styrene per pass of ethylbenzene can reach 63%.

Hence the RCR system must provide a higher conversion, than the two stage adiabatic system. A direct comparison between these two systems is used in the following sections.

The two staged adiabatic system shown in Figure 1 has been simulated by a heterogeneous steady state model, i.e. equations (1) to (6) with the time derivative set to zero. The kinetics used in the numerical solution are as follows:

$$r_1 = k_1 \left(p_{EB} - p_{ST} p_H / K_p \right) / (\alpha + p_{EB} + \beta p_{ST}) \qquad (16)$$

$$r_i = k_i p_H^{i-2} p_{EB} / (\alpha + p_{EB} + \beta p_{ST}) \qquad (17)$$

where $i = 2,3$

$$k_i = 3.032 \times 10^6 \exp(-23050/T) \qquad (18)$$

$$K_p = \exp(16.12 - 15350/T) \qquad (19)$$

$$k_2 = 3.401 \times 10^3 \exp(-20336/T) \qquad (20)$$

and

$$k_3 = 6.679 \times 10^4 \exp(-18820/T) \qquad (21)$$

This set of kinetics for the reactions (13), (14) and (15) were obtained by fitting the experimental data of Bogdanova et al[14] by the Langmuir-Hinshelwood[15] model. The equations were compared[16] with other literature cited kinetics[11,17,18,19,20], and found to give both conversion and efficiency values within reported ranges for all combinations of system parameters.

In industrial processes the first reactor normally gives a 40% styrene conversion and this has been used as a basis for the reactor sizing. The data used in the simulation is listed in Table 1. The inlet temperature of 650°C is the maximum operating temperature of the iron oxide catalyst and a reactor depth of 0.204 m provided the required 40% conversion. Industrial processes do not allow the inlet temperature to the second reactor to exceed 630°C, thus avoiding excessive pyrolysis. The simulation was continued with the temperature increased to 630°C, and the overall conversion was 63.9% with an efficiency of 85.7% for a second reactor of the same depth. This low efficiency is caused by the relatively high pressure in the first reactor. A pressure drop of 0.8 bar was allowed in the first reactor, and assuming 0.7 bar drop in the interstage heater, gives an inlet pressure of 1.6 bar into the second reactor.

THE RCR SYSTEM

The RCR system is assumed to comprise two reactor beds of identical proportions to those of the two staged adiabatic system. The heat transfer medium will be super-heated steam which avoids contamination difficulties. A simple RCR configuration for countercurrent flow is shown in Figure 2. Bed A operates as the reactor, while bed B is being regenerated. The two 4-way valves are switched simultaneously, thus reversing the roles of the beds. It is anticipated that the regenerative steam flow would be ultimately used as the diluent for the reaction. However, as yet the flowrate and temperature are unknown.

Simplified Design Approach

Values of the design variables are obtained from the simplified design approach. The inlet reactant and regenerative steam temperatures are maintained at 650^{o}C to avoid exceeding the maximum catalyst temperature and catalyst temperature profile at the beginning of the reactor stroke is isothermal at 650^{o}C

The rate of temperature fall in the reactor is given by equation (11), and the conversions and rates for various isothermal temperatures are given in Table 2. As expected the maximum rate occurs at the highest catalyst temperature. For a 20^{o}C temperature drop during the reactor stroke, the average conversion will be 68% at an average rate of fall of 0.346^{o}Cs^{-1}. Hence the allowable stroke duration is approximately 58s, which will be extended to 60s to be more practical.

The regenerative steam flowrate is found from equation (12), and for a 60s stroke is 1.672 kg m^{-2}s^{-1}. This is approximately 7 times the required diluent steam flow using a molar steam to ethylbenzene

ratio of 14.0.

Thus the values of the design variables are listed in Table 3 and these are used in conjunction with the values in Table 1 in the full simulation using equations (1) to (9). For the RCR system the reactants must only pass through one bed and so the inlet pressure is taken to be 1.6 bar.

Simulation of the RCR

The cyclic steady state operation was assumed, when the reactor conversion and the outlet temperatures from both beds varied by less than 0.5 x 10^{-4} at the ends of successive cycles. This was achieved after only 3 cycles starting from isothermal beds at 650^{o}C. An average conversion of 67.7% is achieved at an efficiency of 88.6%. Hence not only does the RCR produce a higher conversion, but also an increased efficiency. The latter is caused by the overall lower pressure level in the reactor.

The conversion and temperature profiles along the reactor at the end of each successive stroke are shown in Figure 3. Few cycles are required because saturation is closely approached during the regeneration stroke. Thus the simple design approach provides excellent estimates of the RCR variables for use in the full simulation. This was also verified for a longer stroke duration of 90s, when the simple approach predicted a conversion of 65% and a steam flowrate of 1.033 kgm^{-2}s^{-1}, and the full simulation gave a conversion of 65.3%.

Discussion

The agreement between the simple design approach and the full simulation is not fortuitous. The transients in the RCE system can be controlled by the judicious choice of the parameter values

Table 1 - Reactor data used in the calculations.

C_{pg}	-	2.417	kJ $kg^{-1}K^{-1}$
ϱ_g	-	5.359×10^{-1}	kg m^{-3}
C_{ps}	-	1.047	kJ $kg^{-1}K^{-1}$
ϱ_s	-	1.750×10^{3}	kg m^{-3}
e, e_p	-	0.4	
S_v	-	1240	m^2 m^{-3}
h	-	265.4	W $m^{-2}K^{-1}$
k_g	-	0.1182	m s^{-1}
G	-	0.339	kg $m^{-2}s$
P	-	3.1	bar
SR	-	14.0	
ΔH_1	-	124972	kJ $kmol^{-1}$
ΔH_2	-	101481	kJ $kmol^{-1}$
ΔH_3	-	-65354	kJ $kmol^{-1}$
C_{EBo}	-	0.0015	kmol m^{-3}
α	-	0.093	bar
β	-	8.03	
T_o	-	650	^oC

Table 2 - Steady state conversion and rate of temperature fall at various isothermal temperatures.

Isothermal Temperature (^oC)	Conversion (%)	Temperature fall (Ks^{-1})
650	72.0	0.368
640	67.8	0.348
630	63.1	0.324
620	57.9	0.298

Table 3 - Values of the Design Variables for the RCR.

Inlet temperatures, T_o and T_o	- 650^oC
Stroke durations, t_1 and t_2	- 60s
Steam Flow, G	- 1.672 kg $m^{-2}s^{-1}$
Regenerated Catalyst Temperature T_s	- 650^oC

Figure Captions

Figure 1 - Two stage adiabatic reactor system.

Figure 2 - Schematic RCR system.

Figure 3 - Concentration and temperature profiles at the end of successive strokes.

Figure 4 - Reactor Conversion Profiles.

Figure 5 - Reactor Temperature Profiles.

Figure 6 - Reactor Outlet Conversion and Temperature Profiles.

Figure 7 - Regenerative Temperature Profiles.

Figure 8 - Regenerative Outlet Temperature Profiles.

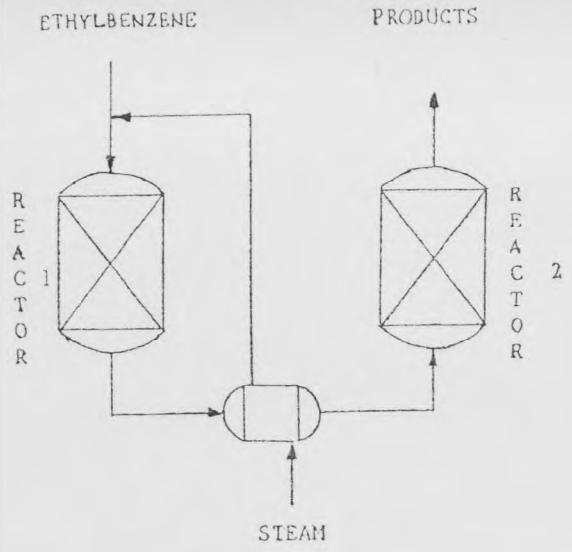

FIGURE 1

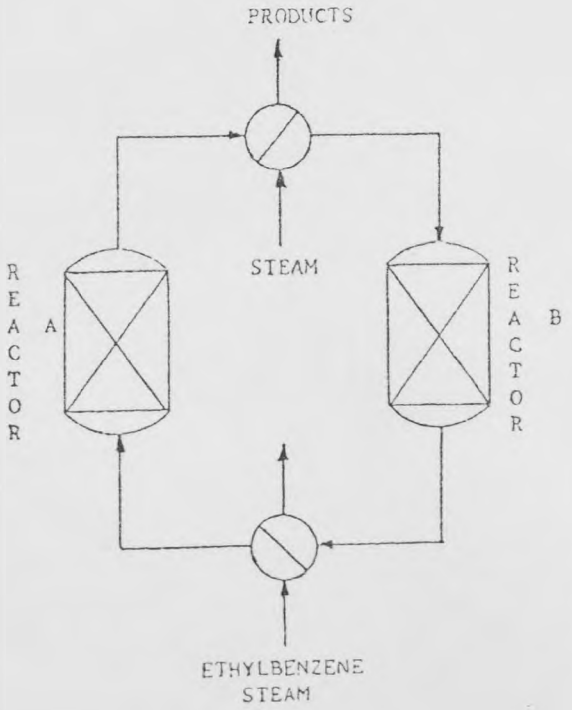

FIGURE 2

and the inherent characteristics of the cyclic mode of operation.

The simple approach assumes that the reactor temperature profile is initially isothermal and that the catalyst support can adequately store the heat of reaction so that a practical cycle time can be maintained. This cycle time should also result in a higher conversion than the steady state adiabatic system. The transients for the RCR system listed in Tables 1 and 3 clearly illustrate how well the assumptions employed in the simple approach are substantiated by the full simulation.

The transient reactor conversion and temperature profiles over the 60s stroke are shown in Figures 4 and 5 respectively. Also included are the corresponding profiles for isothermal and steady state adiabatic conditions. The initial RCR profiles almost coincide with the isothermal profiles and, although they fall as the stoke proceeds, the lower limiting profiles of the adiabatic conditions are not reached after 60s. The temperature level always favours high conversions, because the reactants ultimately experience a rising temperature profile. However the temperature does fall in the entrance region of the reactor, and this follows the adiabatic profile. Thus if the stroke was continued beyond 60s, the adiabatic conditions would eventually be reached.

The variation of the outlet temperature and conversion over the 60s stroke are shown in Figure 6. The response of the conversion is almost linear over the stroke. However, the temperature begins to fall quite steeply at the end of the stroke. The conversion starts at 71.2% and falls to 61.4% with an average of 67.7%. The temperature drops from 650^{o}C down to 642.3^{o}C with an average of 646.7^{o}C. The initial conversion compares well with isothermal value in Table 2 of 72%. However, at the end of the stroke the

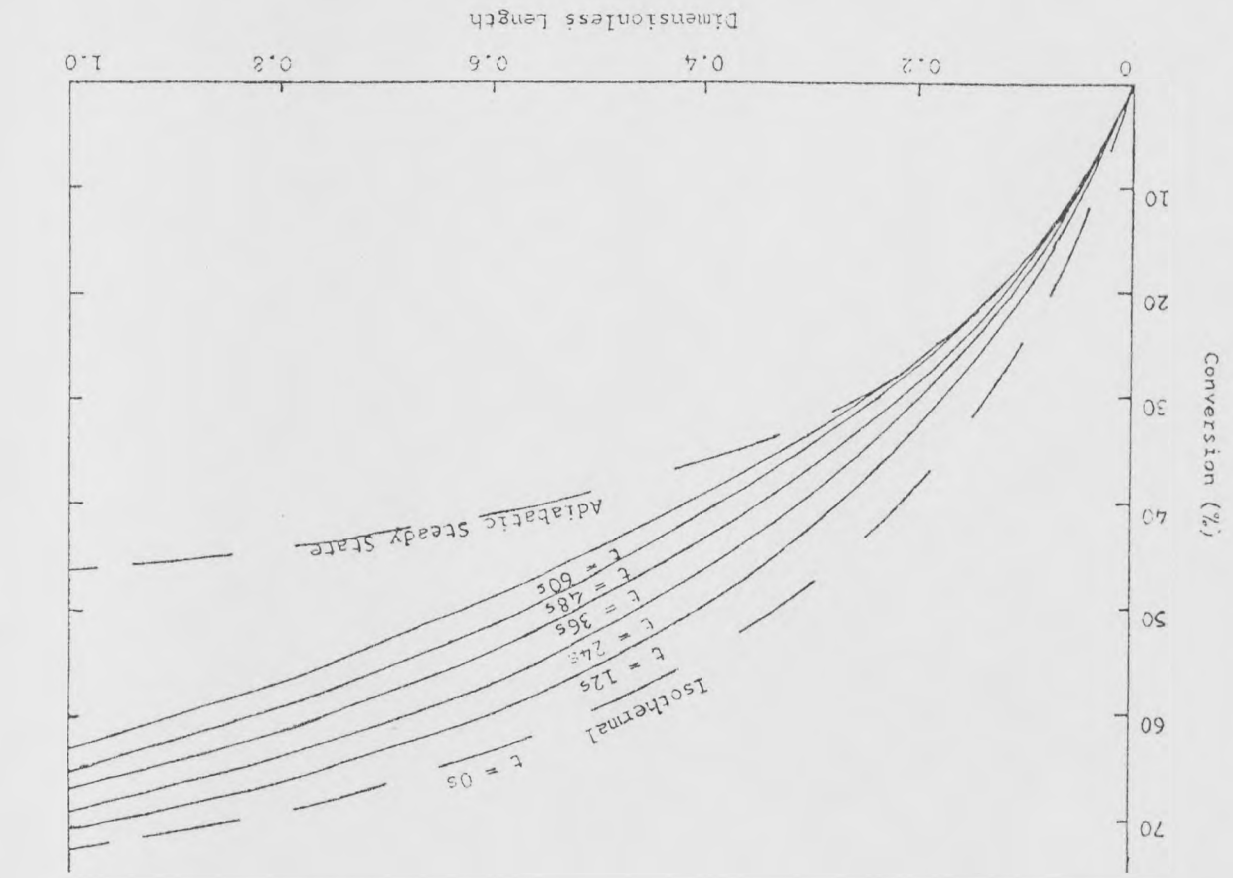

FIGURE 4

-16-

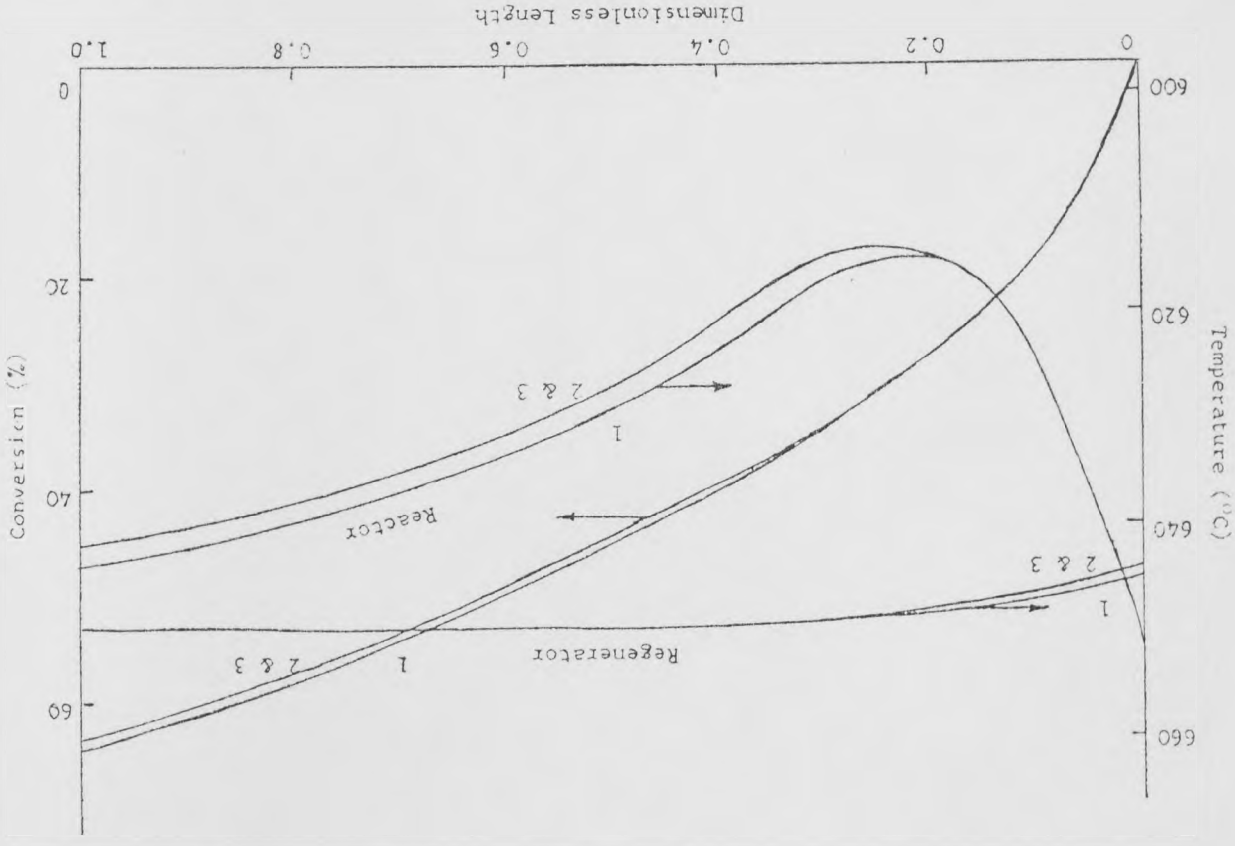

FIGURE 3

-15-

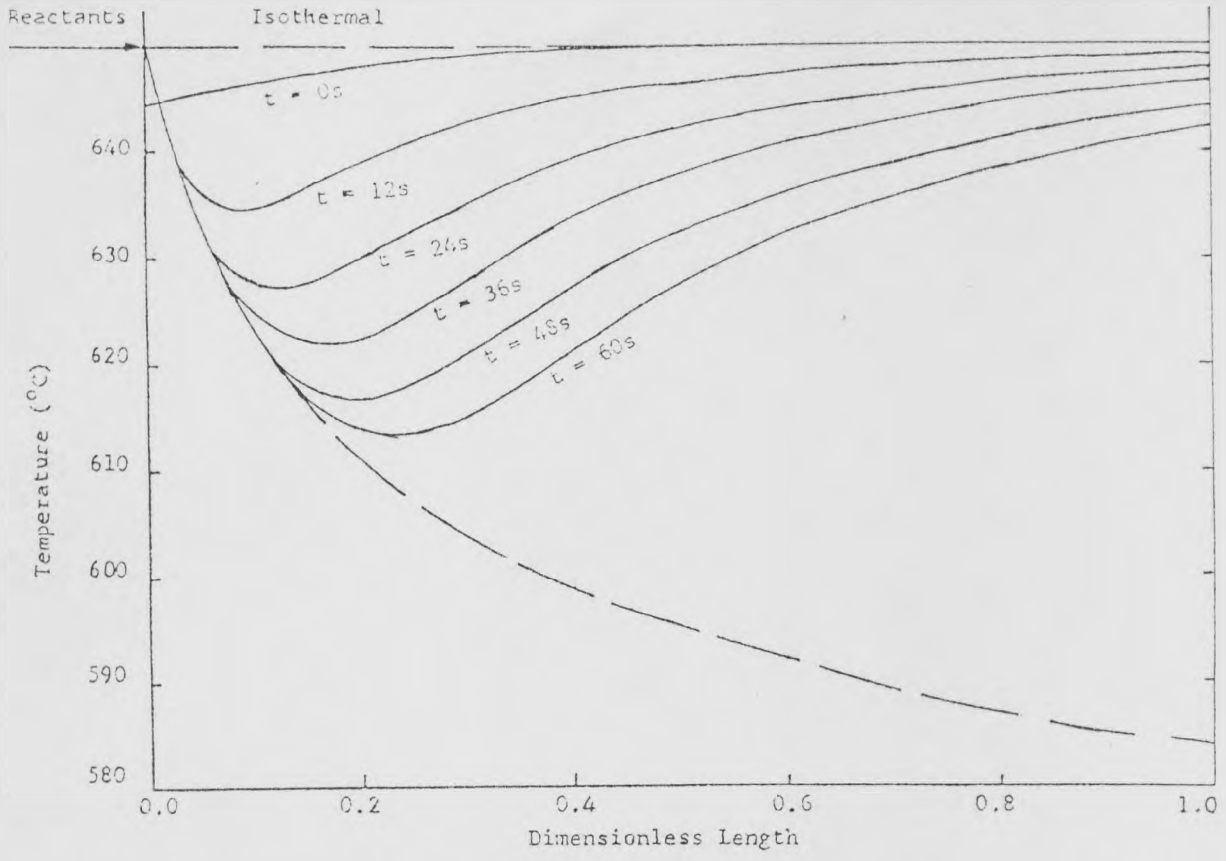

FIGURE 5

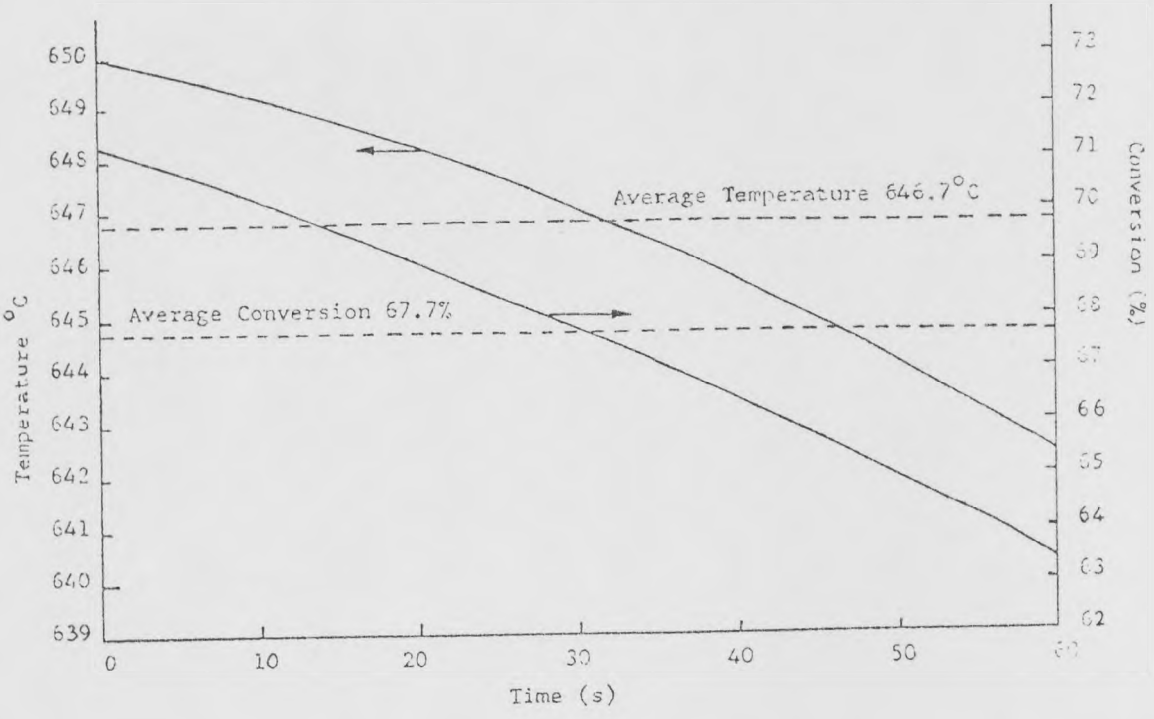

FIGURE 6

conversion is less than that used in the simplified approach of 63%, because the temperature profile is now no longer close to the isothermal value of 630°C. The increasing profile in the latter part of the reactor results in a reasonable conversion nevertheless. Thus, the longer the stroke duration, the RCR moves further away from isothermal conditions.

The temperature profiles during the regeneration stroke are illustrated in Figure 7. The countercurrent flow of steam entering at 650°C adequately regenerates the non-isothermal profile after the reactor stroke almost to an isothermal profile at 650°C. The slight fall in the temperature near the entrance is not crucial, because the reactants during the next stroke enter at 650°C and maintain the required temperature level of 650°C. The variation of the outlet temperature is shown in Figure 8 and reflects the shape of the final reactor profile. There is a distinct minimum in the response at 617°C and the average outlet temperature is 630°C

The full simulation can now be used to investigate the RCR system for the effects of parameter variation. However, shortage of space prevents including this study here. The simulation has been used to define the configuration of a practical RCR system for the dehyrogenation of ethylbenzene, and pilot plant studies are presently being carried out at Leeds University.

CONCLUSIONS

A mathematical model is developed and solved for a regenerative-catalytic-reactor (RCR) system for the dehydrogenation of ethylbenzene to styrene. A simplified design approach is proposed which allows prediction of the design variables. In addition to the reactor space time, the RCR system requires values for the cycle time, the initial catalyst temperature profile, the regeneration flowrate and

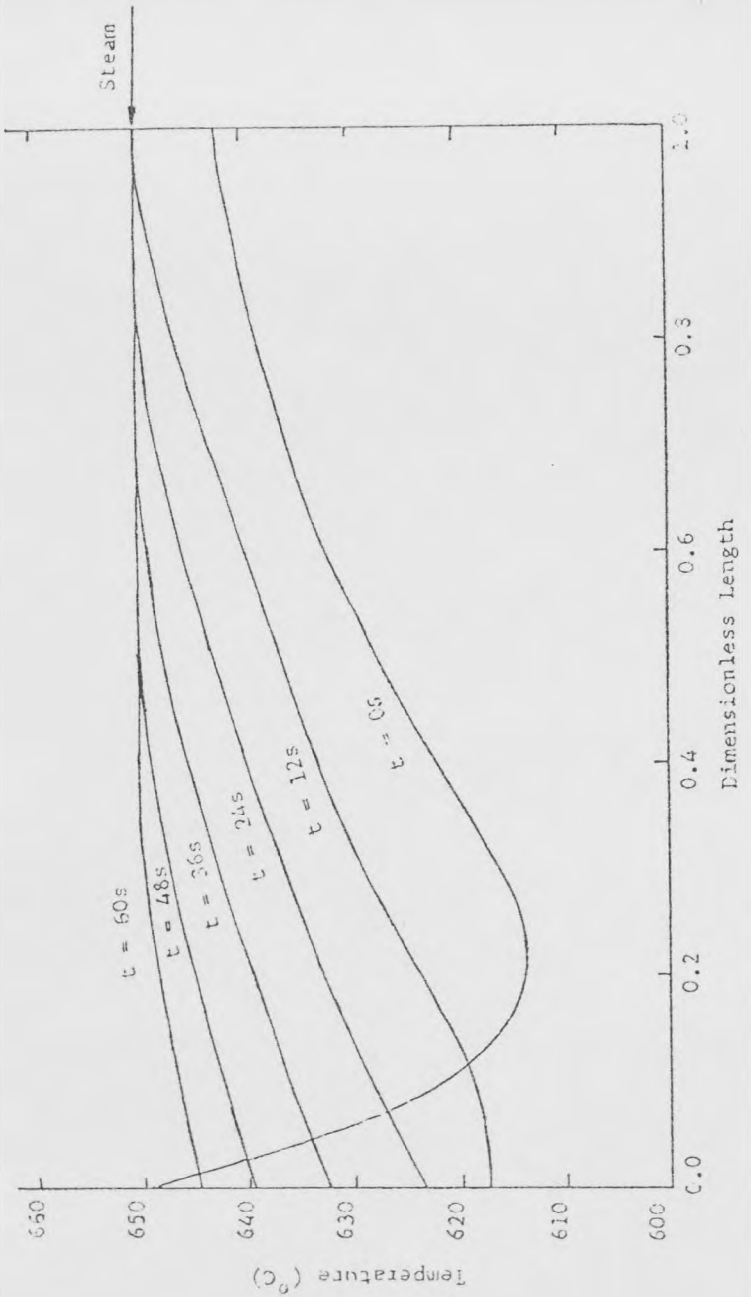

FIGURE 7

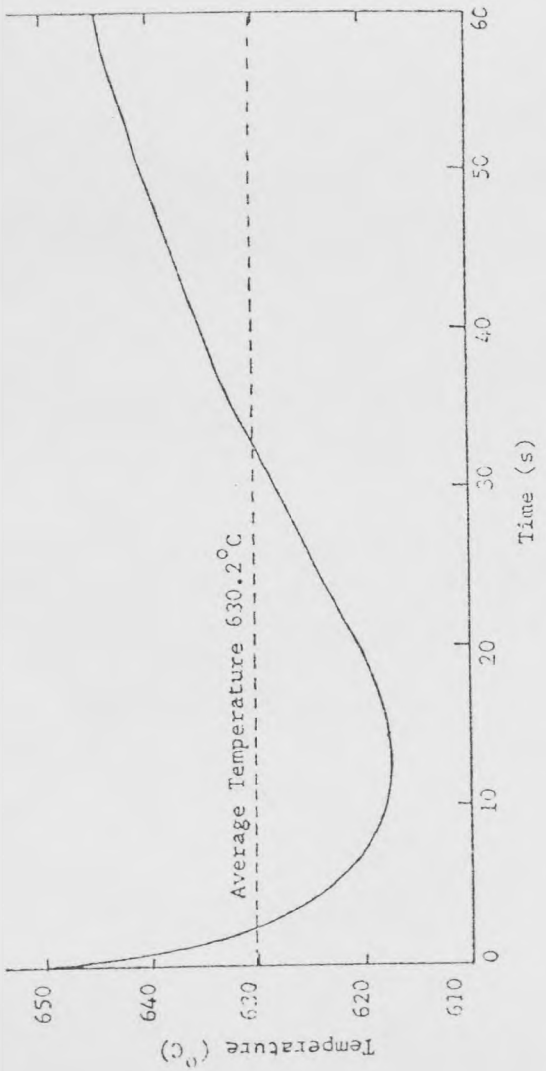

FIGURE 8

the inlet temperatures for each stroke. A direct comparison is made between a two stage adiabatic system and the RCR system. The simple design approach provided excellent predictions of the design variables and the expected conversions in the RCR system. For a 60s stroke duration, the RCR simulation predicted an average conversion of 67.7% at an efficiency of 88.6% against the two stage adiabatic system values of 63.9% and 85.7% respectively. Thus the RCR system has potential economic advantages for the dehydrogenation of ethylbenzene to styrene.

NOMENCLATURE

a	- stoichiometric coefficient	
C_p	- specific heat	kJ $kg^{-1}K^{-1}$
c	- concentration	kmol m^{-3}
e	- voidage	
e_p	- catalyst support porosity	
F	- flowrate	m^3 s^{-1}
G	- mass velocity	kg $m^{-2}s^{-1}$
h	- heat transfer coefficient	W $m^{-2}K^{-1}$
K_p	- equilibrium constant	bar
k_g	- mass transfer coefficient	m s^{-1}
k	- velocity constant	kmol s^{-1}(kg catalyst)$^{-1}$
P	- pressure	bar
p	- partial pressure	bar
r	- reation rate	kmol s^{-1}(kg catalyst)$^{-1}$
SR	- steam to ethylbenzene molar ratio	
S_v	- surface area per unit volume	m^2 m^{-3}
T	- temperature	K
t_1	- duration of the reaction stroke	s
t_2	- duration of the regeneration stroke	s

t	- time	s
V	- reactor volume	m^3
Z	- total reactor length	m
z	- distance from reactor entrance	m

Greek

α	- adsorption coefficient of ethylbenzene	bar
β	- ratio of adsorption coefficients of styrene and ethylbenzene	
ΔH	- heat of reaction	kJ $kmole^{-1}$
δT	- rate of temperature change	K s^{-1}
ρ	- density	kg m^{-3}
τ	- total cycle ($=t_1 + t_2$)	s

Subscripts

f	- exit
g	- gas
i	- component
j	- reaction
o	- entrance
s	- solid
1	- styrene reaction
2	- benzene reaction
3	- toluene reaction

Symbols with a bar refer to the regenerative stroke.

REFERENCES

1. Heggs,P.J., and Cockcroft,C.S., 1976, Proceedings of Design 76, Institution of Chemical Engineers, B-3 University of Aston, U.K.

2. Cockcroft,C.S., and Heggs,P.J., 1975, Revista Portuguesa De Quimica, 16 & 17, 297 (Chempor '75,Lisbon,September 1975).

3. Gavalas,G.R., 1971, Ind.Eng.Chem.Fund.,10, 71.

4. Gavalas,G.R.,1971, AIChE.J.,17,787.

5. Kirk-Othmer (Ed.), 1969, Encyclopedia of Chemical Technology, Volume 19, 55-85, Wiley, New York.

6. Miller,S.A., and Donaldsen,J.W.,1967, Chem.Eng.Progr.48,37.

7. Styrene, 1973, Hydrocarbon Processing, 52, 179.

8. U.S.Pat. 3525776.

9. Styrene, 1973, Hydrocarbon Processing, 52, 180.

10. Heggs,P.J., and Cockcroft,C.S.,1974, Proceedings of 7th Europäisches Symposium "Computer Applications in Process Development", 379, Erlangen.

11. Sheel,J.G.P., and Crowe,C.M., 1969, Can.J.Ch.E., 47, 183

12. Davidson,B., and Shah,M.J., 1965, IBM J.Res.Develop. 9, 389.

13. Mitchell,J.R. 1946, TAIChE. 42, 293

14. Bogdanova,O.K.et al 1962, Petrol Chem. U.S.S.R., 1, 120.

15. Hinshelwood,C.N. 1940, The Kinetics of Chemical Change, Clarendon Press, Oxford, England.

16. Cockcroft,C.S. 1976, Ph.D.Thesis, Leeds University.

17. Modell,D.J. 1972, Chem.Eng.Comput.1,100.

18. Wenner,R.R., and Dybdal,E.C.1948, Chem.Eng.Progr. 44, 275.

19. Abet,F.,et al. 1967, Quad.Ing.Chem.Ital.,3,154.

20. Eckert,E.,et al. 1975, Symposium on Computers in the Design and Erect of Chemical Plants, Karlovy Vary,Czechoslovakia.

NOMENCLATURE

NOMENCLATURE

		Units
A_S	Surface area	m^2
A_t	Throat cross sectional area	m^2
A_x	Cross sectional area	m^2
C	Coefficient of discharge, excluding velocity of approach	-
C_p	Specific heat capacity at constant pressure	$J\ kg^{-1}\ K^{-1}$
c	Concentration	$mol\ m^{-3}$
D,d	Diameter	m
D_H	Hydraulic mean diameter	m
e	Voidage	-
F	Shear stress on surface	$N\ m^{-2}$
F_a	Thermal expansion correction factor	-
F_c	Reynolds number correction factor	-
F_m	Manometer fluids correction factor	-
G	Irradiation	W
G_m	Superficial mean velocity	$kg\ s^{-1}\ m^{-2}$
g	Gravitational constant (= 9.81)	Nm^{-2}
Gr	Grashoff number (= $\beta g\ \Delta T\ l^3\ \rho^2/\mu^2$)	-
h	Heat transfer coefficient	$Wm^{-2}\ K^{-1}$
h_m	Maximum manometer differential head	cm Hg
J	Radiosity	W
j_h	Colburn j-factor for heat transfer (= $St\ Pr^{0.67}$)	-
K_i	Rate constant for the ith reaction	$mol\ kg^{-1}\ s^{-1}$
K_p	Equilibrium constant	-
k	Thermal conductivity	$W\ m^{-1}\ K^{-1}$
L, l	Length	m
M	Mass flowrate	$kg\ s^{-1}$
n	Number of turns	-

		Units
Nu	Nusselt number (= hD/k)	-
P	Pressure	$N\ m^{-2}$
p	Partial pressure	$N\ m^{-2}$
Pr	Prandtl number (= Cp μ/k)	-
Q, q	Heat load	W
$Q^{\cdot}$	Heat load per unit volume	$W\ m^{-3}$
Q_R	Heat load per 'power ring'	W
R	Heat transfer resistance	$K\ W^{-1}$
r	Radius	m
Re	Reynolds number (= u Dρ/μ)	-
Re_m	Modified Reynolds number (= 2 u Dρ/3 (1 - e) μ)	-
rr_i	Rate of the ith reaction	$mol\ s^{-1}\ kg^{-1}$
S	Flowrate index (= $Cz^2/\sqrt{1 - z^4}$)	-
SR	Steam to ethylbenzene molar ratio	-
St	Stanton Number (= h/ρu Cp)	-
T	Temperature	K
U	Overall heat transfer coefficient	$Wm^{-2}\ K^{-1}$
u	Velocity	ms^{-1}
W_m	Maximum 'dry' steam flowrate	$kg\ s^{-1}$
x_e	Equilibrium conversion	-
x_w	Metal wall thickness	m
Y	Fluid expansion correction factor	-
z	Ratio of orifice diameter, d, to the pipe inside diameter, D (= d/D)	-

Greek Letters

β	Coefficient of cubical thermal expansion	K^{-1}
γ	Ratio of specific heat capacity at constant pressure, Cp, to specific heat capacity at constant volume, C_v.	-
γ_f	Specific weight of dry steam	$kg\ m^{-3}$

		Units
ΔH	Heat of reaction	kJ kg mol^{-1}
ΔP	Pressure drop	N m^{-2}
ΔT_{ln}	Log mean temperature difference	K
ε	Emissivity	-
Θ_m	Log mean temperature difference	K
λ	Latent heat of vaporisation	J
μ	Viscosity	Ns m^{-2}
ρ	Density	kg m^{-3}
σ	Stefan-Boltzmann constant (= 5.67 x 10^{-8})	Wm^{-2} K^{-4}
Γ	Mass flowrate per unit length of perimeter	kg s^{-1} m^{-1}
τ	Surface tension	Nm^{-1}

Miscellaneous Letters

$\mathcal{F}_{i \to j}$ Total view factor for radiation from i to j

Subscripts

A	Ambient
AV	Average
b	Bulk
BD	Bead
BH	Base, internal
BZ	Benzene
C	Convective
calc	Calculated
CH	Natural convective, horizontal section
CT	Contact
CV	Natural convective, vertical section
DS	Desuperheating
EB	Ethylbenzene
f	Fluid

FB	Firebar
FL	Flange
G	Gas
GT	Gas to thermocouple
H2	Hydrogen
I	Inner
IN	Inlet
INS	Insulation
NB	Nucleate boiling
NC	Natural convective
O	Outer
obs	Observed
OUT	Outlet
P	Particle
PL	Plate
R	Radiative
S	Surface
SC	Subcooling
SD	Shield
ST	Styrene
T	Total
t	Throat
TBW	Total, bed to wire
TC	Thermocouple
TH	Top, internal
TOL	Toluene
W	Wall
WI	Inner annulus wall
WII	Inner annulus pipe, inner wall
WIO	Inner annulus pipe, outer wall
WIT	Inner annulus wall, top end
WO	Outer annulus wall
WOI	Outer annulus pipe, inner wall
WOO	Outer annulus pipe, outer wall

REFERENCES

REFERENCES

1. Bailey, J. E. and Horn, F.J.M., Chem. Eng. Sci., 27, 109, (1972).
2. Horn, F.J.M., Ind. Eng. Chem., Proc. Des. Develop., 6, 21, (1967).
3. Douglas, M. M., Ind. Eng. Chem., Proc. Des. Develop., 6, 43, (1967).
4. Bailey, J. E., Horn, F.J.M., A.I.Ch.E.J., 17, (3), 550, (1971).
5. Bailey, J. E., Chem. Eng. Comm., 1, 111, (1973).
6. Renken, A., Muller, M., Wandrey, 4th Int. Symp. Chem. Reaction Eng., Germany, (1976).
7. Gavalas, G. K., Ind. Eng. Chem. Fund., 10(1), 71, (1971).
8. Gavalas, G. K., A.I.Ch.E.J., 17, (4), 787, (1971).
9. Assaf, A., Ph.D. Thesis No. 916, University of Leeds, (1981).
10. Cockcroft, C. S., Ph.D. Thesis No. 779, University of Leeds, (1976).
11. Cockcroft, C. S. and Heggs, P. J., Chem. Por. 1981, Caloriste Gulenbian Foundation Centre, Lisbon, Portugal.
12. Cockcroft, C. S. and Heggs, P. J., Chem. Por. 1975, Caloriste Gulenbian Foundation Centre, Lisbon, Portugal.
13. Cockcroft, C. S. and Heggs, P. J., 7 Europaisches Symposium, 2-3 April, 1974, Erlargen.
14. U.S. Patent 2,374,826.
15. Miller, S. A. and Donaldson, J. W., Chem. Eng. Prog., 48, (12), 37, (1967).
16. Mitchell, J. E., Trans. A.I.Ch.E., 42, (2), 293, (1946).
17. Kirk-Othmer (Ed.), Encyclopaedia of Chemical Technology, 19, 55, Wiley, New York, (1969).
18. Degannes, P. N., Ruthven, D. M., Can. J. Chem. Eng., 57, 627, (1979).
19. Fujimoto, K., Kunugi, T., Ind. Eng. Chem. Prod. Res. Dev., 20, 319, (1981).
20. G.B. Patent 892,779.
21. G.B. Patent 966,704.
22. Wett, T., Oil and Gas Journal, July 20th, 1981.
23. Fr. Pat. 1,344,654; Germ. Pat. 1,917,279; U.S. Pat. 3,807,963.
24. U.S. Pats. 3,118,006; 3,308,179; 3,326,996; 3,402,212; 3,502,737; 3,515,763; G.B. Pat. 1,176,916.

25. Sheel, J.G.P. and Crowe, C. M., Can. J. Chem. Eng., 47, 183, (1969).

26. Davidson, B. and Shah, M. J., IBM.J.Res.Develop., 9, 389, (1965).

27. Wenner, R. R. and Dybdal, E. C., Chem. Eng. Prog., 44, (4), 275, (1948).

28. Berdulin, A. Ya., Terekhin, R. M., Yukelson, I. I., Khim. Prom., 45, (9), 662, Moscow (1969).

29. Abet, F., Mauri, M., Piovan, M., Quad. Ing. Chem. Ital., 3, (9), 154, (1967).

30. Modell, D. J., Chem. Eng. Comput., 1, 100, (1972).

31. Eckert, E., Marek, M. and Spevecek, J., Symposium on Computers in the Design and Erection of Chemical Plants, Karlovy Vary, Czechoslovakia (1975).

32. Carra, S. and Forni, L., Ind. Eng. Chem. Develop., 4, (3), 281, (1965).

33. Bogdanova, O. K., Sheheglova, A. P., Balandin, A. A. and Belomestriykh, I. P., Petrol Chem. USSR, 1, (1), 120, (1962).

34. Davidson, B., Shah, M. J., IBM Technical Report, TR 02.340, IBM Systems Develop. Lab., San Jose, California (1965).

35. Ohlinger, H. and Stadelmann, S., Chem. Ingr. Tech., 37, (4), 361, (1965).

36. Catalyst Information and Instructions, Girdler G-64 Catalysts, Girdler-Sudchemie, Munich, (1981).

37. BS 4137: 1967: Guide to the Selection of Electrical Equipment for Use in Division 2 areas.

38. BS 1259: 1958: Intrinsically Safe Electrical Apparatus and Circuits.

39. BS 889: 1965: Specifications for Flameproof Electric Lighting and Fittings.

40. BS 229: 1957: Flameproof Enclosures of Electrical Apparatus.

41. Riddlestone, H. G., "Comparison of National Requirements for Electrical Apparatus for Use in Hazardous Atmospheres", 3rd Symposium on Chemical Process Hazards with special reference to Plant Design, I.Chem.E., 11-12 April, 1967.

42. National Fire Protection Association: "Guide to Fire Prevention in the Chemical Industry, B.C.I. (1968).

43. Flowpack Users Manual, I.C.I. Limited, (1972).

44. Schmidt, F. W., Willmott, A. J., "Thermal Energy Storate and Regeneration", McGraw-Hill, New York, (1981).

45. Simpson, L. L., Chem. Eng., 75, 199, June 17th, 1968.

46. Data Booklet for 'Kaowool' Fibre, Blanket and Paper. Morganite Ceramic Fibres Ltd., Wirral, Merseyside.

47. Spink, L. K., "Principles and Practice of Flow Meter Engineering", 9th edition, Foxboro Publications (1967).

48. BS 1042: 1964: Methods for the Measurement of Fluid Flow in Pipes: Part 1 (Orifice Plates, Nozzles and Venturi Tubes).

49. 'Kanthal' Handbook, Aktie bolaget, Kanthal, Sweden, (1980).

50. 'E-2 Metripump' Handbook, Metering Pumps Ltd., Feltham, Middlesex.

51. Lord, R. L., Minton, P. E. and Slusser, R. P., Chem. Eng. 77, 102, January 21st, 1970.

52. 'Ghlom 80/20' Resistance Wire Data Sheets, Resistance Wires Ltd., Manchester, (1980).

53. Kay, J. M., "An Introduction to Fluid Mechanics and Heat Transfer", 2nd edition, C.U.P., (1963).

54. Patrick, M. A., Trans. I.Ch.E., 46, 516, (1967).

55. Kreith, F., "Principles of Heat Transfer", 2nd edition, In text, Educational Publishers, London (1973).

56. Colburn, A. P., Millar, L. L., and Westwater, J. W., Trans. A.I.Ch.E., 38, 447, (1942).

57. Collier, J. G., "Convective Boiling and Condensation", McGraw-Hill, London, (1972).

58. Coulson, J. M. and Richardson, J. F., "Chemical Engineering", Volumes I, II and III, Pergamon Press, Oxford, (1975).

59. Perry, R. H. and Chilton, C. H., Chemical Engineers Handbook, 5th Edition, McGraw-Hill Publications, New York (1973).

60. British Steam Specialities Data Book and Engineers Catalogues, B.S.S., Leicester, (1980).

61. Gallant, R. W., "Physical Properties of Hydrocarbons", Volumes I and II, Gulf Publishing Co., Houston, Texas.

62. Physical Data for Chemical Engineering Design, B.P. Chemicals (U.K.) Ltd., Engineering Department, London, (1970).

63. Compressed Gas Handbook, N.A.S.A., NASA SP-30545, (1969).

64. Heating Elements Catalogue, Heating Elements Ltd., Leicester, (1976).

65. McAdams, W. H., "Heat Transmission", 3rd edition, McGraw-Hill, (1954).

66. Leuenberger, H. and Person, R. A., "Radiation Shape Factors for Cylindrical Assemblies", Amer. Soc. Mech. Engrs., Paper No. 56-A-144, (1956).

67. GEC—Elliot Calibration Handbook for Metric Series Rotameters, GEC-Elliot Rotameters Ltd., Croydon, (1980).

68. 'Pyrotenax' Thermocouples and Accessories Booklet, BICC (Pyrotenax) Ltd., Hebburn, Tyne and Wear (1979).

69. Heggs, P. J. and Handley, D., Trans. A.I.Ch.E., 46, 251, (1968).

70. 'Isotape' Catalogue, Isopad Ltd., Borehamwood (1981).

71. Clough, D. E. and Ramirez, W. F., A.I.Ch.E.J., 22, 6, 1097, (1976).

72. Kobayashi, H., Kobayashi, M., Catal. Rev., 10, 139, (1975).

73. Bennett, C. O., Catal. Rev., 13, 121, (1976).

74. Scheintuch, M., Schmitz, R. A., Catal. Rev., 15, 107, (1977).

75. Beusch, H., Fieguth, D., Wicke, E., Adv. Chem. Ser., 109, 615, (1972).

76. Billimoria, M. R., Bruns, D. D., Bailey, J. E., A.I.Ch.E.J., 26, 319, (1980).

77. Mehta, P. S., Sams, W. N., Luss, D., A.I.Ch.E.J., 27, 234, (1981).

78. Unni, M. P., Hudgins, R. R., Silveston, P. L., Can. J. Chem. Eng., 51, 623, (1971).

79. Schweich, D., Villermaux, J., Ind. Eng. Chem. Fund., 21, 51, (1982).

80. Dale Wilson, H., Rinker, R. G., Chem. Eng. Sci., 37, 343, (1982).

81. Abdul-Kareen, H. K., Jain, A. K., Silveston, P. L., Hudgins, R. R., Chem. Eng. Sci., 35, 273, (1980).

82. Abdul-Kareem, H. K., Silveston, P. L., Hudgins, R. R., Chem. Eng. Sci., 35, 2077, (1980).

83. Abdul-Kareem, H. K., Silveston, P. L., Hudgins, R. R., Chem. Eng. Sci., 35, 2085, (1980).

84. Jain, A. K., Hudgins, R. R., Silveston, P. L., Can. J. Chem. Eng., 60, 809, (1982).

85. Jain, A. K., Ph.D. Thesis, University of Waterloo, Waterloo, Ontario, Canada (1981).

86. Lee, E. H., Catal. Rev., 8, 285, (1974).

87. 'Isotape' Catalogue, Isopad Ltd., Borehamwood.

88. Clough, D. E., and Ramirez, W. F., A.I.Ch.E.J., 22, 6, 1097, (1976).

89. Clough, D. E., Ph.D. Thesis, University of Colorado, (1975), No. 76-3892.

90. Spencer, S. F., Anal. Chem., 35, 592, (1963).

91. U.S. Patents: 3,702,346; 3,755,482; 3,847,968; 3,855,330; 4,113,787; 4,287,375.

92. Amos, J. A., Cox, N. R., Mohla, D. C., Chem. Eng. Prog., 77, 29, (August 1981).

93. Smith, J. M., "Chemical Engineering Kinetics", 2nd edition, McGraw-Hill, New York, (1970).

94. Kaeding, W. W., Catal. Rev., 8, 307, (1974).

95. British Steel Corporation, Tubes and Fittings Catalogue, Tubes Division, Corby, Northants.

96. U.S. Patent: 4,069,271.

97. Autoclave High Temperature Control Valves, Autoclave Engineers Ltd., Hounslow, Middlesex.